AN INVESTIGATION INTO THE MECHANICS OF REGULAR ARRAYS OF DISCS AND SPHERES

DANIEL JOHN BLACKBURN, B.Sc.

A Thesis submitted for the Degree of

Doctor of Philosophy

at

The University of Aston in Birmingham

February 1983

The University of Aston in Birmingham

An investigation into the mechanics of regular arrays of discs and spheres

A thesis submitted for the degree of Doctor of Philosophy, by Daniel John Blackburn, 1983

SUMMARY

Before the behaviour of granular material can be fully understood, it is necessary to study the simpler case of idealised regular packings. Two approaches towards this end are reported here; one analytical and one using computer simulation.

In the first part of the thesis regular packings of rigid spheres (arranged in a body-centred orthorhombic manner) are analysed in order to define the conditions necessary to cause slip at the contacts. The macroscopic stress and strain-increment tensors are derived to define both the initial yield conditions and subsequent plastic (softening) deformation. The geometry of the corresponding yield surface is described by an oblique cone which rotates during plastic deformation. Plastic strain-increment vectors are at right angles to the cone axis.

The computer simulation uses the Distinct Element Method to study regular packings of discs as they deform under a loading imposed by end plattens. The method employs an explicit finite difference scheme to model the propagation of boundary originated forces and displacements through the assembly. The results of the simulation tests show that end plattens produce discrete shear bands which propagate through the assembly and that softening is associated with gap widening along the existing shear bands.

KEY WORDS

granular material
regular packings
yield conditions
computer simulation
shear band propagation

ACKNOWLEDGEMENTS

I would like to thank my supervisor, Dr.C.Thornton, for his help and enthusiastic support throughout the research period.

Appreciation is also expressed to Suzanne who typed the manuscript; to Charlie and Lyn who traced the diagrams; to Mr.P.Taylor and Dr.L.Hatton of Merlin Geophysical Co. Ltd. for their understanding and generosity while this thesis was being prepared; and to Ann Callcott for her perseverance.

Finally, and most of all, I would like to thank my parents for their constant support and encouragement resulting in the production of this thesis.

CONTENTS

SUMMARY

ACKNOWLEDGEMENTS

CONTENTS 1

LIST OF TABLES AND FIGURES 6

CHAPTER 1 INTRODUCTION 17

1.1 Object and scope of the investigation 17

1.2 Terminology 19

CHAPTER 2 THE STRUCTURE OF REGULAR PACKINGS 20

2.1 Crystallographic unit cells 21

2.1.1 Crystallography - Morphology and Internal Order 21

2.1.2 Unit cells and space lattices 24

2.2 The packing of spheres 26

2.3 The body-centred orthorhombic array 28

2.3.1 The 15 ball dodecahedral unit 29

CHAPTER 3 THE MECHANICS OF REGULAR ARRAYS - A REVIEW 43

3.1 Introduction 43

3.2 Elastic behaviour of spheres 43

3.2.1 Elastic compliance due to normal contact forces 43
3.2.2 Elastic compliance due to combined normal and tangential contact forces 45
3.2.3 Elastic behaviour of regular packings of spheres 47
3.3 Irrecoverable deformation due to interparticle slip 48
3.3.1 Two dimensional rod models 49
3.3.2 Regular arrays of spheres - axisymmetric compression 54
3.3.3 Regular arrays of spheres - plane strain 57
3.3.4 Regular arrays of spheres - general case 61

CHAPTER 4 THE ANALYSIS OF BODY-CENTRED ORTHORHOMBIC ARRAYS OF RIGID SPHERES 70
4.1 Derivation of the strain-increment tensor 71
4.2 Derivation of the stress tensor 74
4.3 Yield conditions for body-centred tetragonal packings 78
4.3.1 Yield surface geometry 80
4.3.2 Plastic potentials and flow rule 84

4.3.3 Hardening/softening laws 86

4.4 Conclusions 87

CHAPTER 5 REVIEW OF COMPUTER SIMULATION 97

5.1 Introduction 97

5.2 Developments in computer simulation 98

5.3 Computer simulation in geomechanics 101

5.3.1 Continuum models 102

5.3.2 Jointed rock models 103

5.3.3 Granular models 106

CHAPTER 6 THE SIMULATION OF PARTICULATE MATERIAL USING THE DISTINCT ELEMENT METHOD 111

6.1 Introduction 111

6.2 The requirements of the model 111

6.2.1 The working space 113

6.2.2 Components of the simulation 114

6.2.3 Dynamic storage 115

6.2.4 Box (or grid) storage 117

6.2.5 Redundant address locations 120

6.3 Program iteration 121

6.3.1 Initialisation of the database 121

6.3.2 Methodology of the iterative cycles 124

6.3.3 Contact detection and reboxing 128

CHAPTER 7 IMPLEMENTATION OF THE SIMULATION PROGRAM 135

7.1 Introduction 135

7.2 Compilation and execution of "BALL" 136

7.2.1 Alterations necessary for compilation 136

7.2.2 Execution of the simulation 142

7.3 Modifications to the model 147

7.3.1 Initialisation of the assembly 148

7.3.2 Boundary control facilities 148

7.3.3 Iteration of the test process 150

7.3.4 Contact summary option 151

7.3.5 Graphical output facilities 152

7.3.6 Command value abstraction 153

7.3.7 Input/output channel allocation 155

7.4 Transfer of the simulation program from the ICL 1904S to the CDC 7600 157

CHAPTER 8 RESULTS OF COMPUTER SIMULATION TESTS 167

8.1 Preliminary tests on 18 disc arrays 169

8.1.1 Selection of control parameters 169

8.1.2 Validation tests 173

8.2 Effect of sample size on mode of deformation 184

8.3 Tests on 124 disc arrays 188

8.3.1 Effect of end restraint 188

8.3.2 Effect of disc rotation (spin restraint) 191

8.4 Further observations 192

CHAPTER 9 CONCLUDING REMARKS 249

APPENDIX A TWO DIMENSIONAL ANALYSIS OF REGULAR RIGID DISC ARRAYS 252

APPENDIX B COMMANDS AVAILABLE FOR "BALL" 256

APPENDIX C PROGRAM LISTING OF "BALL" 263

REFERENCES 264

BIBLIOGRAPHY 272

LIST OF TABLES AND FIGURES

CHAPTER 1

No tables or figures

CHAPTER 2

Table	2.1	Classification of unit cells	32
Figure	2.1	The 14 unit cells according to Bravais	33
	2.2	Typical unit cell showing the lattice parameters	34
	2.3	Arrangement of spheres showing alternating layer structure	35
	2.4	The 14 Bravais lattices ordered according to sphere distribution	36
	2.5	Two face-centred cubic unit cells stacked vertically to show a body-centred orthorhombic unit cell contained within	37
	2.6	Formation of octahedral units from body-centred orthorhombic unit cells	38
	2.7	Diagrammatic representation of interlocking octahedral assemblies	39
	2.8	Exploded view of a dodecahedral unit	40

Figure 2.9 The complete dodecahedron 41
2.10 The 15 sphere hard ball model of a dodecahedral unit 42

CHAPTER 3

Figure 3.1 Deformation of two identical homogeneous, elastic spheres in oblique contact 66
3.2 Typical plot illustrating the variation of inter-particle deformation with applied tangential force 66
3.3 Closest packing arrangement of rods (or discs) showing the packing angles α and β according to Rowe (1962) 67
3.4 Parkin's (1965) general two dimensional model 68
3.5 Parkin's (1965) two dimensional strength solution 68
3.6 Packing angle for initially less dense packings after Thornton (1977) 69
3.7 Solutions resulting from Thornton's (1977) analysis 69

CHAPTER 4

Figure 4.1 Body-centred orthorhombic unit cell showing co-ordinate axes and cell dimensions 89

4.2 Dodecahderal hard ball model showing contact points and gaps 89

4.3 Deviatoric stress-strain plot and the corresponding yield surface (viewed in principal stress space) 90

4.4 Normalised deviatoric yield loci 90

4.5 Effect of interparticle friction 91

4.6 Deviatoric yield loci for body-centred tetragonal packings 91

4.7 Method of superimposing plastic strain-increment vectors on yield points 92

4.8 A plastic potential constructed from plastic strain-increment vectors 92

4.9 Deviatoric yield locus viewed along the axis of the cone (D= 2.0 packing) 93

4.10 Yield cones and strain-increment vectors for body-centred tetragonal packings 94

Figure 4.11 Hardening theories 95

4.12 Plot of yield stress against deformation showing the points corresponding to various intermediate packing types 96

CHAPTER 5

No tables or figures

CHAPTER 6

Figure 6.1 Data storage in the dynamic array 131

6.2 Combination of two "Integers" into a real variable 131

6.3 Data structure within the dynamic array showing the interaction between box and link sections 132

6.4 Diagrams showing the relationships between boxes, contacts and links in the dynamic array 133

6.5 Iteration subroutine tree 134

CHAPTER 7

Figure 7.1 Algorithm for automatic formation of a tight packing 161

Figure 7.2 Automatic wall definition algorithm 162
7.3 Algorithm to iterate a series of commands 163
7.4 Algorithm for contact printout 164
7.5 Algorithm for the plotting subroutine 165
7.6 Algorithm for reading in commands 166

CHAPTER 8

Figure 8.1 Initial arrangement of an 18 disc packing showing plattens, grid and co-ordinate axes 194
8.2 Plot of stress ratio against relaxation cycles 195
8.3 Plots of stress ratio against strain illustrating the effect of loading rate 196
8.4 Forces acting on a typical elastic disc within a close packing 197
8.5 Plots of stress ratio and volumetric strain against longitudinal strain, comparing the theoretical results with those obtained from the simulation, for a frictionless packing 198

Figure 8.6 Plots of stress ratio against strain to illustrate the effects of stiffness 199

8.7 Stress ratio-strain curves illustrating the effect of cell pressure 200

8.8 Plots of stress ratio against strain illustrating the effect of interparticle friction 201

8.9 Stress ratio-strain curve for an 18 disc packing 202

8.10 Deformation of an 18 disc packing at 0.2% strain post peak (1.4% strain) 203

8.11 Deformation of an 18 disc packing at 10.5% strain post peak (11.7% strain) 203

8.12 Stress ratio-strain curve for a 74 disc packing 204

8.13 Deformation of a 74 disc packing at 1.3% strain, with frictionless discs and plattens 205

8.14 Deformation of a 74 disc packing at 1.7% strain, with frictionless discs and plattens 206

8.15 Deformation of a 74 disc packing at 2.8% strain, with frictionless discs and plattens 206

Figure 8.16 Stress ratio-strain curve for an 86 disc packing 207

8.17 Deformation of an 86 disc packing at 1.48% strain, with frictionless discs and plattens 208

8.18 Deformation of an 86 disc packing at 2.2% strain, with frictionless discs and plattens 209

8.19 Deformation of an 86 disc packing at 3.3% strain, with frictionless discs and plattens 210

8.20 Deformation of an 86 disc packing at 4.5% strain, with frictionless discs and plattens 211

8.21 Stress ratio-strain curve for a 95 disc packing 212

8.22 Deformation of a 95 disc packing at 1.3% strain, with frictionless discs and plattens 213

8.23 Deformation of a 95 disc packing at 2.0% strain, with frictionless discs and plattens 214

8.24 Stress ratio-strain curve for a 124 disc packing 215

8.25 Deformation of a 124 disc packing at 1.4% strain, with frictionless discs and plattens 216

Figure 8.26 Deformation of a 124 disc packing at 1.6% strain, with frictionless discs and plattens 217
8.27 Deformation of a 124 disc packing at 2.3% strain, with frictionless discs and plattens 218
8.28 Comparison of stress ratio-strain curves for various packing sizes 219
8.29 Deformation of a 410 disc packing at 2.10% strain 220
8.30 Deformation of a 410 disc packing at 3.25% strain 221
8.31 Stress ratio-strain curve for a 410 disc packing 222
8.32 Stress ratio-strain curve for a 124 disc packing with frictionless plattens 223
8.33 Stress ratio-strain curve for a 124 disc packing with frictional plattens 224
8.34 Deformation of a 124 disc packing at 1.97% strain with frictionless plattens 225
8.35 Deformation of a 124 disc packing at 2.9% strain with frictionless plattens 226

Figure 8.36 Deformation of a 124 disc packing at 3.10% strain with frictionless plattens 227

8.37 Deformation of a 124 disc packing at 3.18% strain with frictionless plattens 228

8.38 Deformation of a 124 disc packing at 3.58% strain with frictionless plattens 229

8.39 Deformation of a 124 disc packing at 5.19% strain with frictionless plattens 230

8.40 Deformation of a 124 disc packing at 2.49% strain with frictional plattens 231

8.41 Deformation of a 124 disc packing at 2.70% strain with frictional plattens 232

8.42 Deformation of a 124 disc packing at 3.10% strain with frictional plattens 233

8.43 Deformation of a 124 disc packing at 3.58% strain with frictional plattens 234

8.44 Deformation of a 124 disc packing at 3.90% strain with frictional plattens 235

Figure 8.45 Deformation of a 124 disc packing at 5.13% strain with frictional plattens 236

8.46 Stress ratio-strain curves for 124 disc packings comparing frictionless and frictional plattens 237

8.47 Stress ratio and contact numbers plotted against strain (calculation cycles) 238

8.48 Stress ratio and contact numbers plotted against strain (calculation cycles) 239

8.49 Deformation of a 124 disc packing at 3.58% strain, with all discs irrotational 240

8.50 Deformation of a 124 disc packing at 3.58% strain, with all discs irrotational 241

8.51 Deformation of a 124 disc packing at 5.19% strain with all discs irrotational 242

8.52 Deformation of a 124 disc packing at 3.58% strain, with boundary discs irrotational 243

8.53 Deformation of a 124 disc packing at 3.58% strain, with boundary discs irrotational 244

Figure 8.54 Deformation of a 124 disc packing at 5.19% strain, with boundary discs irrotational 245

8.55 Stress ratio-strain curves for 124 disc packings (frictionless plattens) illustrating the effect of spin restraint 246

8.56 Stress ratio-strain curves for 124 disc packings (platten friction) illustrating the effects of spin restraint 247

8.57 Deformation of a 124 disc packing at 1.97% strain with frictionless plattens showing the positions of horizontal contact forces 248

APPENDIX A

Figure A.1 Plot of yield stress against deformation showing the points corresponding to various intermediate packing types 255

APPENDIX B

No tables or figures

APPENDIX C

Microfiche listing of program "BALL" (inside back cover)

CHAPTER ONE

1. INTRODUCTION

1.1 OBJECT AND SCOPE OF THE INVESTIGATION

The experimentally observed behaviour of granular material, such as sand, is complex due to its particulate structure. The external behaviour observed in the laboratory is however, in some way, related to the internal behaviour of the particles that together form the overall structure. To attempt to relate theoretically the observed behaviour of sand to what occurs within such a complicated structure would be extremely difficult. It is, therefore, necessary to first examine simpler structures in order that the intrinsic aspects of the internal mechanics may be identified. By studying packings of simple structures and identifying the yield conditions and associated mechanisms, it is hoped that a more fundamental understanding of granular materials will be reached. Previous analyses of regular packings have usually been restricted to one (or two) particular array geometries. In this thesis a more general packing description will be adopted, thereby enabling a general three dimensional analysis to be developed, which is applicable to both the initial yield condition and subsequent deformation. Before this is possible it is necessary to define the physical model and identify the structure.

In Chapter 2 the structure of regular arrays will be discussed and a review of previous analyses of regular arrays will be presented in Chapter 3. Chapter 4 presents the analysis of a class of regular packings that can be defined as Body-Centred Orthorhombic, from which it is possible to identify the effects of structure and inter-particle friction. The relationship between the internal particle mechanics and the macroscopic yield conditions will also be considered.

The second part of the thesis will be concerned with the use of computer simulation as a method of directly modelling the behaviour of granular material. After a general review of computer simulation presented in Chapter 5 a particular technique, the Distinct Element Method, Cundall and Strack (1978), will be described in Chapter 6. This technique is capable of modelling a wide variety of boundary conditions on irregular assemblies of random particles, but as an initial project at the University of Aston attention has been restricted to regular assemblies. The alterations necessary to achieve this, using the available computing facilities will be provided in Chapter 7.

The results of the simulation tests carried out with the ammended program will be presented and discussed in Chapter 8. It will be shown that the stress-strain behaviour is

dependent on the boundary conditions applied, which in turn affect the internal mechanisms. In this context particular attention will be given to the initiation and propagation of discrete shear bands within the assembly. Some final remarks will be provided in Chapter 9, to conclude the presentation.

1.2 TERMINOLOGY

The majority of the symbols and terms contained in this thesis are common to a lot of current soil mechanics research and so are widely agreed upon and unambiguous. However, in certain instances, some terms may convey different meanings to different investigators. In such cases particular attention will be given to clarify the meaning of any possibly ambiguous terms and definitions will be provided of the symbols used at the relevant points in the text.

CHAPTER TWO

2. THE STRUCTURE OF REGULAR PACKINGS

Before examining the mechanics of regular arrays of spheres it is necessary to clearly identify the structure of the physical model. The spacial arrangement of the spheres is analogous to the "hard ball models" of physical metallurgy and crystallography which, in turn, represent the unit cells of the three dimensional space lattices used to describe the structure of crystals.

In order to avoid any ambiguity the unit cell terminology of crystallography will be adopted in this thesis. Consequently, this chapter will first of all consider crystallographic descriptions of structure. This will be followed by a consideration of the ways in which equal spheres may be packed to form regular arrays. Finally the arrangement which will be the subject of the analysis provided in chapter 4 will be examined.

The Bibliography should be consulted for any historical references, mentioned in the text but, not found in the references list.

2.1 CRYSTALLOGRAPHIC UNIT CELLS

2.1.1 Crystallography - Morphology and Internal Order

The earliest work on the nature of crystals was an attempt to describe the observed external polyhedral geometry in terms of the internal order. Both Kepler and Descartes speculated that the configurations exhibited by snow flakes could be explained by the packing of spherical ice particles in a plane. This line of thought was developed by Hooke in 1665 for his work "Micrographia", in which it was noted that all shapes displayed by alum crystals could be achieved by packings of spherical particles. It was postulated by Huygens, in the same century, that the shapes formed by other crystals could be explained by various arrangements of ellipsoidal particles.

A large number of "Laws" were put forward by early crystallographers searching for ways in which to understand the nature of crystals, these "Laws" usually expressed generalities about crystal properties. One of these, the "Law of Constancy of Interfacial Angles", states that for any two crystals of the same substance, the angles between corresponding faces are always the same. This was confirmed by Rome de l'Isle in 1772 after performing extensive crystal measurements.

In 1782, Hauy began to build on the foundations of those, like Hooke, who explained the basic crystal forms by the packing of spherical or ellipsoidal particles. As an alternative building block, Hauy proposed the use of "Molecules Integrantes". These he sketched as parallelepiped - shaped blocks, the equivalent, in modern terms, to the primitive cells of a lattice. These blocks, when packed in parallel arrays, were intended to represent the crystal structure so that the exterior of the collection of blocks corresponded to the morphology of the crystal being modelled. The slopes and shapes of various crystal faces were simulated by leaving steps on the exterior of the building block assemblies.

The geometry of such stacks of blocks was the inspiration for the contribution by Weiss, who in 1808 showed how it was possible to refer crystal faces to a system of axes. The conventions he adopted for the labelling and orientation of the axes persist through to the present day. To refer faces to axes, he defined the faces in terms of their relative intercepts with the three orthogonal reference axes. These ratios constituted the first use of indices to define crystal faces, and he proposed a corresponding "Law" - "The Law of Rational Intercepts". Using this reference system, Weiss was able to distinguish between crystals of different types. The indices used in modern crystallography to represent the orientation of crystal

faces are sets of three numbers that are proportional to the Weiss intercept system. These were proposed in 1825 by Whewell and are commonly called the "Miller Indices" because Millers book, "A Treatise on Crystallography", published in 1839 popularised them.

It was shown by Hessel in 1831 that there are 32 possible forms of symmetry applicable to crystals that can be developed from the external elements of symmetry, axes of rotation, inversion axes and reflection planes. These 32 crystal classes were largely overlooked, however, until Sohncke called attention to them in 1879.

The first space lattices were derived by Frankenheim in 1842, but unfortunately a duplication was made of one of the forms so that it was concluded that there were 15 basic forms of regular packings. This error was rectified in 1851 by Bravais whose geometrical analyses showed that there are only 14 different space lattices, in each of which the environment of every point is identical with that of every other point and is similarly orientated. The parallel orientation of layers of spheres, as required by the Bravais lattices, was at that time considered to be a pre-requisite for homogeneity. However, in 1863, Weiner showed that the homogeneity requirement merely called for any situation in which all arrangements have the same relation to the pattern as a whole. Using this argument Sohncke, in 1876, proposed the "65 point systems".

Sohncke showed that if identity of environment, only, were considered (without similar orientation) there are 65 regular point systems. As a development of this work, another 165 arrangements were discovered by using reflection and inversion operations in addition to those performed by Sohncke. There were three independent derivations deducing the existance of the 230 different types of three dimensional arrangements. These derivations were performed by Barlow in 1883, Fedorov in 1885 and Schoenflies in 1891. Schoenflies, using mathematical group theory in his derivation, probably had the greatest influence on later investigations and it was his work that was responsible for calling the symmetries of the point systems, "Space Groups".

2.1.2 Unit Cells and Space Lattices

In a crystal, the morphology reflects a dependence on the internal arrangement of the component parts. The pattern of this internal order is dependent on individual units, each of which is a group of linked atoms, with a fixed spatial relationship between them. This relationship has to be repeated many times to build up a crystal. Commonly, the smallest unit which, when repeated many times in three dimensions, will build up a crystal, is called a primitive cell. The corners of a primitive cell, (or building block), have the property that each is a point which is indistinguishable from its neighbours. An

array of such points is called a lattice, or a space lattice if it is a three dimensional arrangement.

For three dimensional space lattices, although there are 230 different Space Groups, Bravais (1851) showed that there were only 14 basic types of lattice, as shown in Figure 2.1, and which are referred to as unit cells. Each unit cell is a building block which reflects the symmetries within the structure and, when stacked with like building blocks, forms an infinitely extended mass which has no gaps between the individual blocks.

For each class of unit cell the geometry is defined by three lattice vectors, A, B, and C; three lattice constants (or vector lengths) a, b, c; and the inter-axial angles α , β and γ ; as shown in Figure 2.2. Different crystals have different unit cell types, sizes and (where the angles between edges are not fixed at 90° or 120°) different angles. The unit cell nomenclature may be adopted and used in the analysis of regular packings if spheres are substituted for the atoms so as to form a "hard ball model".

Thus a regular three dimensional array of spheres, when joined together by lines drawn through their centres, form a space lattice. The type of sphere packing arrangement can be represented by one of the 14 unit cells of Bravais. This system will provide a means of identifying

any packing and will avoid ambiguities when describing the work of contributors to this field. Consequently it will be the convention in this work, when describing packings referred to in other works, to call the packing by the name used in the original work, and where the packing description is different to that of the system used herein, the unit cell description will be quoted in brackets afterwards. For example, when reviewing the works of Gratton and Fraser (1935) on the packing of spheres, reference will be made to the tetragonal-sphenoidal (rhombohedral) arrangement.

2.2 THE PACKING OF SPHERES

Using a"hard ball model",Kepler (1611), was the first to recognise that a "close-packed" (face-centred cubic) array of spheres could be obtained either by stacking square or triangular packed planes; and concluded that "In the closest arrangement of solids (spheres), the trigonal order cannot occur without the square, and vice-versa". He demonstrated this by stacking dense packed (triangular) planes of spheres to form a tetrahedron, which he then inverted so that an edge of the tetrahedron, rather than a vertex, was uppermost. He then found that, whenever one ball was removed from the top, the four balls of a square packed plane were revealed.

A systematic study of the symmetrical arrangement of close

packed spheres, compatible with the external symmetry of crystals, was undertaken by Barlow. In 1883 he suggested the, then radical, concept that the separate atoms making up a crystal compound "Occupy distinct portions of space and do not loose their individuality".

An extensive work was performed by Gratton and Fraser (1935) to examine how different regular arrangements of spheres affect the porosity and permeability of the resultant packings. They recognised four different regular packings: the cubic (simple cubic); the orthorhombic (hexagonal); the rhombohedral (face-centred cubic); and the tetragonal-sphenoidal packing (rhombohedral); see Table 2.1. Gratton and Fraser also recognised the existance of 2 "dense-packed arrays", the face-centred cubic and the close-packed hexagonal, however due to their approach, both of these were considered as rhombohedral in their nomenclature.

Gratton and Fraser (1935) noted that the tightest packing, the rhombohedral (face-centred cubic) packing was not of a uniform density. They recognised that the packing was composed of zones of tetrahedral elements and zones of octahedral elements. They observed that the overall porosity of the packing, which is widely quoted as 25.95% is in fact a weighted average of the porosity of the octahedral elements (27.93%) and the porosity of the

tetrahedrons (22.00%). This is due to the way in which the triangular layers are stacked upon each other.

As can be seen in Figure 2.3, it is not possible to place spheres in every available saddle of the lower layer. The regular stacking of layers in an A.B.A.B.A. manner results in the formation of tetrahedral and octahedral gaps. There are many alternatives of this stacking arrangement, for instance A.B.C.B.A.B.C.B.A, which leads to the formation of a hexagonal packed lattice. Such a situation could also occur when a face-centred cubic packing undergoes twinning, the packing that occurs in the twinned zone is in a hexagonal packing arrangement.

2.3 THE BODY-CENTRED ORTHORHOMBIC ARRAY

The 14 unit cells in Figure 2.1 may be grouped into the seven crystal systems as given in Table 2.1. Alternatively, except for the hexagonal and rhombohedral cells, they may be re-grouped according to whether they are simple, body-centred, face-centred, or base-centred, as shown in Figure 2.4.

It is the convention in crystallographic nomenclature to take the symbol ' $\neq$ ' to mean "not <u>necessarily</u> equal to", Buerger (1970). Consequently all the body-centred cells can be described as body-centred orthorhombic, the body-centred cubic and body-centred

tetragonal cells being special cases of the more general body-centred orthorhombic unit cell.

In Chapter 4 the mechanics of body-centred orthorhombic arrays will be analysed. The analysis will be shown to be an extension of previous work, Rennie (1959), Parkin (1965), Thornton (1979) dealing with face-centred cubic arrays. By stacking two face-centred cubic unit cells, an alternative body-centred orthorhombic unit cell can be identified as shown in Figure 2.5. This alternative orthorhombic cell is an equally valid building block. Hence it is clear that the face-centred cubic unit cell is a special case of the general body-centred orthorhombic unit cell.

Consequently, by adopting the body-centred orthorhombic array as the physical model, general solutions can be obtained which will include body-centred tetragonal, body-centred cubic, and face-centred cubic arrays as special cases. Furthermore, for the mode of deformation to be analysed in Chapter 4, as will be shown, the general body-centred orthorhombic description will remain valid throughout the deformation process.

2.3.1 The 15 Ball Dodecahedral Unit

Although the structure is adequately defined by the body-centred orthorhombic unit cell it is more convenient to

adopt an alternative unit element for the analysis of the mechanics of the system.

For regular arrays of rods or discs, Thornton (1977) adopted a rhombic unit element to define the structure. If two body-centred orthorhombic unit cells are stacked, one in top of the other, as shown in Figure 2.6 a, then an octahedral unit can be identified, Figure 2.6 b, which corresponds to a 6-ball"hard ball model",as shown in Figure 2.6 c. Although the octahedron, Figure 2.6 b, might appear to be the three-dimensional equivalent of Thornton's (1977) rhombic element, it is not a valid building block.

As shown in Figure 2.7 a set of equal octahedral units cannot completely fill the space available. However, an examination of the voids in an assembly of octahedrons reveals that, as shown in Figure 2.7, the complete space available can be filled by three sets of interlocking octahedral assemblies. For the general orthorhombic arrangement the octahedral dimensions are different for each set.

Consequently it is possible to identify a dodecahedral unit composed of two octahedral units from each of the three sets. An exploded view of the dodecahedron is shown in Figure 2.8 which clearly illustrates the six octahedral components. The complete dodecahedron is shown in Figure

2.9. If an infinite number of such dodecahedra are arranged to form a body-centred orthorhombic array then the space available will be fully occupied and hence the dodecahedron is a valid building block. The corresponding"hard ball model"is illustrated in Figure 2.10 and consists of 15 spheres. This 15-ball dodecahedral unit will be used to define the physical model for the mechanical analysis provided in Chapter 4.

CRYSTAL SYSTEM	LATTICE PARAMETERS	BRAVAIS LATTICE UNIT CELLS
CUBIC	$a=b=c$, $\alpha=\beta=\gamma=90^0$	SIMPLE CUBIC (1) BODY-CENTRED CUBIC FACE-CENTRED CUBIC (2)
TETRAGONAL	$a=b\neq c$, $\alpha=\beta=\gamma=90^0$	SIMPLE TETRAGONAL BODY-CENTRED TETRAGONAL
ORTHORHOMBIC	$a\neq b\neq c$, $\alpha=\beta=\gamma=90^0$	SIMPLE ORTHORHOMBIC BODY-CENTRED ORTHORHOMBIC FACE-CENTRED ORTHORHOMBIC BASE-CENTRED ORTHORHOMBIC
RHOMBOHEDRAL	$a=b=c$, $\alpha=\beta=\gamma\neq90^0$	RHOMBOHEDRAL (3)
HEXAGONAL	$a=b\neq c$, $\alpha=\beta=90^0\ \gamma=120^0$	HEXAGONAL (4)
MONOCLINIC	$a\neq b\neq c$, $\alpha=\gamma=90^0\neq\beta$	SIMPLE MONOCLINIC BASE-CENTRED MONOCLINIC
TRICLINIC	$a\neq b\neq c$, $\alpha\neq\beta\neq\gamma\neq90^0$	TRICLINIC

NOTES: (1) EQUIVALENT OF THE "CUBIC"OF GRATTON & FRASER (1935)

(2) " " "RHOMBOHEDRAL" " " "

(3) " "TETRAGONAL-SPHENOIDAL" " "

(4) " " "ORTHORHOMBIC" " " "

TABLE 2.1 CLASSIFICATION OF UNIT CELLS.

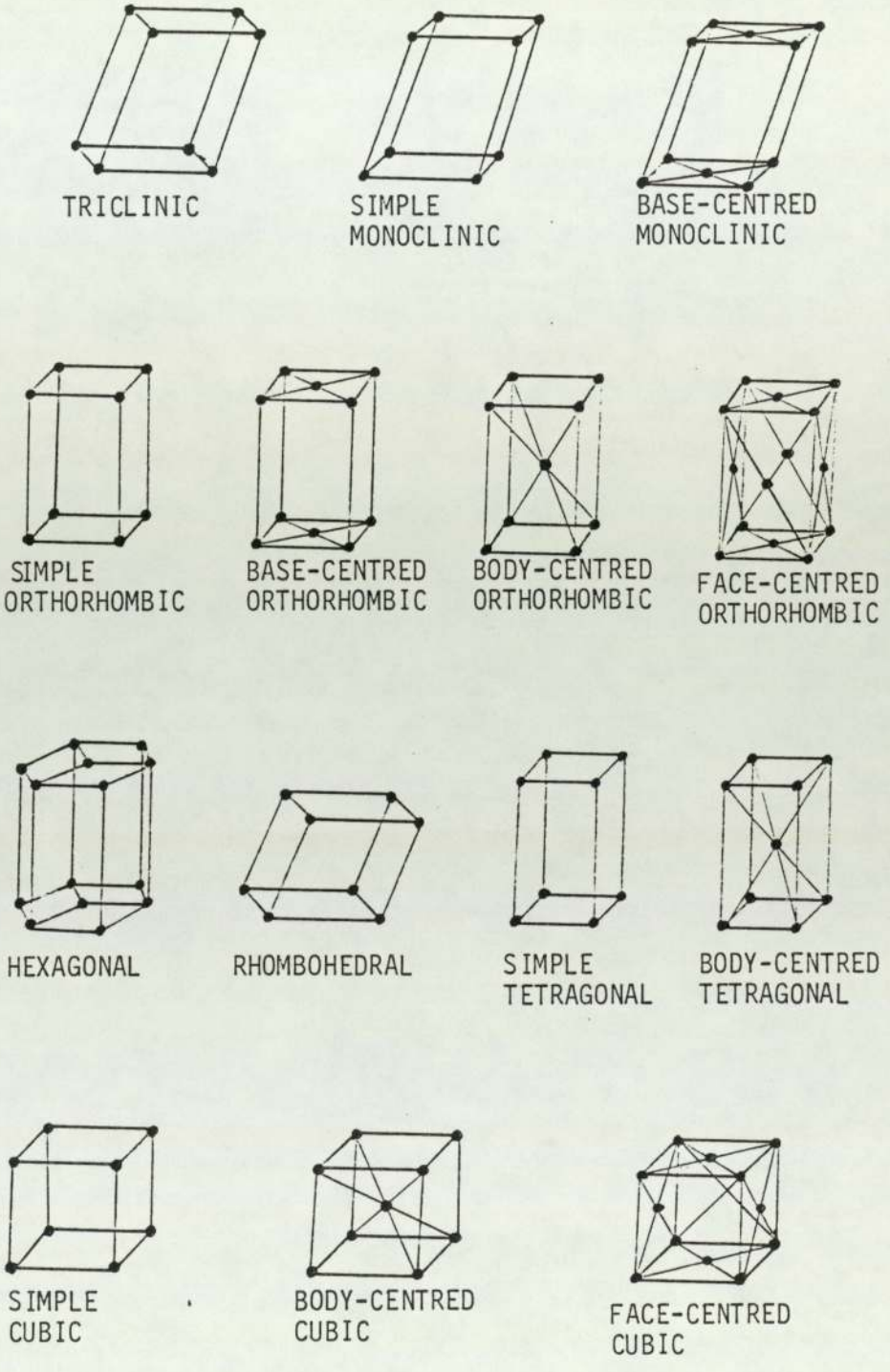

FIGURE 2.1 THE 14 UNIT CELLS ACCORDING TO BRAVAIS

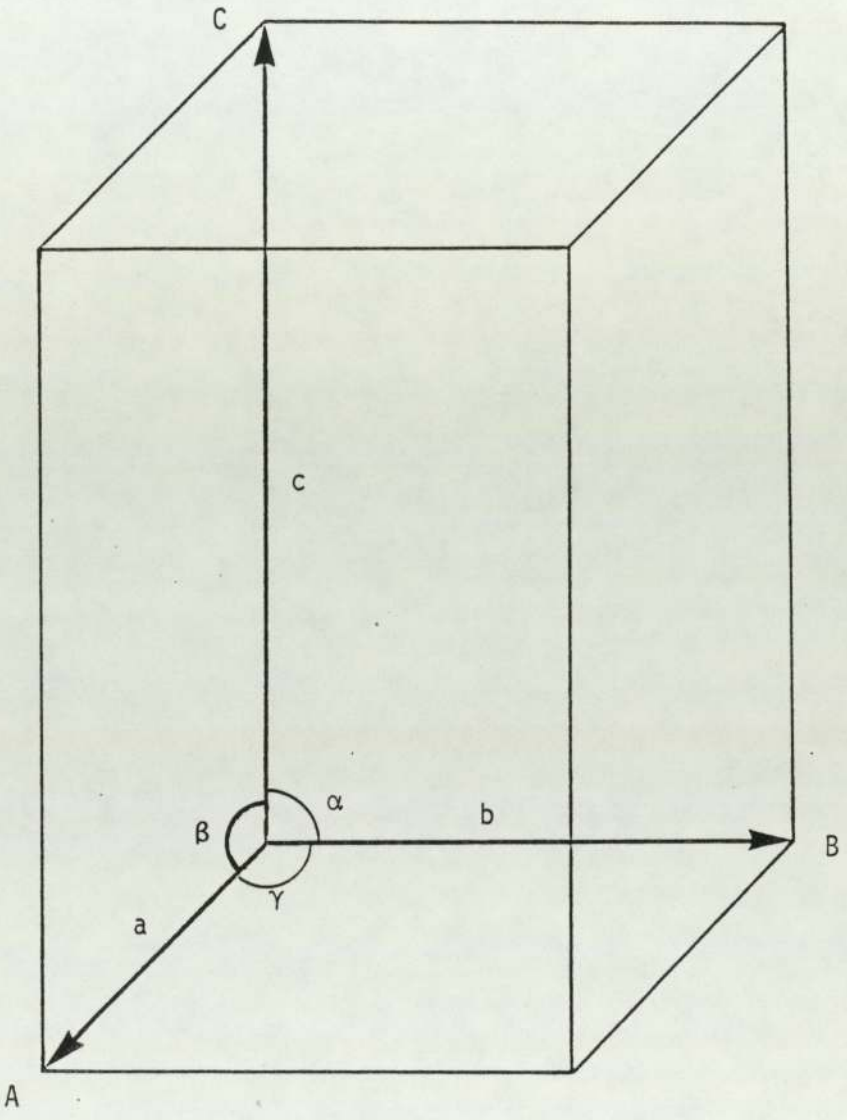

A, B, C - LATTICE VECTORS
a, b, c - LATTICE CONSTANTS
α, β, γ - LATTICE INTER-AXIAL ANGLES

FIGURE 2.2 TYPICAL UNIT CELL SHOWING THE LATTICE PARAMETERS

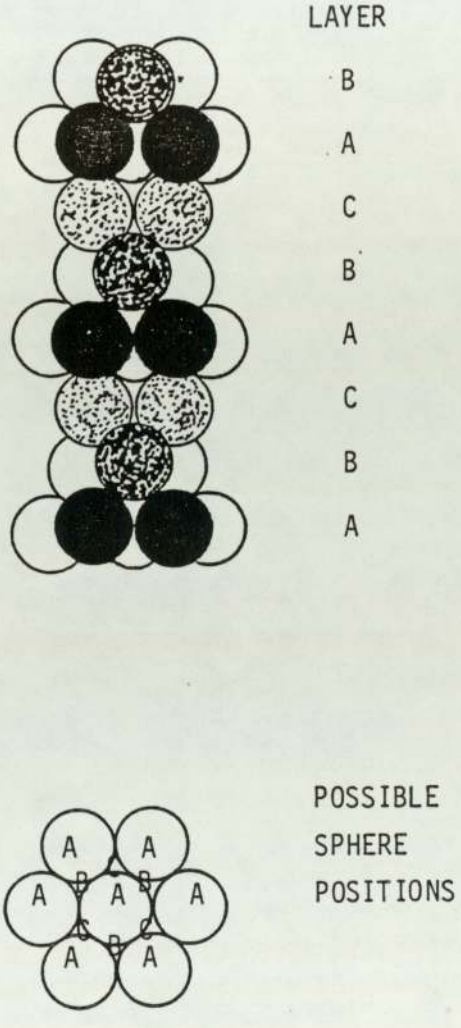

FIGURE 2.3 ARRANGEMENT OF SPHERES
SHOWING ALTERNATING LAYER STRUCTURE

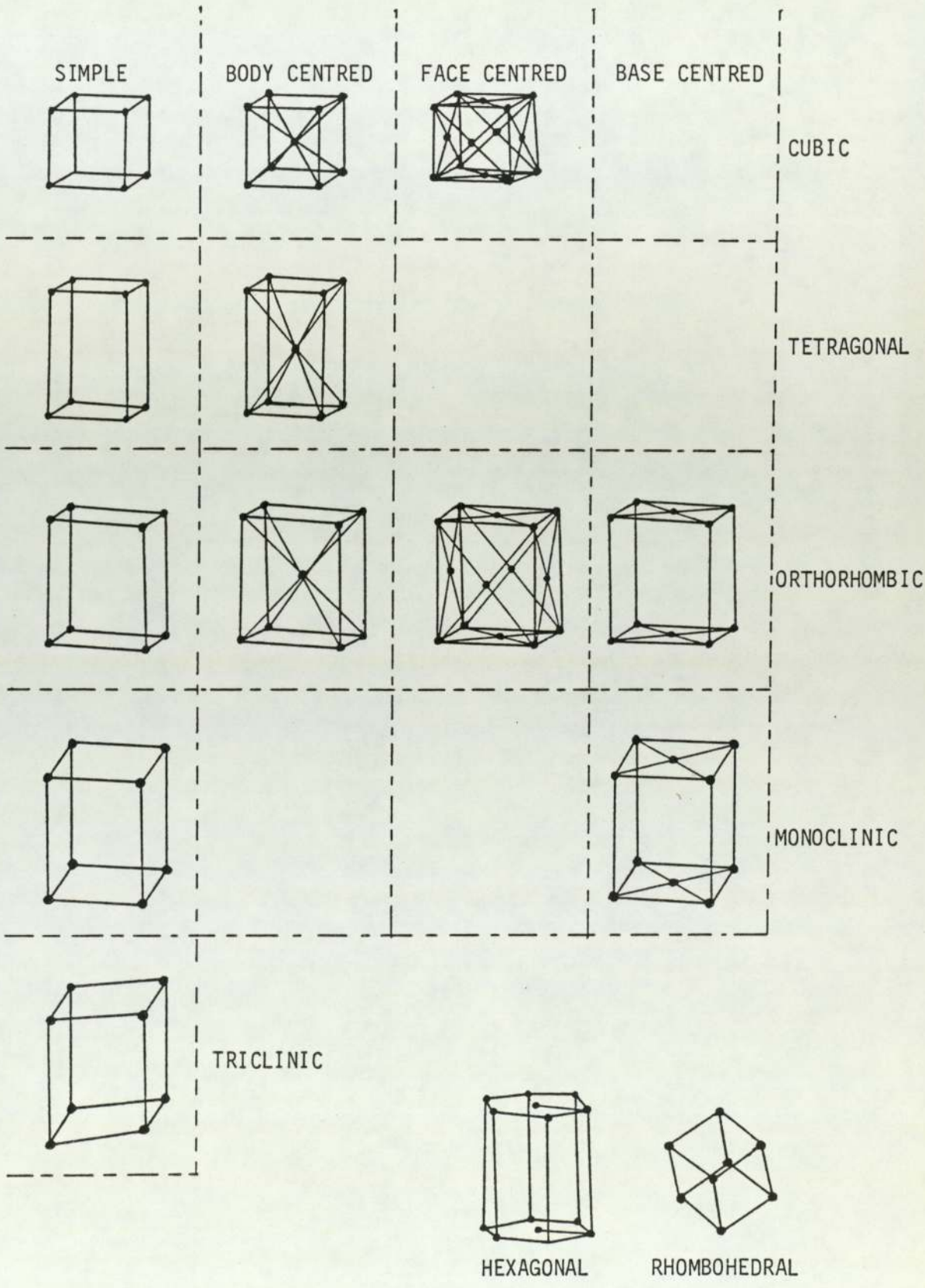

FIGURE 2.4 THE 14 BRAVAIS LATTICES ORDERED ACCORDING TO SPHERE DISTRIBUTION

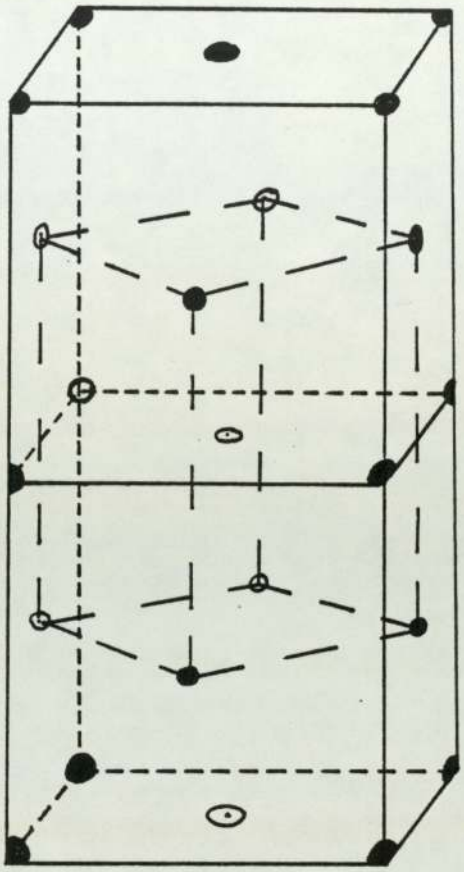

FIGURE 2.5 TWO FACE-CENTRED CUBIC UNIT CELLS STACKED VERTICALLY TO SHOW A BODY-CENTRED ORTHORHOMBIC UNIT CELL CONTAINED WITHIN

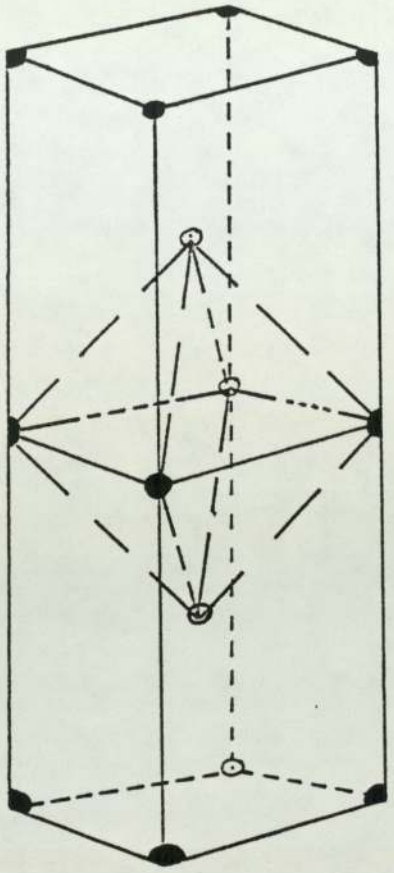

(A) TWO BODY-CENTRED ORTHORHOMBIC UNIT CELLS STACKED VERTICALLY

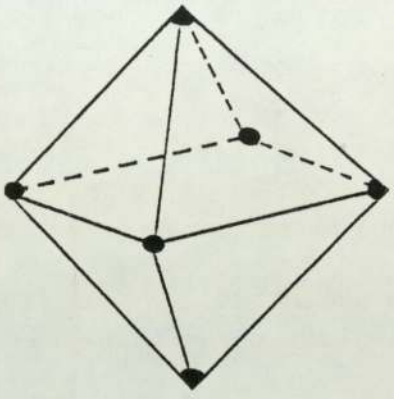

(B) OCTAHEDRAL UNIT

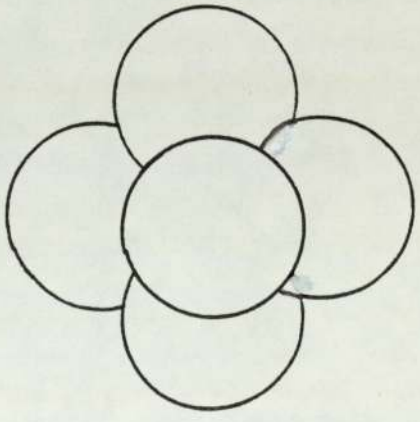

(C) SIX BALL HARD BALL MODEL OF AN OCTAHEDRAL UNIT

FIGURE 2.6 FORMATION OF OCTAHEDRAL UNITS FROM BODY-CENTRED ORTHORHOMBIC UNIT CELLS

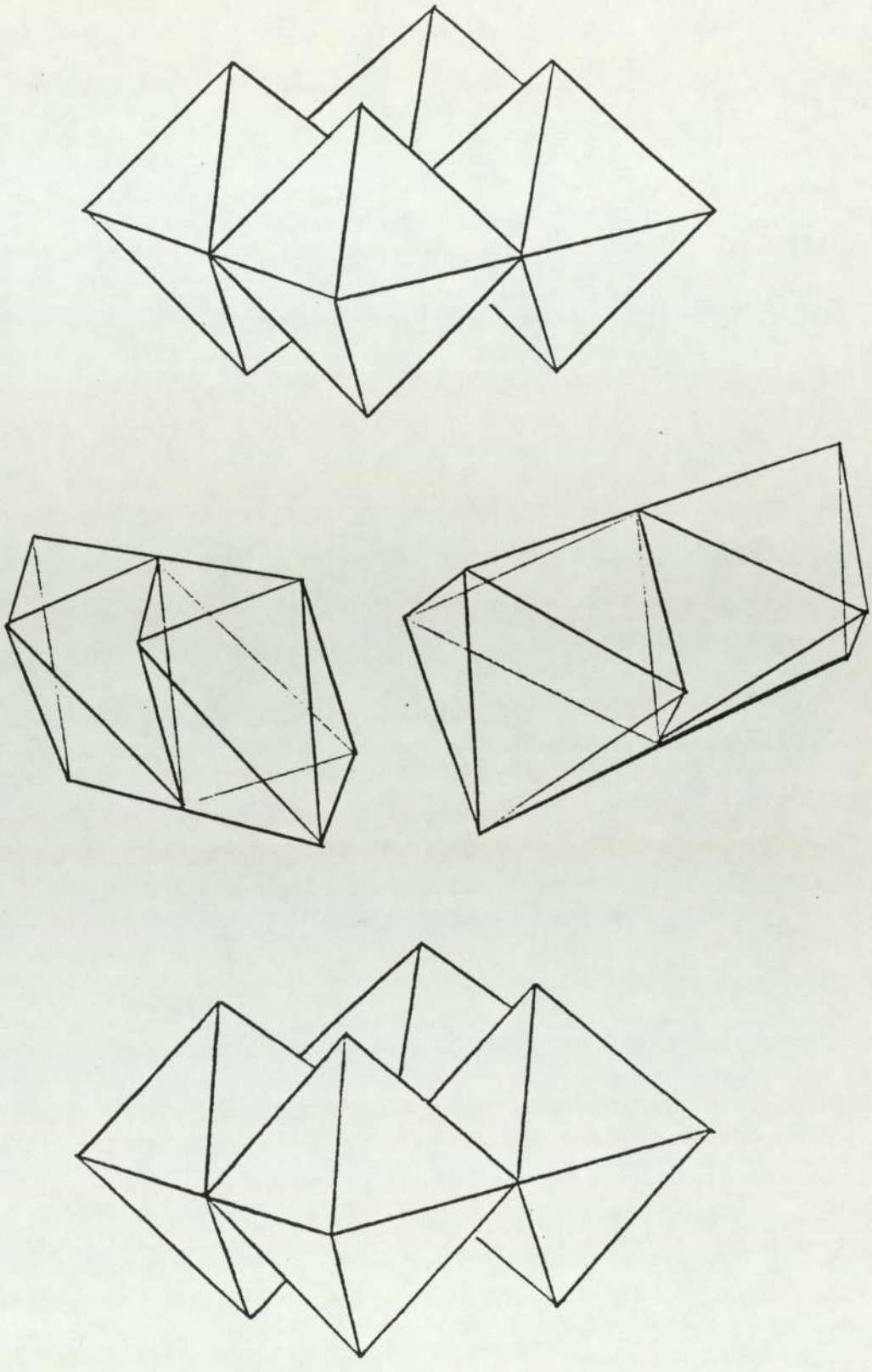

FIGURE 2.7 DIAGRAMMATIC REPRESENTATION OF INTERLOCKING OCTAHEDRAL ASSEMBLIES

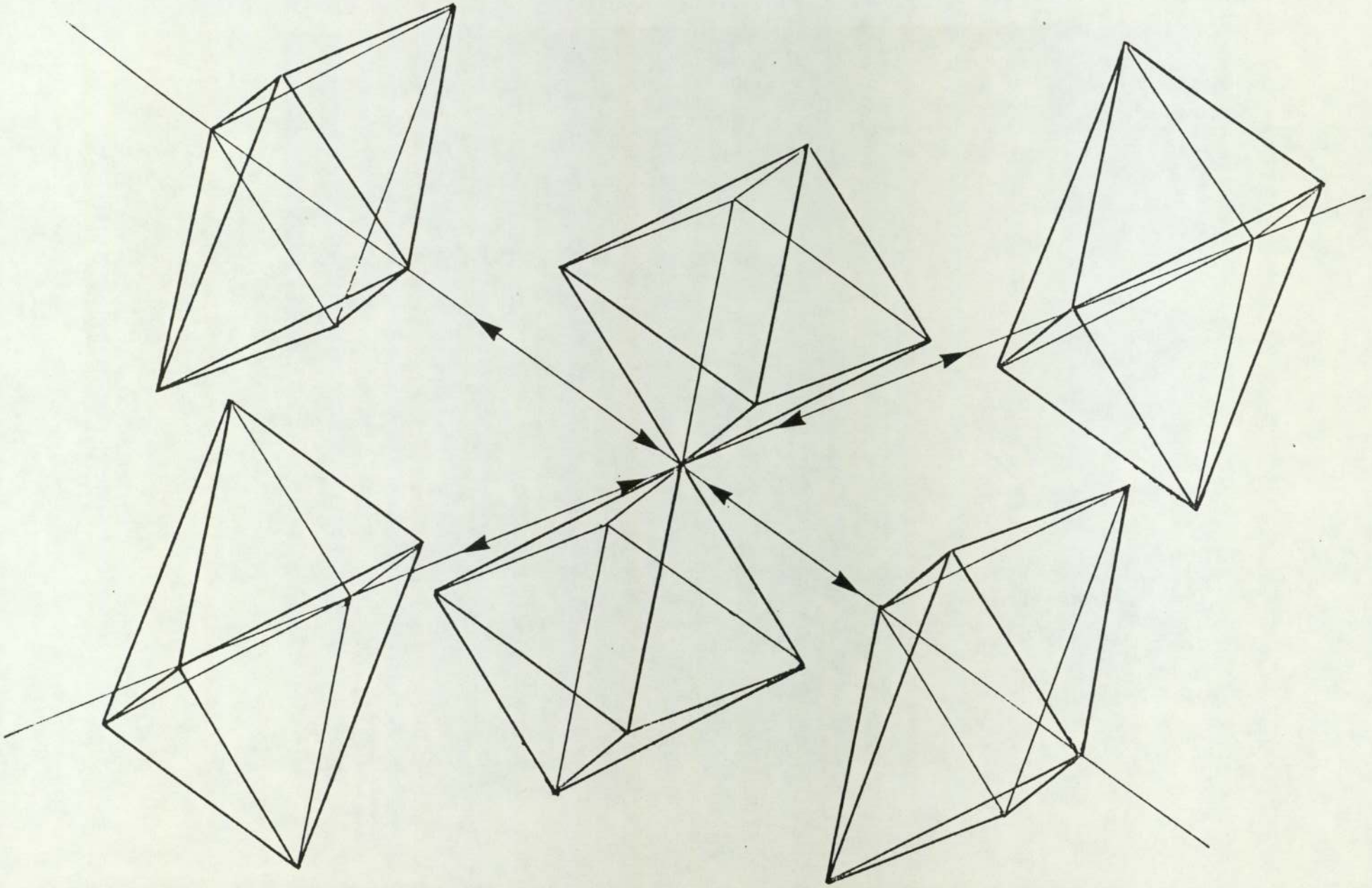

FIGURE 2.8 EXPLODED VIEW OF A DODECAHEDRAL UNIT

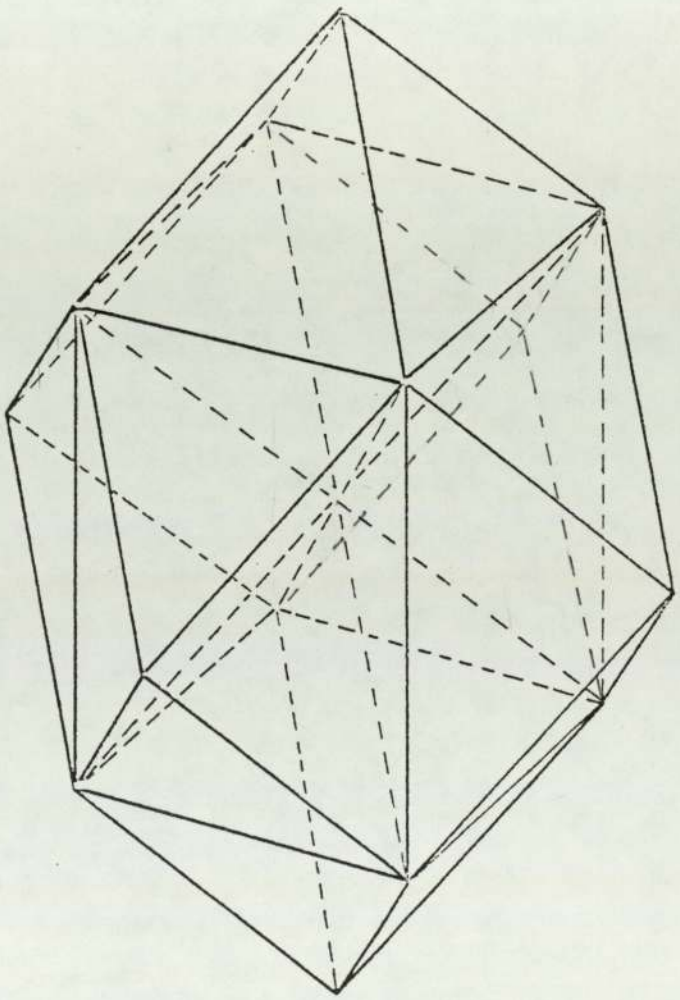

FIGURE 2.9 THE COMPLETE DODECAHEDRON

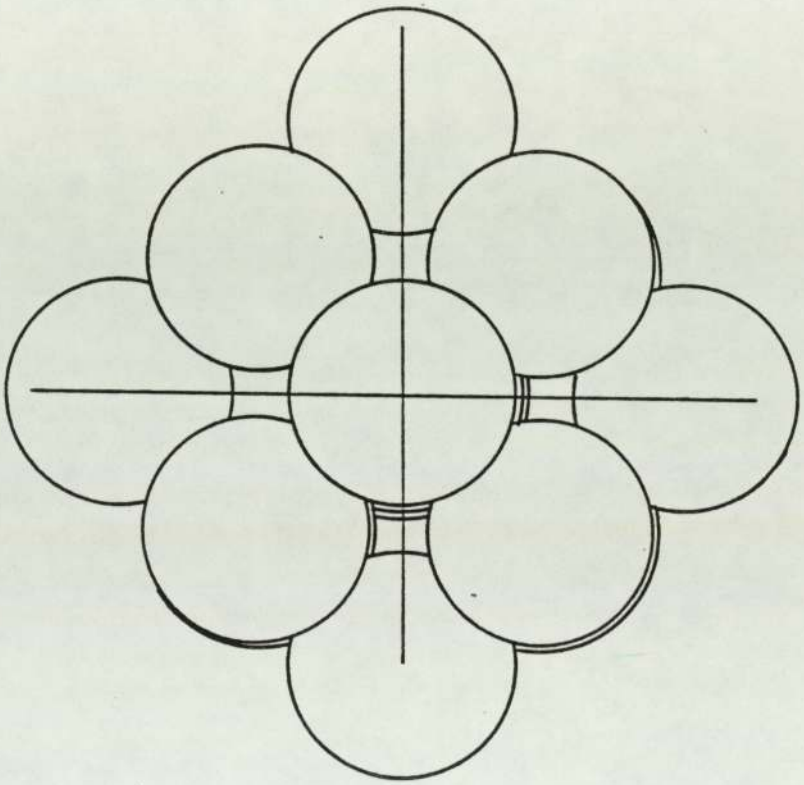

FIGURE 2.10 THE 15 SPHERE HARD BALL MODEL OF A DODECAHEDRAL UNIT

CHAPTER THREE

3. THE MECHANICS OF REGULAR ARRAYS - A REVIEW

3.1 INTRODUCTION

The macroscopic stress-strain behaviour of regular arrays can be related to the force-displacement relationships at the interparticle contacts. The contacts behaviour will be dependent not only on the applied external loadings but also on the geometry of the array and the mechanical properties of the particles. Hence, the overall deformation of the assembly will be due to changes in the geometrical arrangement of the particles and deformation of the particles themselves.

3.2 ELASTIC BEHAVIOUR OF SPHERES

3.2.1 Elastic Compliance due to Normal Contact Forces

If two similar elastic spheres, each of radius R, are in contact under the action of a normal force, N, the theory of Hertz, see Timoshenko and Goodier (1951), states that the radius of the contact area, a, and the normal displacement of the contact, α , are given by

$$a = \{3(1-\nu)NR/8G\}^{1/3} \qquad \ldots(3.1)$$

and

$$\alpha = 2\{3(1-\nu)N/8GR^{\frac{1}{2}}\}^{2/3} \qquad \ldots(3.2)$$

where ν and G are the Poissons ratio and shear modulus for the spheres.

By combining the two equations, Duffy and Mindlin (1957) obtained the following expression for the normal compliance, c

$$c = d\alpha/dN = (1-\nu)/2Ga \qquad \ldots(3.3)$$

Which shows that the load deformation curve is non linear due to the variation of a with N as given by (3.1).

For two spheres in contact having different radii and different elastic properties, similar expressions exist, Timoshenko and Goodier (1951), and take the form

$$a = \{3\pi N R_1 R_2 (K_1+K_2)/4(R_1+R_2)\}^{1/3} \qquad \ldots(3.4)$$

and

$$\alpha = \{3\pi N(K_1+K_2)(R_1+R_2)^{\frac{1}{2}}/4(R_1R_2)^{\frac{1}{2}}\}^{2/3} \qquad \ldots(3.5)$$

where $K_1 = (1-\nu_1^2)/\pi E_1$ and $K_2 = (1-\nu_2^2)/\pi E_2$ define the elastic properties of the two spheres. The normal

compliance can then be determined and is given by

$$c = d\alpha/dN=\{(1-\nu_1)/G_1+(1-\nu_2)/G_2\}/4a \quad ...(3.6)$$

which degenerates to (3.3) if the two spheres possess the same elastic properties.

3.2.2 Elastic Compliance due to Combined Normal and Tangential Contact Forces

Hertzian contact theory was extended by Catteneo (1938) and Mindlin (1949) to account for a tangential force component, T. According to these works, when a uniformly increasing tangential force is added to a contact which is under a constant normal force, then deformation will occur at that contact. As shown in Figure 3.1, the deformation is initiated on the circumference of the contact area and then propagates radially inwards. Thus, the portion on which deformation occurs is an annulus, of outer radius, a, and inner radius, c, where

$$c = a(1-T/\mu N)^{\frac{1}{2}} \quad ...(3.7)$$

and μ is the coefficient of friction between the spheres. The relative tangential movement of the sphere centres was then expressed as

$$\delta = 3\mu N(2-\nu)(1-\{1-T/\mu N\}^{2/3})/8Ga \quad ...(3.8)$$

leading to an expression for the tangential compliance

$$S = d\delta/dT = (2-\nu)/4Ga(1-T/\mu N)^{1/3} \quad ...(3.9)$$

which was confirmed experimentally by Johnson (1955).

The effects produced by reversing the tangential force were studied by Mindlin, Mason, Osmer and Deresiewicz (1951). Their work indicated that, as a result of the distortion at the contact the force-displacement relationship changes upon reversals. Should the tangential force oscillate between $\pm T^*$ (such that $T^* < \mu N$), then it was argued that a stable cycle would occur after the first quarter cycle, see Figure 3.2. The existance of an annulus of deformation, with the subject of equation 3.6 as its inner radius, was experimentally verified in the same work, and was also confirmed by Johnson's (1955) experiments.

A later extension of this theory was provided by Mindlin and Deresiewicz (1953). They considered a varying additional force of constant obliquity applied across a contact under an existing initial normal force. This provided a load-displacement relation for first loading and unloading and then for the subsequent stabilised cycle. In such a stabilised cycle, if the tangential force component oscillated between $\pm T^*$, then tangential compliance during loading would be given by

$$S_R = \frac{2-\nu}{4Ga} \{\theta+(1-\theta)\{1-(1+\theta)(L^*+L)/2(1+\theta L)\}^{-\frac{1}{2}}\} \quad \ldots(3.10)$$

where $L = T/\mu N_o$ $L^* = T^*/\mu N_o$

$\theta = \mu/\beta$ $\beta = dT/dN \geq \mu$

and No is the initial normal force at the contact. For the unloading part of the stabilised cycle, the compliance, Su, is obtained by reversing the signs of θ and L.

A more recent work by Walton (1978), however, considered the case where the contact forces are initially zero and then both tangential and normal forces are increased simultaneously with their ratio constant during the increase. It was found that no slip annulus is formed if $T < \mu N$, and Walton (1978) concluded that if slip occured at all it would take the form of sliding (slip over the whole of the contact area) when $T = \mu N$. Consequently it was suggested that the formation of a slip annulus depends on whether the spheres are first compressed normally and then sheared, or whether the two motions occur simultaneously.

3.2.3 Elastic Behaviour of Regular Packings

The theories pertaining to two similar spheres in contact (Sections 3.1 and 3.2), were used by Duffy and Mindlin (1957) to analyse a Face-Centred Cubic array of elastic spheres. By satisfying both equilibrium and compatability, a relationship was obtained between the relative displacement increments

and the load increments. The resulting non-linear, differential stress-strain relationship, however, requires the integration to be performed over the entire loading history. A similar method of analysis has also been used to analyse other regular arrangements: - Simple Cubic, Deresiewicz (1958); Close-packed Hexagonal, Duffy (1959).

3.3 IRRECOVERABLE DEFORMATION DUE TO INTERPARTICLE SLIP

Both Deresiewicz (1958) and Thurston and Deresiewicz (1959) recognised that if $T = \mu N$ then the tangential compliance $d\delta/dT$ becomes infinity. Hence they deduced that for regular arrays this would constitute failure of the packing since Coulomb type slip would occur between spheres resulting in a change in the configuration of the packing. They noted that the displacements of the spheres due to failure were several orders of magnitude greater than the elastic deformations previously examined and described this arrangement as a "series of shearing displacements of individual layers of spheres".

Since such relative displacements (slips) are irrecoverable on unloading, the corresponding macroscopic strains can be considered as plastic in contrast to the macroscopic elastic strains resulting from the deformation of the spheres themselves. Consequently, investigations of irrecoverable deformation are considerably simplified by assuming the spheres to be

rigid, thereby eliminating the recoverable (elastic) behaviour.

3.3.1 Two Dimensional Rod Models

The closest packing arrangement of discs or rods is shown in Figure (3.3) and was analysed by Rowe (1962), who defined the structure by two angles α and β as shown. As can be seen, β defines the inclination of the contact planes and α defines the orientation of the inclined rows of contiguous rods. The failure mechanism was considered to result in the rods splaying apart in the horizontal directions and moving vertically together into the spaces created by the horizontal movement. The possibility of body rotation of the packing occuring during post-failure deformation was not considered.

By considering separately the statics and kinematics of the system, Rowe (1962) derived the following expressions to define the principal stress ratio and the ratio of principal strain-increments,

$$\sigma_1/\sigma_2 = \tan\alpha.\tan(\phi_\mu+\beta) \qquad \ldots(3.11)$$

$$-\dot{\varepsilon}_2/\dot{\varepsilon}_1 = \tan\alpha.\tan\beta \qquad \ldots(3.12)$$

which were then combined to eliminate α and give

$$-\frac{\sigma_1 \dot{\varepsilon}_1}{\sigma_2 \dot{\varepsilon}_2} = \frac{\tan(\phi_\mu + \beta)}{\tan\beta} \qquad \ldots(3.13)$$

in which ϕ_μ is the angle of interparticle friction and the left side of the equation was taken to be the ratio of work-in to work-out. Rowe (1962) observed that this ratio is unity for frictionless rods; and concluded that, for rods with friction, the 'work ratio' was greater than unity as a result of the convertion of internal work into frictional heat.

Experimental results reported by Rowe (1962) showed good agreement with the predicted relative movements of the rods. The maximum principal stress ratio, however, was significantly less than predicted and was obtained only after a small axial strain. This was attributed to slight imperfections in the rods which resulted in small irregularities in the packing arrangement. Ultimate collapse of the packing was described as a 'catastrophic movement' which occured as the principal stress ratio approached unity. The collapse mechanism consisted of the rods on one plane moving right past the supporting rods to form new contacts on the next row. The rods in the areas to either side of this plane then returned to their original configuration.

Inspection of Figure 3.3 clearly indicates that the structure of the array is not isotropic and hence the strength of the array would be expected to vary with the

direction of the applied stresses. The dependence on the relative orientation of the packing geometry was recognised by Parkin (1964) who considered the orientation of the applied stress system as a variable.

Parkin (1964) identified that failure occured when interparticle friction is overcome on one or more sets of diametrically opposed contact planes and that this leads to the formation of gaps along one of the three sets of contiguous rows of rods. By defining Θ as the angle between the major principal stress plane and the direction of one of the contiguous rows of rods (the potential failure plane), see Figure 3.4, Parkin (1964) obtained the following solution for the strength of the packing

$$\frac{\sigma_1}{\sigma_2} = \frac{\cos(60+2\theta-\phi_\mu)-\cos(60-\phi_\mu)}{\cos(60+2\theta-\phi_\mu)+\cos(60-\phi_\mu)} \qquad \ldots(3.14)$$

which provided the family of solutions shown in Figure 3.5, which have minimum values of

$$\frac{\sigma_1}{\sigma_2} = \tan^2(60+\phi_\mu/2) \qquad \ldots(3.15)$$

when $\theta = 60+\phi_\mu/2$.

Thornton (1977) extended Parkins (1964) analysis to initially less dense arrangements by considering the characteristic packing angle λ (defined in Figure 3.6)

as a variable. The horizontal rows of contiguous rods were considered to be 'the incipient failure planes' and the ratio of the stresses on these planes were determined as

$$\frac{T}{\sigma_n} = \cot(\lambda-\phi_\mu) \qquad \ldots(3.16)$$

which leads to

$$\frac{\sigma_1}{\sigma_2} = \frac{\cos(\lambda+2\theta-\phi_\mu)-\cos(\lambda-\phi_\mu)}{\cos(\lambda+2\theta-\phi_\mu)+\cos(\lambda-\phi_\mu)} \qquad \ldots(3.17)$$

or

$$\frac{\sigma_1}{\sigma_2} = \tan\theta\tan\{(180-\theta)-(\lambda-\phi_\mu)\} \qquad \ldots(3.18)$$

The family of solutions given by (3.18) are shown in Figure 3.7 and have minimum values of

$$\frac{\sigma_1}{\sigma_2} = \cot^2\frac{(\lambda-\phi_\mu)}{2} \qquad \ldots(3.19)$$

when $\theta = 90^\circ - \frac{1}{2}(\lambda-\phi_\mu)$ and exhibit infinite discontinuities at $\theta = 90^\circ - (\lambda-\phi_\mu)$ and 90°.

It was also identified that, for $\theta = 90^\circ - \lambda/2$, the directions of principal stress and strain-increment coincided and that the corresponding solution is

$$\frac{\sigma_1}{\sigma_2} = \cot(\lambda/2)\cot(\lambda/2-\phi_\mu) \qquad \ldots(3.20)$$

and that this corresponds to Rowe's (1962) solution for $\lambda = 60^{\circ}$.

Since λ was considered to be the instantaneous packing angle, the solution given by (3.18) was considered to be also valid during post-failure deformation. This lead Thornton (1977) to consider the solutions in terms of plasticity theory and a flow rule was identified, which was equivalent to (3.18) and expressed in conventional soil mechanics terminology as

$$\sin \phi = \frac{\sin (\phi_{\mu}+\nu)}{\cos (\phi_{\mu}-2\psi)} \qquad \ldots(3.21)$$

where

$$\sin \phi = \frac{\sigma_1-\sigma_3}{\sigma_1+\sigma_3} \qquad \ldots(3.22)$$

and ϕ is the angle if internal shearing resistance. Also

$$\sin \nu = \frac{-(\dot{\varepsilon}_1-\dot{\varepsilon}_3)}{(\dot{\varepsilon}_1+\dot{\varepsilon}_3)} \qquad \ldots(3.23)$$

where ν is the angle of dilatation.

The angle ψ is the deviation angle between the directions of principal stress and strain-increment, and hence when $\psi = 0$ the coaxial flow rule is obtained.

$$\sin \phi = \sin (\phi_{\mu}+\nu) \; / \; \cos \phi_{\mu} \qquad \ldots(3.24)$$

The flow rule corresponding to the minimum strength solutions given by (3.19) was shown to be

$$\sin \phi = \sin (\phi_\mu + \nu) \qquad \ldots(3.25)$$

since this case is obtained when $\psi = \phi_\mu / 2$.

Although both Parkin (1964) and Thornton (1977) considered the relative orientation of the packing to the applied stress system, the amount of rotation of the principal stresses considered was limited to compressive stress states. Complete rotation of the principal stresses so as to include extension conditions was examined by Molenkamp (1980), who showed that the strength in extension was less than the strength in compression.

3.3.2 Regular arrays of spheres - axisymmetric compression

In their analysis of the elastic behaviour of face-centred cubic arrays of equal spheres, Thurston and Deresiewicz (1959) identified limiting conditions which would result in an alteration to the geometric arrangement of the spheres. They considered axisymmetric compression states of stress and obtained an expression for the strength of the array which was given as

$$\frac{\sigma_1 - \sigma_3}{\sigma_3} = \frac{\sqrt{6}+8\mu}{\sqrt{6}-4\mu} \qquad \ldots(3.26)$$

where μ is the coefficient of interparticle friction. This expression can be transformed and expanded to give

$$\frac{\sigma_1}{\sigma_3} = 2 + 2\sqrt{6}\mu + 8\mu^2 + \text{(higher terms in } \mu) \quad \ldots(3.27)$$

However, although they considered axisymmetric stress conditions, the assumed deformation mechanism was described as a series of shearing displacements of adjacent layers which occured in one direction only. It was pointed out by Thornton (1974) that this was a plane strain mechanism and that equation 3.27 agrees with plane stress solutions obtained by Leussink and Wittke (1963) and Rennie (1959), see section 3.3.3.

Both face-centred cubic and close-packed hexagonal arrays were analysed by Dantu (1961) who determined the strength of each array under axisymmetric compression conditions. The stress-ratio to cause failure for the face-centred cubic array was given as

$$\frac{\sigma_1}{\sigma_3} = \frac{2(1 + \mu)}{1 - \mu} \quad \ldots(3.28)$$

which expands to give

$$\frac{\sigma_1}{\sigma_3} = 2 + 4\mu + 4\mu^2 + \text{(higher terms in } \mu) \quad \ldots(3.29)$$

For the close-packed hexagonal packing, failure was defined by

$$\frac{\sigma_1}{\sigma_3} = \frac{4(\sqrt{2} + \mu)}{\sqrt{2} - 2\mu} \quad \ldots(3.30)$$

or, in expanded form

$$\frac{\sigma_1}{\sigma_3} = 4 + 6\sqrt{2}\mu + 12\mu^2 + \text{(higher terms in } \mu) \quad \ldots(3.31)$$

Rowe (1962) also analysed both face-centred cubic and close-packed hexagonal arrangements under axisymmetric compression conditions. Following a similar argument to that which he presented for regular arrays of rods, see section 3.3.1, Rowe (1962) was able to derive general expressions which were valid for both types of array and remained valid during post-failure deformation. The principal stress-ratio was defined by

$$\frac{\sigma_1}{\sigma_3} = \tan\alpha \tan(\phi_\mu + \beta) \quad \ldots(3.32)$$

and the corresponding strain-increment by

$$\frac{-\dot{\varepsilon}_3}{\dot{\varepsilon}_1} = \tfrac{1}{2} \tan\alpha \tan\beta \quad \ldots(3.33)$$

Where α represents the current packing angle and β the angle between the contact plane and the major principal stress direction. Thornton (1974) showed that equation (3.32) was in agreement with Dantu's (1961) strength solutions when the appropriate values of α and β were substituted.

Leussink and Wittke (1963) analysed the strength and deformation of both face-centred cubic and close-packed

hexagonal arrays of rigid spheres. For axisymmetric compression states of stress, they considered that the packing type remained constant during deformation which merely produced a change in the angle of contact between spheres. Consequently, they were able to obtain a general solution for the principal stress ratio which was given as

$$\frac{\sigma_1}{\sigma_3} = 2 \tan j_0 \tan (j_0+\rho) \qquad \ldots(3.34)$$

where ρ is the angle of interparticle friction and j_0 is the angle between the contact normals and the minor principal plane. Equation (3.34) corresponds to Rowe's (1962) solution, equation (3.32), and is therefore also in agreement with equations (3.28) and (3.30) obtained by Dantu (1961) at failure.

3.3.3 Regular arrays of spheres - plane strain

In addition to axisymmetric compression, Leussink and Wittke (1963) also analysed plane strain deformation of both face-centred cubic and close-packed hexagonal arrays. Under plane strain conditions the "type of packing" was considered to alter during deformation and, hence, they were unable to obtain a general solution. The principal stress ratio in plane strain, for the face-centred cubic array, was given as

$$\frac{\sigma_1}{\sigma_3} = 2\tan j_0 \frac{(\tan j_0+\tan\rho/(1+\sin^2 j_0)^{\frac{1}{2}})}{(1-2\tan\rho\tan j_0/(1+\sin^2 j_0)^{\frac{1}{2}})} \qquad \ldots(3.35)$$

and for the close-packed hexagonal case

$$\frac{\sigma_1}{\sigma_3} = \frac{2}{3}\tan j_0(\tan j_0+\tan\rho)/(1-\tan\rho\tan j_0) + \frac{4}{3}\tan j_0\frac{(\tan j_0+\tan\rho/(1+3\sin^2 j_0)^{\frac{1}{2}})}{(1-4\tan\rho\tan j_0/(1+3\sin^2 j_0)^{\frac{1}{2}})} \quad \ldots(3.36)$$

It was shown by Thornton (1974) that the expanded forms of equations (3.35) and (3.36) are

$$\frac{\sigma_1}{\sigma_3} = 2 + 2\sqrt{6}\mu + 8\mu^2 + (\text{higher terms in } \mu) \quad \ldots(3.37)$$

and

$$\frac{\sigma_1}{\sigma_3} = 4+2\sqrt{2}(1+2\sqrt{3})\mu+36\mu^2+(\text{higher terms in } \mu) \quad \ldots(3.38)$$

respectively.

The strength of a face-centred cubic packing of rigid spheres was analysed by Rennie (1959) who recognised that the separation distance between the centre of a typical sphere and the centres of each of the twelve spheres in contact with it cannot decrease during shear. From this observation he was able to demonstrate that for a small strain S to be possible there must be six independent expressions of the form

$$2x'Sx \geq 0 \quad \ldots(3.39)$$

where x defines the co-ordinates of the centre of a

sphere in contact with the reference sphere. The six expressions were given as

$$
\begin{aligned}
&S_{11} \geq 0 \\
&S_{11}+2\sqrt{2}S_{12}-2S_{13}+2S_{22}-2\sqrt{2}S_{23}+S_{33} \geq 0 \\
&S_{11}+2\sqrt{2}S_{12}+2S_{13}+2S_{22}+2\sqrt{2}S_{23}+S_{33} \geq 0 \\
&S_{33} \geq 0 \\
&S_{11}-2\sqrt{2}S_{12}-2S_{13}+2S_{22}+2\sqrt{2}S_{23}+S_{33} \geq 0 \\
&S_{11}-2\sqrt{2}S_{12}+2S_{13}+2S_{22}-2\sqrt{2}S_{23}+S_{33} \geq 0
\end{aligned}
\qquad \ldots(3.40)
$$

It was shown that failure would occur if $S_{11}>0$ with all other expressions equal to zero and the corresponding strain tensor was given as

$$
S = \begin{bmatrix} 2 & 0 & 0 \\ 0 & -1 & 0 \\ 0 & 0 & 0 \end{bmatrix} \qquad \ldots(3.41)
$$

which defines a plane strain condition.

To obtain the stress tensor Rennie (1959) related the discrete forces acting on a typical sphere to the average stress tensor for the assembly as a whole by considering the average stress tensor inside one sphere within the array. The average stress tensor for a typical sphere was taken as the volume integral of the stress tensor through-out a sphere, which was expressed as the summation of the products of the discrete contact forces and the co-ordinates of their points of action on the boundary of the sphere.

Hence the stress tensor was shown to be a multiple of

$$\begin{bmatrix} \frac{\sqrt{3}-2\mu\sqrt{2}+2\mu\phi}{\sqrt{3}} & \phi & 0 \\ \phi & \frac{2\sqrt{3}+2\mu\sqrt{2}-2\mu\phi}{\sqrt{3}} & 0 \\ 0 & 0 & 1+t \end{bmatrix} \qquad \ldots(3.42)$$

where ϕ was taken as the angle between the principal axes of stress and strain. From (3.42) the following equation was obtained

$$\frac{\sigma_1+\sigma_3}{\sigma_1-\sigma_3} = 3\{(1+4\mu\sqrt{2/3}-4\mu\phi/\sqrt{3})^2+4\phi^2\}^{-\frac{1}{2}} \qquad \ldots(3.43)$$

which has a maximum of

$$\frac{\sigma_1+\sigma_3}{\sigma_1-\sigma_3} = \frac{3\sqrt{1+4\mu^2/3}}{1+4\mu\sqrt{2/3}} \qquad \ldots(3.44)$$

when

$$\phi = \frac{\sqrt{3}\mu+4\sqrt{2}\mu^2}{3+4\mu^2} \qquad \ldots(3.45)$$

Hence it was shown that the minimum (and therefore most critical) principal stress ratio was

$$\frac{\sigma_1}{\sigma_3} = \frac{3\sqrt{1+4\mu^2/3}+1+4\mu\sqrt{2/3}}{3\sqrt{1+4\mu^2/3}-1-4\mu\sqrt{2/3}} \qquad \ldots(3.46)$$

Rennie (1959) gave the expanded form of (3.46) as

$$\frac{\sigma_1}{\sigma_3} = 2+2\mu\sqrt{6}+7\mu^2-8\sqrt{6}\mu^3/9+(\text{higher terms in } \mu) \qquad \ldots(3.47)$$

which is incorrect, Thornton (1974), and should be

$$\frac{\sigma_1}{\sigma_3} = 2+2\mu\sqrt{6}+7\mu^2+8\sqrt{6}\mu^3/3+(\text{higher terms in } \mu) \quad ...(3.48)$$

Therefore, by permitting the stresses freedom to rotate about the intermediate principal stress direction, Rennie (1959) demonstrated that the co-axial situation (principal stress directions coinciding with principal strain directions) was not the most favourable orientation for collapse to occur. He concluded that the failure criterion was given by (3.48), which corresponds to a non-coaxial case with ϕ defined by (3.45), but he considered it possible that a rotation of the stresses about some other axis might give an even more favourable orientation.

3.3.4 Regular Arrays of Spheres - General Case

Rennie's (1959) analysis of a face-centred cubic array of spheres was restricted to plane strain conditions. Parkin (1965) extended this work to cover the range between plane strain and axisymmetric compression by considering two inequalities in (3.40). Parkin (1965) considered the possibility of both $S_{11}>0$ and $S_{33}>0$, which corresponds to the case of broken contacts on perpendicular diagonals. The corresponding strain-increment tensor was given as

$$S = a\begin{bmatrix} 2 & 0 & 0 \\ 0 & -1 & 0 \\ 0 & 0 & 0 \end{bmatrix} + b\begin{bmatrix} 0 & 0 & 0 \\ 0 & -1 & 0 \\ 0 & 0 & 2 \end{bmatrix} \quad ...(3.49)$$

where $a + b = 1$.

It was assumed that the intermediate principal axes of stress and strain-increment coincided and a solution was sought for the range $1 \geq a \geq 1/2$. The contribution to the stress tensor of the normal contact forces was the same as that obtained by Rennie (1959), but the tangential force contribution was found to be

$$\frac{2\mu qd}{\sqrt{3/2a^2+ab+3/2b^2}} \begin{bmatrix} 0 & 0 & 0 \\ 0 & -(a+b) & 0 \\ 0 & 0 & b \end{bmatrix} \qquad \ldots(3.50)$$

Taking $\beta = 1-q$ and $F = \sqrt{3/2a^2+ab+3/2b^2}$

Parkin (1965) obtained the following expression

$$\frac{(\sigma_1+\sigma_3)^2}{(\sigma_1-\sigma_3)^2} = \frac{9F^2+12\mu bF(1-\beta)+4\mu^2b^2(1-\beta)^2}{F^2+4\mu F(2a+b)(1-\beta)+4\mu^2(2a+b)^2(1-\beta)^2+8F^2\beta^2} \qquad \ldots(3.51)$$

and by differentiating the right hand side with respect to β , the "critical" value of β was obtained as

$$\beta = \frac{\mu(3a+b)(F+2\mu(2a+b))}{6F^2+4\mu bF+2\mu^2(3a+b)(2a+b)} \qquad \ldots(3.52)$$

For specific values of σ_2/σ_3 the "critical" strength, σ_1/σ_3 was obtained by numerical solutions of (3.51), (3.52) and the relationship

$$\frac{\sigma_2}{\sigma_3} = \frac{F-2b\mu(1-\beta)}{3F+2b\mu(1-\beta)} \cdot (\sigma_1/\sigma_3 + 1) \qquad \ldots(3.53)$$

Thornton (1979) attempted to extend Parkin's (1965) analysis by permitting three degress of rotational freedom to the applied stress system. Changing to the usual soil mechanics sign convention for stresses and strains (compressive positive), and re-labelling the reference axes, Thornton (1979) re-wrote (3.49) to define the strain increment tensor as

$$S = \begin{bmatrix} (a+b) & 0 & 0 \\ 0 & -2b & 0 \\ 0 & 0 & -2a \end{bmatrix} \qquad \ldots(3.54)$$

The normal contact force contribution to the stress tensor was expressed as

$$\frac{d}{V} \begin{bmatrix} \frac{p+q+r+s}{2} & \frac{-p+q-r+s}{2\sqrt{2}} & \frac{p-q-r+s}{2\sqrt{2}} \\ \frac{-p+q-r+s}{2\sqrt{2}} & \frac{p+q+r+s}{4} & \frac{-p-q+r+s}{4} \\ \frac{p-q-r+s}{2\sqrt{2}} & \frac{-p-q+r+s}{4} & \frac{p+q+r+s}{4} \end{bmatrix} \qquad \ldots(3.55)$$

where p, q, r, and s are the normal forces at the four pairs of inclined contact planes, and V was, incorrectly (see Chapter 4) taken as the volume of a typical sphere. The contribution of the tangential forces was derived as

$$\frac{2fd}{VF} \begin{bmatrix} (a+b) & 0 & 0 \\ 0 & -b & 0 \\ 0 & 0 & -a \end{bmatrix} \qquad \ldots(3.56)$$

where $f = \mu n$ and n is the smallest of the normal forces p, q, r and s.

Since the analysis was concerned with stress ratios, Thornton (1979) neglected the component d/V, and using (3.55) obtained the following expressions for the normal contact forces

$$\begin{aligned} s &= 1 + \tau_{yx} + \tau_{zx}/\sqrt{2} + \tau_{zy}/\sqrt{2} \\ r &= 1 + \tau_{yx} - \tau_{zx}/\sqrt{2} - \tau_{zy}/\sqrt{2} \\ q &= 1 - \tau_{yx} - \tau_{zx}/\sqrt{2} + \tau_{zy}/\sqrt{2} \\ p &= 1 - \tau_{yx} + \tau_{zx}/\sqrt{2} - \tau_{zy}/\sqrt{2} \end{aligned} \qquad \ldots(3.57)$$

The stress tensor was then defined as a multiple of

$$\begin{bmatrix} 2+2(a+b)f/F & \tau_{zy} & \tau_{zx} \\ \tau_{yz} & 1-2bf/F & \tau_{yx} \\ \tau_{xz} & \tau_{xy} & 1-2af/F \end{bmatrix} \qquad \ldots(3.58)$$

and the three degrees of rotational freedom were supplied to the applied stress system by arbitrarily varying the shear stress components in (3.58).

However, it was pointed out by Parkin (1981) that this procedure was not admissible since the strain-increment tensor imposes restrictions on the interparticle forces which, therefore, invalidate solutions obtained for rotations about any but the intermediate principal strain-

increment direction. This criticism by Parkin (1981) resulted in a re-examination of the problem by Thornton (1981) who demonstrated that gap formation along perpendicular diagonals was only possible if slip occured at all contacts, with the consequence that the stress and strain increment tensors must be coaxial. This lead to the conclusion by Thornton (1981) that Parkin's (1965) solutions were inadmissible and that the only valid solutions were the original plane strain solution of Rennie (1959) and the general co-axial solution obtained by Thornton (1981).

If slip occurs at all contacts then the normal forces are all equal to n (say) and Thornton's (1979) co-axial solution may be written as

$$\sigma_{ij} = \frac{nd}{V} \begin{bmatrix} 2+2(a+b)\mu/F & 0 & 0 \\ 0 & 1-2b\mu/F & 0 \\ 0 & 0 & 1-2a\mu/F \end{bmatrix} \qquad \ldots(3.59)$$

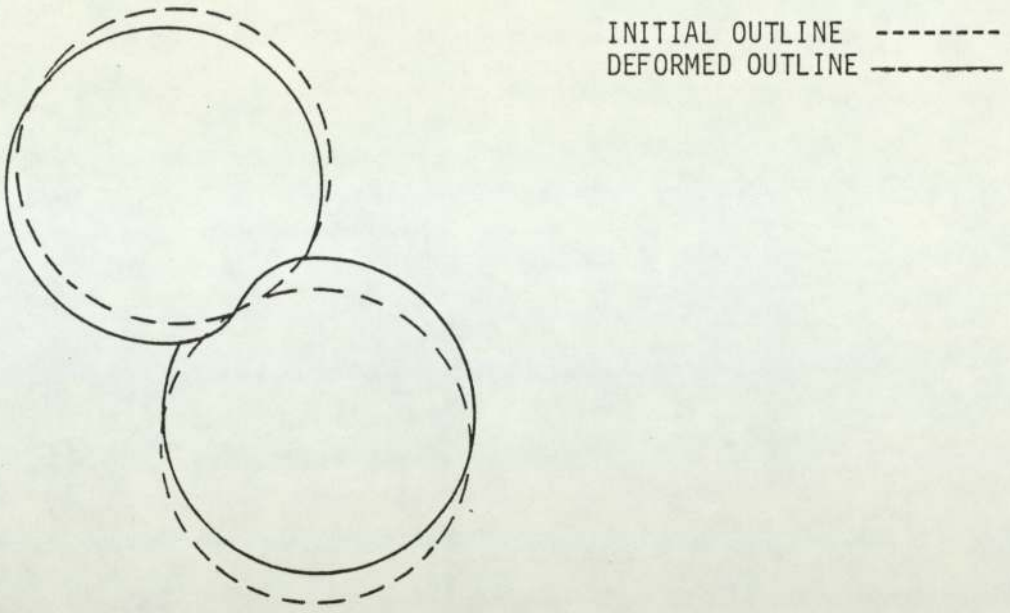

FIGURE 3.1 DEFORMATION OF TWO IDENTICAL, HOMOGENEOUS ELASTIC SPHERES IN OBLIQUE CONTACT

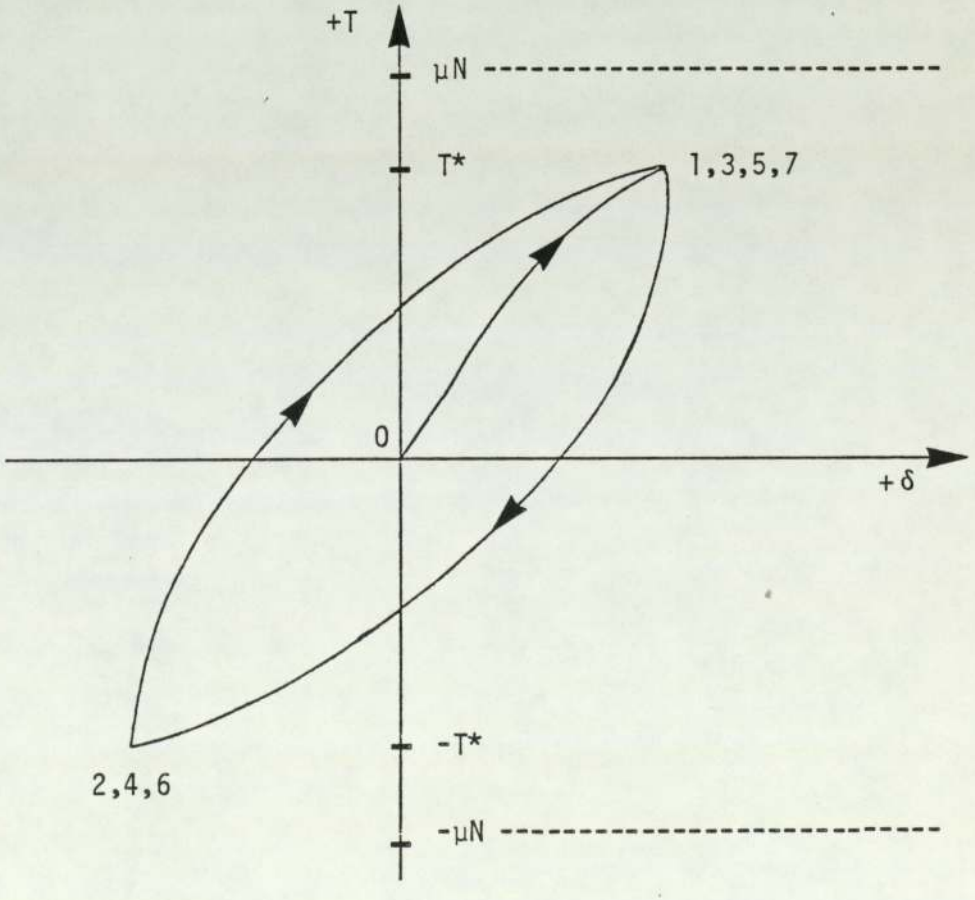

FIGURE 3.2 TYPICAL PLOT ILLUSTRATING THE VARIATION OF INTER-PARTICLE DEFORMATION WITH APPLIED TANGENTIAL FORCE

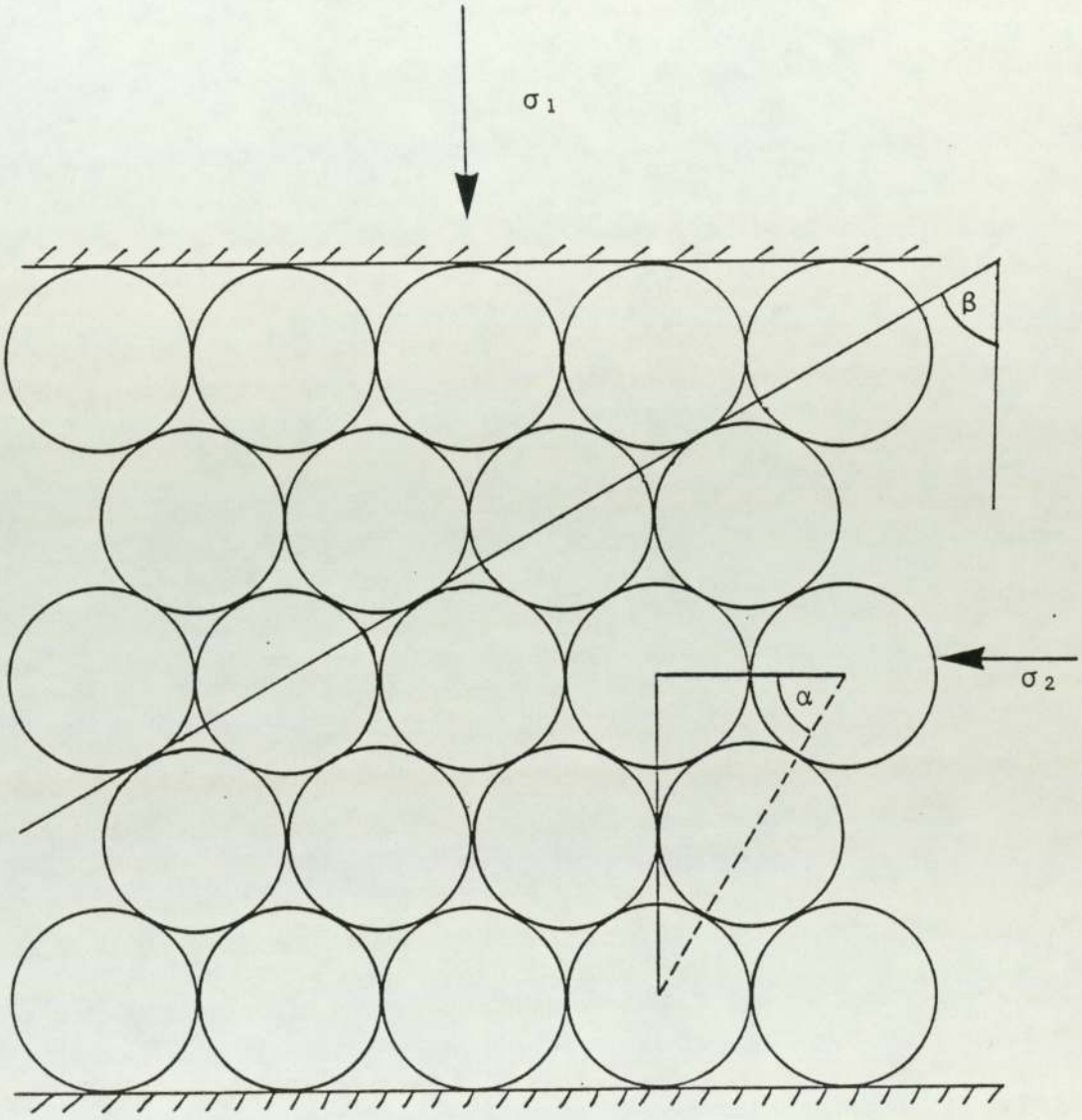

FIGURE 3.3 CLOSEST PACKING ARRANGEMENT OF RODS (OR DISCS) SHOWING THE PACKING ANGLES α AND β ACCORDING TO ROWE (1962)

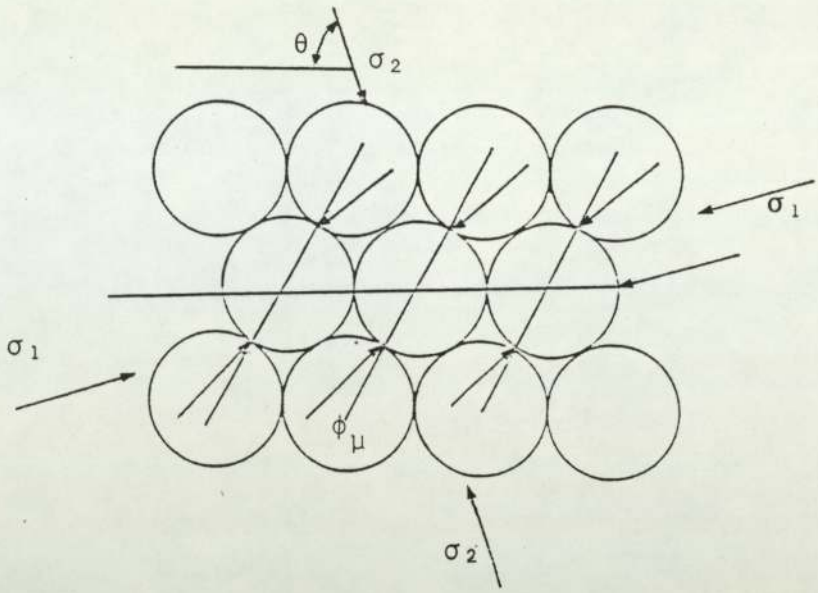

FIGURE 3.4 PARKIN'S (1965) GENERAL TWO-DIMENSIONAL MODEL

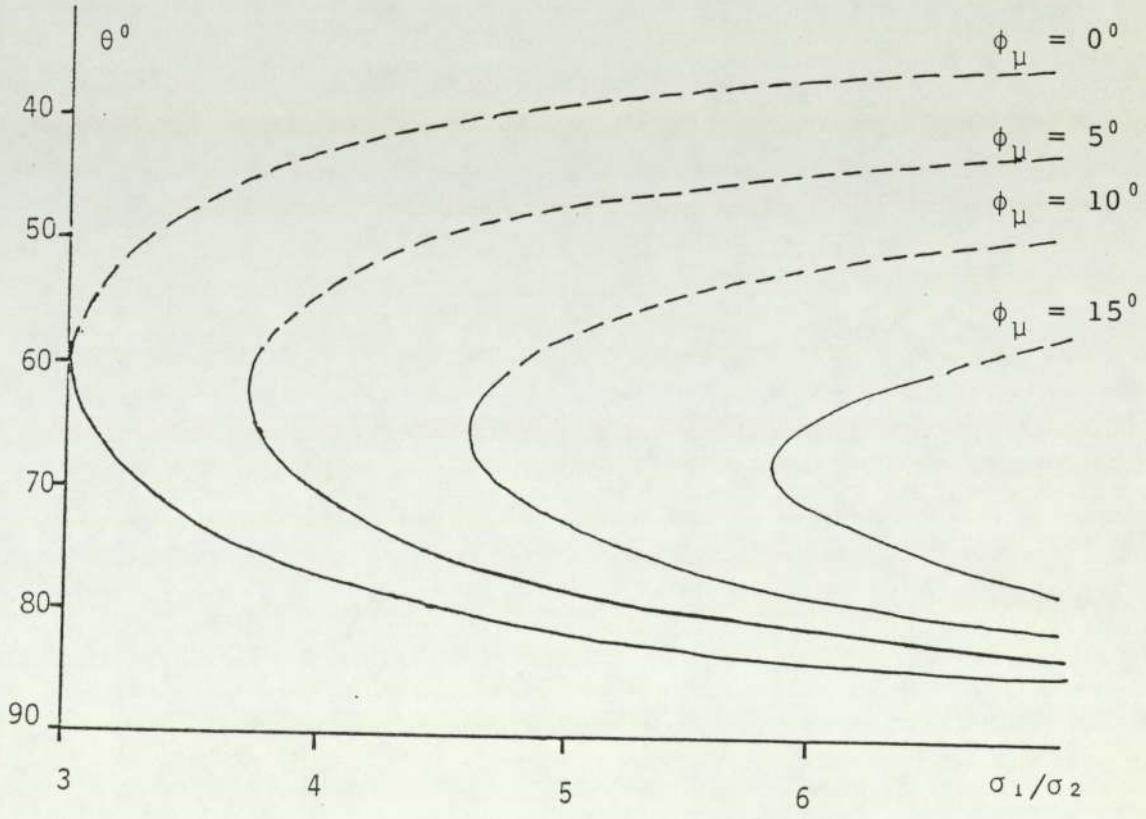

FIGURE 3.5 PARKIN'S (1965) TWO-DIMENSIONAL STRENGTH SOLUTION

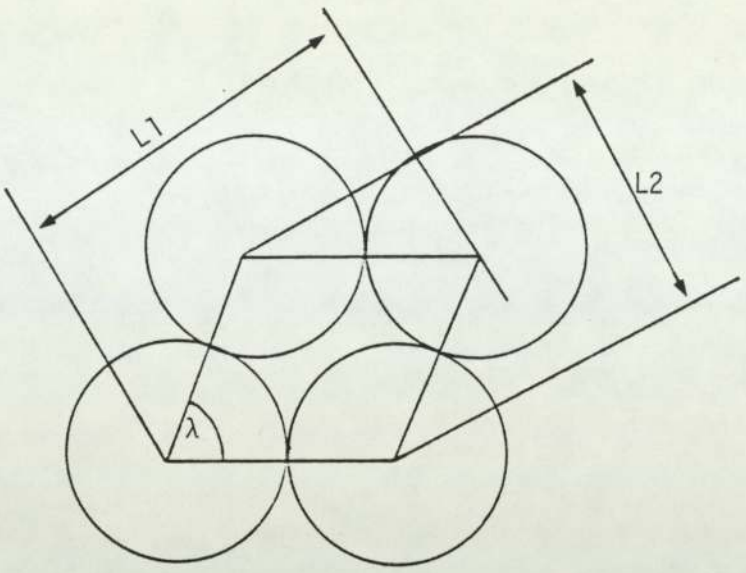

FIGURE 3.6 PACKING ANGLE FOR INITIALLY LESS DENSE PACKINGS AFTER THORNTON 1977

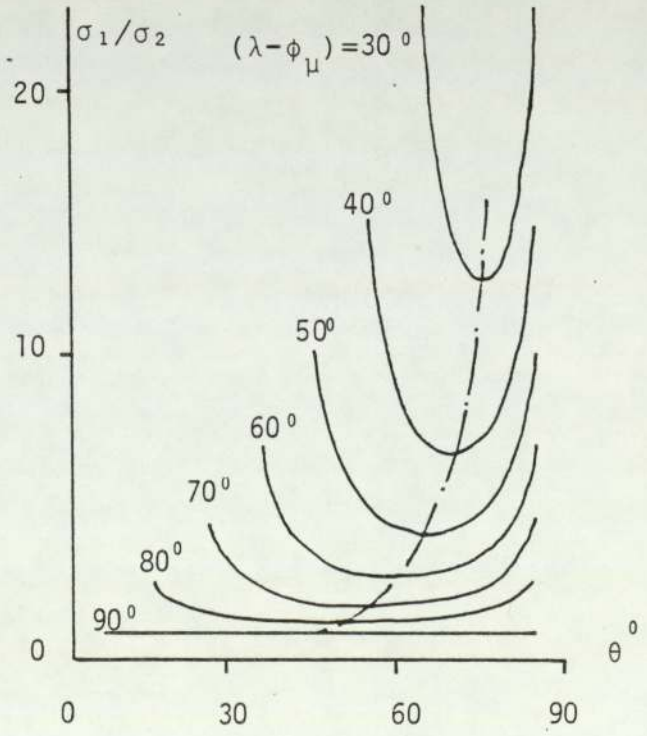

FIGURE 3.7 SOLUTIONS RESULTING FROM THORNTON'S (1977) ANALYSIS

CHAPTER FOUR

4. THE ANALYSIS OF BODY-CENTRED ORTHORHOMBIC ARRAYS OF RIGID SPHERES

This chapter presents an analysis of a class of regular packings which can be termed body-centred orthorhombic, see Section 2.3. The spheres are assumed to be rigid and so the analysis is solely concerned with the conditions which will produce slip at the interparticle contacts. Interparticle slip will result in a change in the geometry of the array and in this way the material (the assembly of spheres) can be said to have yielded.

By examining the conditions necessary for slip to occur the corresponding stress and strain-increment tensors are derived. The results of the analysis are then plotted in principal stress space and, from the geometrical interpretation of the solutions, yield conditions are identified and compared with well known concepts of plasticity theory. The analysis presented in this chapter has been published elsewhere, Thornton and Blackburn (1981).

Throughout the analysis, the usual soil mechanics convention that compressive stresses and strain-increments are positive will be adopted.

4.1 DERIVATION OF THE STRAIN-INCREMENT TENSOR

The body-centred orthorhombic unit cell is illustrated in Figure 4.1 which also shows the cartesian co-ordinate reference frame (x,y,z). The dimensions of the unit cell, as shown, are measured between sphere centres in the x,y and z directions. The terms l,m and n are the direction cosines of the lines joining the sphere centres to the centre of the central sphere, and D is the diameter of the spheres. By altering the values of the direction cosines, different body-centred orthorhombic packings may be analysed. The spheres, however, impose restrictions on the possible values of the direction cosines which must be in the range $1/\sqrt{2}$ to $1/2$.

Although the structure is adequately defined by the unit cell shown in Figure 4.1, it is more convenient to consider the alternative building block of fifteen spheres which, together, form the "hard ball model" of a dodecahedron, Figure 4.2 (a). This permits a clear examination of the kinematics of the body-centred orthorhombic array. It can be seen that the central sphere is in contact with eight other spheres, at contact points P,Q,R and S, where each point represents a pair of contacts on a common diameter. In addition, there are six other spheres separated from the central sphere by gaps at T,U and V (Figure 4.2 (b)).

If such an arrangement were to be subjected to a small, uniform strain-increment, $d\varepsilon_{ij}$, then the change in the square of the distances between the centres of each of the surrounding spheres and that of the central one will be

$$\delta = (X_i+dX_i)\ (X_i+dX_i) - X_iX_i \qquad ...(4.1)$$

which, to a first order approximation in dX_i, leads to

$$\delta = 2X_i dX_i \qquad ...(4.2)$$

but since $dX_i = d\varepsilon_{ij}X_j$ ...(4.3)

$$\delta = 2X_i d\varepsilon_{ij}X_j \qquad ...(4.4)$$

to a first order approximation in dX_i.

From an examination of the geometry of the body-centred orthorhcmbic packing, it has been shown that co-axiality is associated with a "multiple slip" mechanism in which slip occurs at all the contact points, Thornton (1981). As a result there is no gap formation at the P,Q,R and S contact points but the initial gaps at the T,U and V locations may change. Therefore, from equation 4.4, the following equations may be obtained:

$$d\varepsilon_{zz}l^2+d\varepsilon_{yy}m^2+d\varepsilon_{xx}n^2-2d\varepsilon_{zy}lm-2d\varepsilon_{yx}mn+2d\varepsilon_{xz}nl=\delta_p=0 \quad ...(4.5\ (a))$$

$$d\varepsilon_{zz}l^2+d\varepsilon_{yy}m^2+d\varepsilon_{xx}n^2+2d\varepsilon_{zy}lm-2d\varepsilon_{yx}mn-2d\varepsilon_{xz}nl=\delta_q=0 \quad ...(4.5\ (b))$$

$$d\varepsilon_{zz}l^2+d\varepsilon_{yy}m^2+d\varepsilon_{xx}n^2-2d\varepsilon_{zy}lm+2d\varepsilon_{yx}mn-2d\varepsilon_{xz}nl=\delta_r=0 \quad ...(4.5(c))$$

$$d\varepsilon_{zz}l^2+d\varepsilon_{yy}m^2+d\varepsilon_{xx}n^2+2d\varepsilon_{zy}lm+2d\varepsilon_{yx}mn+2d\varepsilon_{xz}nl=\delta_s=0 \quad ...(4.5(d))$$

$$8d\varepsilon_{yy}m^2D^2=\delta_t \quad ...(4.5(e))$$

$$8d\varepsilon_{xx}n^2D^2=\delta_u \quad ...(4.5(f))$$

$$8d\varepsilon_{zz}l^2D^2=\delta_v \quad ...(4.5(g))$$

which shows that

$$d\varepsilon_{zz} = \delta_v/(8D^2l^2) \quad ...(4.6(a))$$

$$d\varepsilon_{yy} = \delta_t/(8D^2m^2) \quad ...(4.6(b))$$

$$d\varepsilon_{xx} = \delta_u/(8D^2n^2) \quad ...(4.6(c))$$

By substituting equations 4.6 into equations 4.5 and solving simultaneously, it is found that the z,y and x axes are principal strain-increment directions.

Using the substitutions

$$a = \delta_u/(8D^2) \quad ...(4.7)$$

$$b = \delta_t/(8D^2) \quad ...(4.8)$$

$$c = \delta_v/(8D^2) \quad ...(4.9)$$

the strain-increment tensor may then be written as

$$d\varepsilon_{ij} = \begin{bmatrix} c/l^2 & 0 & 0 \\ 0 & b/m^2 & 0 \\ 0 & 0 & a/n^2 \end{bmatrix} \qquad \ldots(4.10)$$

with the conditions that a+b+c=0 and that

$l^2+m^2+n^2 = 1$

4.2 DERIVATION OF THE STRESS TENSOR

The forces acting on the surface of the central sphere are discrete forces acting at the points of contacts with adjacent spheres. Consequently the state of stress within the sphere is not homogeneous. However, the average stress tensor within a sphere will be identical for all spheres due to the regular arrangement of the spheres. Therefore, the macroscopic state of stress, σ_{ij}, is obtained directly from the average stress tensor, $\bar{\sigma}_{ij}$, for a typical sphere.

If, within a volume V, there is a state of stress which is in equilibrium, but arbitrarily distributed within the sphere, then the average state of stress $\bar{\sigma}_{ij}$ may be defined as $\bar{\sigma}_{ij} = \frac{1}{V} \int_V \sigma_{ij} dV$ ...(4.11)

Applying Gaus's Divergence Theorem, the above volume integral may be replaced by a surface integral to give

$$\bar{\sigma}_{ij} = \frac{1}{V} \int_S x_i t_j dS \qquad \ldots(4.12)$$

where x_i is the "i" co-ordinate of a point on the surface S, and t_j is the "j" component of the traction acting on S at that particular point.

However, since the tractions are discrete forces, the surface integral may be replaced by a summation over the " n " forces acting on the surface. Therefore, the average stress $\bar{\sigma}_{ij}$ is defined as

$$\bar{\sigma}_{ij} = \frac{1}{V} \Sigma_1^n x_i t_j \qquad \ldots(4.13)$$

where V is the volume of the space occupied by each sphere, on which there are n discrete forces t_j acting at the contacts defined by the co-ordinates x_i. Hence, the individual contributions to the average stress tensor of the normal and tangential contact forces can be obtained by multiplying the orthogonal components of these forces by the co-ordinates of their contact points. The average stress tensor, therefore, can be considered to be the sum of the normal force contribution, $\bar{\sigma}_{ij}{}^N$, and the tangential force contribution $\bar{\sigma}_{ij}{}^T$; thus

$$\bar{\sigma}_{ij} = \bar{\sigma}_{ij}{}^N + \bar{\sigma}_{ij}{}^T \qquad \ldots(4.14)$$

Imposing the restriction of no particle spin, all the tangential forces must be equal in order to satisfy moment equilibrium for each sphere. As coaxiality is associated with slip at all contacts, all the normal forces must be equal. Therefore the normal forces may be denoted by

p and the tangential forces by $f=\mu p$ at every contact.

The normal force contribution is obtained from the product

$$\bar{\sigma}_{ij}^{N} = \frac{2pD}{V}\begin{bmatrix} -l/2 & l/2 & -l/2 & l/2 \\ m/2 & m/2 & m/2 & m/2 \\ -n/2 & -n/2 & n/2 & n/2 \end{bmatrix} \begin{bmatrix} -l & m & -n \\ l & m & -n \\ -l & m & n \\ l & m & n \end{bmatrix} \quad \ldots(4.15)$$

which gives

$$\bar{\sigma}_{ij}^{N} = \frac{4pD}{V}\begin{bmatrix} l^2 & 0 & 0 \\ 0 & m^2 & 0 \\ 0 & 0 & n^2 \end{bmatrix} \quad \ldots(4.16)$$

The direction cosines of the tangential forces are determined by the strain-increment tensor and are given by the expression

$$\frac{dx_i}{(dx_i dx_i)^2} \quad \text{where } dx_i = d\varepsilon_{ij}x_j \; . \quad \ldots(4.17)$$

By considering each contact individually it is found that the direction cosines of the tangential forces are:-

$$\begin{aligned} &-c/Fl \;,\; b/Fm \;,\; -a/Fn \;,\; \text{at the P contacts} \\ &\;\;c/Fl \;,\; b/Fm \;,\; -a/Fn \;,\; \text{at the Q contacts} \\ &-c/Fl \;,\; b/Fm \;,\; \;\;a/Fn \;,\; \text{at the R contacts} \\ &\;\;c/Fl \;,\; b/Fm \;,\; \;\;a/Fn \;,\; \text{at the S contacts} \end{aligned} \quad \ldots(4.18)$$

where $$F^2 = c^2/l^2+b^2/m^2+a^2/n^2 \quad \ldots(4.19)$$

Having thus defined the directions of the tangential forces, the tangential force contribution to the stress tensor is obtained from

$$\bar{\sigma}_{ij}{}^{T} = \frac{2\mu pD}{V} \begin{bmatrix} -l/2 & l/2 & -l/2 & l/2 \\ m/2 & m/2 & m/2 & m/2 \\ -n/2 & -n/2 & n/2 & n/2 \end{bmatrix} \begin{bmatrix} -c/Fl & b/Fm & -a/Fn \\ c/Fl & b/Fm & -a/Fn \\ -c/Fl & b/Fm & a/Fn \\ c/Fl & b/Fm & a/Fn \end{bmatrix} \quad \ldots(4.20)$$

which leads to

$$\bar{\sigma}_{ij}{}^{T} = \frac{4\mu pD}{VF} \begin{bmatrix} c & 0 & 0 \\ 0 & b & 0 \\ 0 & 0 & a \end{bmatrix} \quad \ldots(4.21)$$

Substituting the two individual contributions 4.16 and 4.21 into equation 4.14 the average stress tensor is obtained

$$\bar{\sigma}_{ij} = \frac{4pD}{V} \begin{bmatrix} l^2+\mu c/F & 0 & 0 \\ 0 & m^2+\mu b/F & 0 \\ 0 & 0 & n^2+\mu a/F \end{bmatrix} \quad \ldots(4.22)$$

This equation indicates that the first stress invarient

$$I_1 = \sigma_{zz}+\sigma_{yy}+\sigma_{xx} = 4pD/V \quad \ldots(4.23)$$

and the interparticle contact forces are given by

$$p = I_1 V/4D \qquad \text{and} \qquad f = \mu I_1 V/4D \quad \ldots(4.24)$$

Therefore the average stress tensor may be rewritten as

$$\bar{\sigma}_{ij} = I_1 \begin{bmatrix} l^2+\mu c/F & 0 & 0 \\ 0 & m^2+\mu b/F & 0 \\ 0 & 0 & n^2+\mu a/F \end{bmatrix} \quad \ldots(4.25)$$

The average stress tensor, equation 4.25, applies to all body-centred orthorhombic packings and defines the states of stress which will cause yield, the yield mechanism being defined by the strain-increment tensor, equation 4.10. Given the physical properties of the array (structure and interparticle friction) it is therefore possible, for an arbitrary mean stress, to identify the complete range of stress states which will cause yield by varying the parameters a,b and c.

4.3 YIELD CONDITIONS FOR BODY-CENTRED TETRAGONAL PACKINGS

Before discussing the solutions obtained from equations 4.10 and 4.25, it will be useful to introduce a piece of nomenclature to assist in the identification of the different packings under consideration. It has already been shown that a range of regular packings can be analysed using the body-centred orthorhombic model, the actual type of packing being studied is only dependent on the values allocated to l,m and n as shown in Figure 4.1 and as used in equation 4.10 and 4.25.

The equations of Sections 4.1 and 4.2 apply to the complete range of body-centred orthorhombic packings, but for the sake of simplicity of presentation the remainder of this chapter will restrict its attention to body-centred tetragonal packings. In these packings, two of the

direction cosines are equal and because of symmetry it is sufficient to consider the case where m=n. However, the results would still be valid for the other body-centred tetragonal cases where l=n or l=m.

While a range of values can be allocated to l,m and n, there are limiting cases. These are dictated by the physical arrangement of the spheres. It can be seen from Figure 4.1 that such limiting cases occur when there are no gaps at either T,U or V. These conditions exist when

$$l^2 = 1/2 \ , \ m^2 = 1/4 \text{ and } n^2 = 1/4$$

and

$$l^2 = 1/4 \ , \ m^2 = 3/8 \text{ and } n^2 = 3/8 \qquad \ldots(4.26)$$

These packings and the intermediate ones may be conveniently described by a simple term, referred to in this work as the packing factor, D'. Where,

$$D' = l^2/n^2 \qquad \ldots(4.27)$$

In this way the face-centred cubic packing ($l^2=\frac{1}{2}, m^2=n^2=\frac{1}{4}$) may be referred to as a $D'=2.0$ packing and the body-centred cubic ($l^2=m^2=n^2=\frac{1}{3}$) as a $D'=1.0$ packing. Thus the geometrically limiting conditions referred to above (equations 4.26) can be restated as being the limits $D'=2.0$ and $D'=0.\dot{6}$. Therefore the body-centred tetragonal packings within this range can be analysed using equations 4.10 and 4.25 and as there are an infinite number of such packings, most of which have no distinguishing crystallographic name, it will be convenient to refer to

these packings by using their packing factor, D'.

When slip occurs at the contacts the assembly yields and the yield conditions are defined by equations 4.10 and 4.25. The solutions for the stress tensor, equation 4.25, may be represented geometrically by plotting the results in principal stress space. Such a geometrical representation is analogous to the yield surface concept of conventional plasticity theories. Consequently it would appear possible to identify a macroscopic model in terms of plasticity theory which corresponds to the particle mechanics solutions provided in Section 4.1 and 4.2. For a complete plasticity theory it is necessary to identify a yield surface or yield function, a plastic potential surface or flow rule, and a hardening or softening law. These ideas will be dealt with in the remainder of this chapter.

4.3.1 Yield Surface Geometry

Theories of plasticity were initially developed to describe the behaviour of metals for which the mean (hydrostatic) stress has no significant effect on the yield conditions. Yield conditions may be represented in principal stress space by yield surfaces which enclose all the states of stress which produce only elastic behaviour. An example of a hypothetical, piece-wise linear, stress/strain plot

and the corresponding yield surface on a deviatoric plane is shown in Figure 4.3. While the deviatoric stress is in the region 0-1, shown in the figure, the sample is behaving in an elastic manner and is represented on the deviatoric plane plot as a point within the yield surface. When point 1 is reached the sample yields plastically (section 1-2 on the stress/strain plot). This is shown on the yield surface plot by the points representing states 1 and 2 being identical and located on the yield surface. Should the sample be unloaded and re-loaded (2-3-4) then it would behave in an elastic manner, until it again reached the yield stress (point 4). For continuing strain (4-5) the sample is shown to continue to deform plastically at the yield stress (σ_y) on the stress/strain curve and is depicted by points 4 and 5 on the yield surface plot.

Yield surfaces for metals are usually assumed to be cylindrical since yield is independent of mean stress. The yield conditions for granular material such as sand, however, are dependent on mean stress and hence the yield surfaces would be expected to be conical. In either case, attention is centred upon the shape of the yield locus on a deviatoric plane ($\sigma_1+\sigma_2+\sigma_3$ = constant) of principal stress space.

It is possible to observe the influence of the various

physical packing properties on the yield locus of a packing by varying those parameters relevant to equations 4.10 and 4.25 and then solving the tensors for each case. By plotting the results of the analyses in principal stress space the geometrical definition of the yield envelopes can be identified. By calculating the stresses and dividing them by the first stress invarient ($\bar{\sigma}_{ij}/I_1$) the results can be normalised to a common mean stress and the yield conditions can then be conveniently presented in terms of the ratio of octahedral shear to normal stress on a common deviatoric plane. This is illustrated in Figure 4.4 which shows the deviatoric yield locus for the body-centred cubic packing ($\dot{D}=1$) together with the yield loci corresponding to the two limiting cases ($\dot{D}=2.0$ and $\dot{D}=0.\dot{6}$). It can be seen that the yield locus for the body-centred cubic packing is a circle centred at the origin. From the shape of the yield locus for the $\dot{D}=1$ packing it might be expected that the geometrical arrangement within the packing would be isotropic, which is clearly incorrect. The geometry of the body-centred array, however, is identical in the three principal directions and hence the behaviour is in effect isotropic for the irotational mode of deformation considered. For body-centred tetragonal arrays the spacial arrangement is only identical in two of the principal directions and this is reflected in the elliptical yield loci which are symmetrical about one of the axes shown in Figure 4.4.

According to the strain-increment tensor (equation 4.4) all states of stress identified by the circular ($\dot{D}=1$) yield locus, are associated with a zero rate of volumetric strain. For all the other body-centred tetragonal packings, the rate of volumetric strain depends on the deformation state. It is interesting to note that for the body-centred cubic packing, the radius of the yield locus is proportional to the coefficient of interparticle friction. This corresponds to the force obliquity on the contact planes of the physical model, indicating that the size of the yield surface is controlled by the interparticle friction, see Figure 4.5 and that the shape is related to the structural anisotropy of the packing, Figure 4.6.

This figure shows the yield loci on a normalised deviatoric plane for a number of body-centred tetragonal packings. It is clear that the yield surfaces are cones. These cones may be either right cones rotated about the origin of principal stress space or they may be oblique cones. It is possible to test whether the yield surfaces are right or oblique cones by solving the average stress tensor (equation 4.10) for different values of interparticle friction. For a given packing this will result in different sized yield loci on the normalised deviatoric plane. Since an oblique plane through a right cone produces an ellipse whose centre is offset from the axis of the cone.

Varying the interparticle friction will produce a set of ellipses which are not concentric if the cones are right cones. Figure 4.5 illustrates the effect of interparticle friction for a face-centred cubic (D^{I}=2.0) packing. The result is a set of concentric ellipses, which demonstrates that the cones are oblique.

4.3.2 Plastic Potentials and Flow Rule

A yield surface is a geometrical representation of the stress tensor, but to represent the complete yield conditions it is necessary to include the strain-increment tensor in some way. This is achieved by superimposing the plastic strain-increment vectors, on the corresponding points along the yield surface in principal stress space. If the strain-increment vectors are normal to a common surface then this surface is termed the plastic potential surface.

Let the state of stress associated with yield be represented by the point P in Figure 4.7. Taking the point representing the state of stress as the origin for the corresponding plastic strain-increment vector the strain-increment tensor, and its components, may then be represented by vectors. The magnitude of the vectors is arbitrary provided that the ratio of the component vectors are correct as this gives the direction of the total plastic strain increment vector. Once the direction of the vector has been established, the line

that is perpendicular to the vector, passing through the vectors origin can be constructed. This line is a tangent to the plastic potential. The plastic potential is then defined by the curve (or surface in three dimensional space) that is normal to all the strain-increment vectors, Figure 4.8. The way in which the plastic potential is related to the yield surface is called the flow rule. Should the plastic potential and the yield surface coincide (as is assumed for metals) then the condition in known as normality and the corresponding theories are termed associated flow theories.

It follows that if the yield surfaces are also plastic potentials the plastic strain-increment vectors will be normal to the yield envelopes. By superimposing the strain increment vectors on the yield surfaces and then viewing the deviatoric planes perpendicularly, it is found that normality does not occur; except for the body-centred cubic packing. For the body-centred cubic packing, the space diagonal is concurrent with the axis of the cone. When the deviatoric yield loci are examined by viewing them along the axes of the cones, the strain increment vectors appear as normals to the yield loci, Figure 4.9. However, on the $\sigma_z : \sqrt{2}\sigma_x$ plane (Figure 4.10) the strain increment vectors are perpendicular to the axes of the cones and therefore there is a lack of normality between the strain increment vectors and the yield surfaces.

4.3.3 Hardening/Softening Laws

During plastic deformation of real materials the yield surface is continuously changing and as a result of these changes, the material is said to harden. The way in which the surface changes determines what type of hardening is exhibited by the material.

A widely used approach is to assume that the initial yield locus undergoes a uniform expansion when the stress path reaches the yield surface. Such uniform expansion is termed isotropic hardening, see Figure 4.11 (a). This hardening implies that no anisotropy is introduced during plastic deformation. The overall geometry of the yield locus is retained, as is its centre, but the new yield locus is a larger concentric version of the previous one. Should unloading occur (section 2-3-4 of Figure 4.11 (a)), then the material response becomes elastic until it reaches the new yield locus, (at point 4 in the figure), at which point yield occurs resulting in further plastic deformation.

Another approach, often used, is to assume that the yield locus undergoes a rigid translation, see Figure 4.11 (b), this is known as kinematic hardening. As yield occurs (section 1-2 of the figure) the whole yield locus moves in stress space, as a rigid body, in the direction of the stress path at the yield point. Unloading results in the material behaving elastically until it reaches the yield

locus (sections 2-3-4) again, whereupon plastic deformation is initiated.

If the yield locus becomes distorted during hardening, but its centre does not move, as in the case when a circular yield locus becomes elliptical (Figure 4.11 (c)), the type of hardening is known as anisotropic hardening.

By considering that the $D'=2.0$, $D'=1.0$ and $D'=0.\dot{6}$ are all merely special cases of one packing (the body-centred tetragonal packing), it follows, for the irrotational mode of deformation considered, that under axisymmetrical compression a $D'=2.0$ packing would deform to a $D'=0.\dot{6}$ packing after passing through the infinite number of packings which have D' values between these two limits. The way in which the yield stress alters with this deformation is shown in Figure 4.12, on which are marked the points corresponding to the various yield loci of Figure 4.6. These figures show that as the regular packing deforms, it undergoes a combined kinematic and isotropic softening.

4.4 CONCLUSIONS

It is shown by the expression for the average stress tensor (equation 4.25) that the size of the yield surface depends on the interparticle friction and the mean stress.

The shape of the yield surface, however, is related to the structure of the packing, which itself is defined by the geometrical distribution of the particles. The structure of the packing also controls the inclination of the yield surface which, inturn, dictates the rate of dilation. It has been shown that the yield surfaces obtained can be defined by oblique cones which have deviatoric planes as base planes. The angle of inclination of the axis of each cone depends on the geometry of the packing (l,m and n). For each separate yield surface, the plastic potentials consist of an infinite number of equally oblique cylinders. Each of which is only applicable to one value of mean stress. The plastic potentials, therefore, reduce to an infinite number of bands around the oblique cone, the width of each band being infinitessimally small.

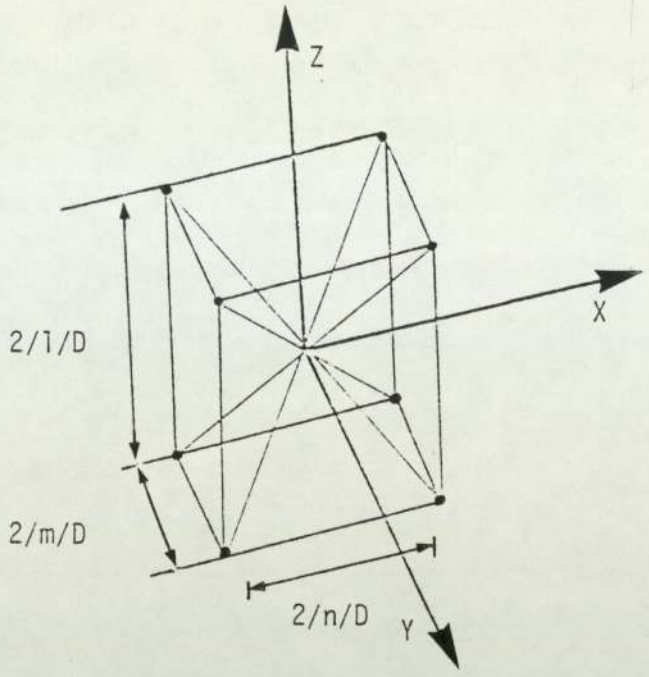

FIGURE 4.1 BODY-CENTRED ORTHORHOMBIC UNIT CELL SHOWING COORDINATE AXES AND CELL DIMENSIONS

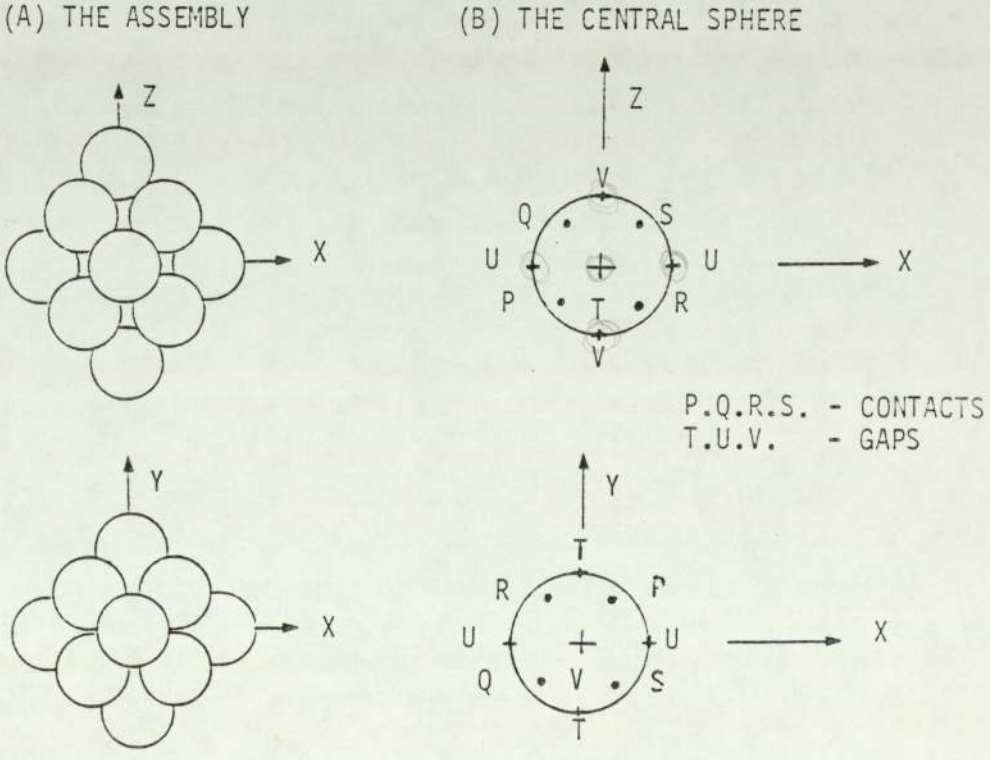

FIGURE 4.2 DODECAHEDRAL HARD BALL MODEL SHOWING POINTS AND GAPS

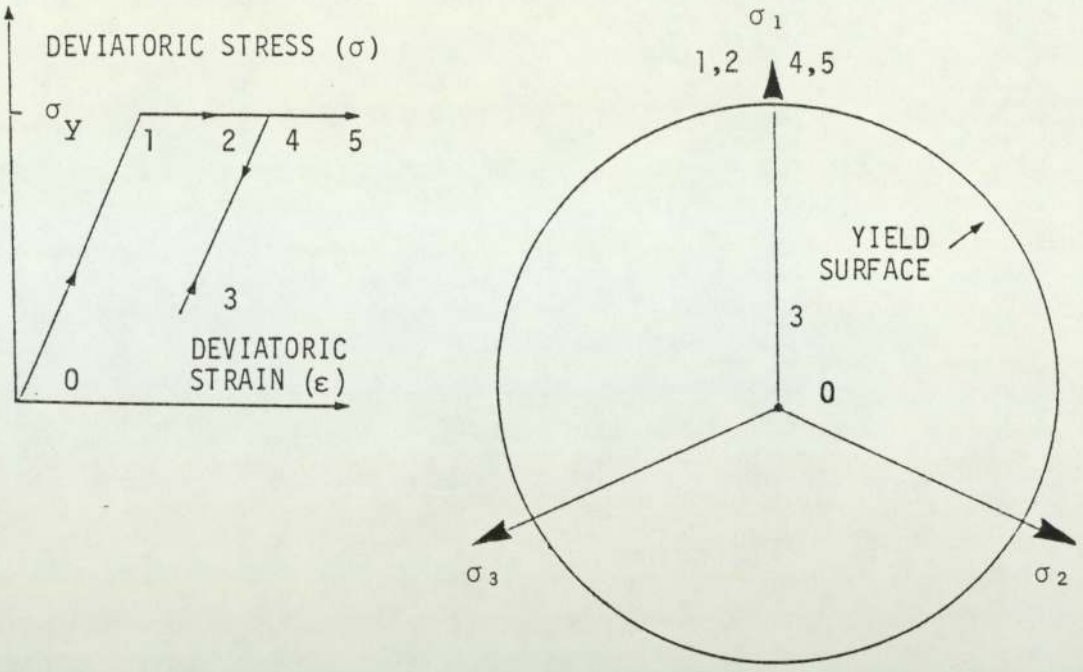

FIGURE 4.3 DEVIATORIC STRESS/STRAIN PLOT AND THE CORRESPONDING YIELD SURFACE (VIEWED IN PRINCIPAL STRESS SPACE)

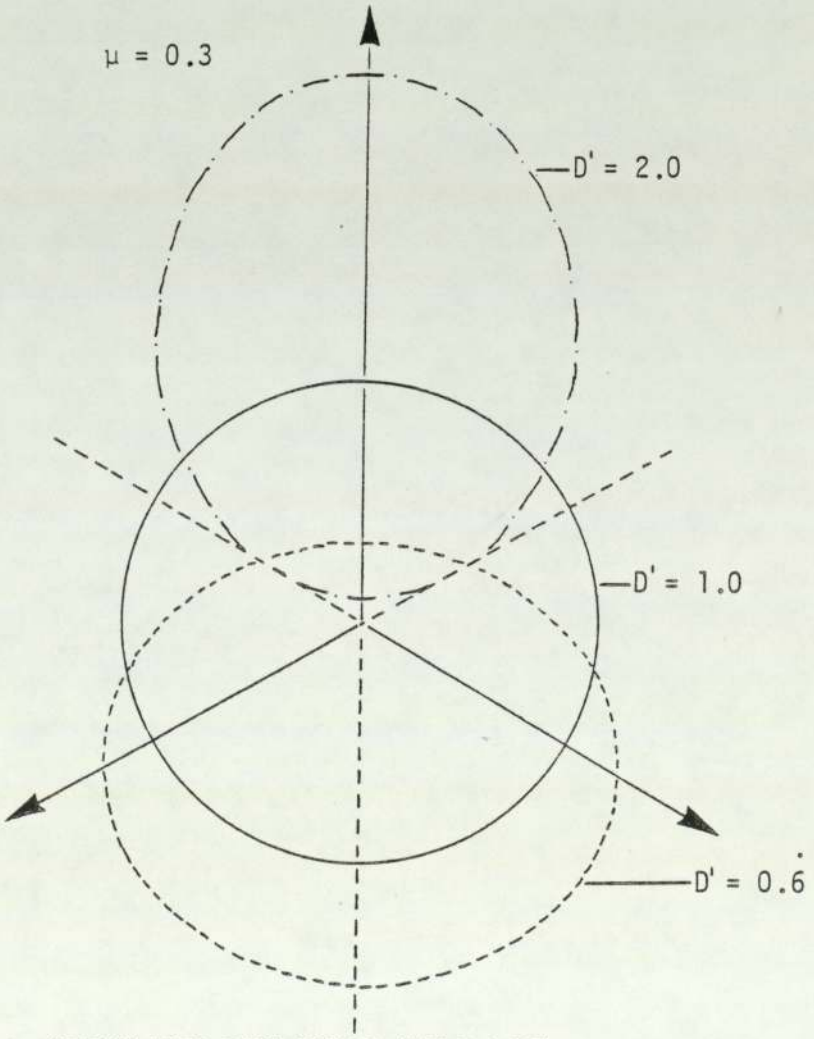

FIGURE 4.4 NORMALISED DEVIATORIC YIELD LOCI

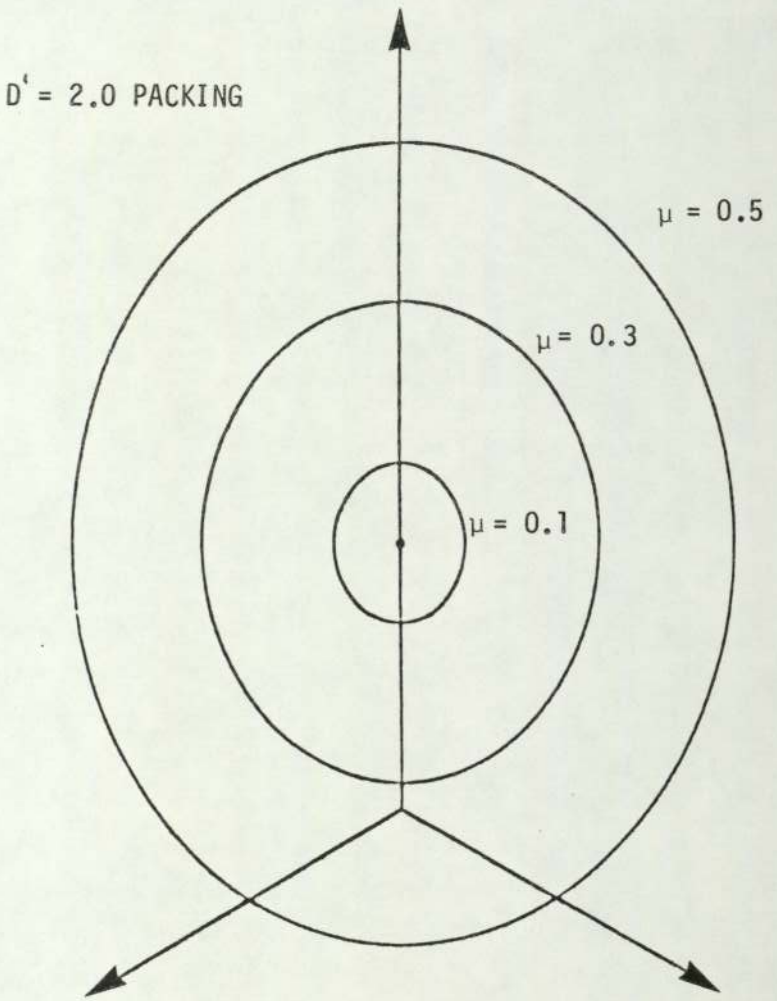

FIGURE 4.5 EFFECT OF INTERPARTICLE FRICTION

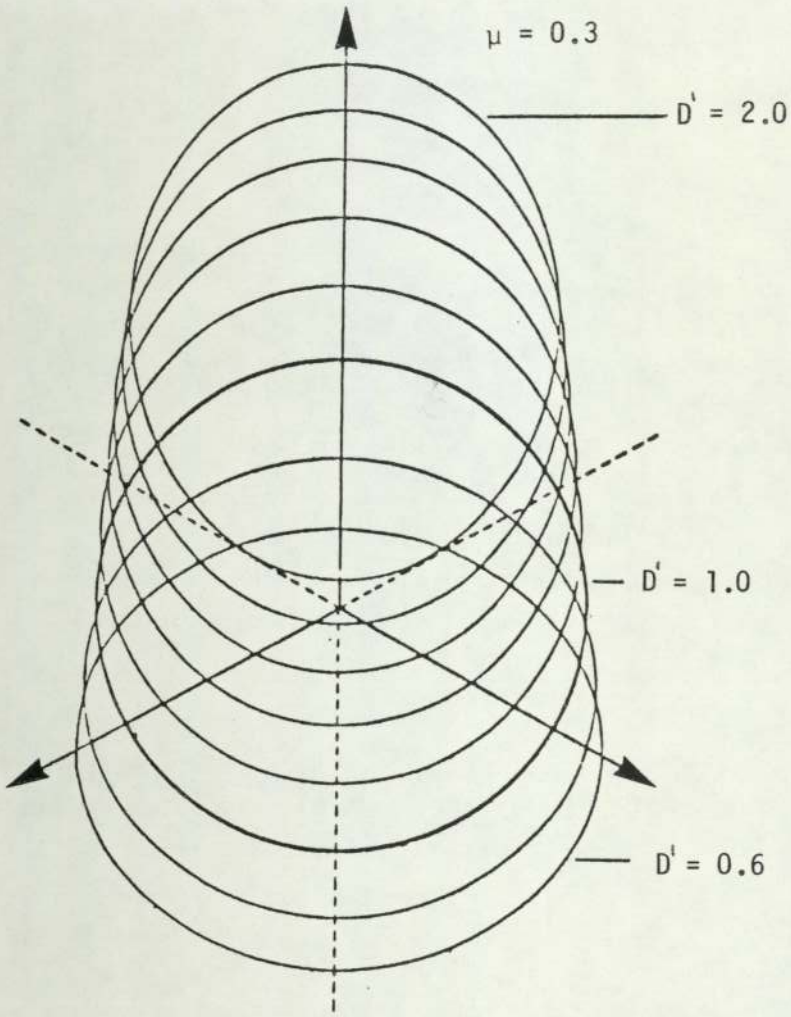

FIGURE 4.6 DEVIATORIC YIELD LOCI FOR BODY-CENTRED TETRAGONAL PACKINGS

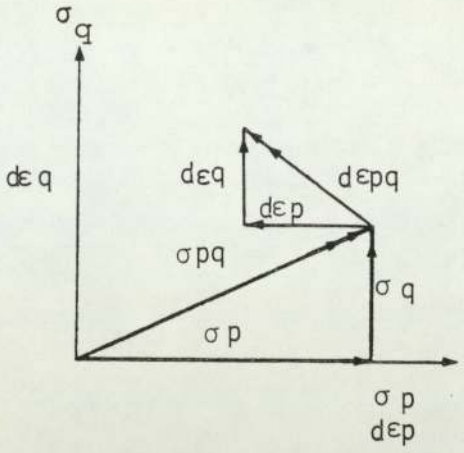

σq, $d\varepsilon q$ = OCTAHEDRAL NORMAL STRESS AND PLASTIC STRAIN INCREMENTS RESPECTIVELY

σp, $d\varepsilon p$ = OCTAHEDRAL SHEAR STRESS AND PLASTIC STRAIN INCREMENTS RESPECTIVELY

FIGURE 4.7 METHOD OF SUPERIMPOSING PLASTIC STRAIN - INCREMENT VECTORS ON YIELD POINTS

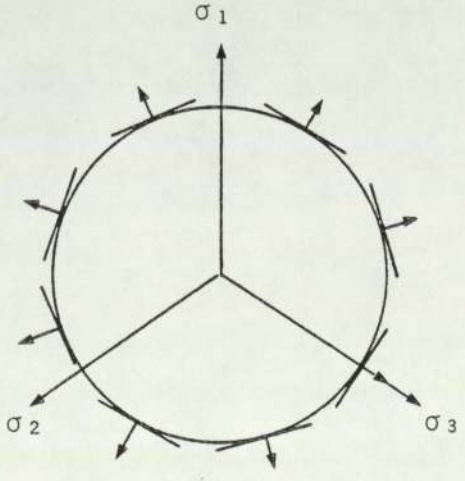

FIGURE 4.8 A PLASTIC POTENTIAL CONSTRUCTED FROM PLASTIC STRAIN-INCREMENT VECTORS

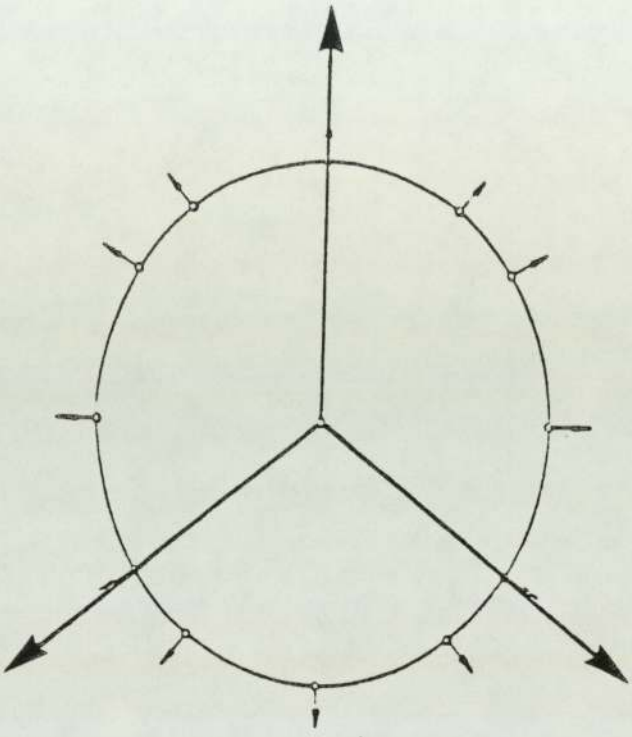

FIGURE 4.9 DEVIATORIC YIELD LOCUS VIEWED ALONG THE AXIS OF THE CONE (D' = 2.0 PACKING)

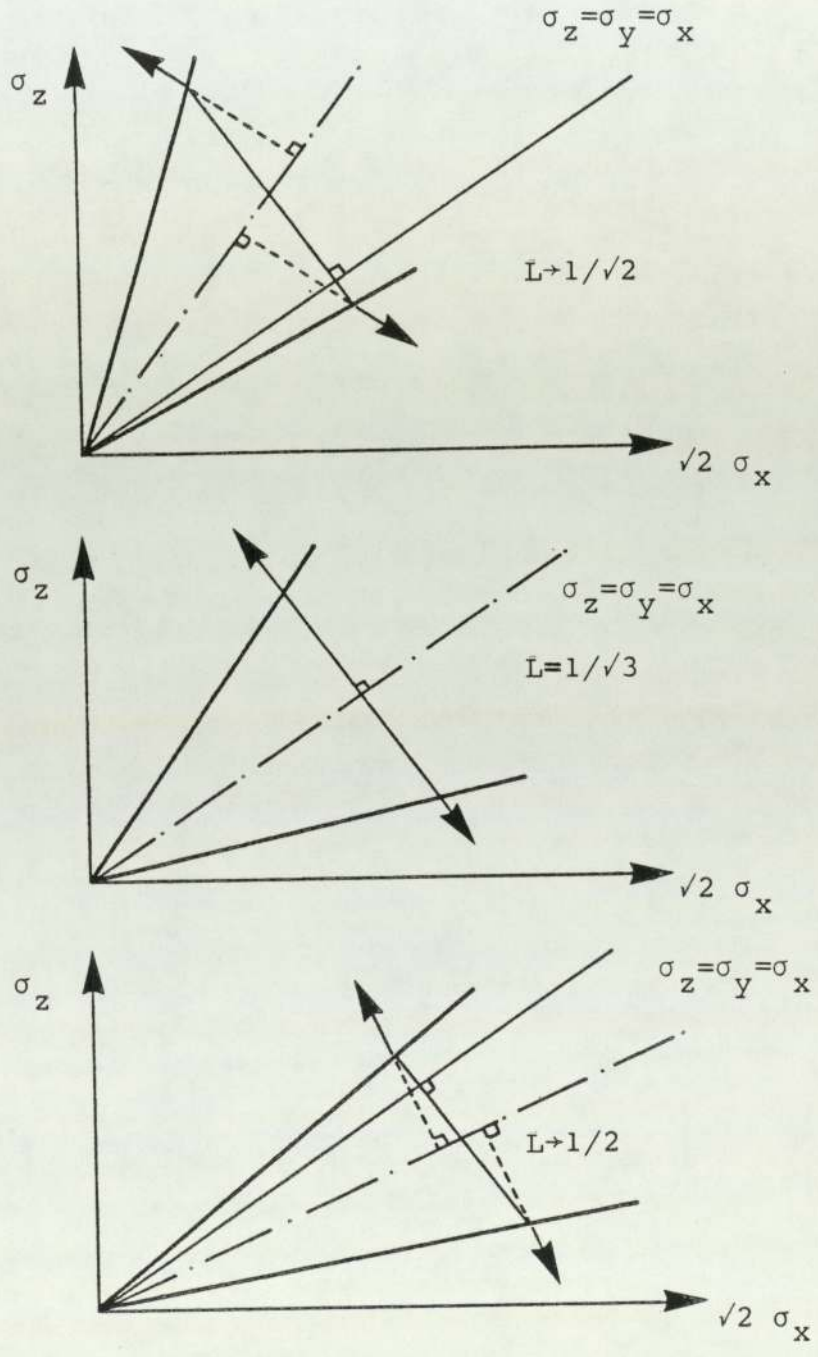

FIGURE 4.10 YIELD CONES AND STRAIN-INCREMENT VECTORS FOR BODY-CENTRED TETRAGONAL PACKINGS

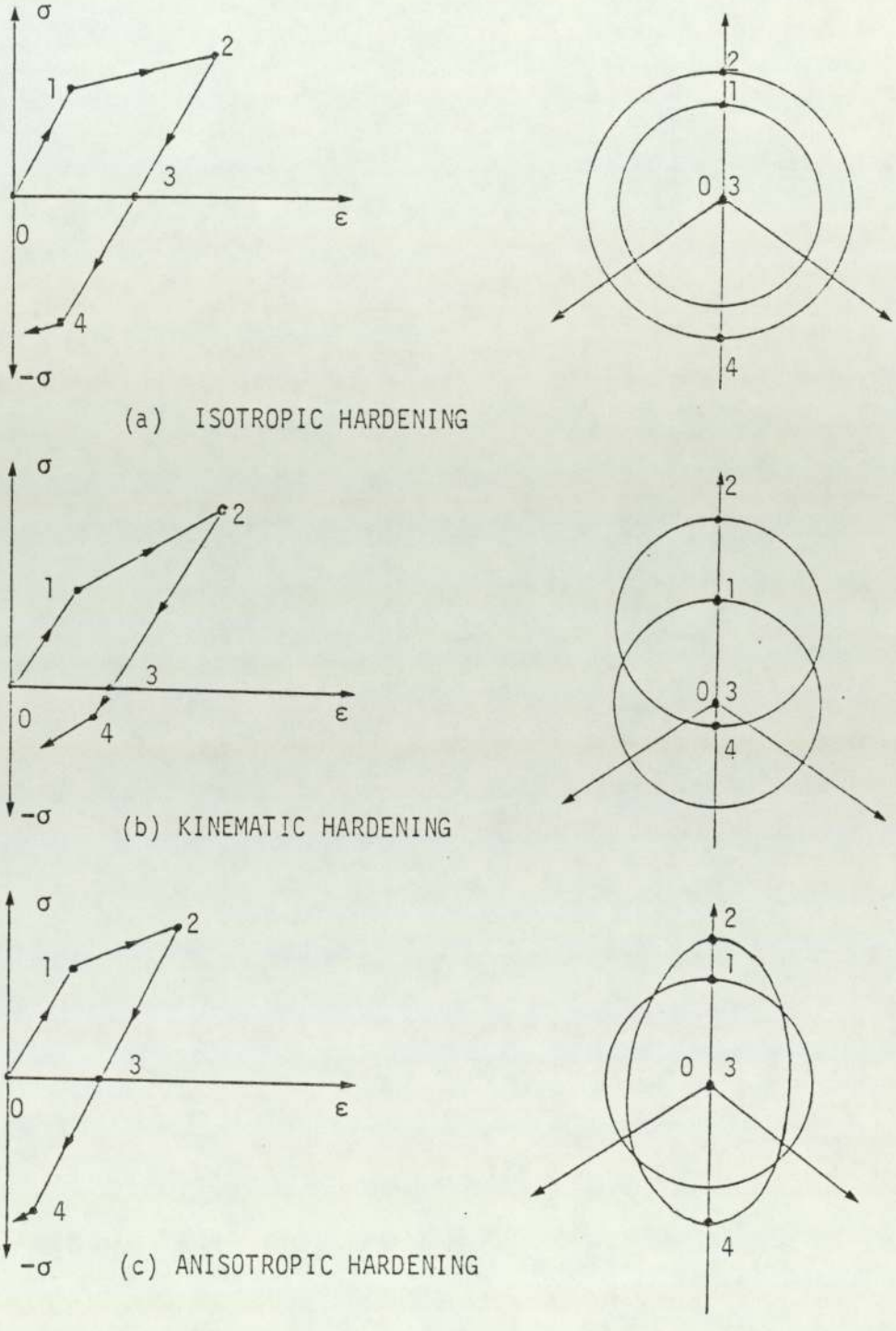

FIGURE 4.11 HARDENING THEORIES

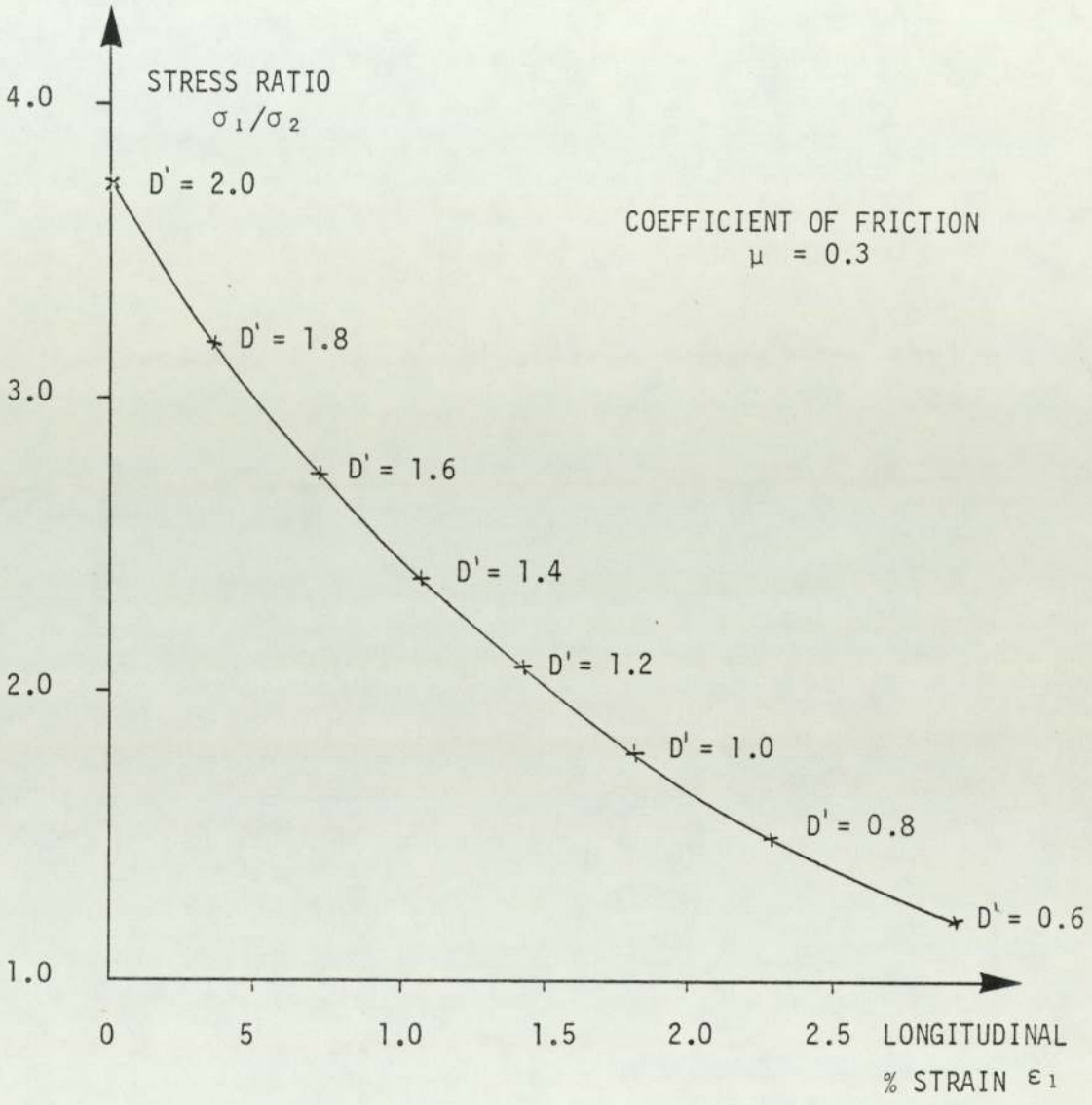

FIGURE 4.12 PLOT OF YIELD STRESS AGAINST DEFORMATION SHOWING THE POINTS CORRESPONDING TO VARIOUS INTERMEDIATE PACKING TYPES

CHAPTER FIVE

5. REVIEW OF COMPUTER SIMULATION

5.1 INTRODUCTION

"No substantial part of the Universe is so simple that it can be grasped and controlled without abstraction. Abstraction consists of replacing that part of the Universe under consideration by a model of a similar but simpler structure", Rosenblueth and Wiener, (1945).

Simulation is essentially the act of setting up a model of a real situation and then performing experiments on that model. Various simulation techniques have been used for scientific purposes for over three hundred years. The purpose of these techniques is to advance the understanding of the behaviour of physical systems, by providing measured observations of the behaviour of models which represent those systems. Models can be divided into two categories, physical models and mathematical ones. A common type of physical modelling is the construction of scale models. These normally take the form of small scale replicas which are tested under controlled conditions. Typical examples of scale modelling in geomechanics include retaining wall and foundation

experiments, and more recently the use of centrifuge models. An alternative type of physical modelling can be performed by the construction of an analogue system. If the real situation obeys certain mathematical relationships then these relationships can be modelled by a physical analogue, as is the case for seepage which can be modelled using either electrically conductive paper or by electrical resistance networks. If,however, the real situation is governed by definitive mathematical rules which can be expressed in the form of equations, then the system may be modelled by mathematical abstractions. Prior to the introduction of modern computers, such mathematical abstraction had to be restricted to relatively simple problems, but modern computing facilities now make it possible to simulate complex three dimensional situations.

5.2 Developments in Computer Simulation

Electrical Resistance Networks, as are used to simulate real situations as ground water flow, can also be used as a calculating device to solve differential equations. Problems of this type have been modelled by Network Analysis, using electrical circuit elements, since the 1920's. General purpose mechanical differential analysers, developed from the wheel and disc integrator (1876), have been used since the 1930's to study problems involving differential equations. Electrical relays were used to aid in the development of an automatic calculator, the

predecessor of the modern day computers which have made numerical simulation so accessable.

The general purpose analogue computer, developed in 1943 at the Massachusetts Institute of Technology, comprised of various electronic units which were capable of performing simple mathematical operations on voltages. Under such an arrangement, each physical factor was represented by a computer variable (a voltage) and the computer units were so inter-connected that the variables could be constrained to obey the same equations that dictated the behaviour of the actual problem variables. The simulation user could then join together the separate units by inserting plugs joined by wires into various sockets on a patch panel. The results were then observed and measured by oscilloscopes, graphical recorders and data-loggers. More modern analogue computers owe their speed of operation to the parallel nature of their construction. All the separate units operate simultaneuously so that all the variables can change together, in the same way as they would do in an actual problem. In order to optimise the usage of the resulting high speed solutions, digital logic and small digital computers were included in the design (around 1960) of some analogue computers to form Hybrid systems. In such a system, the digital section controls and monitors the operation of the analogue section and provides space for program and data storage.

The first really practical proposal for a computer which was capable of storing programs in its memory was commissioned in 1949 at Cambridge University. This early machine was based on work done by Von Neumann who extended earlier ideas put forward by Eckert and Mauchly. The Eckert-Mauchly UNIVAC was introduced in 1951 and soon developments were made which enabled computers to be programmed (Fortran I was developed in 1956) to solve differential equations by numerical ingegration. This technique was called Digital Simulation and offered the advantages of simplicity and accuracy over the analogue simulation models. In digital computer simulations, a system is represented by a set of algebraic/differential/logical equations, these are then solved by the computer and the results presented in some form of tabular or graphical output.

Initially, the major disadvantage of Digital Simulation was that of speed. Digital Simulation depended upon a sequence of simple mathematical processors passing through the central processor, each of which took a finite length of time and, prior to the introduction of transistors in computers (1958), the vacuum tubes used were both slow and of a short design life. The subsequent introduction of integrated circuits in 1966 meant that a lot of the problems associated with hard wire computers (such as overheating, system breakdowns and component failure) were to a great extend eradicated.

Further developments such as input/output interrupts, timesharing, satellite links, mini and micro-computers, and interactive programming, have all contributed to make computing faster and cheaper. Consequently digital simulation has become one of the most attractive forms of modelling.

5.3 Computer Simulation in Geomechanics

In order to perform a computer simulation of a real system, that system must be described in a form that is both acceptable to the computer and realistic to the system under consideration. If a system can be characterised by a set of variables, with each combination of variable values representing a state or condition of the system, then manipulation of the variable values simulates movements of that system from state to state, Prikster and Pegden (1979). Simulation could thus be described as a numerical technique for conducting experiments on a digital computer, which involves certain types of mathematical and logical models that describe the behaviour of a system over extended periods of real time. For complex systems, the techniques used can yield valuable insights into which variables are most influential in that system and how the variables interact.

5.3.1 Continuum Models

A method commonly used for analysing continuous media on digital computers is the Finite Element Method. In the Finite Element Method the procedure is to idealise the subject into a continuum which is then subdivided into a large number of discrete elements. It is then assumed that these elements are only connected to each other at their common nodes or joints. Within each such element, it is normal to assume that the displacements and the strains are determined entirely by the nodal displacements. For this purpose a "Displacement Function" is assumed which specifies, in advance, the manner in which each joint within the element deforms. It is then assumed that the stresses within an element are those derived from the strains associated with the displacement function. The stiffness matrices for each element are assembled together to form an "Overall Stiffness Matrix" for the system. Once this has been achieved, ordinary matrix models can be used to obtain the solution of many diverse engineering problems. The Finite Element Method, was, initially, restricted to the analysis of material which was, or was assumed to be, linear elastic. Subsequent developments, however, have extended its use to materials which obey non-linear and elasto-plastic constitutive laws.

A Finite Element approach is capable of modelling limited

progressive mechanisms, as it is possible to perform a number of calculation iterations during the solution of any problem. Thus, as the model parameters change, iterations may be performed using the revised values. However, the initally selected arbitrary discretisation of the material cannot be altered subsequently because it would then be necessary to construct a new overall stiffness matrix which would make the analysis very expensive.

5.3.2 Jointed Rock Models

As stated in the previous section, ground models may be treated as a continuum. However, there are cases when this is not entirely satisfactory when the ground behaves in an essentially discontinuous manner. One common example is that of jointed rocks. The importance of joints and seams in rock has long been recognised by engineers. Tunnelling and the stability of rock slopes are both cases which are more dependent on the joint properties of rock than the characteristics of the intact rock itself.

It is probably more realistic to treat jointed rock as an aggregate of massive rock blocks, separated by joints which possess their own properties, than to consider it as a continuum, whose overall characteristic properties are somehow altered due to the influence of discontinuities within the mass.

Goodman et al (1968) suggested a method of joint representation which could be incorporated into a Finite Element analysis in order to provide a more faithful simulation for jointed rock problems. In this work, as well as defining the mass properties, different elements were defined for the joints where they passed through the otherwise continuous material. The joint elements were described by their own properties (normal and shear stiffnesses and strength). Several situations were modelled, including a simulated tunnel through a staggered rocky block system. From the results obtained it was concluded that the inclusion of joint elements in an otherwise standard Finite Element computer program provided a method of analysis that adequately handled joints that failed through tension, rotation and shear. Using this modification observations were made of collapse patterns commonly observed in real situations. It was noted that the inclusion of discontinuities in the mathematical model improved comparisons between the model and the prototypes, the results being significanlty superior to those obtained from analytical and experimental methods where a continuum model was used. This work on joints was developed by Zienkiewicz et al (1970) who further modified the joint elements to allow modelling of curved and variable thickness joints. By defining the middle surface of the joint (using a shape function) and then establishing the normal and tangential directions to this surface at the node points, the coordinates of connecting nodes could be established. Several models of mass rock behaviour were

discussed, including a stratified or laminar model and a limited tensile stress model which could accommodate load reversals (previously tensile stresses developed in such analyses were relieved to zero, this implied that no compressive stresses could be developed until joint closure occured). The model permitted stress analysis of more realistic rock configurations, possibly with complex joining properties. The solution of these simulations were obtained from an iterative process whose convergence to the solution was dependent on the proximity of the structure to its failure state. For cases of non-uniformly applied load, it was noted that the stress-strain relationship was not necessarily unique and so special care had to be taken, though the technique was still claimed to be applicable.

A different approach for jointed rock was adopted by Cundall (1971). A computer program was described to simulate a system of "semi-rigid rock blocks" in which the interaction between blocks was governed by friction, contact stiffness and the simple laws of motion. Each block was treated as a separate entity with unlimited translation and rotation possible. The program was dynamic, employing a simple explicit time-marching finite difference scheme, thus enabling progressive failure to be modelled.

Using this technique it was possible to study the effects of joint geometry, joint properties and loading conditions. It was also suggested that rock-bolts and water pressure in the joints could also be simulated.

5.3.3 Granular Models

Although soil is usually treated as a continuum it consists of discrete particles which interact with each other. It would not, however, be feasible to treat soil as discontinua by considering individual particles, in order to provide a predictive tool for Geotechnical analyses. Soil, inspite of its discrete internal structure, behaves en-mass as a continuum and a continuum approach using the Finite Element Method is expected to remain the most universal and economic tool for computer simulation in geomechanics. Such an approach however depends on the validity of the constitutive laws incorporated into the formulation and, to date, no entirely satisfactory constitutive model for soil exists. This is due to the complex macroscopic behaviour of soil which is the result of its internal discrete nature.

It is therefore attractive to attempt to use computer simulation to model the internal deformation processes which may occur in particulate assemblies. In this way a better understanding of the mechanics of particulate

material can be obtained from which it is possible to develop more realistic constitutive laws which may then be incorporated into conventional Finite Element programs.

Serrano and Rodriguez-Ortiz (1973) described a computer program that was capable of generating a model of a granular media according to any given particle size distribution. The simulated soil particles were placed in a random manner, thus allowing natural soil structure to form and then be observed. It was suggested that the assemblies could be simulated using the Finite Element Method in which a stiffness matrix was constructed which took into account the geometry of the assembly and the stiffnesses at each contact. Incremental displacements were determined from the last known forces by inverting the overall stiffness matrix. In order to deal with slip at the contacts, iteration procedures were necessary and only one contact was allowed to slip at a time. A big disadvantage of this approach was that it was necessary to reform the stiffness matrix whenever a contact was made or broken. However, the results were reported as being promising.

Another numerical model for discontinua was described by Trollope and Burman, (1980). Their model for a granular wedge was simulated by a mass of rigid particles, the compliance of which was seen to be governed by the

stiffness characteristics at the interparticle contacts or joints. It was demonstrated that, irrespective of particle shape, the model could be reduced to a lattice-like analogue whose nodes were at the particle centroids. The resulting nodal displacements were determined by the movements associated with the dislocation of each joint or contact. Because of the manner in which the lattice represented mass behaviour as being the result of the composite interactions between adjacent particle centroids it was considered to be a discrete model, and as the model was dominated by the stiffness characteristics, the technique was labelled the Discrete Stiffness Model.

Extending the application of the method previously used for jointed rock, Cundall (1971), Cundall (1978) carried out numerical experiments on random assemblies of discs. The disc assembly could be contained within boundaries that were free to move in any desired manner. The characteristics of the discs and the contacts between discs could be prescribed by the user and there was no restriction on the amount of displacement permitted to the discs.

The method of analysis was called the Distinct Element Method and was described as an explicit numerical scheme in which the interaction of the particles is monitored contact by contact and the motion of the particles modelled particle by particle.

The particles within the assembly could be generated by a built-in random particle generator which could create discs to fill a given area, the discs conforming to any chosen particle size distribution. It was argued that only a simple placement algorithm was needed since mechanical compaction from an initially less dense state was preferable to any scheme that fitted particles closely together by using a non-physical numerical procedure, especially as mechanical compaction often forms the first stage of any physical experiment. The total number of discs that could be modelled at any time was claimed to be 5000 although the maximum number of discs that have actually been used in reported tests is 1000. With such large assemblies it was necessary to make extensive use of graphical output facilities in order to facilitate the interpretation of the results.

Further examples of numerical simulation of random disc arrays were provided by Cundall and Strack (1978), (1979a) and (1979b). In these works the method was used to simulate experiments on photo-elastic discs presented by de Josselin de Jong and Verruijt (1969) and Oda and Konishi (1974). The comparison between the results of the physical tests and those of the computer simulations were used as a validation of the method.

The authors suggested that although the comparison was qualititive, the Distinct Element Method was a valid tool for research into the fundamental behaviour of granular assemblies. Cundall and Strack (1979b) also described a three dimensional version of the Distinct Element Method program which was used to simulate a triaxial test on a Face-Centred Cubic arrangement of spheres reported by Rowe (1962). Comparison with Rowe's experimental results was encouraging.

A more detailed description of the Distinct Element Method will be provided in Chapter Six.

CHAPTER SIX

6. THE SIMULATION OF PARTICULATE MATERIAL USING THE DISTINCT ELEMENT METHOD

6.1 INTRODUCTION

The program published by Cundall and Strack (1978) was specifically designed to assist in the development of constitutive laws for soil. It was intended that such laws would result from numerical tests performed on assemblies of discrete particles simulated on a computer by use of the Distinct Element Method program - "BALL". Features of such a purpose-designed package included the facility for applying force or displacement boundary conditions to the assemblies of particles, which in turn could be specified as having various values of inter-particle friction, cohesion and stiffness. By the use of in-built graphics routines, the mechanisms occuring within the granular assembly during a test could be studied and the results used to confirm or invalidate existing theories and form the basis for new ideas.

6.2 THE REQUIREMENTS OF THE MODEL

The simulation program BALL, (version 1.1) was written specifically to meet the special needs of modelling a

particulate material. Unlike the structural elements of a building, whose relative orientation are often assumed fixed, a granular material (which is capable of being loaded in a variety of ways and undergoing considerable strain) exhibits a greater amount of relative movement between its constituant granules. It is,therefore, necessary for a simulation program to accurately model the conditions which cause such large internal relative movements. This, in many cases, will produce a grain structure that is considerably different from the original internal configuration. To allow for such movements to occur it is necessary to have a sophisticated system of linking information for any individual grain to any other element it might come into contact with, (which in the extreme case is any other element in the assembly), not just its immediate neighbours. To allow for such individual movement (and hence independence) it is necessary to have associated with each grain its own individual grain properties (particle size, density, cohesion and surface friction) as all the grains need not be identical.

It is also necessary to simulate some system of controlling the boundaries of the particulate assembly which may be either stress-controlled or strain-controlled. A common method of deforming elements of soil in the laboratory is to employ controlled boundary plattens which apply a uniform deformation to the boundary of the element. The data structure of such a platten would have to be modelled along similar lines to the material grains, allowing it to

move during a simulation run, while permitting the positions along the platten where it contacts particles to also vary.

To improve the efficiency of information retrieval and data co-ordination so that the program is viable in terms of computer execution time, it is vital that all the relevant information is readily available for each disc and platten.

6.2.1 The Working Space

It is necessary to define a two dimensional co-ordinate system for use in "BALL" and to declare the upper and lower bounds which the computer program has to consider while performing the simulation. The program is set up to accept the maximum width and height that the user expects to need. This area can be considered as a physical "working space" in which the elements of the simulation can interact. The lower left corner of the working space is implicitly taken as the origin of the resultant co-ordinate (X,Y) system. On this working space the program user specifies the size of grid that is required and this is then set up in both the horizontal (X) and vertical (Y) directions. Having divided the working space into the relevant number of boxes to form a continuous grid over the entire working space, the simulation program uses the boxes formed by this grid as an extra reference system. This is used to limit search areas for particles, by eliminating the need to check all particles for possible

contacts (and hence interactions) with the particle currently under scrutiny. The grid thus acts as a rapid reference system for any point or set of neighbouring points on the working space.

6.2.2 Components of the Simulation

Once a co-ordinate system with its grid has been set up, it is possible to define discs and walls (or plattens) which map onto the working space.

A disc is placed so that its centre is at the co-ordinates specified by the user. The disc then occupies the area of working space concomitant with its radius. Where two similar discs over-lap, the contact is assumed to be at the mid-point of the over-lap. To ease reference for such contacts, each disc is mapped into the grid boxes that its circumscribing square covers and a record is kept of which boxes are covered (even partially) by which discs. A similar procedure is followed for the walls (or plattens) of the simulation problem. As each wall is defined its co-ordinates and length, (see appendix B for a detailed explanation of BALL program commands), enable the program to map which grid boxes will be within the bounds of the wall. This information is stored by the program so that a record can be kept of which boxes contain wall elements.

6.2.3 Dynamic Storage

Information and data used in the simulation is stored in one of two distinct forms. Data constants, such as the radii or densities of the different disc types are normally constant throughout any one simulation run, such constant-value data items are stored in various separate arrays. Examples of such constants are: the values of disc radii, the coefficients of disc and wall friction and the normal and shear stiffnesses. However there is a need to have some storage set aside for non-constant data. Such data, which will be constantly liable to access and variation, is referred to as "Dynamic Data" and the corresponding form of storage as "Dynamic Storage".

The data base in which the dynamic information is stored in BALL, is composed of a one dimensional array. This array contains information concerning the co-ordinates of, and the kinematics and out of balance forces associated with, each individual disc and wall. Space in the array string is also reserved for information concerning each of the boxes formed by the grid and some space is maintained for a "Linked-List" (see section 6.2.4) whenever there is a need for additional information concerning the grid boxes.

All the above information is grouped into separate sections of the dynamic data array. The partitions between

sections are indicated by markers which provide a flexibility for expansion or contraction of any section of the array as the simulation proceeds. The structure of the dynamic storage is shown in Figure 6.1, which provides an overall memory map and guide to storage for users of BALL.

As stated above, the information stored in this manner is organised in a one-dimensional array, this saves storage in computer-core and thus minimises the size of the program storage requirement. Sometimes, however, the program requires to place two pieces of information into the same location in the array. This is achieved in the program by the use of the Fortran "EQUIVALENCE" statement. As each array location is implicity allocated two accessable words of storage, these can be either split-up and used individually for holding INTEGER values or combined to hold a REAL number. (See Figure 6.2).

The program is coded so that whenever it is necessary to access a single integer, the whole data-location is equivalenced to an integer array of size two, this then permits either of the integers to be retrieved. For storage purposes and because most of the data in the program is of a REAL type, the dynamic array stores all values as REAL. Thus two integers which occur at one memory position are stored as the equivalenced real number in the computer -

this is usually an apparently meaningless "junk" form of data bits, but because the data is always accessed in the same way (by equivalencing to arrays) these "junk" values become invisible to the computer and are returned to the program in their original form.

6.2.4 Box (or Grid) Storage

As was remarked in section 6.2.2, information is stored in the relevant part of the array storage for all discs or walls which overlap into any box of the grid. An individual section of the dynamic array is allocated to the boxes. Each box has two "words" of storage allocated to it, and there are seven different box conditions that the contents of a box may depict, (see Figures 6.3 and 6.4).

State 1. If there are no discs or walls in a particular box then both words of storage are set to zero values.

State 2. If there is one entry in a box, then the starting address of the data relevant to that particular disc or wall is placed in one word of the box and the other word is set to a zero value.

States 3 and 4. When there are two or more elements in the area covered by a box, it may be necessary to access information for which there would be insufficient storage space in the box-section of the storage array. If there is no contact between the elements in the box, a zero is placed in one word of the storage location

and the address of a "Link" element is placed in the other word of box storage. The link address refers to a data location outside the box-section. At the location given by the address in the non-zero box-word a pointer is set-up. This pointer consists of two words of storage, each containing the starter-address of one of the particles in the grid area.

Should the two elements in the grid area be in contact, then instead of a zero in one word of store, a contact address is inserted. This address refers to the start of a section of data which is set-up to accommodate information pertaining to the contact. This exists outside the area of data allocated to boxes. The starter address refers to the first piece of information relevant to that particular contact. Storage is allocated for information on the shear and normal displacements, and the shear and normal contact forces, in addition to this there is a two word space for the starter address of the two bodies in contact (cross-referenced) and a two word space is reserved for a pointer to another contact - for cases where more than one contact occurs in the same physical grid area of the working space. The second word of box-storage contains the link to the starter addresses for the two bodies in contact - the same as before.

States 5 and 6. For the more complex case where there are three bodies in the same area of box-grid, then one word of store is either a zero (State 5 - no contacts occuring in that box) or the starter-address

of a contact list, (State 6). The starter-address of a contact list has the same function as described above, except this time (more than one contact in a box), the final piece of data in the contact information is a pointer to another contact starter-address. The other word of the box-storage contains a pointer to linking information outside the box-section of storage. The information at the pointer address is made up of two words; one word points to the starter-address of one of the elements in the box, while the other word contains a pointer to another location which in turn contains the starter addresses of the other two bodies in that box.

State 7. The most general and hence most complex situation is where there are many bodies in one box. In this case, the words of storage concerned with that particular box contain a pointer to a contact list and a pointer to the particle addresses. The information at the location given by the particle-address pointer is divided into two words, one contains the starter-address of one of the particles in that box, while the other word contains a pointer to another link. At the address of the link (as given by the pointer), the data is again divided into two parts, one giving the starter-address of a particle, while the other contains a pointer to another link and so on, until the last link is reached, in which case it contains two particle starter-addresses. The algorithm for this section of storage is summarised in Figure 6.4.

6.2.5 Redundant Address Locations

An important feature of the "BALL" simulation program is the way in which it handles the array tidying process. As has been shown in section 6.2.4, information is recorded of contacts occuring in any grid box of the physical working space, however the storage capacity requirements would soon increase excessively if contact data, which was no longer applicable, was preserved in the dynamic array. As contact information is discarded, the storage space becomes redundant and if no facility was provided in the program for the re-use of such storage space, the dynamic array would soon be burdended with excessive amounts of out-of-date or redundant information.

The program BALL maintains two "Empty" lists, these are lists of un-used box-links discarded by the program. Whenever a contact is discarded or a link becomes redundant its address is entered at the top of the relevant empty list. Consequently whenever a contact is created or a link is required, the empty-lists are consulted to see if there is any redundant space in the dynamic array and if any memory is available then the old memory locations are re-addressed and re-used. The empty-lists work as a last in - first out stack and thus ensure that all available space is re-used efficiently before new memory space is allocated.

6.3 PROGRAM ITERATION

To enable the reader to more easily understand the subroutine calling sequence used by BALL, a brief description of the logic governing a typical iteration cycle will be presented in this section and the reader should refer to Figure 6.5 which shows the subroutine calling sequence.

6.3.1 Initialisation of the Data Base

Step (1). On the initial instruction to the simulation program to commence a number of iteration cycles, the program calls Subroutine INIT to calculate the values of the masses, moments of inertia and the normal and shear stiffnesses for all the different particle types (the maximum number of different types of particles has been arbitrarily set to fifty). As part of this initial setting-up process, Subroutine REBOX is called.

Step (2). Subroutine REBOX updates a particle's contacts with walls and dics - and reviews the boxes in which it has entries, by scanning the boxes that should show an entry for that particle. Which boxes to search are dictated by the radius of the particle and the co-ordinates of its centrod. REBOX then calls subroutines SEARCH and UPDATE.

Step (3). Subroutine SEARCH searches the box which it

has been instructed to examine by REBOX. The purpose of this search is to delete any entries for a particle found in that box that should not be there; to insert entries to that box for a particle which should be there, but has not been found; and to call Subroutine TEST if any particle (other than the one passed to SEARCH from REBOX) is found in a box.

Step (4). A call to Subroutine TEST is a dummy call. One of the subroutine parameters between REBOX and SEARCH is a text variable, (in this case BTEST). On being transferred to SEARCH the text value is allocated to the variable TEST. Thus, whenever Subroutine TEST is called from this subroutine, TEST has the value BTEST and consequently Subroutine BTEST is called. This form of call theoretically enables Subroutine SEARCH to call many other program segments. Indeed, later in the execution of the program, it is necessary to use SEARCH for monitoring a wall, in which case the value allocated to variable TEST is not BTEST but WTEST, which tests the properties of a wall.

Step (5). In the current context, Subroutine SEARCH would call Subroutine BTEST. This subroutine is only called when SEARCH finds an object in a box which is different from the particle being considered. BTEST then tests whether the two

elements are in contact, if a contact exists then the starter-address of the object is put into a buffer, (unless it is already there) and the buffer counter incremented. A similar process would be set in motion if WTEST had been called, except that no disc address would be passed to the TEST sub-routine, instead a wall would be examined.

Step (6). Once Subroutine BTEST ends, control is returned to Subroutine SEARCH and then to Subroutine REBOX. The above process (Steps (2) to (5)), is repeated until all the relevant boxes in the Working Space have been examined and when this has been done, Sub-routine UPDATE is called.

Step (7). The function of UPDATE is to use the information stored in the buffer (as mentioned in Step (5)) in order to create new contacts, should they now exist but have not been found - and to re-box any existing contacts that are now in an in-correct grid-box. The number of tasks that this subroutine has to perform is relayed to it by the value of the buffer counter. Before using new space for any additional information that has to be recorded, the re-usable memory list is consulted to see if there is any old-memory space available, and if there is, then the old-memory space is re-used.

Once this process has been completed, control

is returned, via REBOX, to Subroutine INIT. The data base necessary for the simulation to proceed is then fully initialised.

6.3.2 Methodology of the Iterative Cycles

Once a suitable data base has been prepared, it is possible to proceed with the discrete time-marching approach of the simulation. Details of the simple force and motion algorithms have been omitted from the following description so as not to cloud the logic behind the program. The equations are described in detail by Cundall (1978) and shown on the program listing microfiche in appendix C . Figure 6.5 should be consulted while reading this section.

The driver-routine which controls the calculation loop is Subroutine CYCLE, this calls the subroutines which govern disc movement, wall movement and inter-element forces, incrementing the model-time at the end of each cycle.

Step (1). The first task of Subroutine CYCLE is to scan all the discs that have been declared in the Working Space. For each of these discs it calls Subroutine MOTION.

Step (2). Subroutine MOTION calculates the new velocities and displacements for each disc, from the forces and movements acting on it. Once the

new disc velocities, (X-direction, Y-direction, and angular), are calculated, they are stored in the dynamic array in the section set aside for disc information. From the new disc velocities, Subroutine MOTION calculates the new co-ordinates of the disc centres and stores these values as it did the velocities. Having calculated the above information, MOTION checks to see if any disc has moved sufficiently (see Section 6.3.3 for an explanation of the reboxing and contact detection algorithms), to set a flag which indicates it is necessary to re-examine that particular particle - using the REBOX series of subroutines, (explained in Section 6.3.1). Once this check has been made, control is returned to Subroutine CYCLE.

Step (3). Subroutine CYCLE immediately examines the flag which could have been set during Subroutine MOTION, if the flag has been set then the REBOX subroutine is called and action is taken as described in Section 6.3.1. Should no flag be set, then MOTION is called for the next disc and step (2) is repeated until Subroutine MOTION has been called for all the discs.

Step (4). Once CYCLE has finished updating the disc information, it starts to work on the walls. For each wall, CYCLE calls Subroutine WALMOT,

this subroutine updates the position of one wall, (per call to the subroutine), by using the wall velocity, (a user-dependent variable). In a manner similar to that described in step (2), if the wall has moved sufficiently to warrant re-examination, a flag is set and control is passed back to Subroutine CYCLE. On re-entry to CYCLE, a check is made to see if the logic flag has been set, indicating the need for a call to rebox the wall. Should this be necessary then a call is made to Subroutine REBOXW.

Step (5). Subroutine REBOXW has a similar function to Subroutine REBOX, except that it acts on a wall. To aid in the scanning of the grid-boxes along the track of a wall, REBOXW calls Subroutine SCAN.

Step (6). Subroutine SCAN searches the boxes along the length of the wall for entries that indicate the wall's presence. To do this it calls Subroutine SEARCH but sets the text parameter to WTEST, thus indicating that a wall is the subject of the investigation. Subroutine SEARCH acts in the same way as described in Section 6.3.1, but on calling Subroutine TEST, this time it is really calling Subroutine WTEST. After SEARCH has returned control to SCAN, SCAN calls Subroutine UPDATE to create new contacts and rebox any existing ones where

necessary - as described in Section 6.3.1.

Step (7). Once all the walls have been processed as described in steps (4) to (6), Subroutine CYCLE proceeds to examine all the contacts, both disc-to-disc and disc-to-wall. To do this the dynamic array is accessed at the pointer which indicates the start of the section which contains the data for the boxes. The boxes are scanned to find those with no more than one element, (either disc or wall), in. For such a box, Subroutine FORD is called.

Step (8). Subroutine FORD calculates the forces at a single contact. In this routine the stiffnesses of the particles are assumed to act in series and if the two particles have differing cohesion or frictional values, then the smaller value is used in the calculation. Once the interparticle forces have been calculated, they are put into the disc information section of the dynamic array and control is returned to CYCLE.

Step (9). Where there is more than one contact in a single box, the information is linked as described in Section 6.2.4 - in this way all interparticle forces are accounted for and calculated using Subroutine FORD.

Step (10). Steps (1) to (9) describe the basic algorithm for one iteration cycle. There is a loop within the CYCLE subroutine which allows the total

iteration-sequence to be repeated as many times as requested by the simulation user.

6.3.3 Contact Detection and Reboxing

The maximum distance a disc can move in both the X and Y directions before a contact search and reboxing check is initiated is one unit, whereafter the integer value of the relevant co-ordinate must change. In many cases a search is activated before such a distance is moved. For the extreme case of unit movement in both directions, by both discs forming a contact, the incremental movement between discs is $2\sqrt{2}$ units. This figure is arrived at by doubling the hypotenuse of a right angled traingle of unit base length. In the simulation, a constant is set to this extreme value and all particles within this distance of each other are assumed to be potentially in contact and space is reserved for such contacts. A potential contact does not contribute any force sums to the particle until the distance between perimeters falls below zero.

When the integer part of either the X or Y co-ordinate of a disc centroid alters, the REBOX series of subroutines is called for that disc. Subroutine REBOX examines the boxes that have entries for that particular disc and determines if the box entries are still correct. If the box entries need altering then REBOX creates and deletes entries as necessary. Similarly, Subroutine REBOXW governs

the monitoring of boxes for a wall when it has moved sufficiently to change the integer value of one of its co-ordinates.

The use of such a simple reboxing trigger-mechanism places some restrictions on the co-ordinates that can be used efficiently, but while doing so it saves a considerable amount of memory, as old co-ordinates do not have to be stored and compared with current ones for a number of cumulative movements. Cundall (1978) comments on the effiency of such a co-ordinate system approach and concludes that while the actual co-ordinates used for Work Space will not affect the statics/dynamics of a particular simulation, the choice of co-ordinates will have a bearing on the degree of efficiency achieved by the simulation. The extent of such effects would depend on the relative radii of the discs. Cundall illustrates this point by saying that large radii will lead to smaller memory requirements, (contact space will only be allocated to discs which are then relatively close to each other), but that there will be a corresponding increase in execution time as reboxing and up-dating would have to be performed more frequently. Alternatively, the use of smaller radii would lead to higher memory requirement - as contact space will then be reserved for relatively distant neighbours, but a corresponding lower execution time is used, (as reboxing and up-dating will be less frequent).

It is apparent that in such a situation, it is the responsibility of the individual user to assess the capabilities of the computer, on which the simulation program is to be mounted and to specify the co-ordinates in a manner which will lead to the optimum use of both machine time and storage.

SYMBOLS M1 TO M5 ARE THE POINTS WHICH INDICATE THE STARTER ADDRESSES OF EACH DATA GROUP

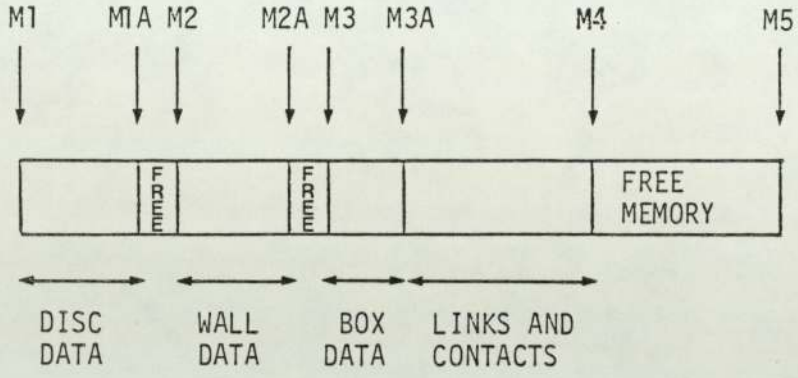

FIGURE 6.1 DATA STORAGE IN THE DYNAMIC ARRAY

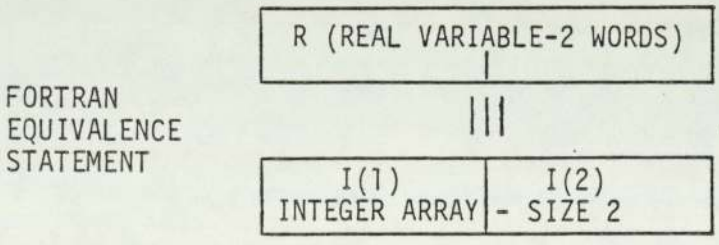

FIGURE 6.2 COMBINATION OF TWO "INTEGERS" INTO A REAL VARIABLE

(AFTER CUNDALL 1978)

(AFTER CUNDALL 1978)

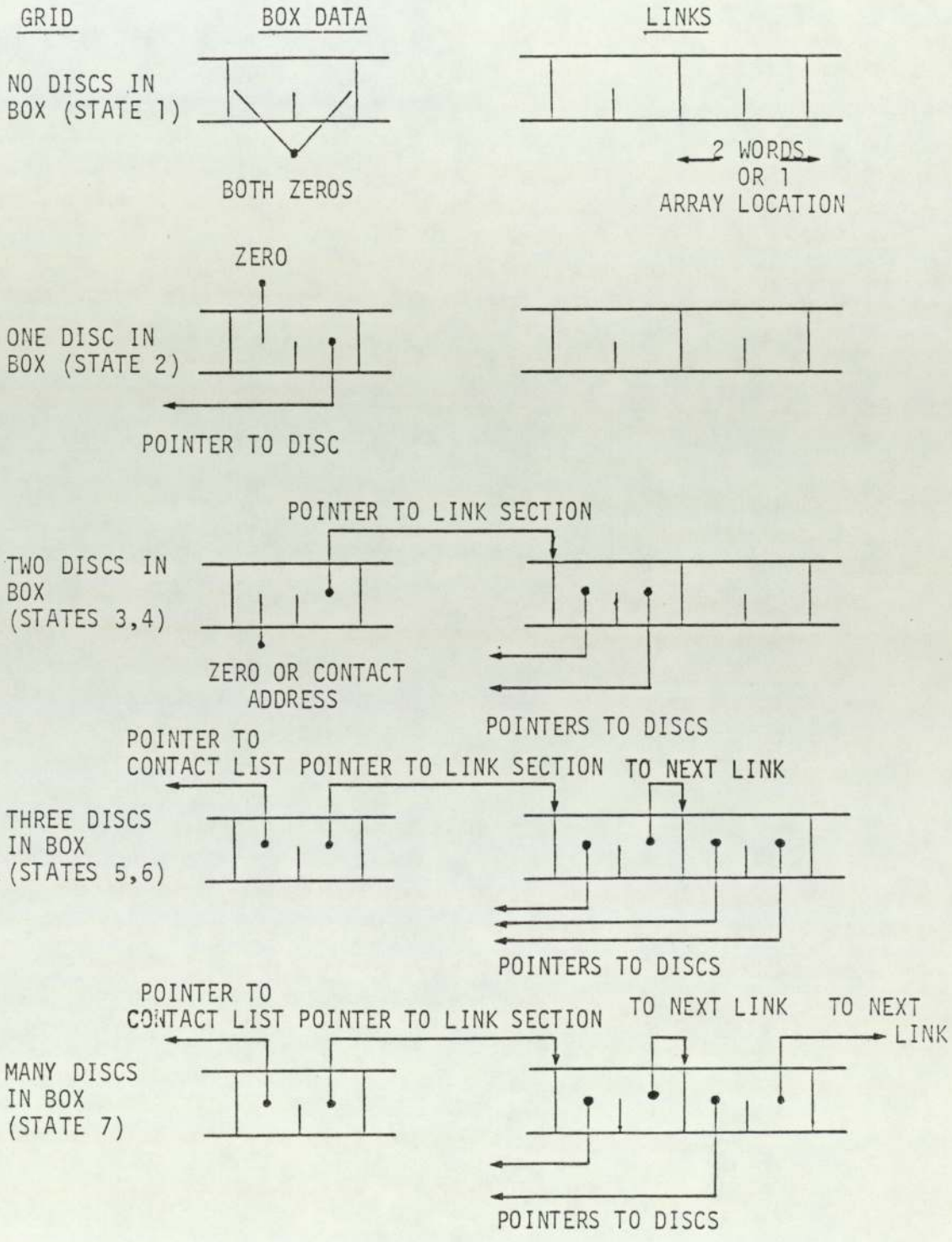

FIGURE 6.3 DATA STRUCTURE WITHIN THE DYNAMIC ARRAY SHOWING THE INTERACTION BETWEEN BOX AND LINK SECTIONS

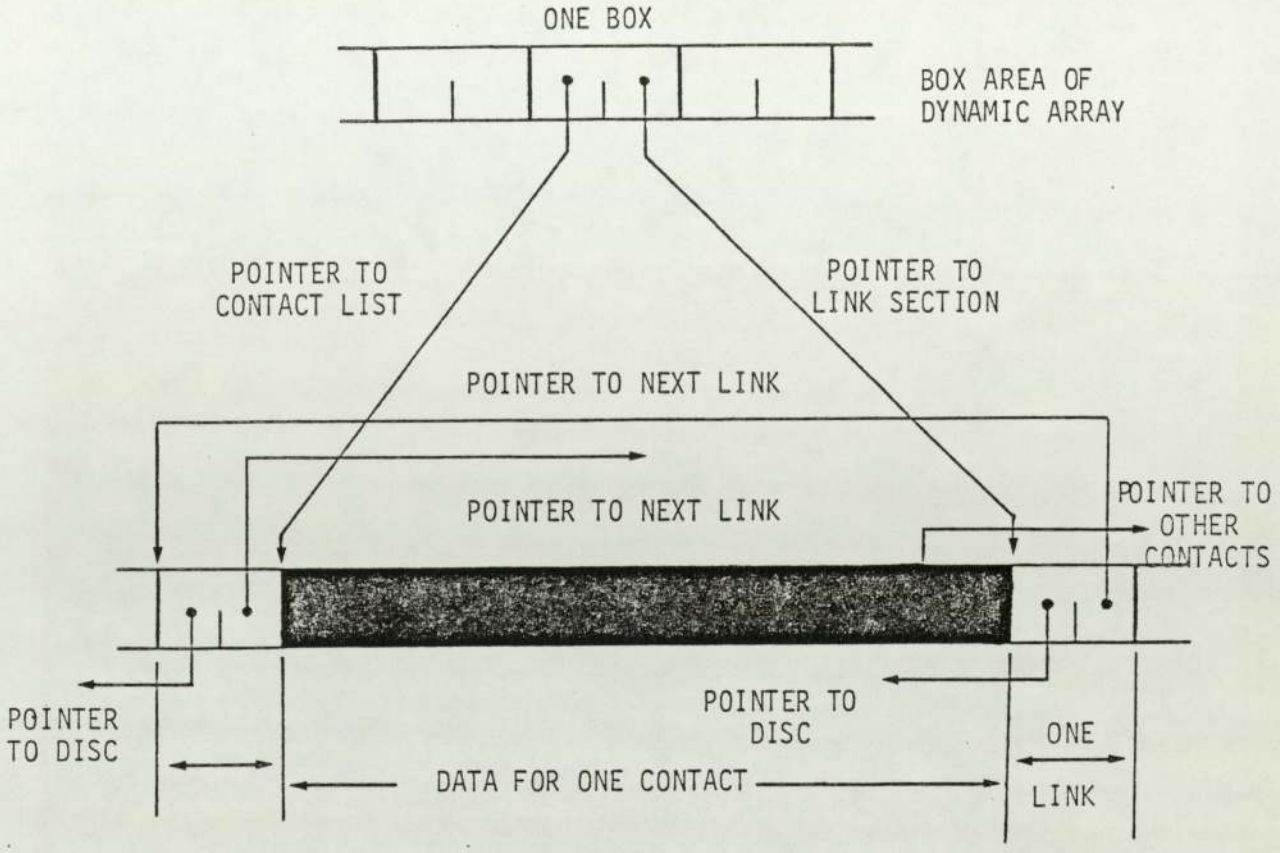

PART OF THE LINK/CONTACT AREA OF
DYNAMIC ARRAY

KEY TO CONTACT DATA

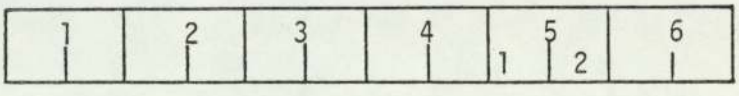

1. NORMAL DISPLACEMENT
2. SHEAR DISPLACEMENT
3. NORMAL CONTACT FORCE
4. SHEAR CONTACT FORCE
5. ADDRESSES OF THE TWO PARTICLES IN CONTACT
6. POINTER TO NEXT CONTACT

(AFTER CUNDALL 1978)

FIGURE 6.4 DIAGRAMS SHOWING THE RELATIONSHIPS BETWEEN BOXES, CONTACTS AND LINKS IN THE DYNAMIC ARRAY

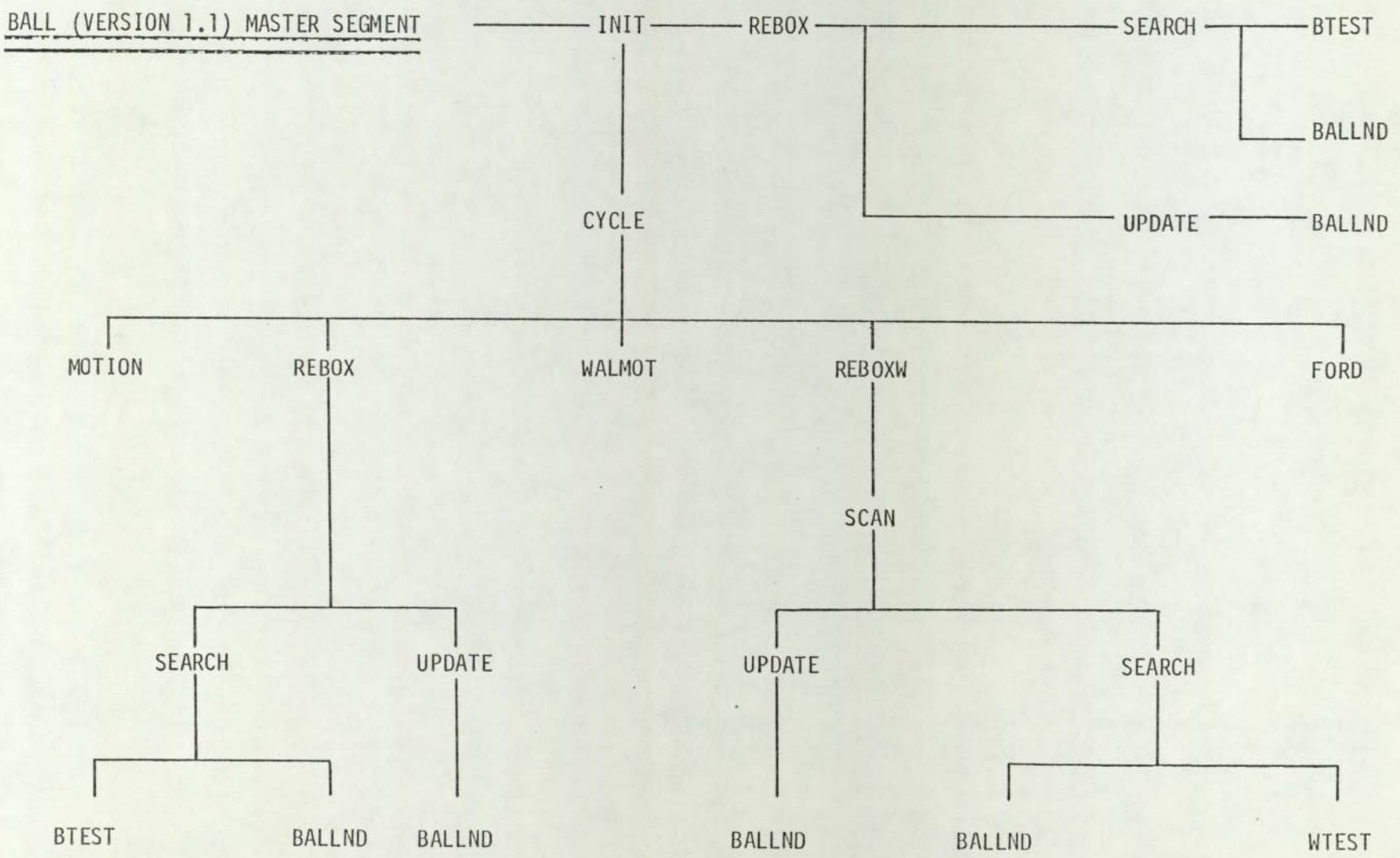

FIGURE 6.5 ITERATION SUBROUTINE TREE

CHAPTER SEVEN

7. IMPLEMENTATION OF THE SIMULATION PROGRAM

7.1 INTRODUCTION

The correct functioning of any computer program is dependent upon the system on which it is run. Therefore when moving a program from one computer system to another it can be expected that a number of alterations will have to be made; the number and extent of these alterations depending on the differences between the original and the proposed computer systems. Once the requirements of the new system have been identified, the necessary alterations made, and the program successfully run, it is then possible to modify the program so that it may, more efficiently, fulfil the reason for its implementation.

The computer program "BALL", version 1.1, was originally set up on a PDP 11/45 and an Interdata 8/32. After consideration of the computing facilities at Aston, it was decided to initially implement the program on the ICL 1904S available there but due to the computing resources needed to develop the simulation, it later became necessary to again transfer the program, this time to the CDC 7600 computer at the University of Manchester Regional Computer Centre (UMRCC). The process for the

implementation of the "BALL" simulation program on the available computer facilities is described in this chapter together with a description of the modifications made to the model.

7.2 COMPILATION AND EXECUTION OF "BALL"

Compilation of a computer (source) program is the process whereby instructions written in a programming language are converted into Machine Code. The resulting (object) program can then be read and acted upon by the computer. In order to produce the object program the Compiler translates each language statement into its Machine Code equivalent. Only a program that is grammatically correct can be successfully compiled. Any syntactical errors in the program will be detected by the Compiler.

The original version of "BALL" was written in PDP-11 FORTRAN (known as FORTRAN IV PLUS), this conforms to the American National Standard Institute (ANSI) FORTRAN IV specifications, as does 1900 EXTENDED FORTRAN which is used on the ICL 1904S. For this reason, the majority of the program instructions were common to both languages, changes only being necesssary where the two dialects fail to overlap.

7.2.1 Alterations necessary for compilation

"Ball",version 1.1, was set-up originally on a PDP 11/45

(Dames and Moore, London) and on an Interdata 8/32 (University of Minnesota). The program was written for byte-orientated machines, that is, machines in which memory "words" are composed of multiples of 8 bits. In order to use this type of memory most efficiently, all addresses and pointers were assumed to be 16-bit quantities. By implication, this limits the size of the Dynamic Array (see Chapter 6) to 32,767 elements, which is the largest number that will fit into 16 bits. By contrast, on the ICL 1904S, which uses 24-bit words, the largest integer number that can be stored is 8,388,607.

In order to optimise the use of memory all addresses and pointers used in the original versions of the program were assumed to be 16-bit quantities and the dynamic array was structured to allow two 16-bit words to share the memory of a two-word "dummy" variable. This was achieved on the PDP11 using a FORTRAN "EQUIVALENCE" statement in the following manner:

```
INTEGER*4       IAL
INTEGER*2       II
DIMENSION       IL(2)
EQUIVALENCE     (IAL,IL)          ...(7.1)
```

In the above FORTRAN coding, the two 16-bit words of array "IL" share the same memory locations as the 32-bit variable "IAL". Although different computers use different conventions for storing such two-word variables,

the internal arrangement of variables, in such cases, is transparent to the program provided that the variables are transferred between 16 and 32 bit variables using EQUIVALENCE statements only. The terms INTEGER*4 and INTEGER*2 refer to the number of bytes allocated to the variables in PDP11 FORTRAN. This facility, however, is not available in the ICL 1900 EXTENDED FORTRAN. Thus, since the ICL 1904S is a word-orientated machine, it was necessary to permit some variables to be twice the bit length of others. This is achieved by using the declarations INTEGER and REAL. Under such circumstances INTEGER variables consist of one 24-bit word of storage while REAL variables consist of two 24-bit words. (This assumes that the statement "COMPRESS INTEGER AND LOGICAL" has been used in the program desription segment of the ICL 1904S job). The revised coding suitable for the ICL 1904S is:

```
REAL          IAL
INTEGER       IL
DIMENSION     IL (2)
EQUIVALENCE   (IAL,IL)                    ...(7.2)
```

It is apparent that this particular aspect of the simulation program will not be adversely affected by transferal to the ICL 1904S. In fact the transfer will result in greater accuracy (more bits allocated to each word of storage) whilst at the same time the underlying

logic, on which the program is based, has been retained.

Another major difference between the two FORTRAN dialects is the way in which they deal with "TEXT" data. A TEXT-type quantity is a string of characters. FORTRAN contains only a limited text handling capability. The manipulation of variables or array elements holding TEXT values must be performed by compiler-dependent character handling routines. In the original program, TEXT is inputted one record (80 characters) at a time. The first four characters of a record are converted to ASCII (American Standard Code for Information Interchange) format, by using an "ENCODE" statement, and allocated a variable name. This variable is then tested for equality to various TEXT constants by using a "logical IF" statement. For example, consider the following PDP11 FORTRAN statements:

```
      DIMENSION            LINE (80)
      READ (1,500)         LINE
  500 FORMAT               (80A1)
      ENCODE (4,6,ALINE)   (LINE (I), I=1,4)
    6 FORMAT               (4A1)
      IF (ALINE.EQ.4HREST) GOTO 10              ...(7.3)
```

This declares an array (LINE) of eighty elements. Eighty TEXT characters are then read into the array "LINE". The first four of these characters are converted into ASCII code and are contained in variable "ALINE". A "Logical IF" is then performed, which compares the contents of

"ALINE" with the TEXT string "REST", control being passed to Label 10 should the comparison show that the two are identical. Such an "ENCODE" statement facility was not available on the ICL 1904S and so an alternative coding was required, this is given below:

```
          DIMENSION    LINE(20)
          DATA   IREST/4HREST/
          READ   (1, 500) (LINE (K),K=1,20)
      500 FORMAT     (20A4)
          II=4
          IF  (ICOMP(II,LINE(1),1,IREST,1).EQ.0)
                                        GOTO 10        ...(7.4)
```

This would result in an INTEGER array (LINE) of twenty elements being declared and a TEXT constant (IREST) being initiated with a value "REST". A line of information is then read into "LINE", every element of which would contain four characters. Then, by using an ICL 1900 EXTENDED FORTRAN character routine, "ICOMP", the four characters in the first element of "LINE" are compared with the characters allocated to the variable "IREST". Should the comparison show that the two sets of text are identical then the character routine ICOMP returns an integer value of zero, if not, a value of unity is returned. The returned value is then compared with zero in a "logical IF" statement and if ".TRUE." then control is passed to label 10.

As a great deal of the flexibility of the simulation program

is derived from the use of TEXT strings, it is important to retain as much as possible of the logic surrounding TEXT comparisons. For example all simulation command sequences are initialised by TEXT "KEY-WORDS" which are read from a data-file. The TEXT that is read in is then compared, via a "look-up table" with permissible KEYWORDS and control passed to the relevant section of the program, which is associated with that KEYWORD. In addition to commands issued during a simulation run, (including the command to "STOP" a run), a TEXT input is necessary for the initialisation of all simulation runs. This TEXT value informs the program whether it is to restart a previous set of runs or whether it is to commence a new series. The difference in KEYWORDS directs the computer either to read in a new set of initialisation data, or to consult a Magnetic Tape which was previously written to by a preceeding simulation run. This facility to re-start a previously run simulation, and then continue it, is one of the most important features of the simulation program.

As it was intended to run the modified program as a back-ground job on the ICL 1904S, it would not have been possible to interrupt the simulation and interrogate it, mid-run, without abandoning the whole job. The "RESTART" facility, once implemented, enables a run to be set in motion and then halted so that an inspection can be made of the progress of the simulation. Once inspected, the run can then be RESTARTed and the modelling parameters

altered, if required.

The comprehensive graph-plotting subroutines incorporated in the original program were unable to be implemented on the plotting device connected to the ICL 1904S. This meant that compatible graph plotter commands had to be substituted for the original ones. The alternative graphics routines were provided using the GINO graph plotter library facility. One advantage of GINO is its portability to other Universities which have an ICL 1900 series computer.

Due to the inherent slowness of the operation of the graph plotting process, the computer would be very inefficiently used if the plotter was controlled directly from a users program. Instead of directly controlling the plotter, therefore, the plotting codes for pen and paper movements that are generated by a program are output to a filestore file. On completion of a program, the file containing the plotting codes is accessed by a special "System Program" to produce the actual graphical output. This operation occurs sometime after the originating program has been processed. In this way the slow speed of the graph plotter does not slow down the rate at which the computer can process the simulation.

7.2.2 Execution of the Simulation

The program "BALL" requires a considerable amount of

computer core and execution time. In order to ensure that the simulation is completed relatively quickly on an already partially congested time sharing multi-programming system, it is important to understand how the computer system works so that jobs can be submitted in the manner most beneficial to the rapid processing of the simulation.

Because of its availability, the ICL 1904S (at the University of Aston in Birmingham) is a heavily used computer. In order to optimise the efficiency of the running of the computer, jobs are started in an order which makes the most efficient use of the system. This ordering is carried out by a part of the Operating System known as the High Level Scheduler. This requires information about each job, such as the amount of core storage, the execution time required by the job, and its priority. This information is supplied by the user, as each job is submitted, in the form of a Job Description parameter. The jobs are then streamed into one of four categories (A to D) depending on the Jobtime and core size. A job that requires a short running time will be directed into the 'A' stream, while a job needing a large amount of core and/or execution time, will be directed into the 'D' stream.

Jobs in streams 'A' and 'B' are permitted to run 24 hours a day, while the running of stream 'C' jobs is limited

to between 17:00 hours, and 08:00 hours. The largest jobs, those in stream 'D' are only run between 22:00 hours and 08:00 hours. The order in which jobs are run, within the stream limitations, is determined by each jobs individual Index value. This is dependent on the user's previous usage of the computer, the number of shares allocated to that user and the priority which that user attaches to the job. Jobs submitted with a high priority can get through relatively quickly but will adversely affect the turnaround of subsequent jobs of that user. Both index schemes (users index and job index) are subject to an exponential time decay; thus a user may compensate for a high index by not using the user number, or a job with an initially high index will achieve a lower index if it remains in the job queue for a long enough period of time. Before deciding on the approach to adopt towards the job queuing system, it will be beneficial to study the operation characteristics of a typical "BALL" simulation run.

The rate of program execution is referred to in disc-cycles per second. For example, if the program was operating at 100 disc-cycles per second, an execution time of 5 seconds would be sufficient for an array of 50 discs to be simulated for 10 full calculation cycles. An execution speed of typically 150 disc-cycles per second was obtained from the program when it was working on the ICL 1904S, but this rate of calculation is dependent on what tasks are required of the simulation (graphical output, disc information printout, alteration of operating

conditions, etc.). As a typical simulation run requires about 60,000 simulation cycles, an eighty six disc array (as used in part of this work) will require an execution time of approximately 34,400 seconds (or about 9.5 hours) for the calculation cycles alone. An approximation of about ten percent of this time should be added-on for the production of graphical output and information printouts. It is thus necessary to run the program over a series of jobs, rather than as one big run; (maximum job-time in 'D' stream being 3600 seconds). How many jobs depends on the stream in which the user intends to run the simulation. Typically, on the available installation, it was found that a complete, adequately tabulated and illustrated simulation experiment would take:

either	11	stream 'D' jobs
	47	stream 'C' jobs
	126	stream 'B' jobs
or	629	stream 'A' jobs

As the processing time for running 'C' and 'D' stream jobs was so restricted, it was decided to run the simulation in the 'B' stream. As shown above this requires the running time of 126 jobs; the ability of the program to stop and be restarted is consequently very important. The program writes to a Magnetic Tape file when it has finished the individual job execution and this file is retained in backing store until it is called up as data for another program run. The nature of such a procedure is that a

Magnetic Tape File must be written to and closed, before it can be recalled and opened. Thus the seperate jobs, that make up the whole simulation run, must be run sequentially rather than concurrently.

On some multi-programming computer systems this could lead to problems as it is possible that more than one of the simulation jobs could be loaded into core at the same time; thus they would both use the same "Restart" files, perform the same calculations, output the same results and possibly cause problems to the next job to be run. Fortunately the High Level Scheduler on the ICL 1904S is set-up so that it allows only one job from a user to be run at any one time.

Ten hours of computing time is quite considerable, especially when it has to be obtained in competition with other users. When running at maximum capacity, the central processor can deal with four 'B' stream jobs in core, thus for the optimum turn-around time, the simulation user has to aim at monopolising one channel of core for the full required time. Even if this was possible, it would still take longer than ten hours to run the program; this is because the ICL 1904S is a time-sharing system. This effectively means that even though a program is in core, so are three others from different users. While work is in progress on one of these programs, the others are being ignored. The program being used alters when an 'Interrupt' is generated. This can be caused by a number of events, typically an Input/Output request or Time slice exceedence. When an

interrupt is encountered, transfer is effected to another program in core, thus not holding up the relatively fast Central Processor with a relatively slow peripheral request. By processing jobs in discrete modules, it can be seen that just because a job has a scheduled execution time of 300 seconds, it is probable that the length of run-time needed will be considerably greater. It should therefore be clear that efficient use of the High Level Scheduler will permit the simulation test to be completed sooner.

7.3 MODIFICATIONS TO THE MODEL

Although the "BALL" simulation program had already been used in connection with random arrays, with the limited time available (program"Ball",Version 1.1 became available in October 1979), it was decided that it would not be realistic to contemplate a thorough examination of the behaviour of random assemblies. Since the current work had been concerned with regular arrays (Part 1 of this thesis), it seemed logical, since the published use of "BALL" in connection with regular arrays was minimal, to apply program "BALL" to regular arrays in this research project. In addition, it was thought that the experience gained in the use of "BALL" on regular arrays would be beneficial to the future application of random packings. Consequently this aspect of the research is to some extent an exploratory investigation into the use of "BALL" as a simulation technique to investigate the behaviour of particulate systems.

The necessary modifications to the existing program are described in this section.

7.3.1 Initialisation of the assembly

The original method of creating discs meant that the co-ordinates of the centroid had to be declared and a command issued to create a disc. This logic has been retained, but as the modified program was to be used to simulate regular packings, it would be beneficial to have a section of the program generate the disc centroids from information given to it concerning the number of rows and columns of discs required. This not only avoids possible user-errors, but also cuts the number of read statements necessary to set up the total packing (and hence reduces the number of interrupts - see Section 7.2.2). Such an algorithm ensures that even very small overlaps, or gaps, are avoided. The algorithm governing this piece of programming is shown in Figure 7.1, which illustrates the way in which the co-ordinates are generated for any arbitrary number of columns, rows and disc radius inputted by the user. Although this refinement may appear to be trivial, its effect on possible interrupts is such that it can significantly affect the initial job run-time.

7.3.2 Boundary Control Facilities

Having created the disc assembly, the next step is to simulate a hydrostatic stress applied to the boundaries

of the array. To do this it is necessary to apply discrete forces to all boundary discs. This is done in the program by setting up two arrays (one for horizontally constrained discs and one for vertically constrained discs). The first element contains the number of discs constrained, the other elements containing the starter addresses of the constrained discs.

When the assembly has been consolidated under the desired hydro-static stress the plattens are then introduced. To avoid wasting computer time, the initial wall description was automatically related to the position of the four corner discs after consolidation. The algorithm is contained in Figure 7.2.

In the original version of "BALL", all the discs are free to spin if and when they want to. Spin is naturally restricted at a wall interface, but no similar restrictions existed for stress-controlled boundaries. Since laboratory samples of soil are normally contained within flexible rubber membranes which provide restraint on the boundary particles, it was decided to incorporate a general particle spin restraint option. In this way it is possible to deny some, or all, of the discs the freedom to rotate. The spin-constraint array is set-up in a similar manner to the horizontal and vertical constraint arrays, already mentioned. There is, however, a special case for the spin constraint case, namely the condition where all the discs are required to be irrotational (instead of, say, merely the boundary ones). In this case there is no need to feed

in the starter address of every disc, instead a default value (in excess of 1000) should be allocated to the 'disc-number' element. The value of this element is tested later in the program and the necessary action taken then. This avoids the need for an iterative process dealing with each disc in turn; instead a flag is set which re-routes the execution through a part of the program which allows no particle spin. Spin restraint is useful for dealing with problems involving boundary effects on the outer discs.

7.3.3 Iteration of the Test Process

After consolidation, the assembly was to be loaded in shear with the hydrostatic stress constraint. Under these conditions the discrete forces used to simulate the hydrostatic stress are dependent on the current dimensions of the array. Originally there was a command "CYCLE" which simply called subroutine CYCLE and performed the required number of calculation cycles. This did not allow for any change in dimensions during the iterations. It was therefore necessary to write an algorithm around the "CYCLE" command. This calculates the dimensions of the packing before each call to "CYCLE", thus enabling the out-of-balance forces on the discs to be adjusted before each iteration cycle is performed. After each iteration cycle has been completed, the horizontal and vertical out-of-balance force-sums are calculated along with the longitudinal strain (in the direction concurrent with platten movement). This information may be passed to a file, which

subsequently contains all the stress ratios and strain values for the entire test, cycle by cycle, thus enabling the user to study a particularly critical part of the test in detail. This also acts as a check to ensure that the test is not run too quickly. A run that has been performed too rapidly (wall movement) will show oscillations in the stress ratio over a large number of cycles. This whole procedure is then repeated for the total number of iteration cycles requested in the original command input. The algorithm is shown in Figure 7.3.

7.3.4 Contact Summary Option

Discs that have been in contact, but have recently broken contact cannot always be observed from the graph-plots, especially for small gaps in the packing. To overcome this it was necessary to obtain a way of listing the discs in contact, together with the normal and shear forces at the contacts. In the original program there was a command "PRINT" which obtains a printout of certain sections of program storage, the existing options being printouts of disc and wall information. This command was extended to include contact information. In a separate file, a record is kept of the total number of non-zero contacts and the cycle number at which this number existed. The algorithm is shown in Figure 7.4.

7.3.5 Graphical Output Facilities

For simulation runs involving large numbers of cycles, it was decided that it would be convenient to have a regular plot of the disc positions every few thousand cycles. This provides the user with a visual record of what is actually happening to the discs. While such plots are of little use quantitatively, they are useful in assessing the state of the simulation run, as it is easier to scan pictorial output for information than it is to study large numbers of tabulations. While the original program needed individual PLOT commands for each plot, it was decided that an automatic plot should be set up, whereby the program generates plot information without the need for a PLOT command. The piece of programming necessary for this was inserted in CYCLE, the plot interval being supplied to the program via a single PLOT request in the command data. (See Appendix B for a list of the various simulation commands). At the same time, a facility for selecting alternative forms of output media (for example micro-film or microfiche) was incorporated.

On entry into the plotting subroutine the output option is checked and the relevant type of plotting file initialised. The algorithm for the plotting subroutine is shown in Figure 7.5. This subroutine is entered everytime a call is made for graphical output. Standard GINO-F routines are used for the instructions to draw lines and characters.

The plotting subroutine determines if the current call is the first one in a job run. If the current call is the initial one, then this subroutine opens the relevant type of graphical output file and then declares the plot scale and the origin of the co-ordinate system used in the graphics system. The character size is set to the scale of the plot and then an iteration is performed which takes each disc in turn, accessing the information stored in the Dynamic Array, obtaining the co-ordinates of the disc centroid. A circle is then drawn (radius scaled down) at the corresponding location of the disc. A counter is incremented and the process repeated. When this has been performed for all the discs, a similar sequence of events is followed for the walls. In order to provide a clear indication of movement and relative position, the working space grid was superimposed in a different colour, on the plot. As a means of reference and to make post-simulation examination of the plots easier, a title informing the user of the total number of cycles performed when the plot was produced, was also added.

7.3.6 Command Value Abstraction

A seemingly over-complicated feature of the original simulation program, was the way in which commands, once read in, were directed to a parsing subroutine to abstract the associated data values. Originally, a TEXT

comparison was performed between the first four letters of the command word and the KEY WORDS in the LOOK-UP table. Once the correct keyword was established, a ten digit integer number was associated with the command and control passed over to Subroutine PARSE. This subroutine deduced from the ten digit number how many arguments were to be expected with the keyword and their type. The subroutine compared the line of data read in as TEXT with the keyword (ignoring any number of blanks and commas) and then associated the dummy variables with the relevant types of argument. In this way a single TEXT value was read into the program from the command data file, the TEXT was split into individual TEXT variables by using the relevant digit code and then the TEXT values were converted to REAL, INTEGER or ALPHANUMERIC values, as stipulated by the digit code and allocated to dummy variables to be fed back to the calling subroutine.

This subroutine used the functions ENCODE and DECODE available on the PDP 11/45 to transform data from and to ASCII code. Such a subroutine, while being very "user-friendly" in terms of data handling, seemed over-complicated and was not feasible on the available computer. Instead, free-format input statements were used. The algorithm describing the logic of this modified section of the program is shown in Figure 7.6. This shows that the concept of a command/look-up table comparison is retained, but instead of an integer code being passed across to PARSE, the keyword number is

transmitted. This number is used in a computed GOTO statement to direct control to that section of PARSE which contains the appropriate READ statements. The command values are allocated to dummy variables and control is then passed back to the calling routine. The keyword number is used again in a computed GOTO, this time to direct control to the relevant part of subroutine NEXT. The dummy variables are then used in this section and upon completion of the command, control is passed back to the start of the subroutine, ready for the next command to be read in. This has the advantage that it is easier to follow the logic, easier to modify for implementation of additional commands and has greater portability between different computer systems.

7.3.7 Input/Output Channel Allocation

The allocation of channel numbers is very much a machine dependent arrangement, but for completeness the channels used in the modified simulation program are as follows:-

1:	Input File	6:	Void
2:	Output File	7:	Plot File
3:	Total Contacts File	8:	Wall Force History File
4:	History File	9:	Complete Stress-Ratio/ Strain Record File
5:	Stress-Ratio/Strain Summary File	10:	Restart File

The Input File contains a sequence of commands, (as given in Appendix B), it is this file which dictates

the operation of the simulation.

The Output File acts as a logging device, it echoes all input commands and is the main output channel for the program.

The Total Contacts File, is a tabulation of the total numbers of non-zero contacts at the end of each complete set of calculation cycles.

The History File contains a periodic dump of all wall variables. This file can be accessed by post-processor programs to plot stress-strain curves.

The Stress-Ratio / Strain Summary File contains the stress-ratio and corresponding strain at the end of each set of iteration cycle commands.

The Plot File is the channel to which all plot commands have to be written, due to the off-line nature of the graph plotting device.

The Wall Force History File is really a dummy file, it was used as a monitoring file during the calibration stage of the model and is now retained as an empty file.

The Full Stress-Ratio/Strain Record File is similar to the Stress-Ratio / Strain Summary File, except that it contains the state of the simulation, calculation cycle

by calculation cycle. This file tends to be a very long one and because of this, the file option is normally unused.

The Restart File is overwritten by the program whenever it reaches a normal exit state and is used to restart the program from the point at which it stopped.

7.4 TRANSFER OF THE SIMULATION PROGRAM FROM THE ICL 1904S to the CDC 7600

Because of the arrangement of the ICL 1904S services available, it became apparent that for larger tests (more discs, bigger strains or both), the machine time needed for a reasonably well documented simulation experiment would cause a great deal of inconvenience to other users. After performing several such experiments, it was recommended that the program should be transferred and run on the CDC 7600 at Manchester. Due to the time restrictions necessary for such a move, the alterations to the program were kept to a minimum, although the CDC 7600 did offer some interesting Fortran extensions.

The use of linked lists in the simulation (as described in Chapter 6), requires the facility to compress two INTEGER variables into one REAL variable location in the Dynamic Array. On the ICL 1904S it is possible to compress INTEGER variables so that they occupy one word

of storage only and as REAL variables are allocated two words, the system of linked lists works adequately well. On the CDC 7600 however, both INTEGER and REAL variables are allocated one 60-bit word of storage. To circumvent this, it was necessary to use DOUBLE PRECISION variables for the Dynamic Array. This, naturally, increased the memory requirements of the program; since DOUBLE PRECISION variables are allocated two 60-bit words of store. However, the storage available at UMRCC on the CDC 7600 is far greater than that on the ICL 1904S, (64K words of Small Core Memory and 250K words of Large Core Memory) and so no memory difficulties were encountered.

One feature of the CDC 7600 is the speed in which it executes jobs. A simulation run (one job) at Aston on the ICL 1904S typically took twenty times longer to execute, thus by submitting a job of an allocated executable time of 1280 seconds (the maximum amount of time on the CDC 7600, turnaround usually over-night), it was the equivalent of running 25,600 seconds worth of jobs on the ICL 1904S.

Other available features included: the use of "SHIFT" functions, these effectively allow the storage of values anywhere within the 60-bit word configuration. In this way it would be possible to store four 15-bit values within one variable (or two 30-bit values, etc) as long as care was taken when accessing such values. This could be applied in future developments of the program to reduce

the storage requirements of the Dynamic Array. Another way of optimising the storage of the Dynamic Array is to declare it in a "BLANK COMMON" statement. On the CDC 7600, any such declarations are placed at the end of the program storage area in core. Thus, as the CDC 7600 is not a multi-programming system, it is impossible to damage other jobs in core. Thus, an array in a BLANK COMMON declaration can have a declared size of unity in the program and can be expanded as required from inside the program. This means that there is no need to estimate the eventual size of the Dynamic Array, as has to be done on the ICL 1904S, to avoid "Privalage Violation-Array out of Bounds" types of run-time errors.

Another facility of the Manchester service was the provision of Computer Output on Microfilm or Microfiche (COM), this avoids producing unmanageable quantities of printout and is available for both lineprinter copy and graphical output.

The use of UMRCC facilities is not totally without job time and job size restrictions because the Manchester service is shared by other Universites in the region, each having a percentage share in the system. The total filestore available to the University was approximately 40,000 blocks, a figure that can be exceeded if there is any difficulty with the COM hardware, and graphical

plots are not erased. The total job allocation to the University is currently 1280 job units per day. A 1280 second simulation run would typically use 640 of these units. However it can be seen that running the simulation program to model a whole experiment, (up to 5% strain) can be achieved in three days, at the rate of one run per day, which is a considerably faster, (and more convenient to others), turnaround time than could be expected from other available computers.

```
INPUT              (number of rows, number of columns,
                    disc type, disc radius).
Initialise the Row Counter to a negative number
Initialise the disc co-ordinates (X,Y) to a suitable
          position on the Working Space.  (XSTART,YSTART)
Calculate the horizontal and vertical distance between
centroids (dX,dY)

XSTART=XSTART-dX
YSTART=YSTART-dY
ITERATE FOR REQUESTED NUMBER OF ROWS
   |        Y=Y+dY
   |
   |        Row Counter = - Row Counter
   |        IF (Row Counter -ve) X=XSTART
   |                             and No. of discs in row=
   |                                 No. of columns
   |        IF (Row Counter +ve) X=XSTART + RADIUS
   |                             and No. of discs in row=
   |                                 No. of columns - 1
   |        ITERATE FOR NUMBER OF DISCS IN A ROW
   |            |                X = X + dX
   |            |
   |            |                ENTER EXISTING DISC
   |            |                CREATION ROUTINE, CREATE
   |            |                A DISC AT X,Y
   |            |
   |        END LOOP
   |
END LOOP
INFORM user of number of discs created.
OBTAIN a graphical printout of the disc arrangement.
```

FIGURE 7.1 ALGORITHM FOR AUTOMATIC FORMATION OF A TIGHT PACKING

INPUT starter addresses of corner discs.

SET variables, relative to corner discs, in order to define lower wall.

SET wall counter = 1.

GOTO existing wall definition section.

DEFINE ONE WALL

IF not first wall

THEN ——————→ END OF SECTION

GOTO remainder of Auto-wall definition section.

SET variables, relative to corner discs, in order to define upper wall.

SET wall counter = 2.

GOTO existing wall definition section.

END OF SECTION

FIGURE 7.2 AUTOMATIC WALL DEFINITION ALGORITHM

```
INPUT       (number of cycles, cell pressure, addresses
             of corner discs).
IF          total number of previous cycles is zero
            THEN original height = Y distance between
                 end disc + 2 * radius.
ITERATE     from 1 to number of cycles.
            CALCULATE current packing dimensions.
   |        IF walls are present
   |        THEN current height = distance between walls.
   |        CALCULATE horizontal and vertical forces
   |                  which correspond to the requested
   |                  cell pressure.
   |        SET force sums to zero
   |        IF  there are any Horizontally constrained
   |            discs and if the horizontal force is non-
   |            zero
   |            THEN add in the restraining horizontal
   |                 force to each horizontally constrained
   |                 disc.
   |      IF  there are any Vertically constrained discs
   |          and if the vertical force is non-zero
   |          THEN add in the restraining vertical
   |               force to each vertically constrained
   |               disc.
   |      IF  total number of cycles is zero
   |          THEN  CALL SUBROUTINE INIT \Both routines acting
   |                CALL SUBROUTINE CYCLE \as originally
   |                   (for 1 cycle)      \  specified.
   |      CALCULATE resulting Horizontal and Vertical
   |                force sums on discs
   |      CALCULATE stress ratio and percentage strain
   |      IF printout option flag set
   |         THEN printout stress ratio and percentage
   |              strain
END LOOP
PRINT       iteration successfully completed message
END OF SECTION
```

FIGURE 7.3 ALGORITHM TO ITERATE A SERIES OF COMMANDS

```
SET UP HEADINGS
INITIALISE      contact counter
POSITION        marker at the start of the box
                information (M3) in the Dynamic Array
RETRIEVE        information at marker address <----------+
IF              a contact exists in that box             |
                THEN obtain normal and shear forces <--+ |
                     across the contact and the        | |
                     starter addresses of the objects  | |
                     in contact.                       | |
                     Printout information.             | |
                     Increment the contact counter if  | |
                     the contact is a non-zero one.    | |
                     Check the contact list for other  | |
                     contacts in the same box.         | |
                     IF another contact exists THEN ---+ |
INCREMENT       box counter by one                       |
IF              still in box section of the Dynamic      |
                Array                                    |
                THEN ------------------------------------+
PRINTOUT        total number of contacts
END OF SECTION
```

FIGURE 7.4 ALGORITHM FOR CONTACT PRINTOUT

```
START
IF              this is the initial call
THEN            initialise the appropriate output
                file.  Set the scale and plot origin.
SET             character size
FOR             all discs
                        draw a circle of given scaled
                        radius around disc centroid
                        and insert the disc's starter
                        address.
FOR             all walls
                        determine the wall lengths
                        and positions. Draw them.
DRAW            the grid over the Working Space.
PRINT           the cycle number
START           a new page

END OF SECTION
```

FIGURE 7.5 ALGORITHM FOR THE PLOTTING SUBROUTINE

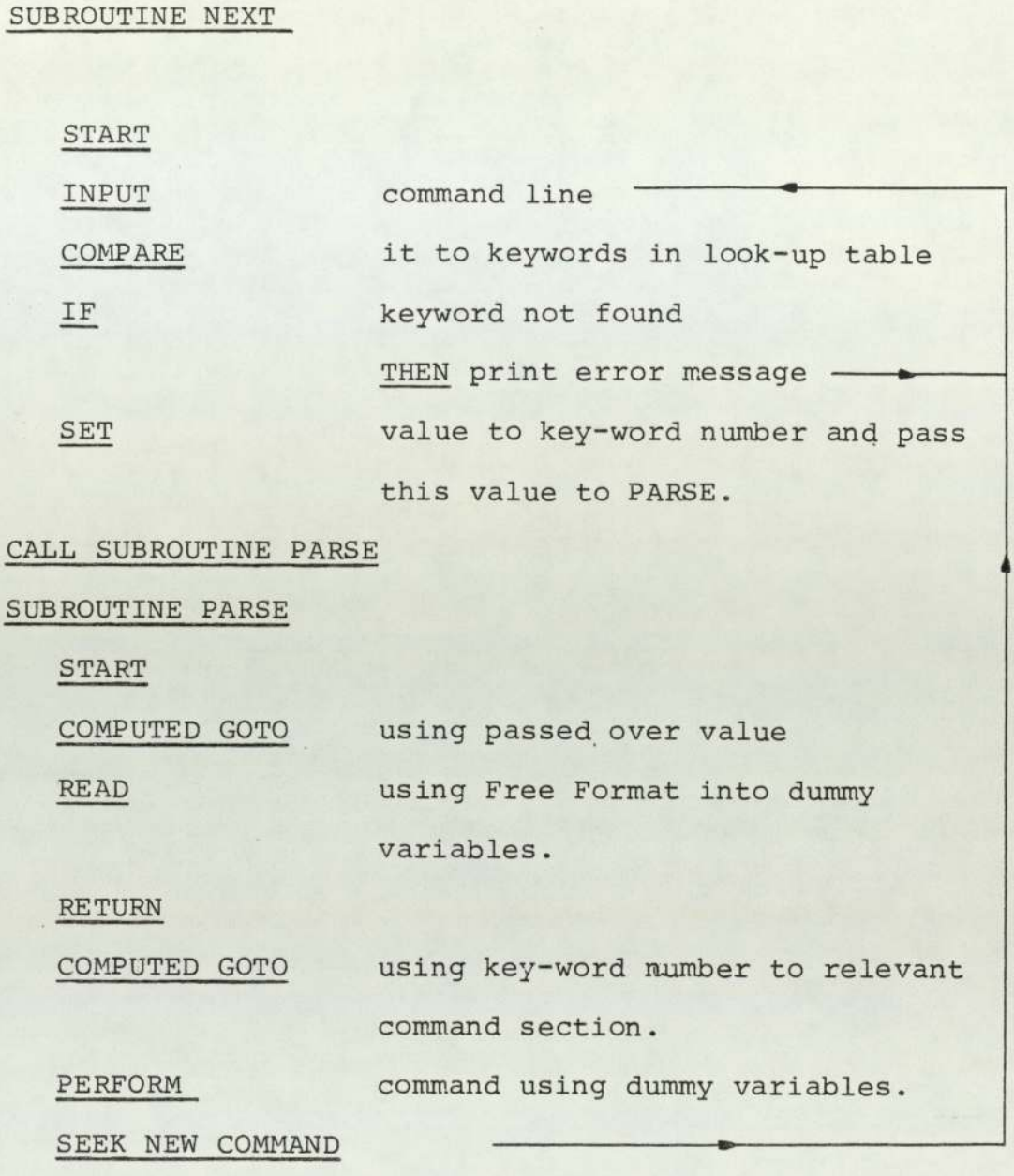

FIGURE 7.6 ALGORITHM FOR READING IN COMMANDS

CHAPTER EIGHT

8. RESULTS OF COMPUTER SIMULATION TESTS

This chapter presents the results of tests performed on various regular arrangements of discs using the computer program BALL. It was decided to simulate a series of biaxial tests in which a rectangular sample (consisting of a regular close packed array of discs) is bounded by plattens on two opposite sides, the remaining two sides being stress controlled boundaries. Stress controlled boundaries were simulated by applying discrete out of balance forces to each of the boundary discs at the beginning of each calculation cycle. As the length of the stress controlled boundary altered, the discrete forces on the discs were adjusted accordingly. For reference purposes, the direction of platten movement is denoted the y-direction and the x-direction is taken to be perpendicular to this, in the plane of the sample. The stress ratio, σ_y / σ_x , consequently refers to the stress on the plattens divided by the constant stress applied to the stress controlled boundaries.

Three main groups of tests were performed, on packings with different numbers of discs - the packing sizes were of 18, 86 and 124 discs. Initially, tests were performed on 18 disc arrays. This small packing has the advantage of being processed relatively quickly on the ICL 1904S computer at the University of Aston (see section 7.2.2). The 18 disc

tests were used to check that the results obtained from the simulation runs were not unreasonable. By altering the boundary conditions and the disc properties, changes were observed on the stress-strain curves that could be directly linked to the changes in the test conditions. The choice of platten velocity was particularly critical to the results and so a number of tests were performed to establish the optimum choice of this parameter.

Having established a suitable platten velocity and examined the effects of various particle properties, further simulation tests were performed on larger arrays to study the effect of boundary conditions on the overall behaviour of the packings. The behaviour of the smaller sample was felt to be disproportionately influenced by boundary effects. On the ICL 1904S computer, the 86 disc packing was chosen as the largest test sample size that could be processed repeatedly in the remaining research time available and consequently tests were performed on this configuration.

Due to improvements in the available computing facilities, it later became possible to transfer the simulation program to the CDC 7600 computer at the University of Manchester. The tests subsequently performed on this computer employed a larger packing size of 124 discs. From the results of these tests, it was possible to study the effects of interparticle slip and gap formation on the resulting stress-strain curves.

8.1 PRELIMINARY TESTS ON 18 DISC ARRAYS

The 18 disc array was generated so as to provide an initial arrangement as shown in Figure 8.1. In order to facilitate reference to individual discs, the data starter-address of each disc (see Section 7.2) was printed within the area occupied by each disc. Because it was not possible to simulate rigid discs, elastic discs of a high stiffness were used. The close packing arrangement of discs was then "consolidated" by simulating a hydrostatic stress acting on the sample. This consolidation was necessary because the internal contact forces (and overlaps) associated with the desired confining stress need to have developed naturally as a result of the simulation technique. Consolidation was considered complete when no further changes occurred in the packing dimensions and the stress ratio had returned to unity. Both top and bottom plattens were then introduced and were located so as to be in contact with the boundary discs (but with no overlaps). With the hydrostatic stress still applied and held constant, the sample was then sheared in compression by specifying equal and opposite velocities to the two plattens. The percentage (engineering) strain in the y-direction and the stress ratio σ_y/σ_x were recorded after each calculation cycle.

8.1.1 Selection of Control Parameters

The simulation model, as already described in chapters

6 and 7, is essentially a dynamic simulation model and as such there can be problems when using it to model a quasi-static situation, due to the resulting motion of the particles. To counter this problem, there is provision in the program for a "damping" of the calculated motions of the elements. This prevents the occurance of vibration of particles in contact (contact damping) and also prevents the particles from moving, as a body, around in the sample area (global damping).

Global damping acts on the velocities of the discs and is introduced into the equations of motion. The effect is similar to having dashpots connecting each particle to its current position. This damping therefore operates on the components of the velocity vectors and on the spin. Contact damping, however, operates on the relative velocities at the contacts. This acts rather like dashpots in the directions of the normal and shear forces at the contacts. The contact damping, in the direction of shear, is not applied when sliding occurs; the damping then is due to friction alone. The contact damping adjustments are introduced into the equations for the out of balance forces.

As explained by Cundall (1978) the damping scheme used requires the input of four parameters, λ_{min}, f_{min}, Im and Ik; where f_{min} is the frequency at which minimum damping occurs,

λ_{min} is the fraction of the critical damping at that frequency and Im and Ik are flags which control the section of parameters in the following damping equation

$$[C] = \alpha[M] + \beta[K] \qquad \ldots(8.1)$$

where $[C]$ is the damping matrix, $[M]$ is the mass matrix, $[K]$ is the stiffness matrix and α and β are constants. If, the flag, Im = 1 then α is set to zero and if Ik = 1, β is set to zero.

The damping parameters used, in the simulations presented here, were $\lambda_{min} = 0.5, f_{min} = 0.5$, Im = 0, Ik = 1 (thus using the global damping option); as used by Cundall (1978) and Cundall and Strack (1979), who remarked that the results they obtained were independent of the values chosen for the damping parameters, for simulations using low platten velocities. A more detailed explanation of the damping systems involved is discussed elsewhere, Cundall (1978), Cundall and Strack (1978).

As the aim of the computer simulation was to simulate a quasi-static test, it was necessary to determine platten velocities suitable for this purpose. Should the platten velocities be temporarily interrupted and cycling continued, then there would be a decrease in the stress on the plattens because some time is required for the damping within the system to bring the discs to equilibrium. This is illustrated

in Figure 8.2 which shows the reduction in stress on the plattens with time, after the platten velocity has been zeroed. It is possible to choose a sufficiently small platten velocity so that such decreases are negligible, however such low velocities require an inordinate amount of computer time to simulate small movements of the plattens. There is a point at which the modelling becomes too expensive in computer time, to justify the small extra precision gained. Equally, if the chosen platten velocity is relatively high - although the required deformation state is quickly attained - the number of extra cycles required, after the platten velocities have been zeroed, would be excessive. There is, therefore, a need to compromise and the decision was made to continuously move the plattens, at a low velocity, with no rest cycles.

The effect of platten velocity on the overall stress-strain behaviour is shown in Figure 8.3. Three tests are illustrated. Two tests, A and B, were performed with continuous platten displacement. A velocity of 0.001 units per cycle was applied in the case of test A and a velocity of 0.002 units per cycle was used in test B. In the third test, C, a velocity of 0.002 units per cycle was applied for 80 cycles and then, with the platten velocity zeroed, a further 400 cycles of calculation time were performed to allow the system to reach equilibrium; this pattern being repeated throughout the test.

It can be seen from Figure 8.3 that the pre-peak behaviour is not affected by the rate of deformation, for the platten velocities chosen. The method of controlling the wall movement does, however, affect the post-peak stress-strain curve. As shown in Figure 8.3, the post-peak stress ratios are lower for the slower rate of continuous deformation, but even lower values are obtained in test C. This indicates that the slower velocity employed in test A was not sufficiently slow as to avoid significant dynamic effects. However, it is clear from the figure that the small amount of precision gained by doubling the calculation time needs to be weighed against the increased cost in computer time. The relatively slow platten velocity of 0.001 units per cycle was used in all the tests on larger samples in this chapter, while the higher platten velocity of 0.005 units per cycle was used in the earlier validation tests on small sample sizes.

8.1.2 Validation tests

Before examining the results of tests performed to evaluate the influence of particle properties, a theoretical analysis of elastic discs - using an approach similar to that used in Chapter 4, will be presented.

Consider the case of frictionless elastic discs in contact. The forces on such a disc are shown in Figure 8.4 (a). To be consistent with the computer simulation the elasticity of the discs may be represented by linear springs acting in the normal and tangential directions at the contacts.

Let the displacements at the contacts be,

$$\delta p \text{ at } P, \ \delta q \text{ at } Q \text{ and } \delta t \text{ at } T \qquad \ldots(8.2)$$

Assuming the stress within the discs to be

$$\sigma_{ij} = \frac{1}{V} \sum_{1}^{n} x_i N_j \qquad \ldots(8.3)$$

Where Nj are the normal forces and x_i are the co-ordinates of the contact points, this can be expanded to give

$$\sigma_{ij} = \frac{2D}{V} \begin{bmatrix} \sqrt{3}/4 & -\sqrt{3}/4 & 0 \\ 1/4 & 1/4 & 1/2 \end{bmatrix} \begin{bmatrix} \sqrt{3}p/2 & p/2 \\ -\sqrt{3}q/2 & q/2 \\ 0 & t \end{bmatrix} \qquad \ldots(8.4)$$

Where D is the diameter of the disc.

or

$$\sigma_{ij} = \frac{D}{V} \begin{bmatrix} 3/4\ (p+q) & \sqrt{3}/4\ (p-q) \\ \sqrt{3}/4\ (p-q) & 1/4\ (p+q)+t \end{bmatrix} \qquad \ldots(8.5)$$

However, for the problem under consideration,

$\sigma_{12} = \sigma_{21} = 0$ as σ_{11} and σ_{22} are principal stresses and therefore p = q. This leads to

$$\begin{bmatrix} \sigma_1 & 0 \\ 0 & \sigma_2 \end{bmatrix} = \frac{D}{2V} \begin{bmatrix} 3p & 0 \\ 0 & p+2t \end{bmatrix} \qquad \ldots(8.6)$$

Which for linear springs, where $p = K\delta_p$ and $t = K\delta_t$ gives

$$\begin{bmatrix}\sigma_1\\ \sigma_2\end{bmatrix} = \frac{DK}{2V}\begin{bmatrix}3 & 0\\ 1 & 2\end{bmatrix}\begin{bmatrix}\Sigma\delta_p\\ \Sigma\delta_t\end{bmatrix} \qquad \ldots(8.7)$$

The strain-increment tensor can be obtained as per Thornton (1979), thus

$$2X_i d\varepsilon_{ij} X_j = (D+2\delta)(D+2\delta)-D^2 \qquad \ldots(8.8)$$

which, at P, gives

$$2\begin{bmatrix}\sqrt{3}D/2 & D/2\end{bmatrix}\begin{bmatrix}d\varepsilon_{11} & d\varepsilon_{12}\\ d\varepsilon_{21} & d\varepsilon_{22}\end{bmatrix}\begin{bmatrix}\sqrt{3}D/2\\ D/2\end{bmatrix} = 4\delta_p D \qquad \ldots(8.9)$$

or $\frac{3}{4}d\varepsilon_{11}+\sqrt{\frac{3}{4}}d\varepsilon_{12}+\sqrt{\frac{3}{4}}d\varepsilon_{21}+\frac{1}{4}d\varepsilon_{22} = 2\delta_p/D \qquad \ldots(8.10)$

Similarly at Q,

$$2\begin{bmatrix}-\sqrt{3}D/2 & D/2\end{bmatrix}\begin{bmatrix}d\varepsilon_{11} & d\varepsilon_{12}\\ d\varepsilon_{21} & d\varepsilon_{22}\end{bmatrix}\begin{bmatrix}-\sqrt{3}D/2\\ D/2\end{bmatrix} = 4\delta_q D \qquad \ldots(8.11)$$

or $\frac{3}{4}d\varepsilon_{11}-\sqrt{\frac{3}{4}}d\varepsilon_{12}-\sqrt{\frac{3}{4}}d\varepsilon_{21}+\frac{1}{4}d\varepsilon_{22} = 2\delta_q/D \qquad \ldots(8.12)$

and at T

$$2\begin{bmatrix}0 & D\end{bmatrix}\begin{bmatrix}d\varepsilon_{11} & d\varepsilon_{12}\\ d\varepsilon_{21} & d\varepsilon_{22}\end{bmatrix}\begin{bmatrix}0\\ D\end{bmatrix} = 4\delta_t D \qquad \ldots(8.13)$$

or

$$d\varepsilon_{22} = 2\delta_t/D \qquad \ldots(8.14)$$

Since $p = q$, $\delta_p = \delta_q$, $d\varepsilon_{12} = d\varepsilon_{21} = 0$ (as there is no rotation)

$$3/2\ d\varepsilon_{12}+1/2\ d\varepsilon_{22} = 4\delta_p/D \qquad \ldots(8.15)$$

Therefore, from (8.14) and (8.15)

$$\begin{bmatrix} \delta_p \\ \delta_t \end{bmatrix} = \frac{D}{8} \begin{bmatrix} 3 & 1 \\ 0 & 4 \end{bmatrix} \begin{bmatrix} d\varepsilon_{11} \\ d\varepsilon_{22} \end{bmatrix} \qquad \ldots(8.16)$$

and for linear elastic discs

$$\begin{bmatrix} \Sigma\delta_p \\ \Sigma\delta_t \end{bmatrix} = \frac{D}{8} \begin{bmatrix} 3 & 1 \\ 0 & 4 \end{bmatrix} \begin{bmatrix} \varepsilon_1 \\ \varepsilon_2 \end{bmatrix} \qquad \ldots(8.17)$$

We can, therefore, substitute (8.17) into (8.7) to obtain

$$\begin{bmatrix} \sigma_1 \\ \sigma_2 \end{bmatrix} = \frac{D^2K}{16V} \begin{bmatrix} 3 & 0 \\ 1 & 2 \end{bmatrix} \begin{bmatrix} 3 & 1 \\ 0 & 4 \end{bmatrix} \begin{bmatrix} \varepsilon_1 \\ \varepsilon_2 \end{bmatrix} \qquad \ldots(8.18)$$

which gives

$$\begin{bmatrix} \sigma_1 \\ \sigma_2 \end{bmatrix} = \frac{D^2K}{16V} \begin{bmatrix} 9 & 3 \\ 3 & 9 \end{bmatrix} \begin{bmatrix} \varepsilon_1 \\ \varepsilon_2 \end{bmatrix} \qquad \ldots(8.19)$$

but $V = \sqrt{3}D^2/2$, leading to

$$\begin{bmatrix} \sigma_1 \\ \sigma_2 \end{bmatrix} = \frac{K}{8\sqrt{3}} \begin{bmatrix} 9 & 3 \\ 3 & 9 \end{bmatrix} \begin{bmatrix} \varepsilon_1 \\ \varepsilon_2 \end{bmatrix} \qquad \ldots(8.20)$$

or

$$\begin{bmatrix} \sigma_1 \\ \sigma_2 \end{bmatrix} = \frac{3\sqrt{3}K}{8} \begin{bmatrix} 1 & 1/3 \\ 1/3 & 1 \end{bmatrix} \begin{bmatrix} \varepsilon_1 \\ \varepsilon_2 \end{bmatrix} \qquad \ldots(8.21)$$

The analysis for discs with friction is similar to that presented above, the forces on a disc are illustrated in Figure 8.4 (b). The average stress tensor within the disc is made up of normal and tangential force contributions

$$\sigma_{ij} = \sigma_{ij}^{(N)} + \sigma_{ij}^{(T)} \qquad \ldots(8.22)$$

The normal force contribution is

$$\sigma_{ij}^{(N)} = \frac{D}{V}\begin{bmatrix} 3/4\ (p_n+q_n) & \sqrt{3}/4\ (p_n-q_n) \\ \sqrt{3}/4\ (p_n-q_n) & 1/4\ (p_n+q_n)+t_n \end{bmatrix} \ldots(8.23)$$

which is similar to (8.5) for the frictionless case. The tangential force contribution is

$$\sigma_{ij}^{(T)} = \frac{2D}{V}\begin{bmatrix} \sqrt{3}/4 & -\sqrt{3}/4 & 0 \\ 1/4 & 1/4 & 1/2 \end{bmatrix}\begin{bmatrix} p_t/2 & -\sqrt{3}p_t/2 \\ -q_t/2 & -\sqrt{3}q_t/2 \\ t_t & 0 \end{bmatrix} \qquad \ldots(8.24)$$

which leads to

$$\sigma_{ij}^{(T)} = \frac{D}{V}\begin{bmatrix} \sqrt{3}/4\ (p_t+q_t) & -3/4\ (p_t-q_t) \\ 1/4\ (p_t-q_t)+t_t & -\sqrt{3}/4\ (p_t+q_t) \end{bmatrix} \ldots(8.25)$$

Representing the disc compliance by linear springs (both normal and tangential) the relationship between the contact forces and contact displacements are

$$p_n = K\Sigma\delta_p \qquad p_t = K\Sigma\Delta_p$$
$$q_n = K\Sigma\delta_q \qquad q_t = K\Sigma\Delta_q$$

For the problem under consideration

$$\sigma_{12} = \sigma_{21} \quad \text{hence} \quad t_t = q_t - p_t \quad \text{and} \quad \Delta_t = \Delta_q - \Delta_p$$
$$\sigma_{12} = 0 \quad \text{therefore} \quad p_n - q_n = \sqrt{3}(p_t - q_t)$$

From inspection, isotropic compression occurs with $t_t = 0 = q_t = p_t$ and, for shear with $\Delta\sigma_2 = 0$ $t_t = 0$, therefore $q_t = p_t$ and $p_n = q_n$ which when substituted into (8.23) and (8.25) give

$$\begin{bmatrix} \sigma_1^{(N)} \\ \sigma_2^{(N)} \end{bmatrix} = \frac{D}{2V} \begin{bmatrix} 3p_n & 0 \\ 0 & (p_n+2t_n) \end{bmatrix}$$

$$= \frac{DK}{2V} \begin{bmatrix} 3 & 0 \\ 1 & 2 \end{bmatrix} \begin{bmatrix} \Sigma\delta_p \\ \Sigma\delta_t \end{bmatrix} \qquad \ldots(8.26)$$

and

$$\begin{bmatrix} \sigma_1^{(T)} \\ \sigma 1^{(T)} \end{bmatrix} = \frac{D}{2V} \begin{bmatrix} \sqrt{3}p_t & 0 \\ 0 & -\sqrt{3}p_t \end{bmatrix}$$

$$= \frac{DK}{2V} \begin{bmatrix} \sqrt{3} \\ -\sqrt{3} \end{bmatrix} \Sigma\Delta_p \qquad \ldots(8.27)$$

where $V = \sqrt{3}D^2/2$ and hence

$$\begin{bmatrix} \sigma_1 \\ \sigma_2 \end{bmatrix} = \frac{K}{D} \begin{bmatrix} \sqrt{3} & 0 & 1 \\ 1/\sqrt{3} & 2/\sqrt{3} & -1 \end{bmatrix} \begin{bmatrix} \Sigma\delta_p \\ \Sigma\delta_t \\ \Sigma\Delta_p \end{bmatrix} \qquad \ldots(8.28)$$

The strain increment tensor is likewise seen to be made up of two components

$$\varepsilon_{ij} = \varepsilon_{ij}^{(N)} + \varepsilon_{ij}^{(T)} \qquad \ldots(8.29)$$

Where $\varepsilon_{ij}^{(N)}$ is the contribution due to the normal displacement and $\varepsilon_{ij}^{(T)}$ is the contribution due to the tangential displacement. It follows from (8.17) that

$$\begin{bmatrix} \Sigma\delta_p \\ \Sigma\delta_t \end{bmatrix} = \frac{D}{8} \begin{bmatrix} 3 & 1 \\ 0 & 4 \end{bmatrix} \begin{bmatrix} \varepsilon_1^{(N)} \\ \varepsilon_2^{(N)} \end{bmatrix} \qquad \ldots(8.30)$$

and

$$\begin{bmatrix} \varepsilon_1^{(N)} \\ \varepsilon_2^{(N)} \end{bmatrix} = \frac{2}{D} \begin{bmatrix} 4/3 & -1/3 \\ 0 & 1 \end{bmatrix} \begin{bmatrix} \Sigma\delta_p \\ \Sigma\delta_t \end{bmatrix} \qquad \ldots(8.31)$$

The remaining part, due to the tangential forces, is given by

$$\begin{bmatrix} \varepsilon_1^{(T)} \\ \varepsilon_2^{(T)} \end{bmatrix} = \frac{2}{D} \begin{bmatrix} 1/\sqrt{3} \\ -\sqrt{3} \end{bmatrix} \Sigma\Delta_p \qquad \ldots(8.32)$$

which follows from the analysis for rigid discs (Appendix A). Combining (8.31) and (8.32)

$$\begin{bmatrix} \varepsilon_1 \\ \varepsilon_2 \end{bmatrix} = \frac{2}{D} \begin{bmatrix} 4/3 & -1/3 & 1/\sqrt{3} \\ 0 & 1 & -\sqrt{3} \end{bmatrix} \begin{bmatrix} \Sigma\delta_p \\ \Sigma\delta_t \\ \Sigma\Delta_p \end{bmatrix} \qquad \ldots(8.33)$$

Slip occurs when $\Sigma\delta_t = 0$ and $\Sigma\Delta_p = \mu\Sigma\delta_p$, therefore from (8.28) and (8.33) we obtain

$$\sigma_1 = K/D\ (\sqrt{3} + \mu)\ \Sigma\delta_p \qquad \ldots(8.34a)$$

and

$$\sigma_2 = K/D\ (1/\sqrt{3} - \mu)\ \Sigma\delta_p \qquad \ldots(8.34b)$$

from which

$$\frac{\sigma_1}{\sigma_2} = \frac{\sqrt{3}\ (\sqrt{3} + \mu)}{(1 - \sqrt{3}\ \mu)} \qquad \ldots(8.35)$$

which agrees with Rowe (1962) and Thornton (1977).

Considering the strains to failure, it follows that, at slip $\varepsilon_{2f} = \frac{-2\sqrt{3}\ \mu\Sigma\delta_p}{D}$ where $\Sigma\delta_p = \frac{\sqrt{3}D}{(1-\sqrt{3}\mu)}\ \frac{\sigma_2}{K}$

and therefore

$$\varepsilon_{2f} = \frac{-6\mu\sigma_2}{(1-\sqrt{3}\mu)K} \qquad \ldots(8.36)$$

$$\varepsilon_{1f} = \frac{2\Sigma\delta_p}{\sqrt{3}D}\ (4/\sqrt{3} + \mu)$$

$$\varepsilon_{1f} = \frac{2\sigma_2}{\sqrt{3}K}\ \frac{(4 + \sqrt{3}\mu)}{(1 - \sqrt{3}\mu)} \qquad \ldots(8.37)$$

All the above values of strain include the strains during consolidation. During consolidation with $\sigma_1 = \sigma_2$,

$$\varepsilon_1 = \varepsilon_2\ ,\ \Sigma\Delta_p = 0\ ,\ \Sigma\delta_t = \Sigma\delta_p$$

Therefore $\Sigma\delta_t = \Sigma\delta_p = \frac{D}{\sqrt{3}K}\sigma_2$ and $\varepsilon_1 = \varepsilon_2 = \frac{2}{D}\Sigma\delta_p = 2\sigma_2/\sqrt{3}K$

Thus, the failure strains developed during shear are

$$\varepsilon_{1f} = \frac{2\sigma_2}{\sqrt{3}K}\ \frac{\{3+2\sqrt{3}\mu\}}{\{1-\sqrt{3}\mu\ \}} \qquad \ldots(8.38)$$

$$\varepsilon_{2f} = \frac{-2\sigma_2}{\sqrt{3}K} \frac{(1+2\sqrt{3}\mu)}{(1-\sqrt{3}\mu)} \qquad \ldots(8.39)$$

and

$$\varepsilon_{vf} = \frac{4\sigma_2}{\sqrt{3}K(1-\sqrt{3}\mu)} \qquad \ldots(8.40)$$

Therefore

$$\frac{\varepsilon_{vf}}{\varepsilon_{1f}} = \frac{2}{(3+2\sqrt{3}\mu)} \qquad \ldots(8.41)$$

which is affected by friction, and

$$\frac{R-1}{\varepsilon_{1f}} = \frac{(1+\sqrt{3}\mu)}{(\sqrt{3}+2\mu)} \frac{K}{\sigma_2} = M \qquad \ldots(8.42)$$

(where $R = \sigma_1 / \sigma_3$)

which is the modulus of the stress ratio-strain curve.

It is therefore possible to provide theoretical curves for an array of regular elastic discs, which are assumed to act elastically up to some peak value and then deform in a plastic (strain-softening) manner afterwards, Figure 8.5. These curves result from a combination of the elastic theory presented in this section and the plastic analysis presented in Appendix A.

Figure 8.5 provides a comparison between the results of a computer simulated test on a 124 disc array of friction-less particles and the theoretical predictions. The stress ratio values simulated by the computer program are seen

to be lower than those predicted, both in the pre-peak and the post-peak sections. Possible causes could be the small number of discs involved (hence the large effects of the boundaries) and the effect of allowing the particles the freedom to spin. This latter point is further examined in section 8.3.2. The volume change curve shows very good agreement pre-peak, but the post-peak values deviate from the predicted curve. However, for the post-peak simulated tests, the packing is not exhibiting uniform deformation, some areas of the packing are much denser than others. The non-uniform deformation will be discussed in detail in Sections 8.2 and 8.3.

Figure 8.6 shows four stress-strain curves for packings of different disc stiffnesses. It can be seen that as the stiffness of the discs increases, the stress-strain curves peak earlier in the tests with a slight increase in the peak stress ratio. This trend is in agreement with equations (8.38) and (8.42) and is explained by the fact that slip can only occur when gaps are created between horizontally contiguous discs. In the simulation test, consolidation of the packing leads to the formation of overlaps at the horizontal contacts between the discs. These overlaps imply contact forces are present and slip cannot occur until the packing has deformed sufficiently to reduce these overlaps (and contact forces) to zero. With packings of rigid discs, there are no overlaps created during "consolidation" and therefore, when sheared, no

deformation is required before slip occurs.

A similar series of tests was performed to illustrate the effects of cell pressure on the assembly and these test results are illustrated in Figure 8.7. It is seen that, in agreement with equation (8.38), the peak strength occurs at greater strains as the cell pressure is increased. High cell pressures during consolidation lead to high forces on the discs at the horizontal contacts. As failure cannot occur until these forces become zero, it follows that the higher the contact force generated during consolidation, the greater is the amount of packing deformation needed before slip can occur.

The effects of interparticle friction are illustrated in Figure 8.8, which shows stress-strain curves for packings with different coefficients of interparticle friction. It can be seen that the slope of the pre-peak curve steepens with increases in interparticle friction and that the strain required to reach peak stress ratio increases. These trends are supported by equations (8.38) and (8.42). The increase in slope of the stress-strain curve (and hence the increase in the packing stiffness) can be explained by the friction allowing a greater force obliquity at the contacts before friction gives way to slip. Similarly, the delay in reaching peak stress that occurs with increasing friction is also due to the delay before slip occurs and slip is necessary to cause the gap opening which is associated

with failure and consequently post-peak behaviour.

From the preceeding test results, the most economic tests (computer time) would appear to be on frictionless discs, under a low cell pressure with all the discs having a high stiffness. Unfortunately, such a choice of conditions, when combined, lead to tests which are very sensitive to the boundary conditions. Platten velocity again becomes the critical factor and in order to avoid unduly slow platten speeds, a compromise has to be reached. All tests subsequenly described in this chapter were simulated using the following data*, unless otherwise stated:

Platten Friction	0.0 or 0.3
Disc Friction	0.0 or 0.3
Confining Stress	4000
Stiffness	1500000
Damping parameters	0.5,0.5,0,1
Platten Velocity	0.001 or 0.005

8.2 EFFECT OF SAMPLE SIZE ON MODE OF DEFORMATION

A series of tests were performed on samples with different numbers of discs in order to examine the effect of sample size and shape on the mode of deformation and the stress strain behaviour. The simulation parameters used in this series of tests were: frictionless discs, frictionless plattens, a cell stress of 4000 units and a disc stiffness

* Due to the nature of the program, all units are dimensionless.

of 1.5×10^6 units. The sample sizes used were 18, 74, 86, 95, 124 and 410 discs.

The smallest sample used (18 discs) reached a maximum stress ratio, σ_y/σ_x , around 1.2% strain, see Figure 8.9. At 1.4% strain, gaps were observed at all but five of the original horizontal contacts. This is illustrated in Figure 8.10. Further deformation resulted in progressive widening of these gaps as shown in Figure 8.11. This figure shows the geometry at 11.7% strain and it can be seen that not all the gaps are of equal size and that some discs remain in contact with each other throughout the test. Unfortunately this packing size is too small to examine, in detail, the causes which lead to the observed non-uniform deformation pattern. It is, however, clear that the gaps shown in Figures 8.10 and 8.11 are associated with the formation of discrete shear bands within the sample.

A larger (74 discs) packing was tested and the resulting stress ratio - strain curve is shown in Figure 8.12. The geometry of the packing, corresponding to three stages of the test, is illustrated in Figures 8.13 - 8.15. These figures show the progressive development of shear bands during the test and it can be seen from Figures 8.12 and 8.13 that the shear bands were initiated before the stress ratio, σ_y/σ_x had reached a maximum. Maximum stress ratio was reached at 1.4% strain. The packing

geometry at 1.3% strain is illustrated in Figure 8.13 which shows that shear bands had already formed and were initiated at the stress controlled boundaries, adjacent to the four corners of the assembly. These shear bands propagate through the array until they reach the platten controlled boundaries, Figure 8.14. It is interesting to note that at this stage of the test, 1.7% strain (0.3% post-peak), observations based on the locations of boundary discs alone would give no indication of the very non-uniform deformation occuring internally. Further deformation results in the shear bands being reflected back at the platten boundary and subsequently transversing the packing, to reach the opposite platten as shown in Figure 8.15 which corresponds to a strain of 2.8%. The shear band pattern is seen to be symmetrical as would be expected for the boundary conditions imposed in the test.

Exactly the same pattern of shear band propagation was observed during a test on an 86 disc packing, the results of which are illustrated in Figures 8.16 - 8.20. Tests on 95 disc and 124 disc packings also confirmed the shear band propagation pattern, as shown in Figures 8.21 - 8.27.

The sample size and shape, however, do have an effect on the size and shape of the groups of contiguous discs which are separated from each other by the shear bands. This affects the ability of the packing to transmit the platten

loads through the sample, and consequently affects the resulting stress ratio-strain curve as illustrated in Figure 8.28. This figure shows that although the elastic pre-peak behaviour is not significantly affected, the maximum stress ratio and post-peak behaviour is very much dependent on the size and shape of the packing.

The largest array of discs examined (410 discs) cannot be directly compared with the other packings reported so far since, unlike the other packings which consisted of frictionless discs, the 410 disc array was composed of discs with an assigned value of interparticle coefficient of friction of 0.3. Nevertheless, it can be seen from Figures 8.29 and 8.30 that the shear band propagation pattern was similar to that of previous tests. The difference between the results of the 410 disc test and the other tests reported in this section was that, although shear bands were initiated at the corners of the assembly, two adjacent shear bands were formed, one starting from the stress controlled boundary the other from the platten boundary. This is illustrated in Figure 8.30 which also shows that, the two adjacent shear bands propagate from each corner until two sets of shear bands meet. Subsequent deformation results in the arrested propagation of one of the shear bands in each set. As can be seen from Figure 8.30, only the shear bands which were initiated at the stress controlled boundary continue to propagate so as to reach the opposite platten boundary. The stress ratio - strain curve generated by the

test on the 410 disc packing is provided in Figure 8.31.

8.3 TESTS ON 124 DISC ARRAYS

8.3.1 Effect of End Restraint

Two tests on the 124 disc packing were simulated in order to examine the effect of end restraint. One test was carried out using a coefficient of platten friction of 0.3; the other test simulated frictionless plattens (coefficient of platten friction = 0.0). In both tests the confining stress was 4000 units, the disc stiffness was 1.5×10^6 units, and the coefficient of interparticle friction was 0.3.

The stress ratio-strain curves obtained from these two tests are shown in Figures 8.32 and 8.33. Figures 8.34 - 8.39 show the geometry of the array at various stages of the test (as indicated in Figure 8.32) for the case of frictionless plattens. The manner in which the geometry changes for the case of plattens with friction is illustrated in Figures 8.40 - 8.45, the corresponding strains being indicated in Figure 8.33. A direct comparison of the two stress ratio-strain curves is provided in Figure 8.46.

It can be seen from Figure 8.46 that the two curves diverge after approximately 1% strain. This divergence is associated with local conditions at the corners of the sample tested with

frictionless plattens which resulted in the initiation of shear bands at about 1.4% strain. The stress ratio developed in the test with frictionless plattens reached a maximum of 2.4% strain and then decreased showing significant post-peak softening behaviour. For the test with friction along the plattens, shear bands were only initiated at about 2% strain when the stress ratio was already greater than the maximum stress ratio attained using frictionless plattens. Following the initiation of the shear bands there was only a small further increase in stress ratio until about 3% strain, after which the stress ratio gradually decreased.

Figure 8.34 shows that, for the test with frictionless plattens, shear band initiation occurred along the platten boundaries adjacent to the corner disc. The shear bands then propagated diagonally from the corners into the packing until two shear bands meet, as shown in Figure 8.35 which depicts the array geometry at 2.9% strain. The propagation of these original shear bands is arrested during post peak behaviour which is associated with the formation of a second, third, and fourth set of shear bands as shown in Figures 8.36 - 8.39. It would appear from the above figures that the post-peak shear bands propagated from within the assembly and were initiated, in each case, at the mid-height of the sample.

The deformation of the sample tested using plattens with friction is shown in Figures 8.40 - 8.45. The general

pattern of shear band formation is similar to that created in the test with frictionless plattens. However, due to the frictional restraint at the plattens, the original shear band is initiated not at the platten boundaries but at the stress controlled boundaries adjacent to the corner discs, Figure 8.40. Platten friction also inhibits the propagation of the shear bands through to the platten boundaries. Figure 8.43 shows the array geometry at 3.58% strain when the shear bands have just reached the central part of the platten boundaries. Further deformation leads to a widening of the existing gaps and this is associated with a continuous reduction in stress ratio as shown in Figure 8.33.

The mechanism of failure can be described as that of gap creation along inclined discrete shear bands. Gap creation results in a reduction in the number of contacts between the discs. Figures 8.47 and 8.48 show how the number of contacts reduce during a test, for the case of frictionless plattens and plattens with friction respectively. It can be seen from these two figures that the stress ratio-strain curve is linear until the first gaps are created and that the change in slope of the curve is related to the number of gaps created. Platten friction delays the start of the gap formation process but the process is always initiated when the stress ratio is still increasing. From figures 8.47 and 8.48, and the other figures referred to in this section, it is clear that maximum stress ratio occurs when there is a continuous (though not necessarily straight) line of gaps between the two platten boundaries. It can also be

seen from Figures 8.47 and 8.48 that platten friction inhibits the speed of propagation of shear bands through the sample and thus delays the attainment of maximum stress ratio. During post-peak behaviour there is no significant reduction in the number of contacts, Figures 8.47 and 8.48, the softening behaviour being due to the widening of existing gaps.

8.3.2 Effect of disc rotation (spin restraint)

In all the tests that have been reported in this chapter the individual discs of an assembly have been permitted the freedom to rotate (or spin) as naturally dictated by the internal conditions at any stage of a test. In this section the effect of spin restraint will be examined. Two levels of restriction were adopted: either rotational freedom was denied to all discs; or to boundary discs only.

Figure 8.55 shows the effect of spin restraint on the stress ratio-strain curve for tests using frictionless plattens. By comparing this figure with Figure 8.46 it can be seen that the effect of spin restraint is not as great as that of end restraint. However, even if only the boundary discs are denied rotational freedom there is a significant delay in the initiation of shear bands. Figures 8.38, 8.52 and 8.49 provide a comparison of the array geometry at 3.58% strain for the three curves shown in Figure 8.55. It is clear from these figures that spin restraint inhibits the propagation of shear bands throughout a test.

The effect of disc rotation for tests employing plattens with friction is shown in Figure 8.56. It can be seen that there is no significant effect until after 3% strain. For the three stress ratio-strain curves shown, the array geometry at 3.58% strain is illustrated in Figures 8.43, 8.53 and 8.50. The delayed development of shear bands due to spin restraint, which can be seen from a comparison of these three figures, accounts for the fact that the stress ratio is still increasing at this stage for the two cases of spin restraint. Figures 8.45, 8.54 and 8.51 provide another comparison of the three packings at about 5.2% strain. At this stage of the test only the sample with rotational freedom denied to all discs exhibits an increasing stress ratio, Figure 8.56. As can be seen from Figure 8.51 this is due to the much slower propagation of shear bands which, for complete spin restraint, have not yet reached the platten boundaries, even at this relatively large strain.

8.4 FURTHER OBSERVATIONS

Although it would be desirable to verify the regular packing theory, presented in the first part of this thesis, by practical laboratory experiments on regular assemblies of discs and spheres, it is not possible to ensure that the particles would be exactly identical - which is necessary to obtain a truly regular packing, as noted by Rowe (1962) and Leussink and Wittke (1963). It was therefore attractive to employ the

computer simulation approach using the Distinct Element Method proposed by Cundall and Strack (1978). However as has been shown in this chapter, the guaranteed initial regular arrangement is not sufficient to ensure a subsequent uniform deformation pattern. Both packing size and boundary conditions result in the formation of discrete shear bands and this, in turn, results in a deviation from the predictions of the ideal regular packing theory.

The discrete shear band patterns, shown in this chapter, are based on observations of gaps created at horizontal contacts. While it is apparent that there are no contact forces once a gap exists, it is also possible to have a zero contact force at a contact without a gap. Figure 8.57 indicates the locations of horizontal contact forces during a test on a 124 disc packing using frictionless plattens. This figure, when compared with the corresponding shear band patterns, Figure 8.34 indicates the metastable condition of contacts at locations other than in the shear bands. Figure 8.57 suggests that subsequent deformation would take the form of a diffused (pure shear) mode of deformation spreading out from the centre of the sample. This in fact did not occur, as shown in this chapter, due to the existance of the discrete shear bands shown in Figure 8.35, which provided, in effect, planes of weakness.

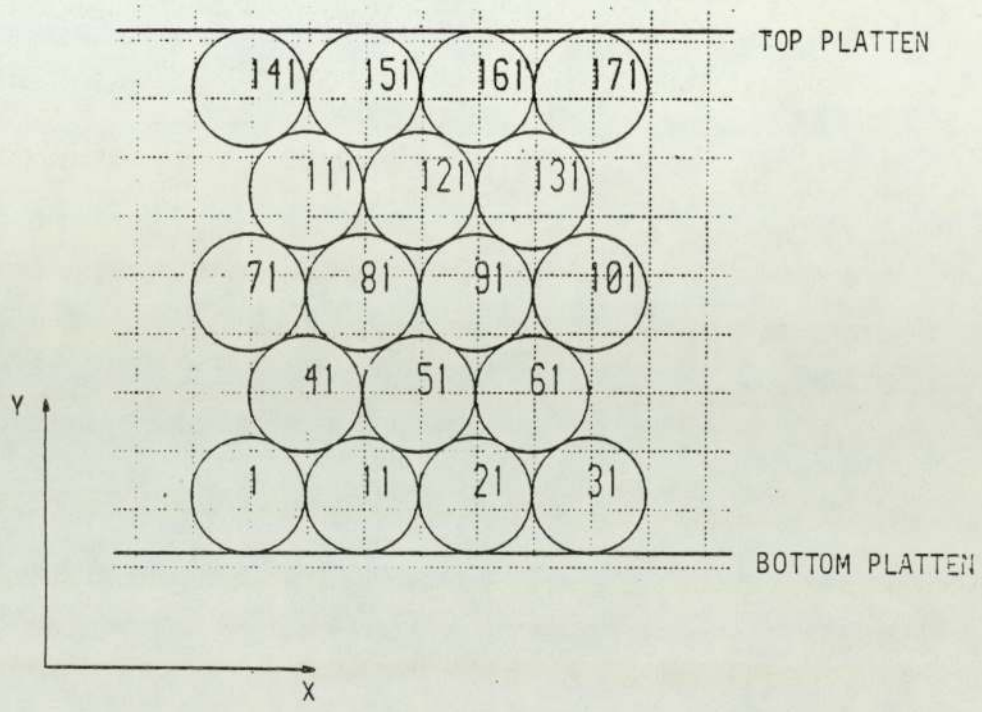

FIGURE 8.1 INITIAL ARRANGEMENT OF AN 18 DISC PACKING SHOWING PLATTENS, GRID AND COORDINATE AXES

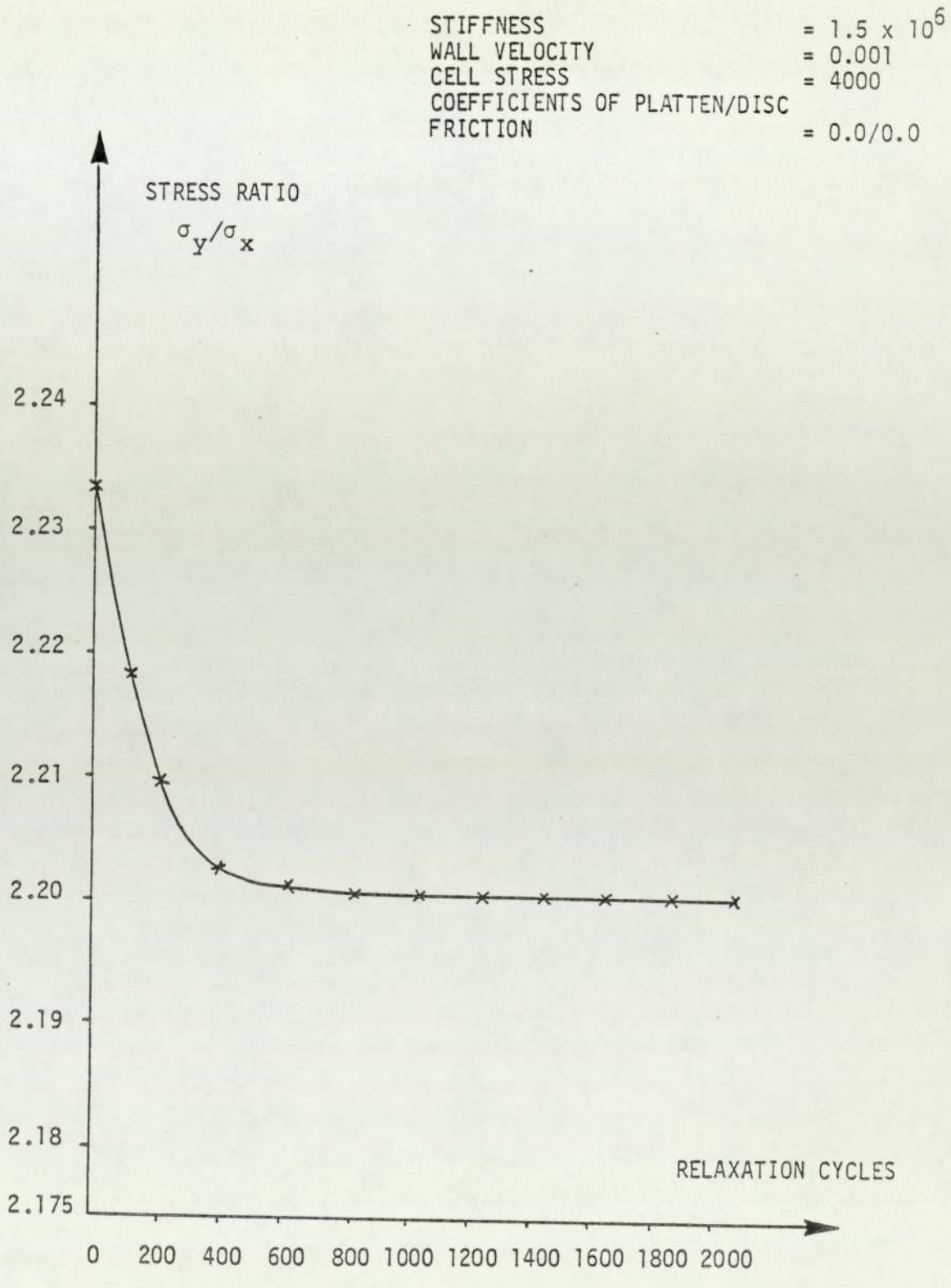

FIGURE 8.2 PLOT OF STRESS RATIO AGAINST RELAXATION CYCLES

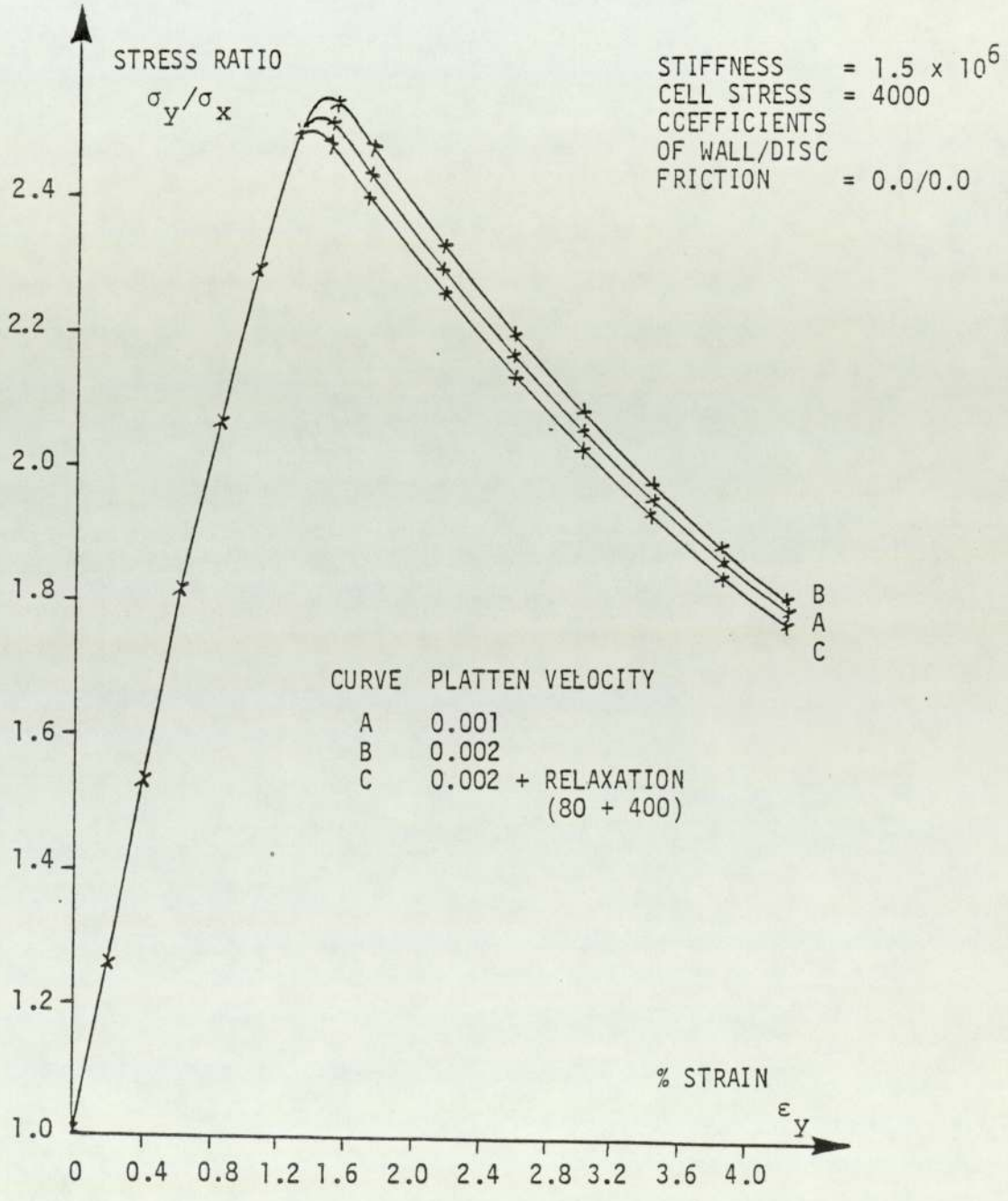

FIGURE 8.3 PLOTS OF STRESS RATIO AGAINST STRAIN ILLUSTRATING THE EFFECTS OF LOADING RATE

(A) FRICTIONLESS DISCS

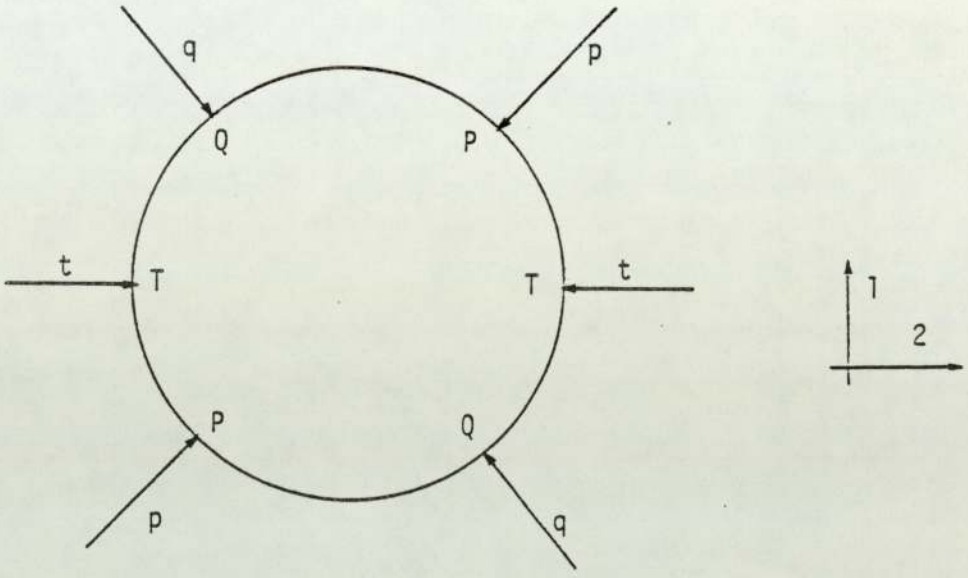

(B) DISCS WITH SURFACE FRICTION

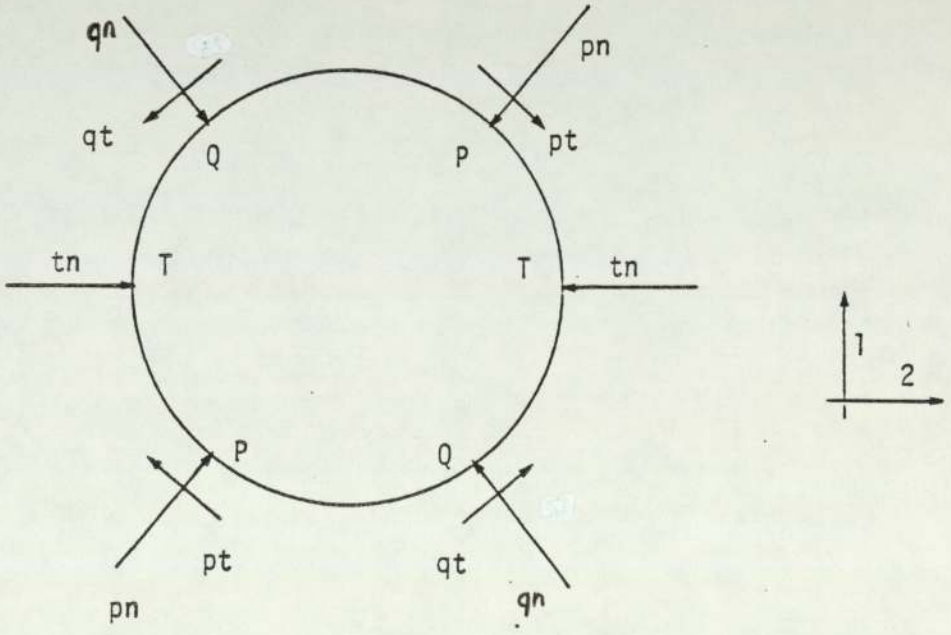

FIGURE 8.4 FORCES ACTING ON A TYPICAL ELASTIC DISC WITHIN A CLOSE PACKING

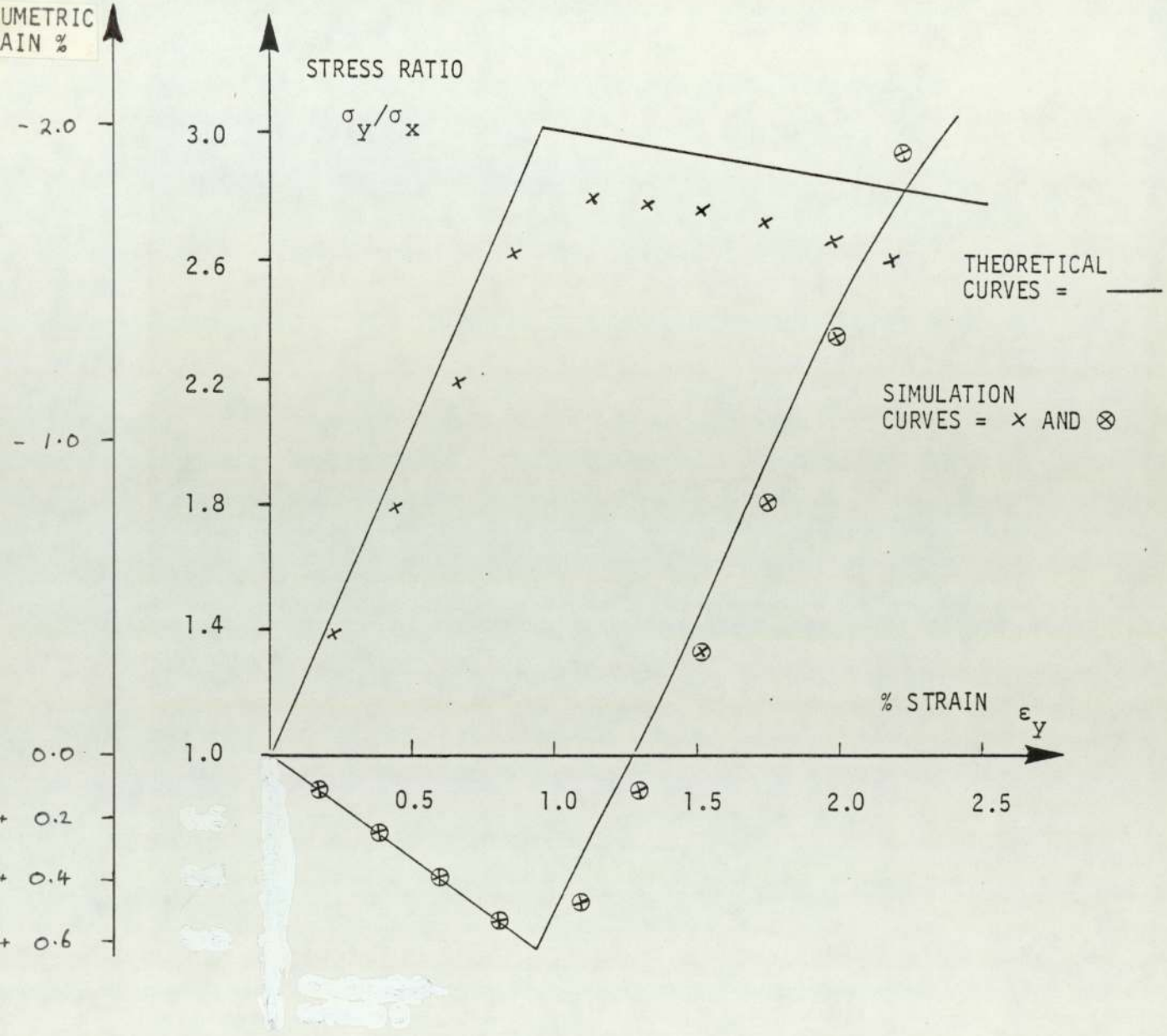

FIGURE 8.5 PLOTS OF STRESS RATIO AND VOLUMETRIC STRAIN AGAINST LONGITUDINAL STRAIN, COMPARING THE THEORETICAL RESULTS WITH THOSE OBTAINED FROM THE SIMULATION, FOR A FRICTIONLESS PACKING

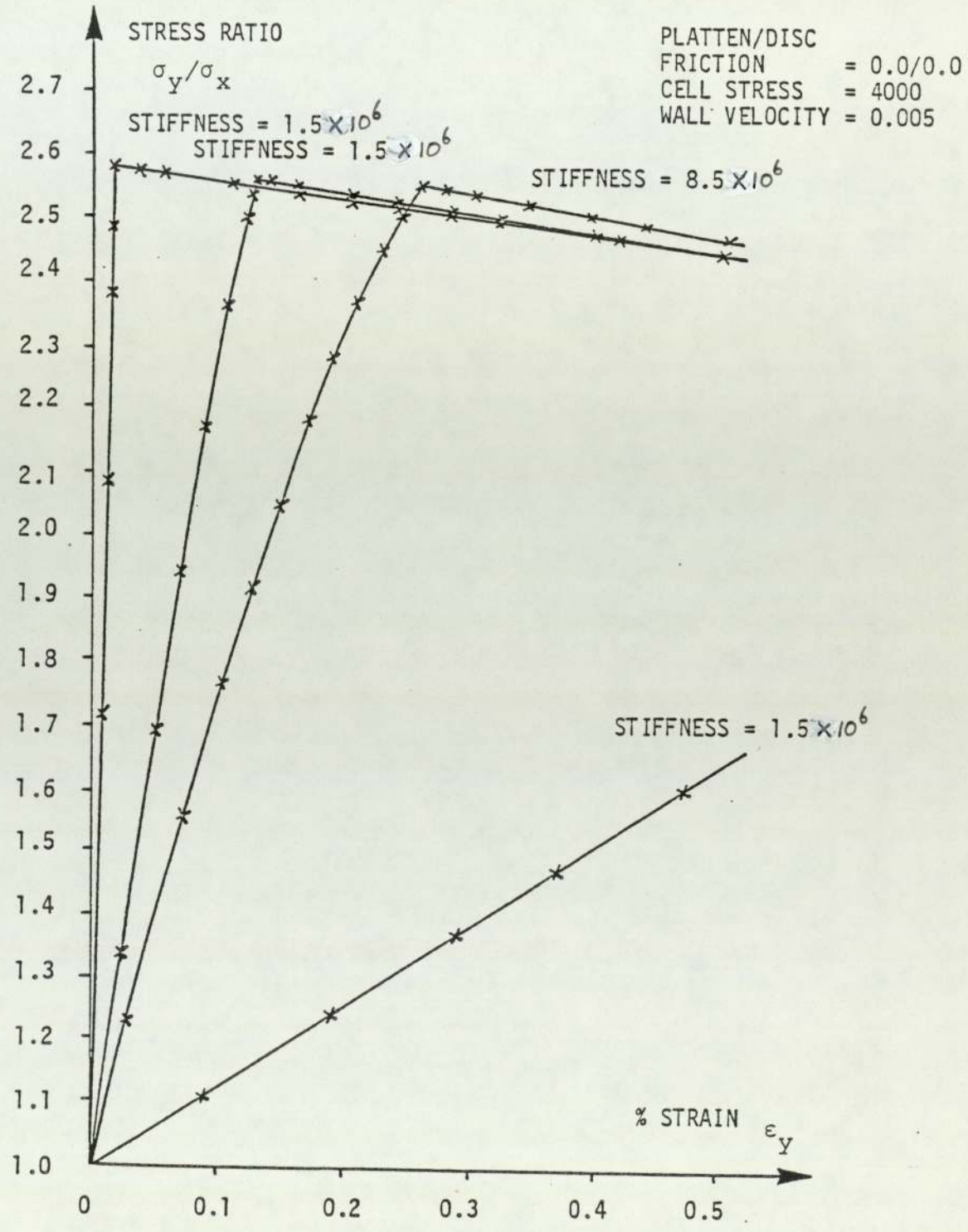

FIGURE 8.6 PLOTS OF STRESS RATIO AGAINST STRAIN TO ILLUSTRATE THE EFFECTS OF STIFFNESS

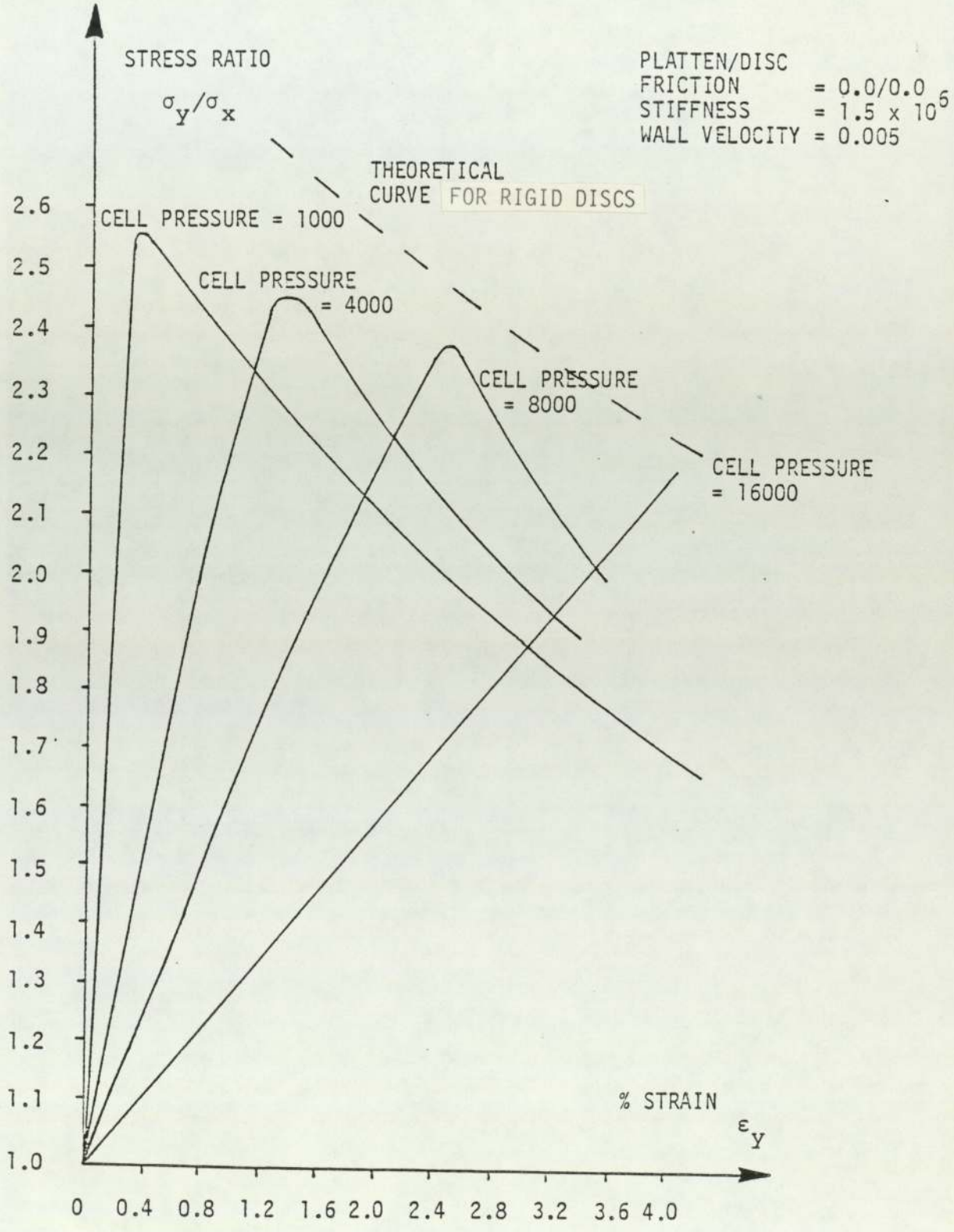

FIGURE 8.7 STRESS RATIO - STRAIN CURVES ILLUSTRATING THE EFFECTS OF CELL PRESSURE

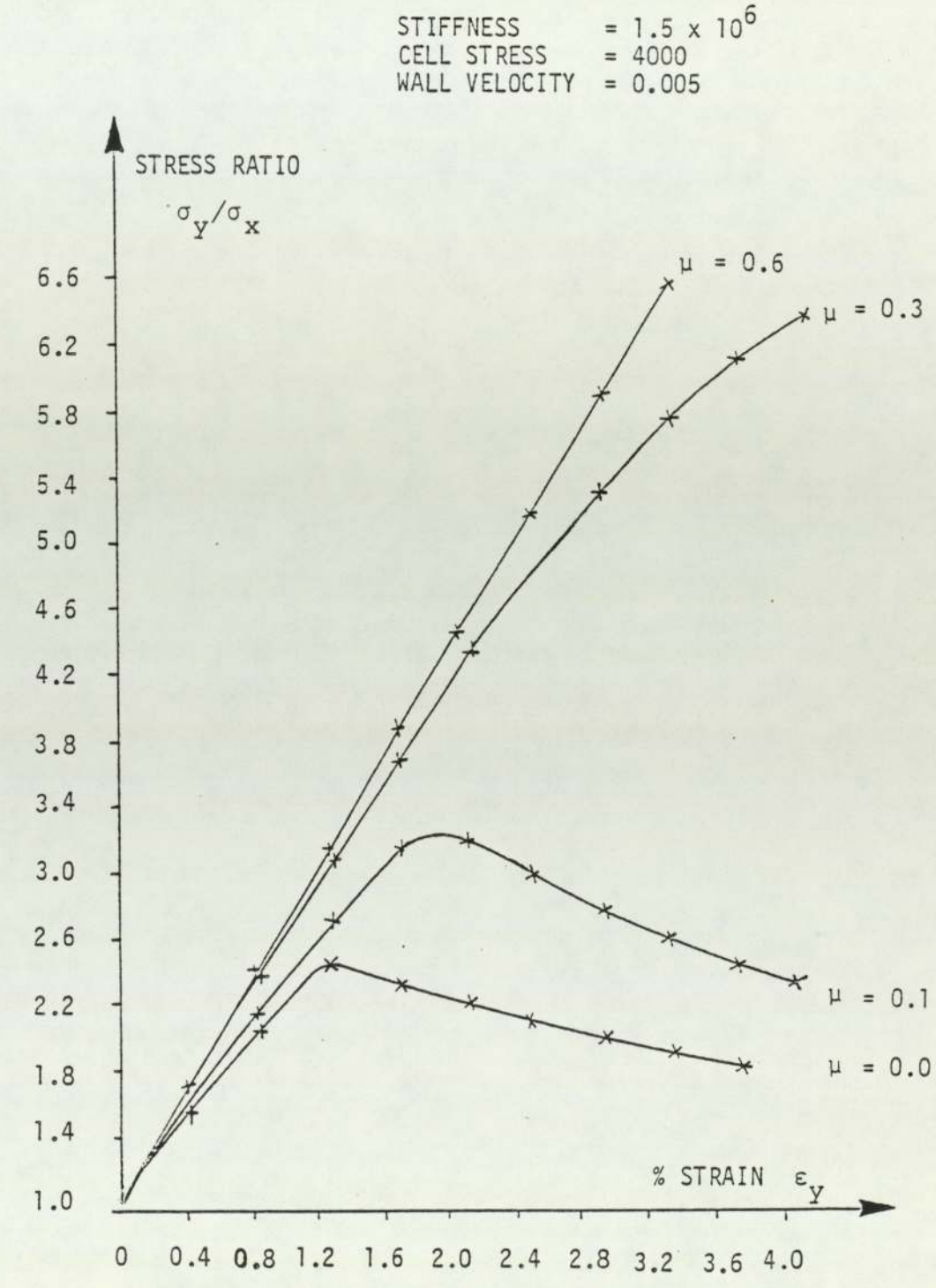

FIGURE 8.8 PLOTS OF STRESS RATIO AGAINST STRAIN ILLUSTRATING THE EFFECT OF INTER PARTICLE FRICTION

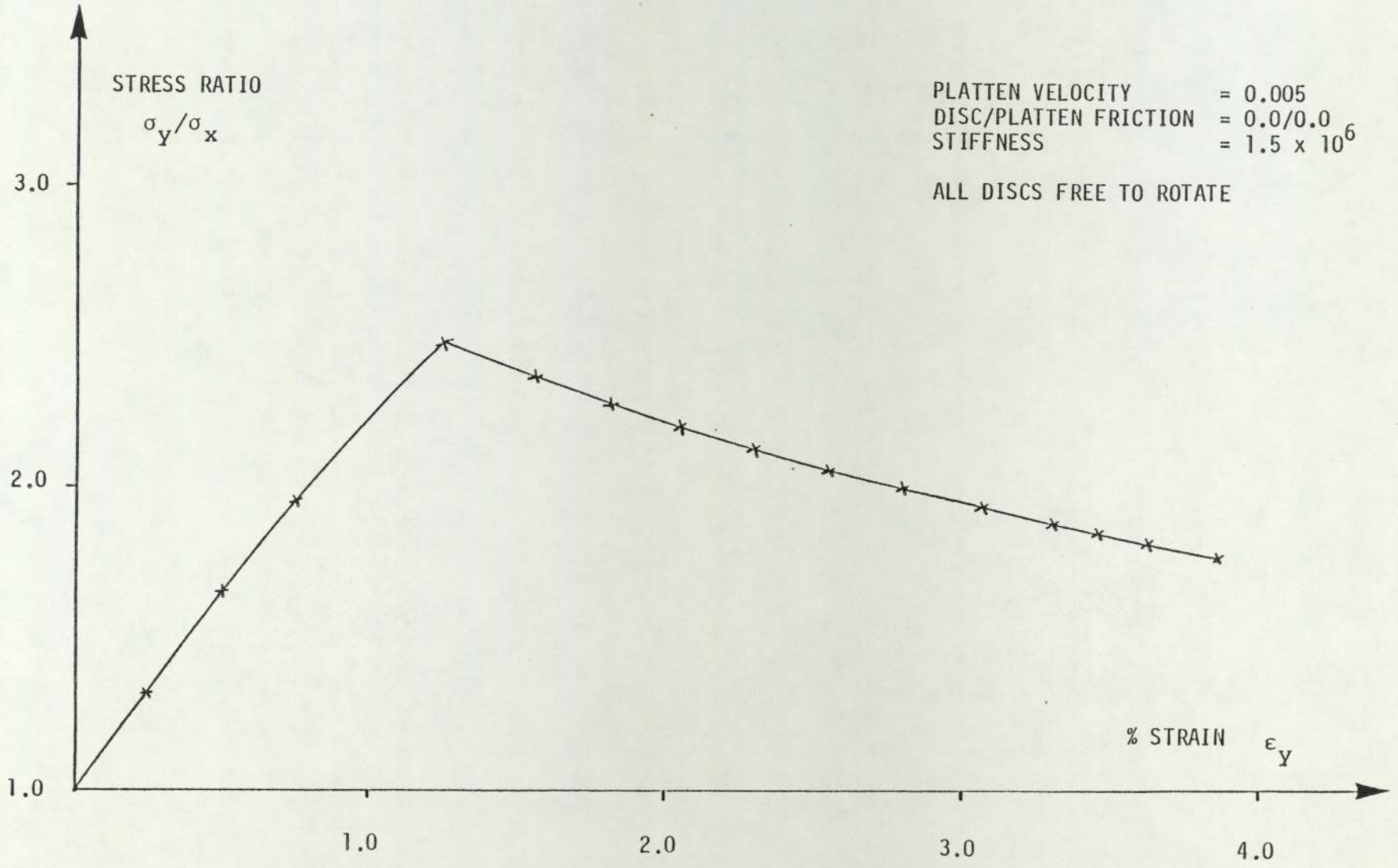

FIGURE 8.9 STRESS RATIO - STRAIN CURVE FOR AN 18 DISC PACKING

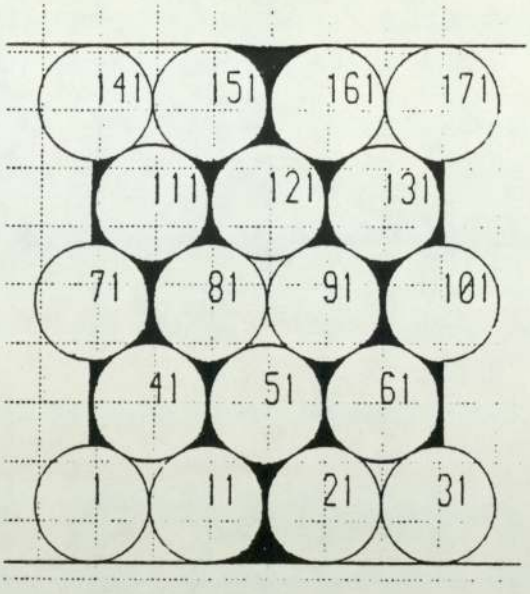

FIGURE 8.10 DEFORMATION OF AN 18 DISC PACKING AT 0.2% STRAIN POST PEAK (1.4% STRAIN)

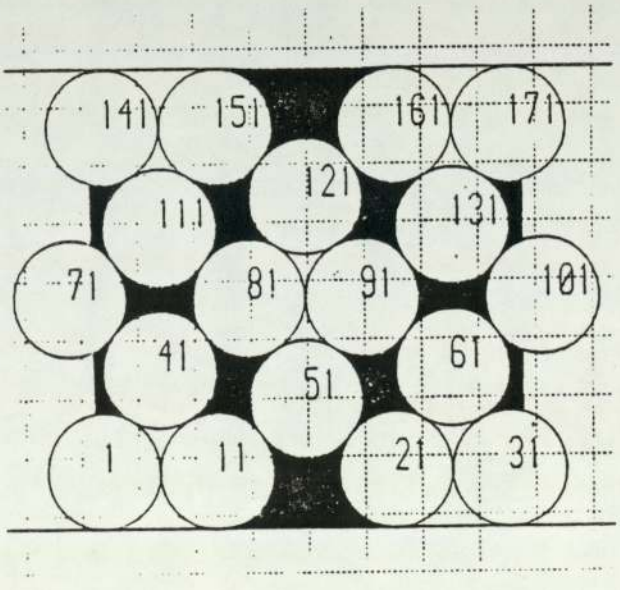

FIGURE 8.11 DEFORMATION OF AN 18 DISC PACKING AT 10.5% STRAIN POST PEAK (11.7% STRAIN)

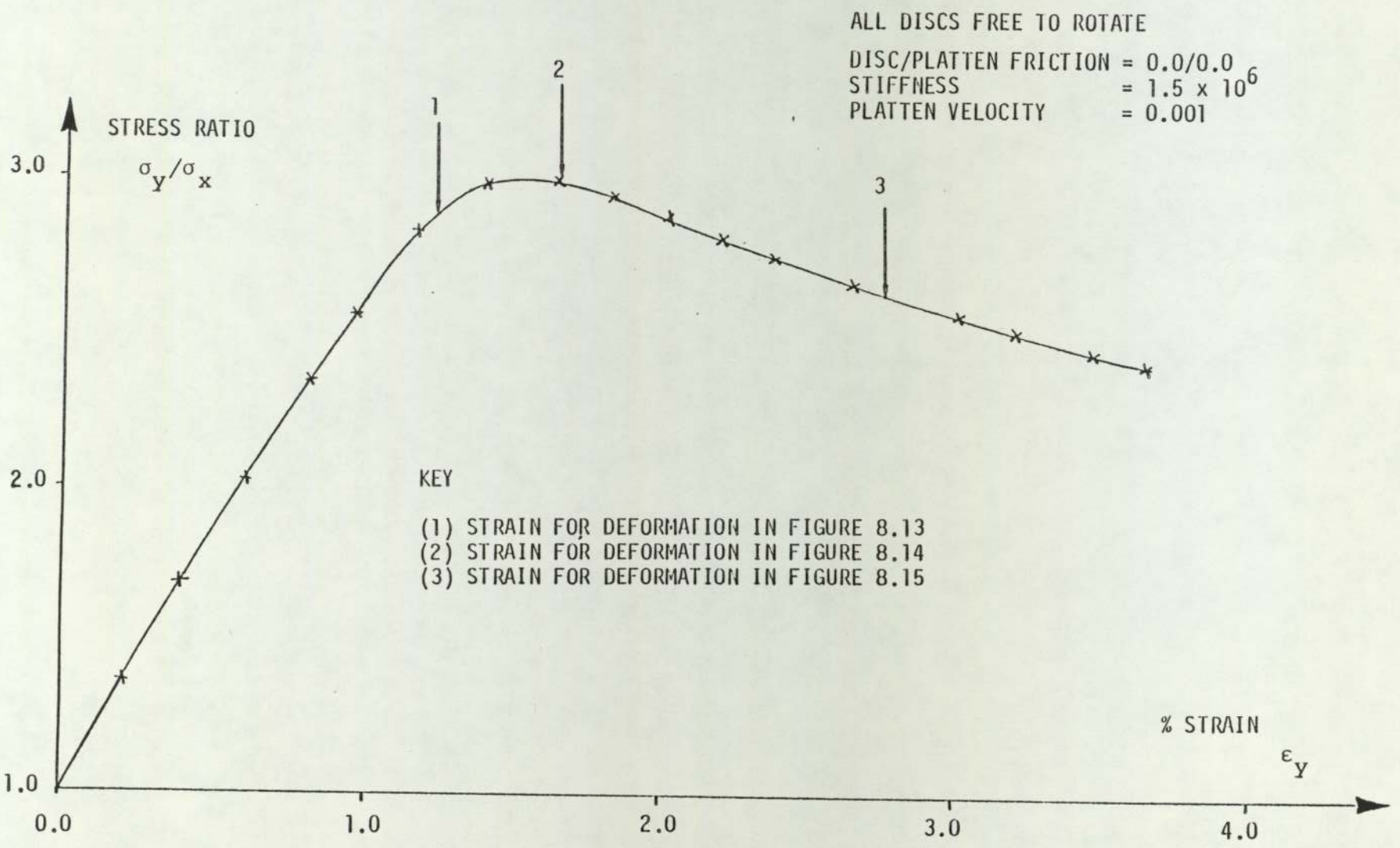

FIGURE 8.12 STRESS RATIO - STRAIN CURVES FOR A 74 DISC PACKING

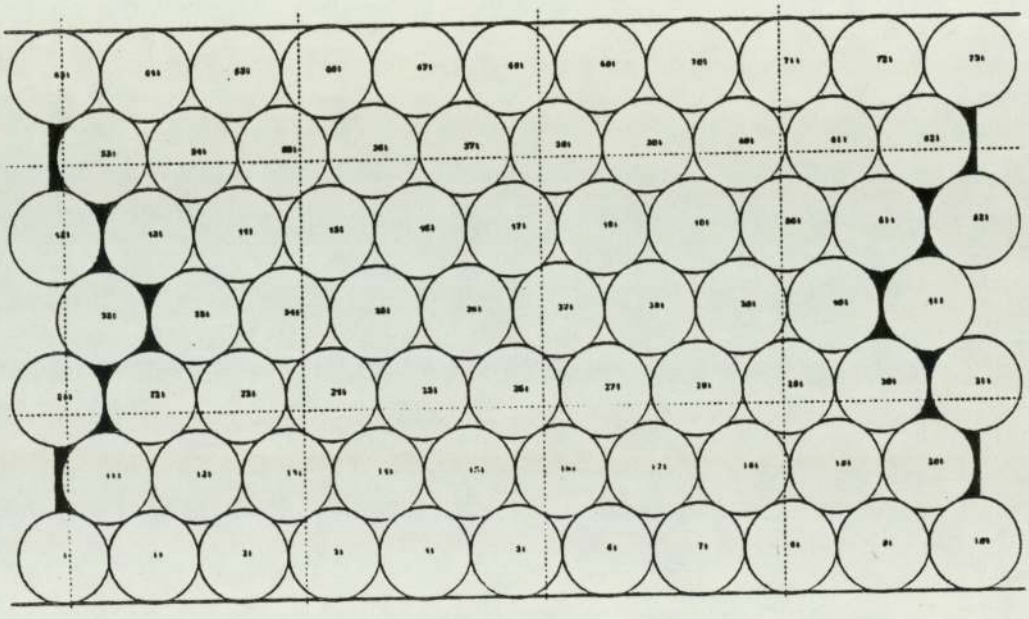

FIGURE 8.13 DEFORMATION OF A 74 DISC PACKING AT 1.3% STRAIN, WITH FRICTIONLESS DISCS AND PLATTENS

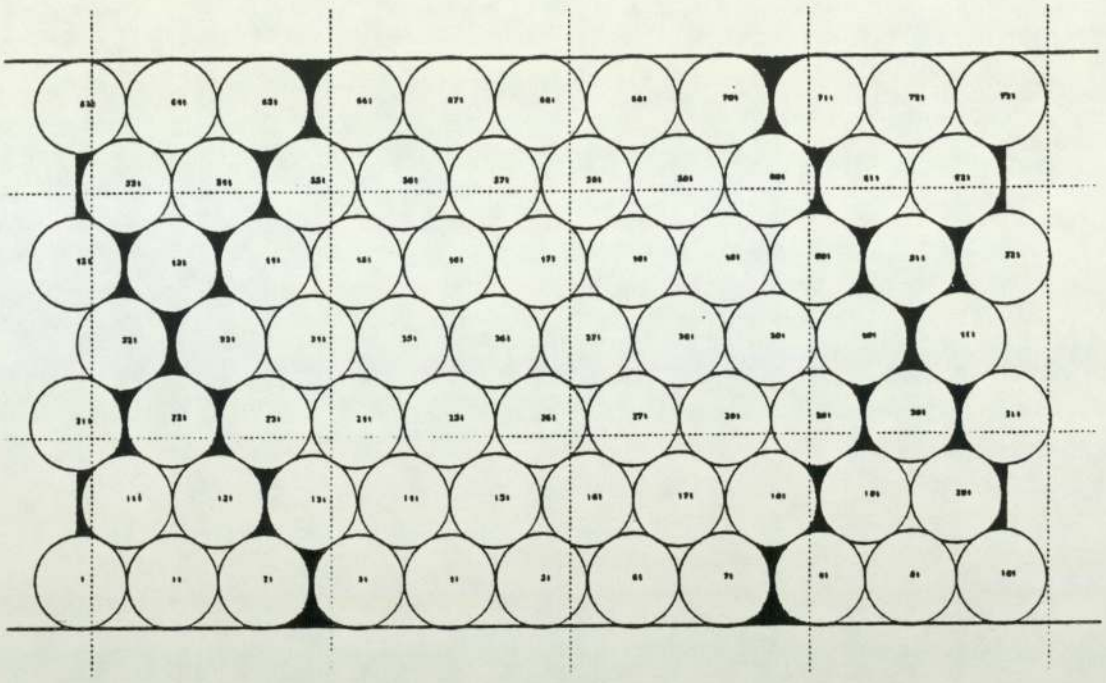

FIGURE 8.14 DEFORMATION OF A 74 DISC PACKING AT 1.7% STRAIN, WITH FRICTIONLESS DISCS AND PLATTENS

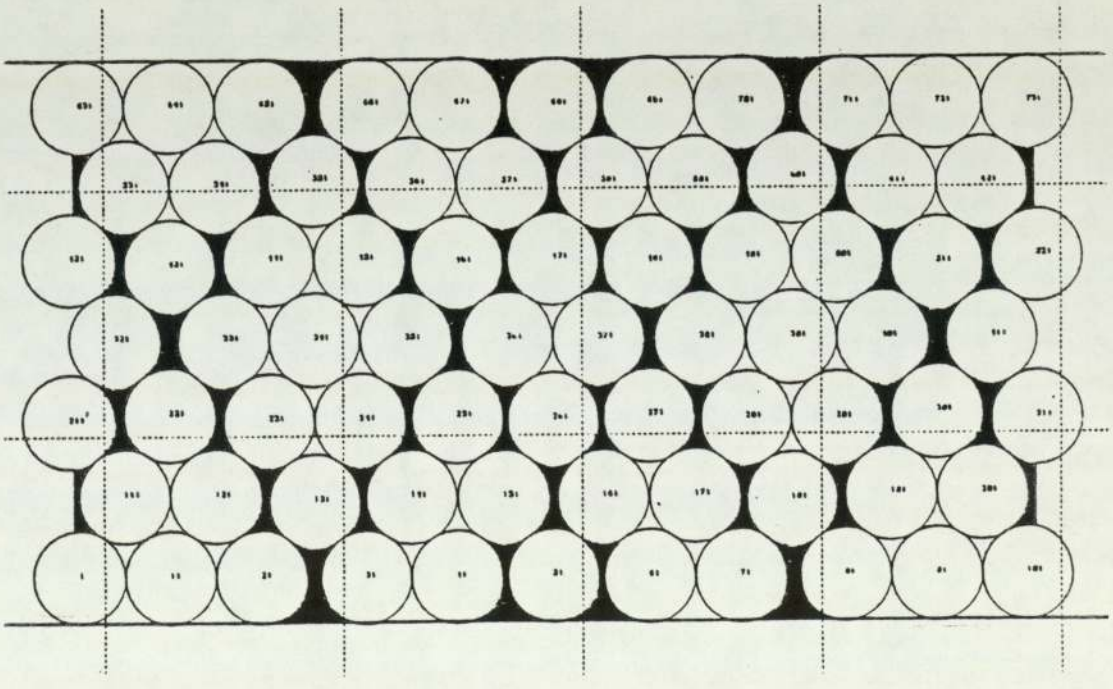

FIGURE 8.15 DEFORMATION OF A 74 DISC PACKING AT 2.8% STRAIN, WITH FRICTIONLESS DISCS AND PLATTENS

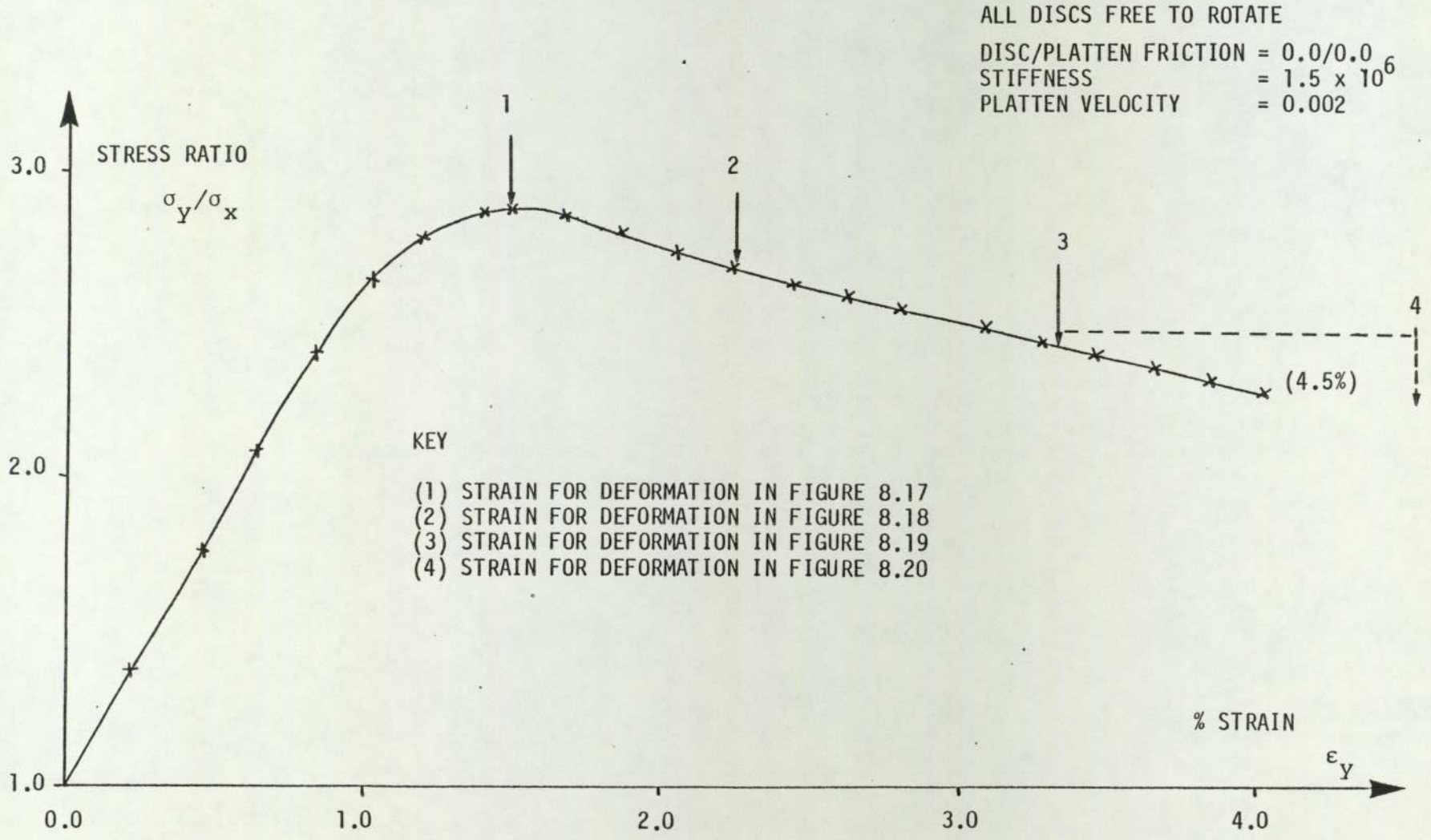

FIGURE 8.16 STRESS RATIO - STRAIN CURVE FOR AN 86 DISC PACKING

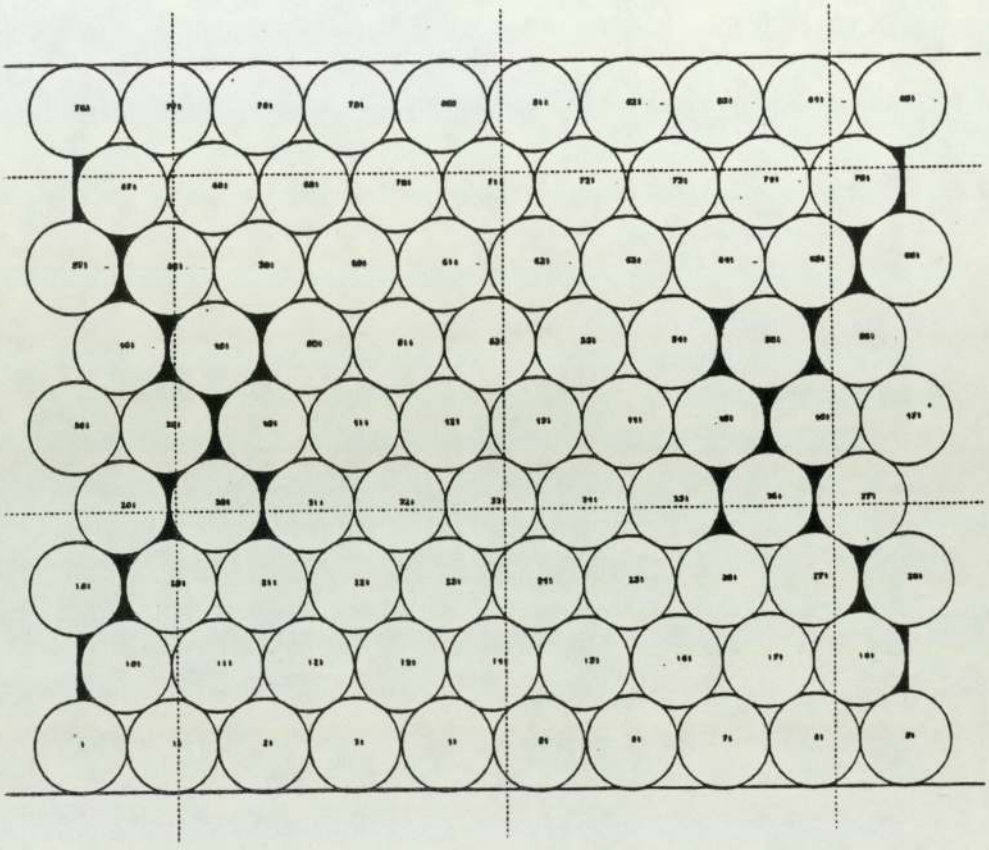

PLATTEN VELOCITY = 0.002

FIGURE 8.17 DEFORMATION OF AN 86 DISC PACKING AT 1.48% STRAIN, WITH FRICTIONLESS DISCS AND PLATTENS

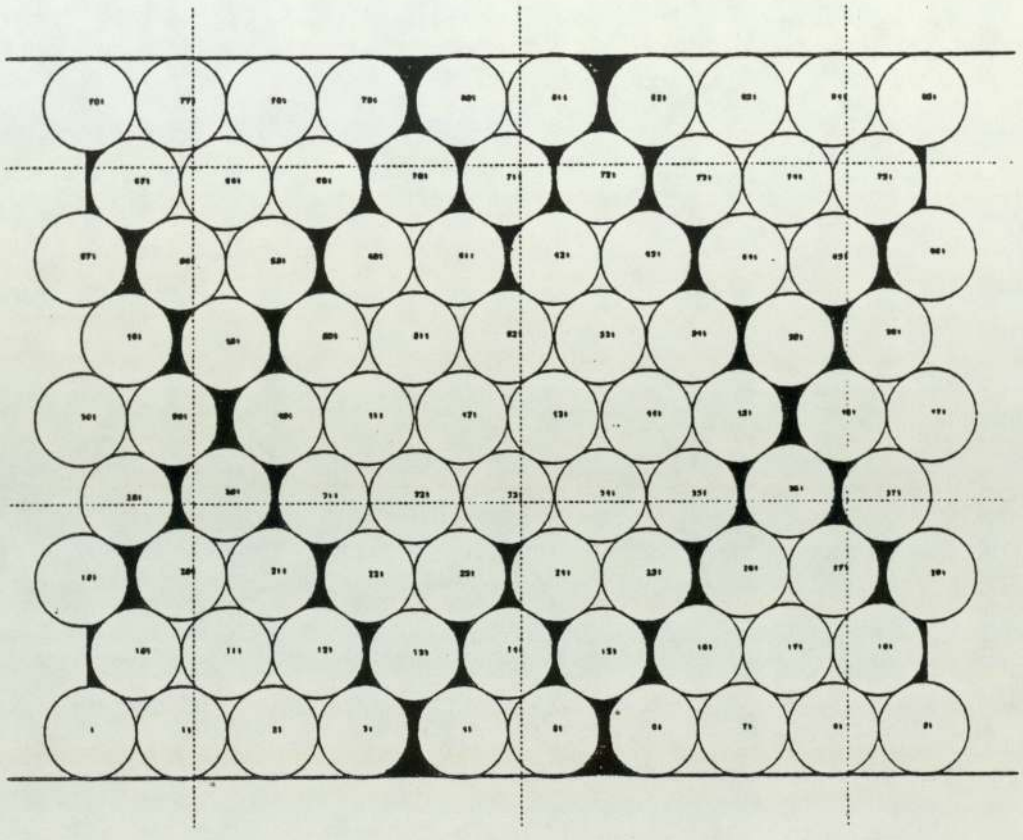

PLATTEN VELOCITY = 0.002

FIGURE 8.18 DEFORMATION OF AN 86 DISC PACKING AT 2.2% STRAIN, WITH FRICTIONLESS DISCS AND PLATTENS

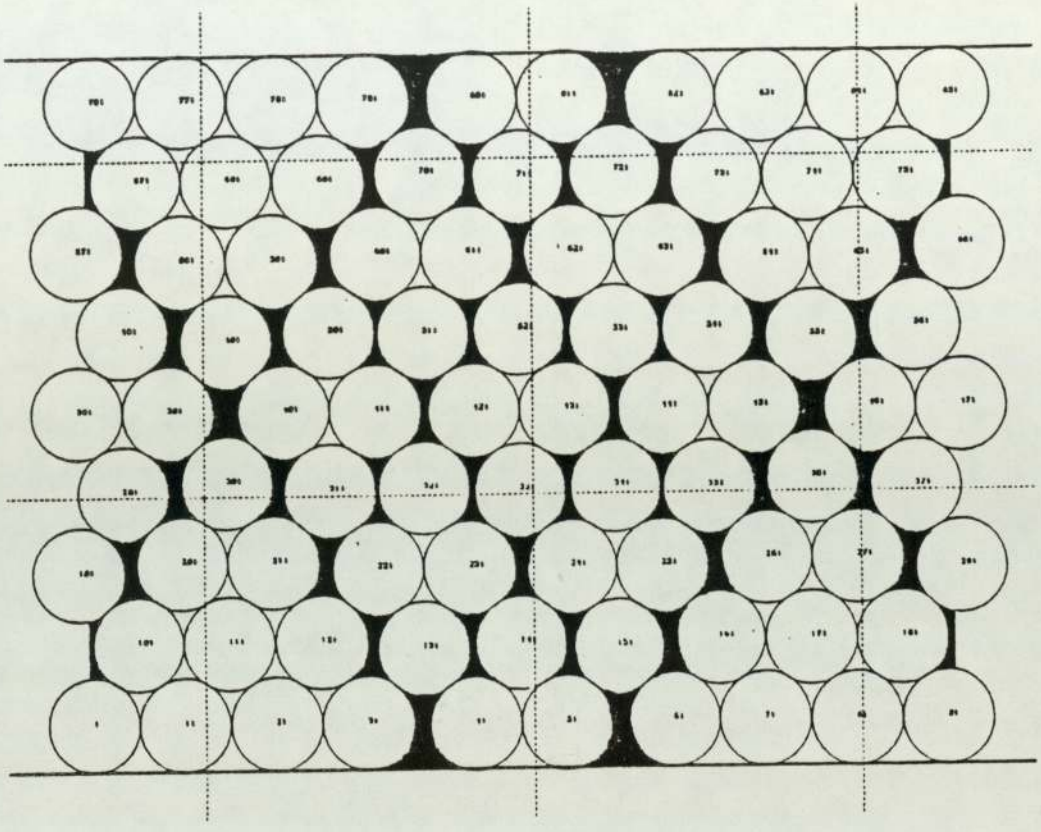

PLATTEN VELOCITY = 0.002

FIGURE 8.19 DEFORMATION OF AN 86 DISC PACKING AT 3.3% STRAIN, WITH FRICTIONLESS DISCS AND PLATTENS

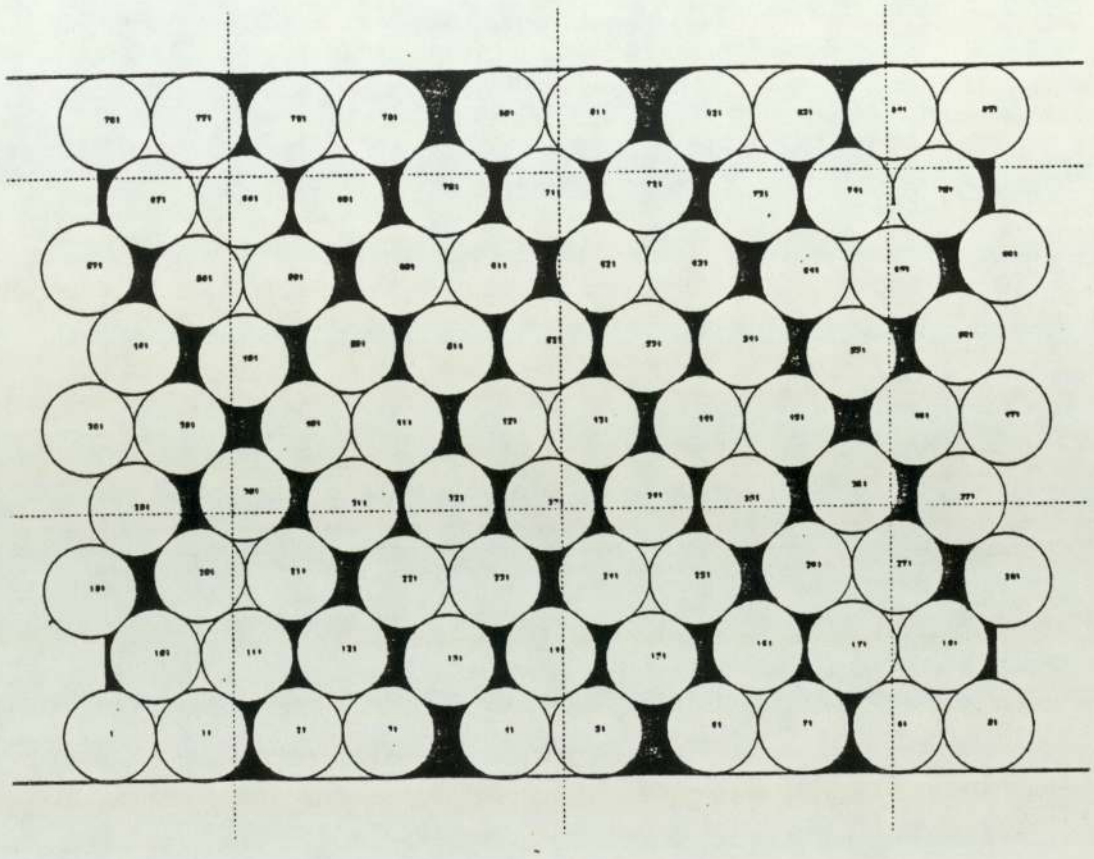

PLATTEN VELOCITY = 0.002

FIGURE 8.20 DEFORMATION OF AN 86 DISC PACKING AT 4.5% STRAIN, WITH FRICTIONLESS DISCS AND PLATTENS

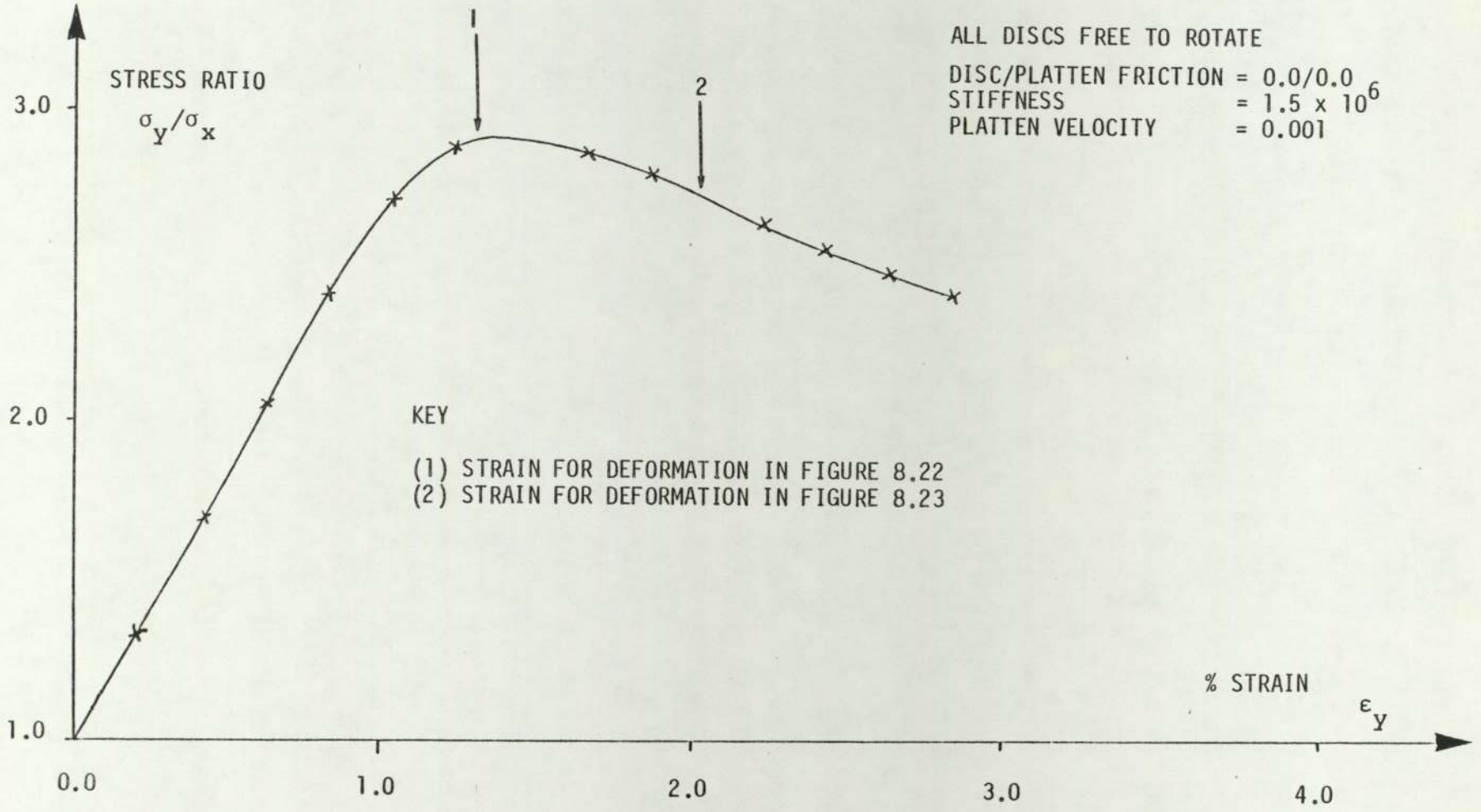

FIGURE 8.21 STRESS RATIO - STRAIN CURVE FOR A 95 DISC PACKING

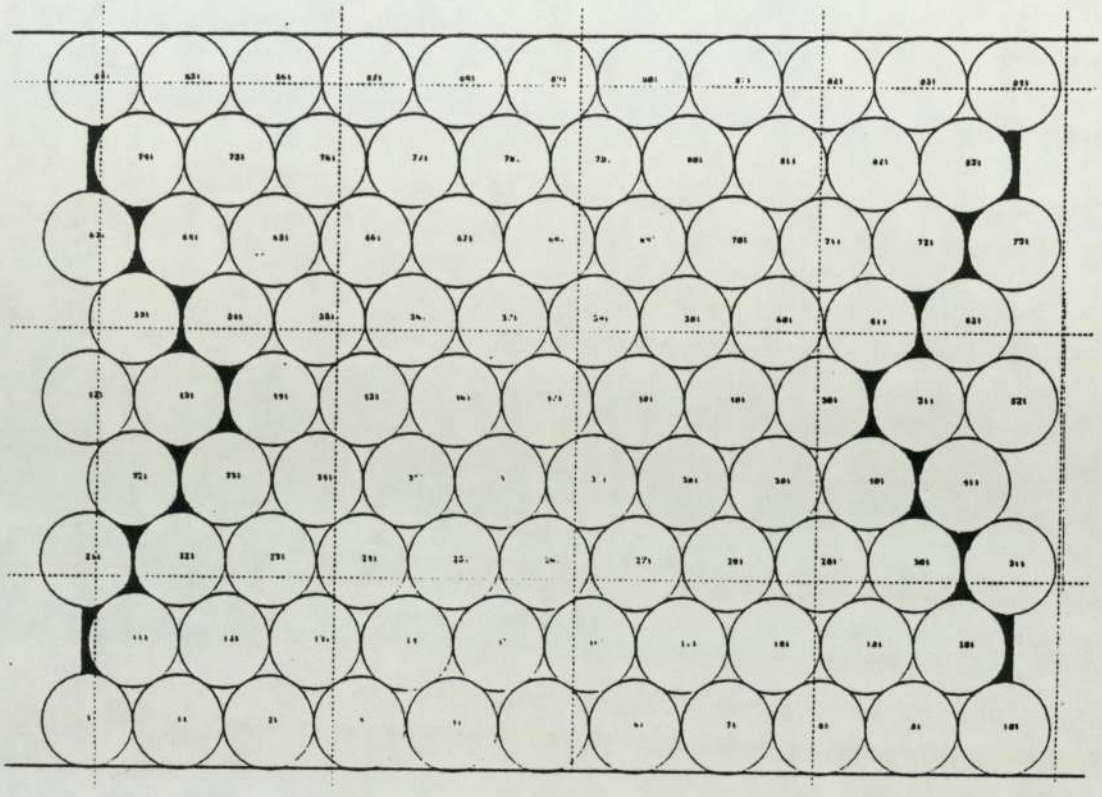

FIGURE 8.22 DEFORMATION OF A 95 DISC PACKING AT 1.3% STRAIN, WITH FRICTIONLESS DISCS AND PLATTENS

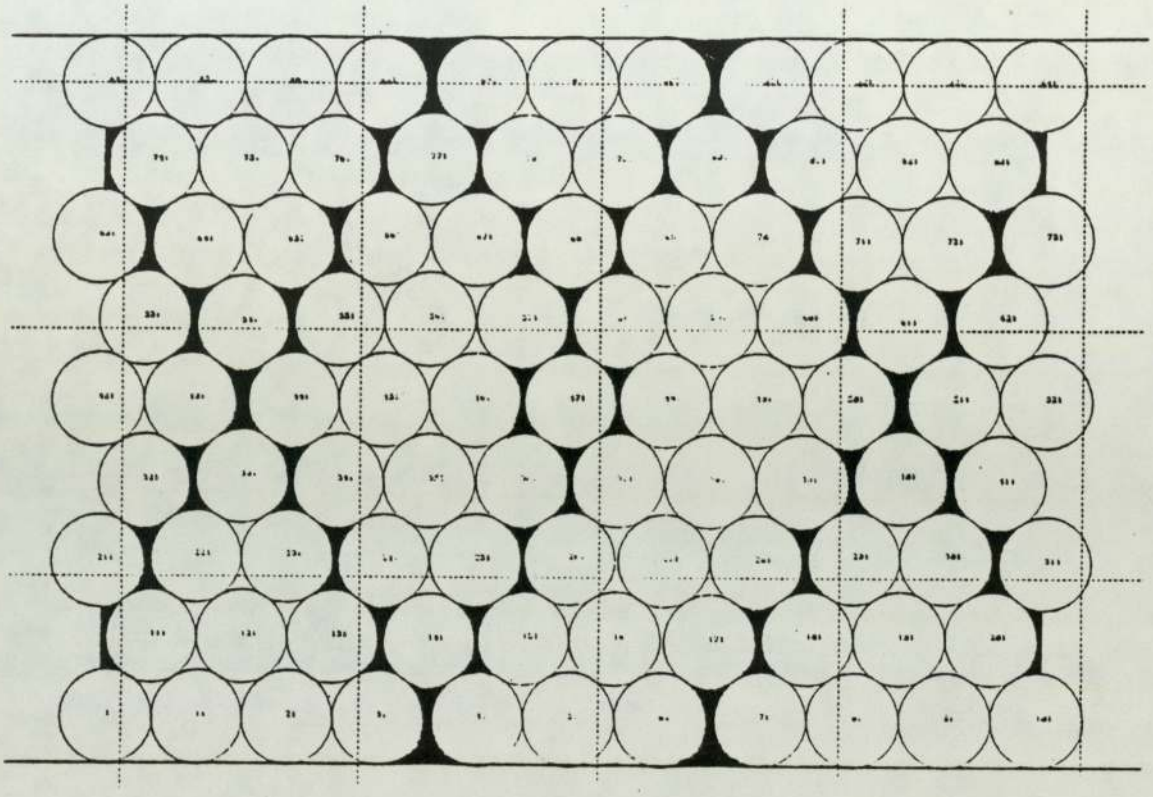

FIGURE 8.23 DEFORMATION OF A 95 DISC PACKING AT 2.0% STRAIN, WITH FRICTIONLESS DISCS AND PLATTENS

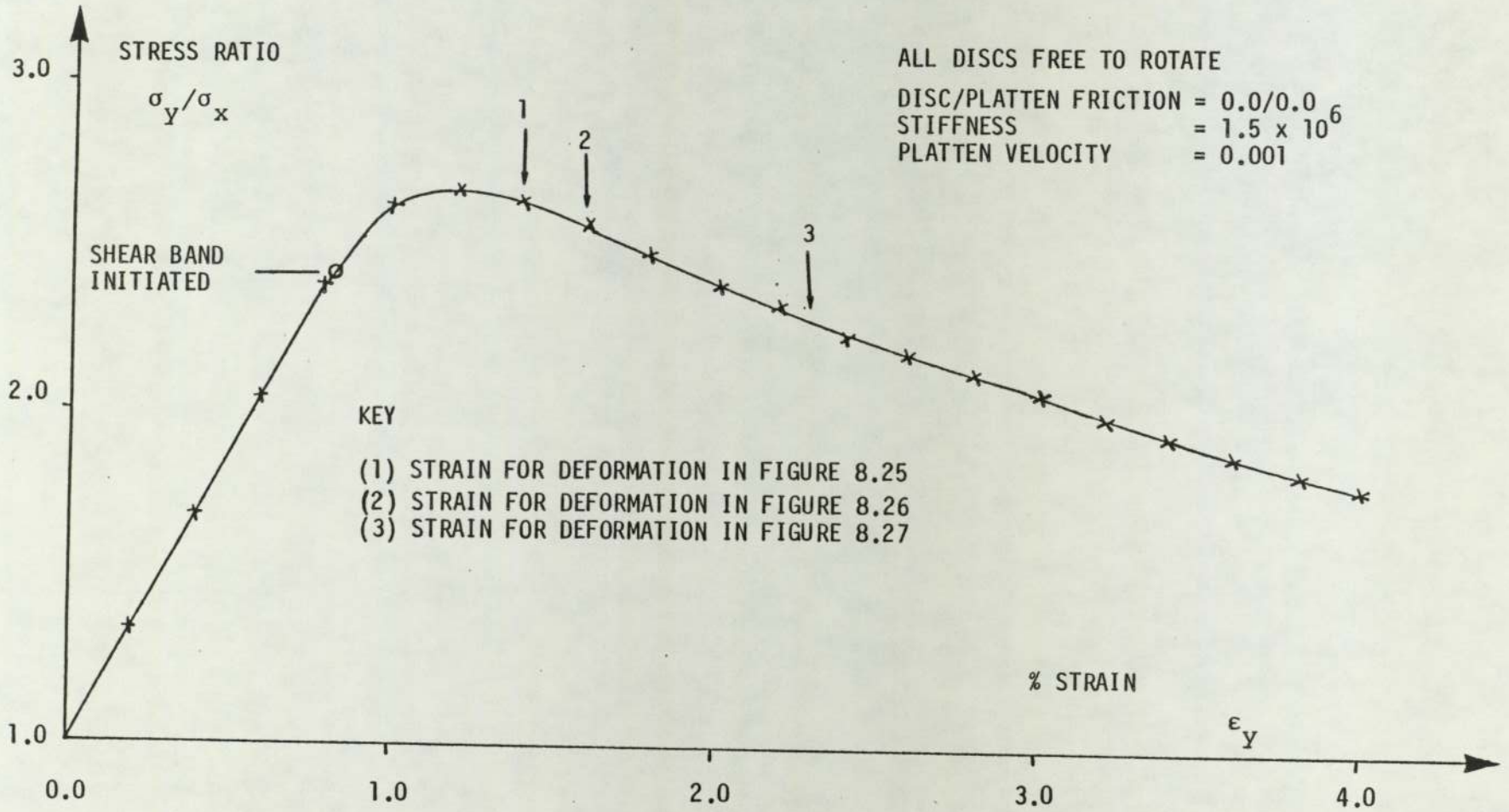

FIGURE 8.24 STRESS RATIO - STRAIN CURVE FOR A 124 DISC PACKING

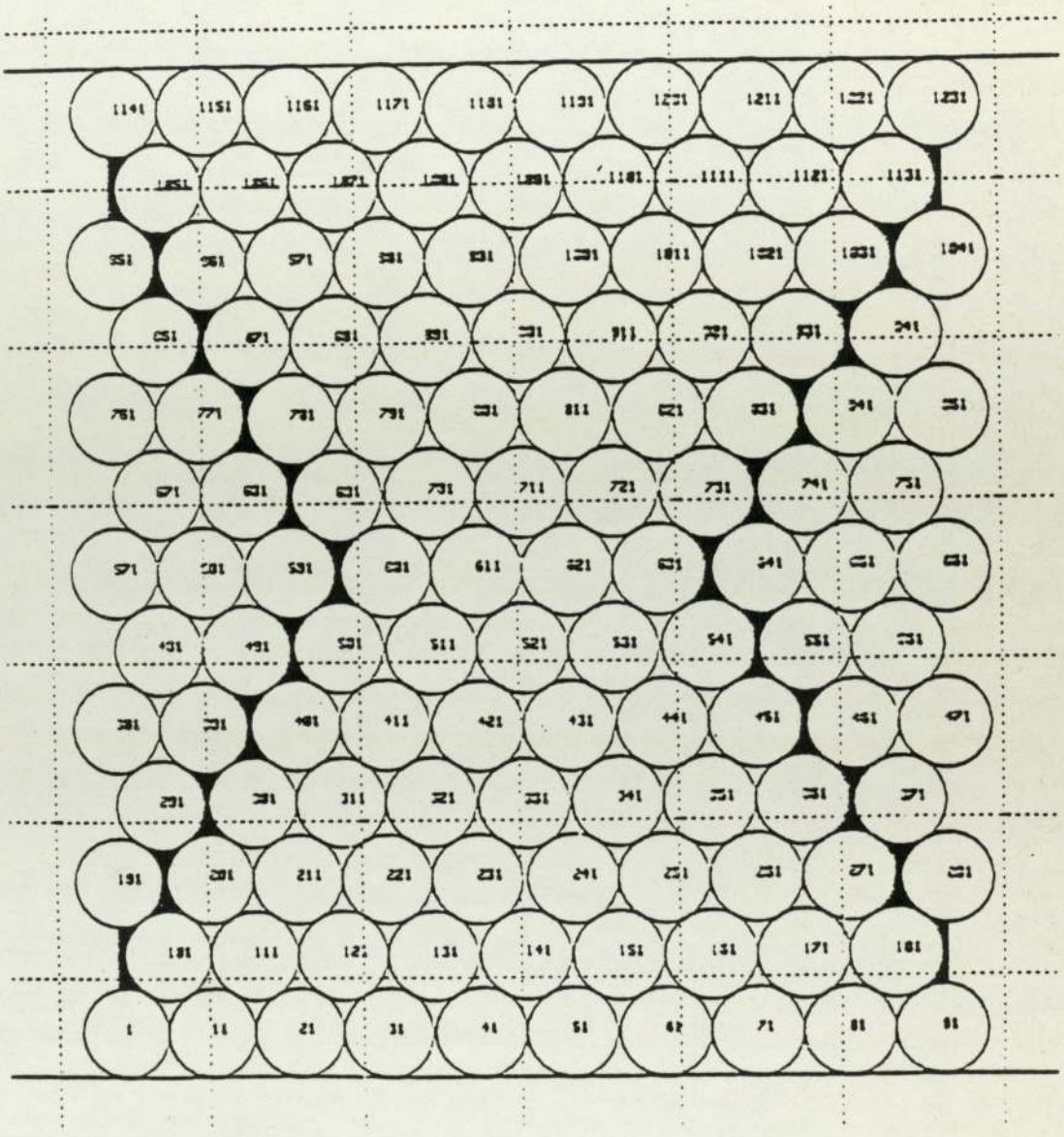

FIGURE 8.25 DEFORMATION OF A 124 DISC PACKING AT 1.4% STRAIN, WITH FRICTIONLESS DISCS AND PLATTENS

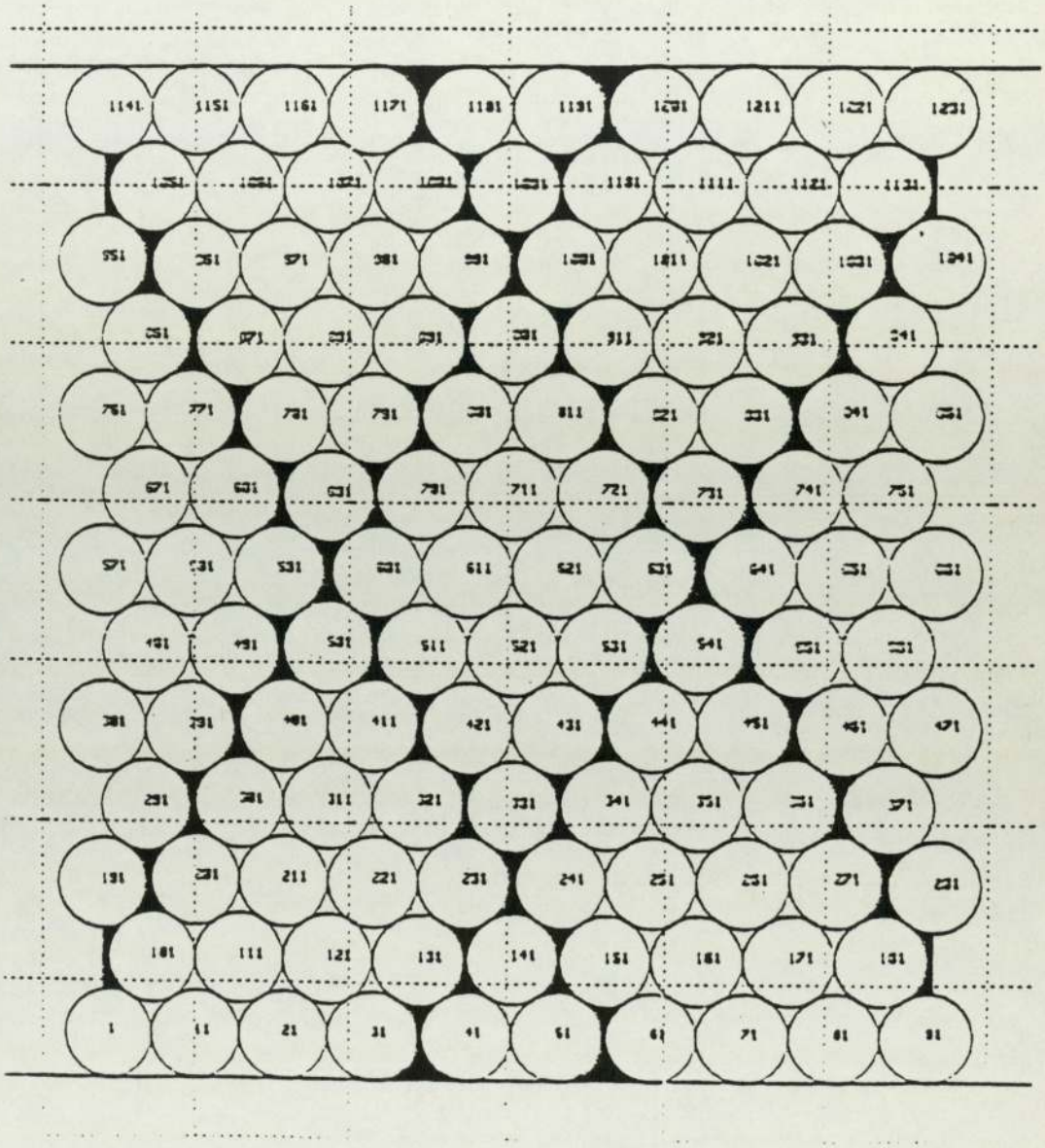

FIGURE 8.26 DEFORMATION OF A 124 DISC PACKING AT 1.6% STRAIN, WITH FRICTIONLESS DISCS AND PLATTENS

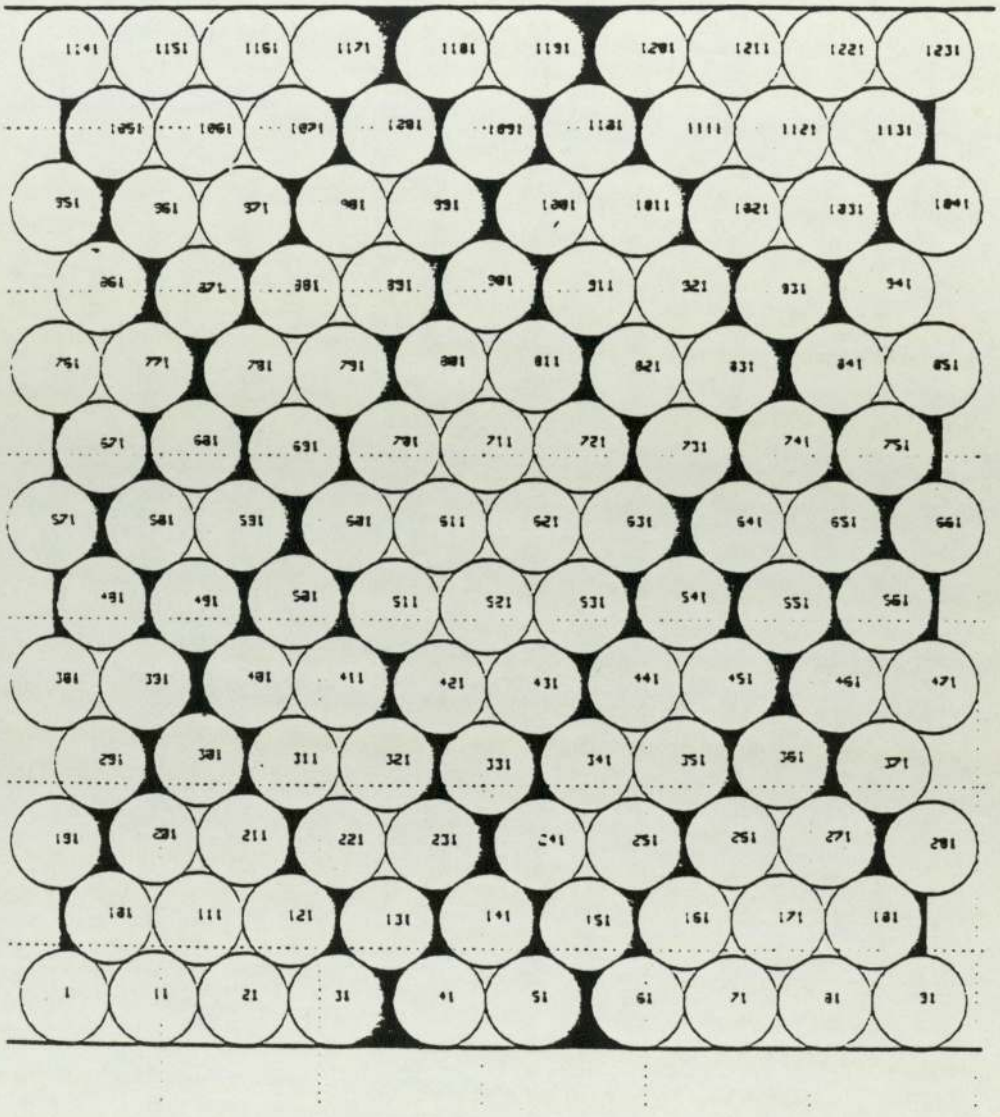

FIGURE 8.27 DEFORMATION OF A 124 DISC PACKING AT 2.3% STRAIN, WITH FRICTIONLESS DISCS AND PLATTENS

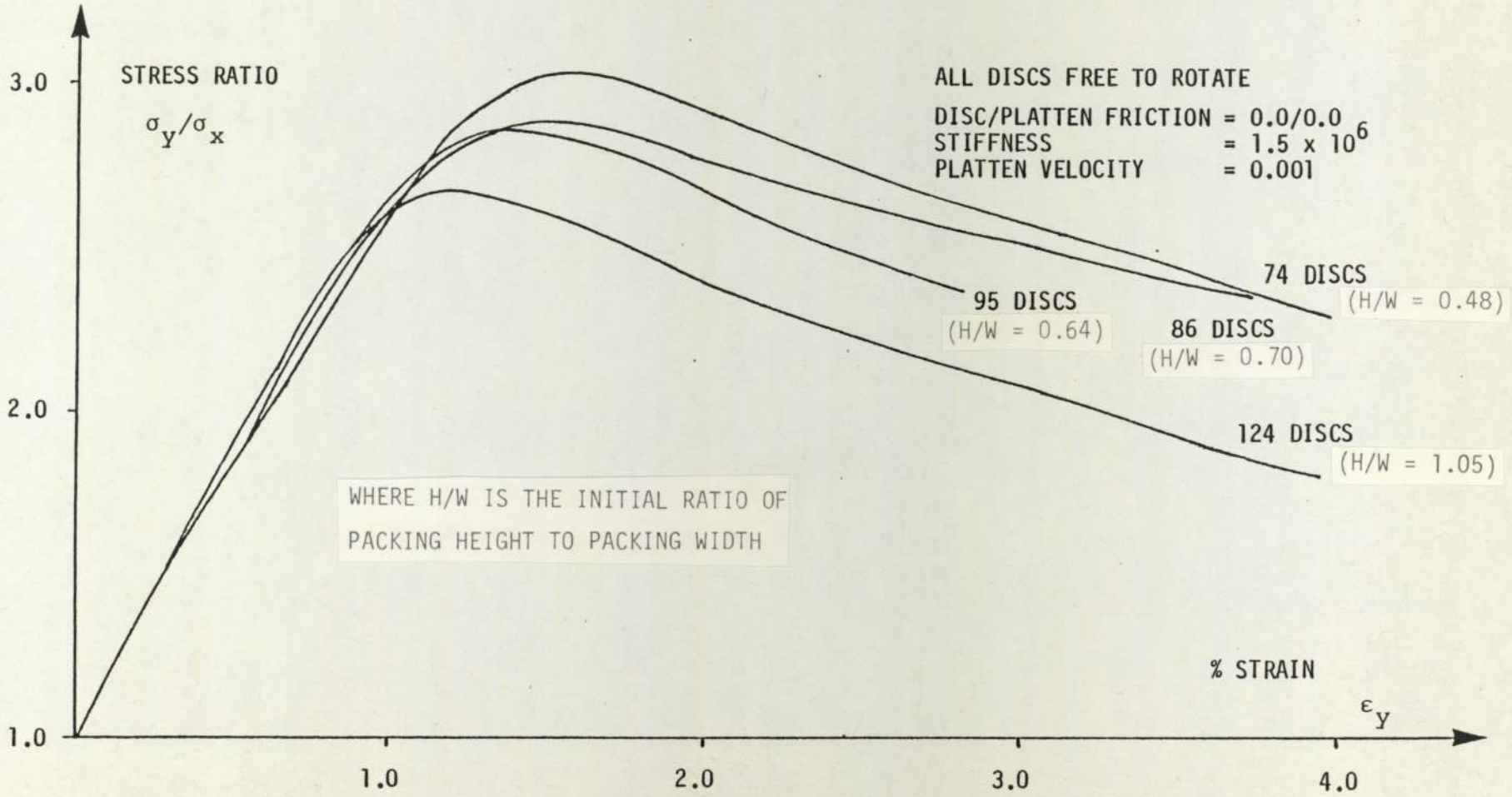

FIGURE 8.28 COMPARISON OF STRESS RATIO - STRAIN CURVES FOR VARIOUS PACKING SIZES

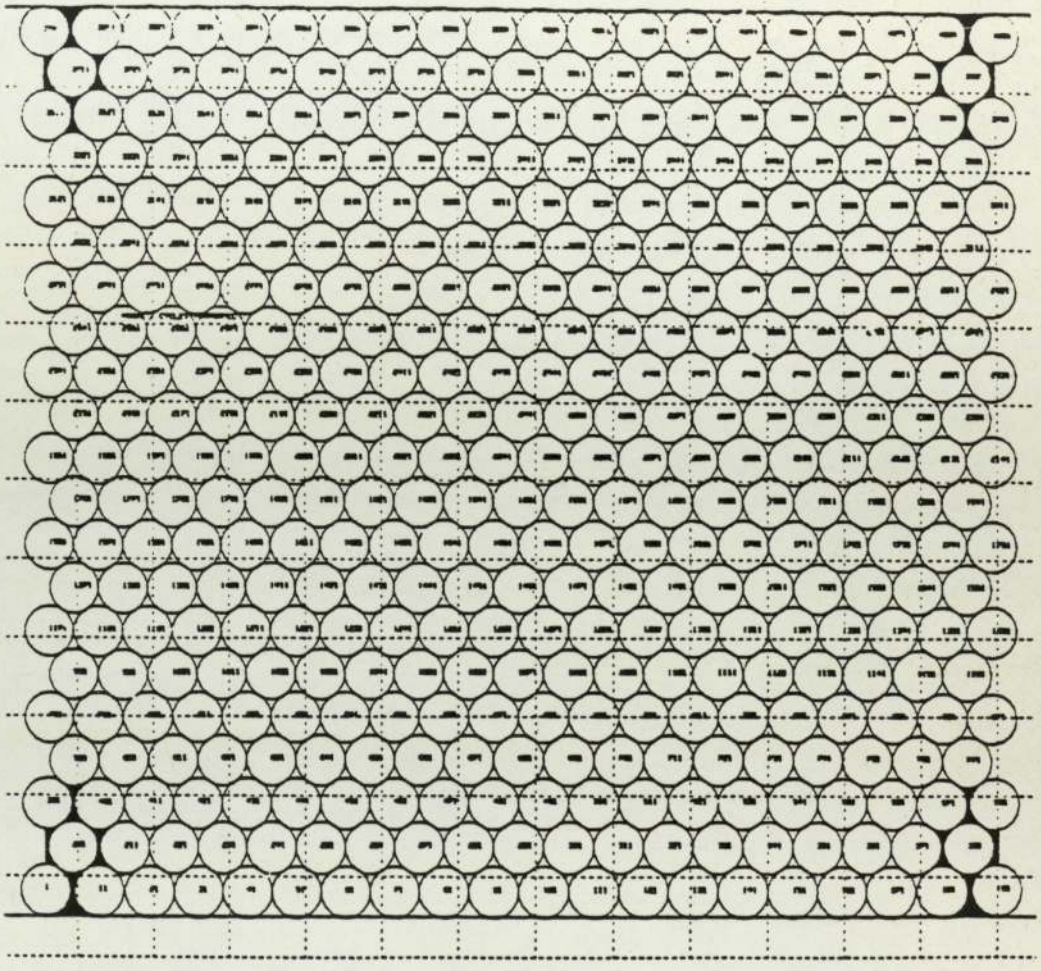

DISC FRICTION = 0.3

PLATTEN FRICTION = 0.0

FIGURE 8.29 DEFORMATION OF A 410 DISC PACKING AT 2.10% STRAIN

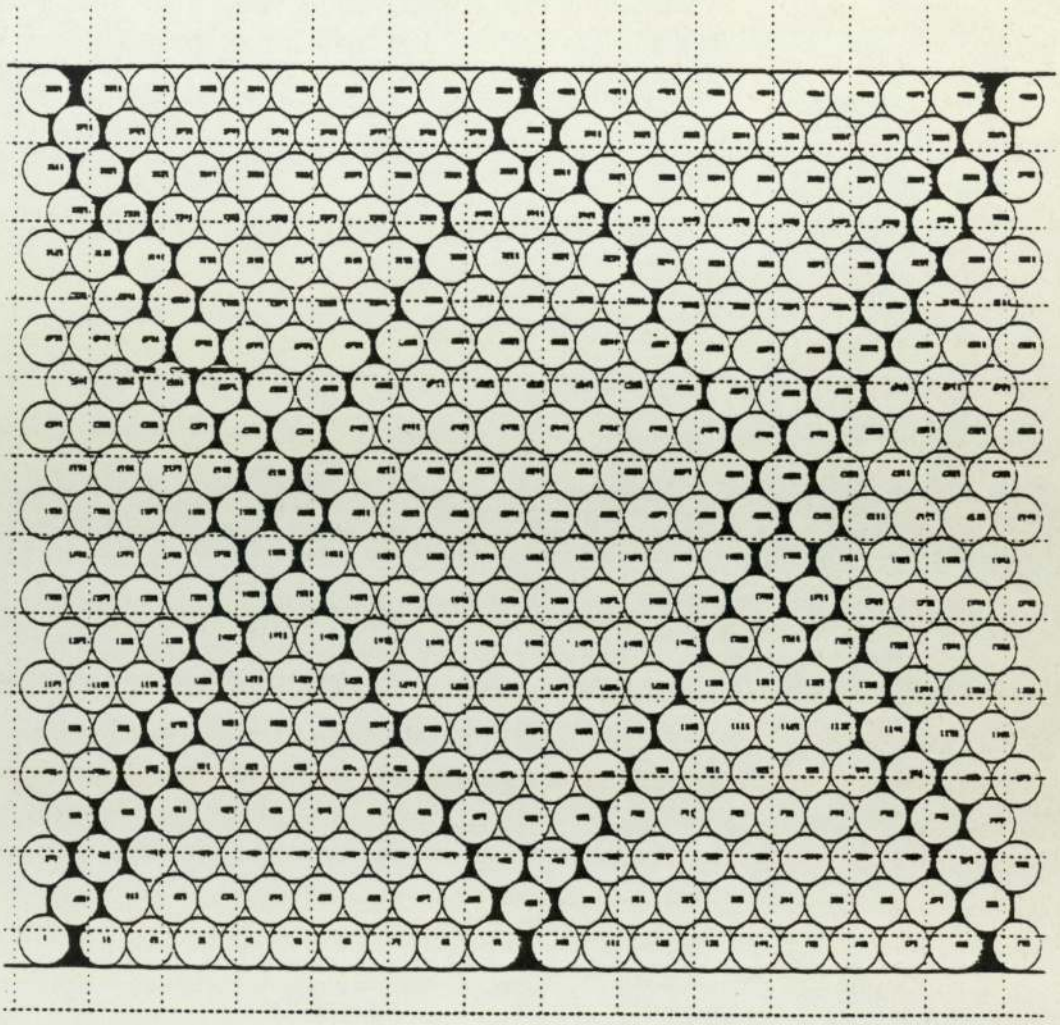

DISC FRICTION = 0.3

PLATTEN FRICTION = 0.0

FIGURE 8.30 DEFORMATION OF A 410 DISC PACKING AT 3.25% STRAIN

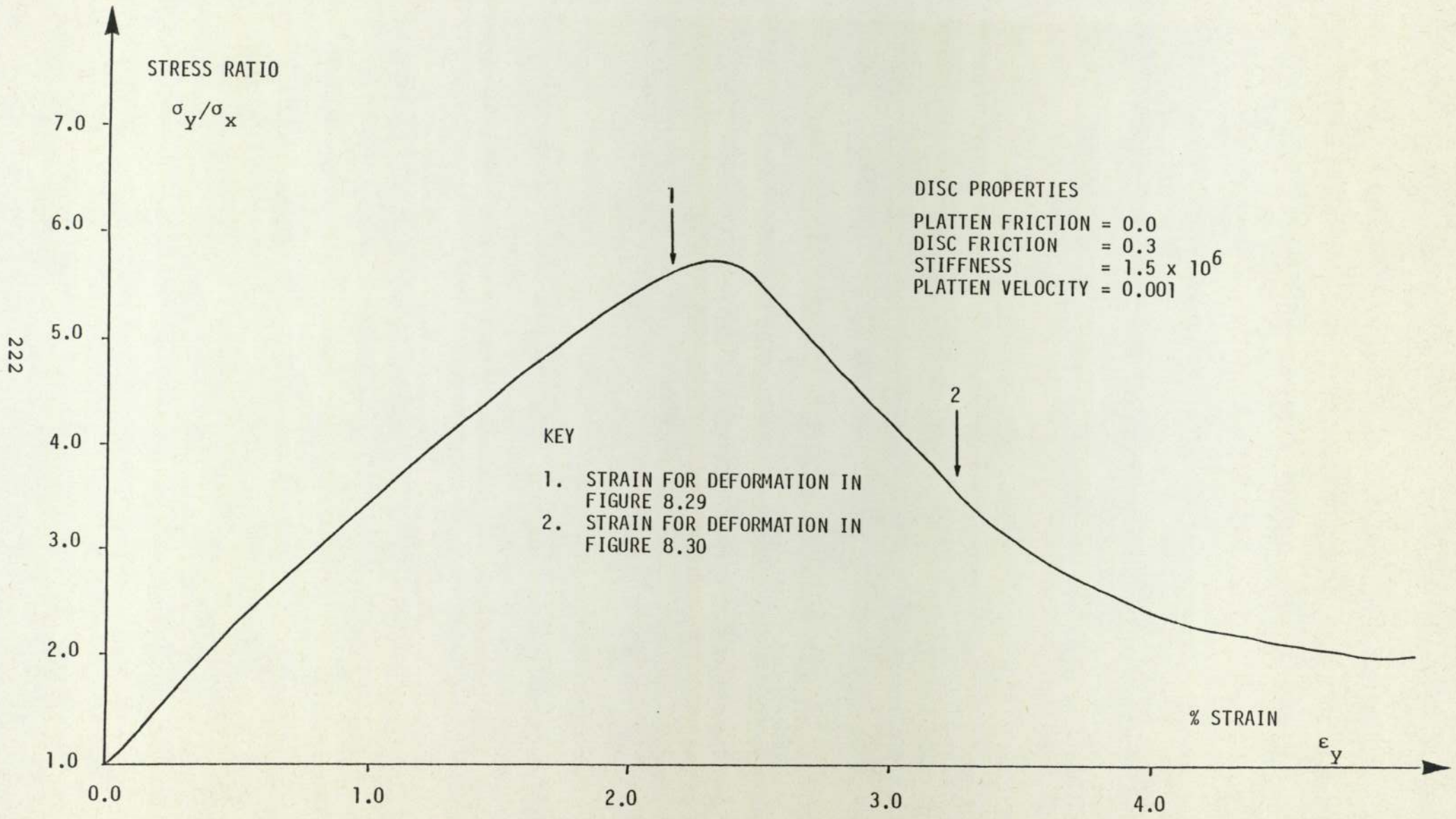

FIGURE 8.31 PLOT OF STRESS - RATIO AGAINST STRAIN FOR A 410 DISC PACKING

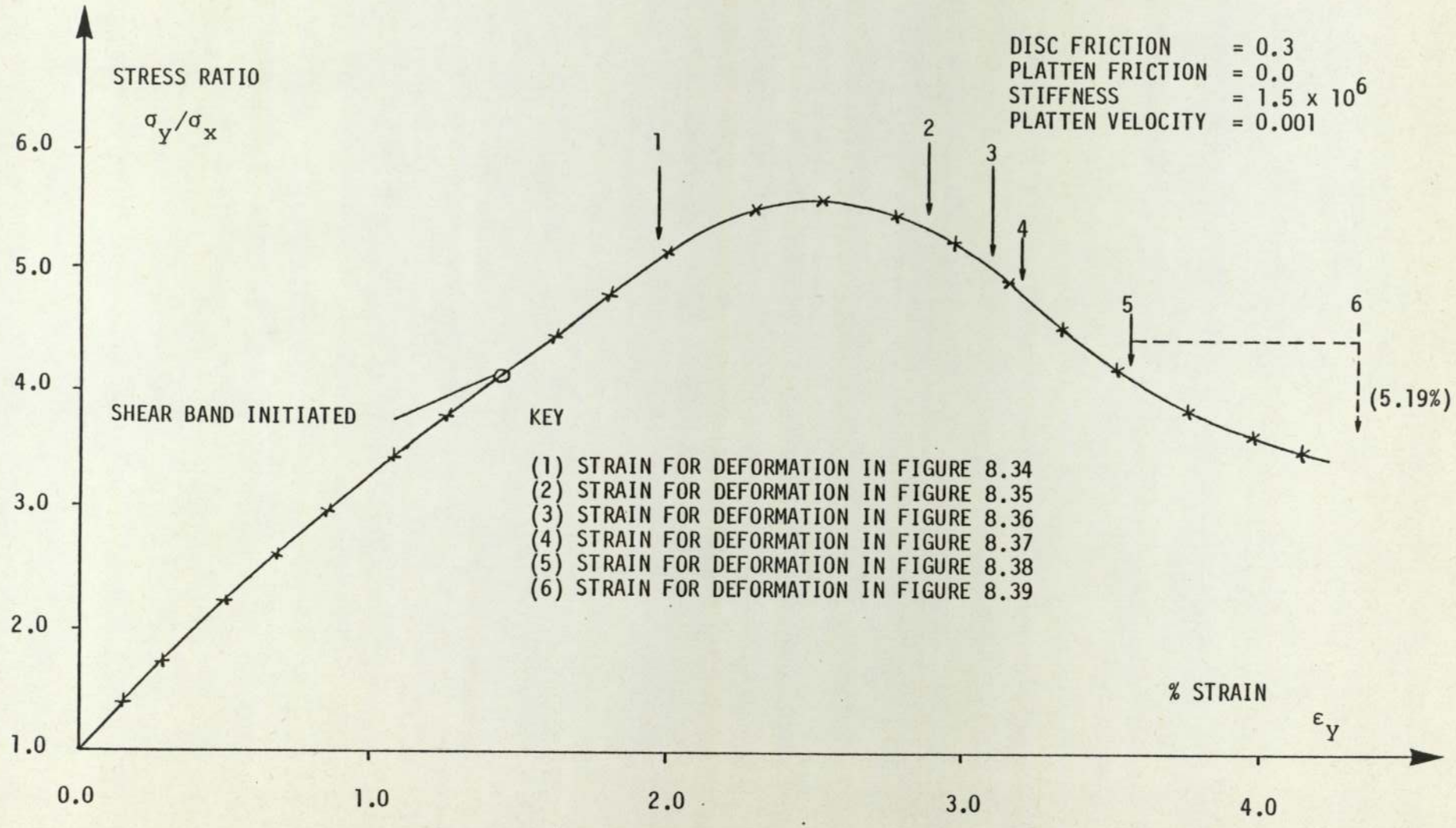

FIGURE 8.32 STRESS RATIO - STRAIN CURVE FOR A 124 DISC PACKING WITH FRICTIONLESS PLATTENS

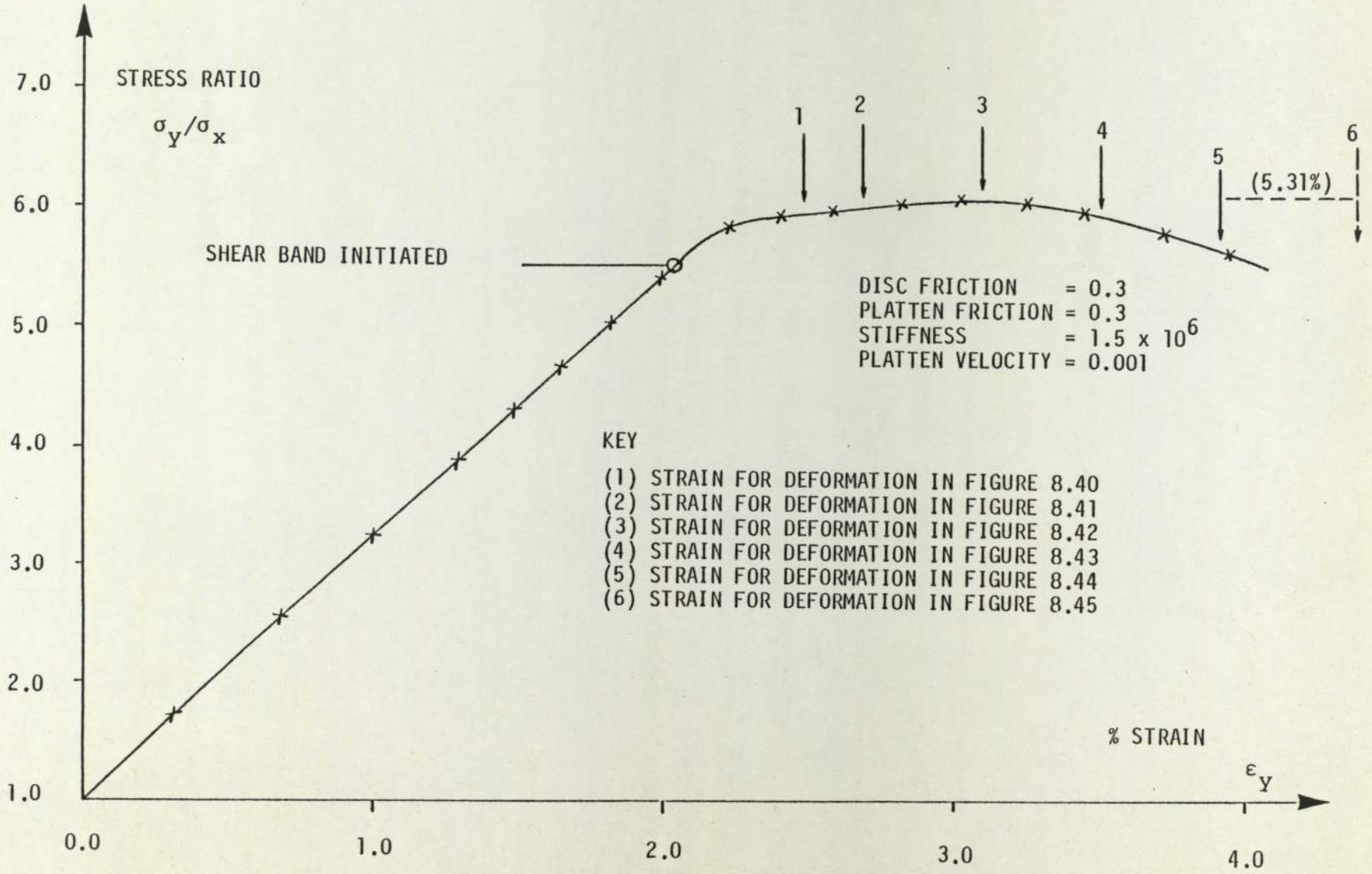

FIGURE 8.33 STRESS RATIO - STRAIN CURVE FOR A 124 DISC PACKING WITH FRICTIONAL PLATTENS

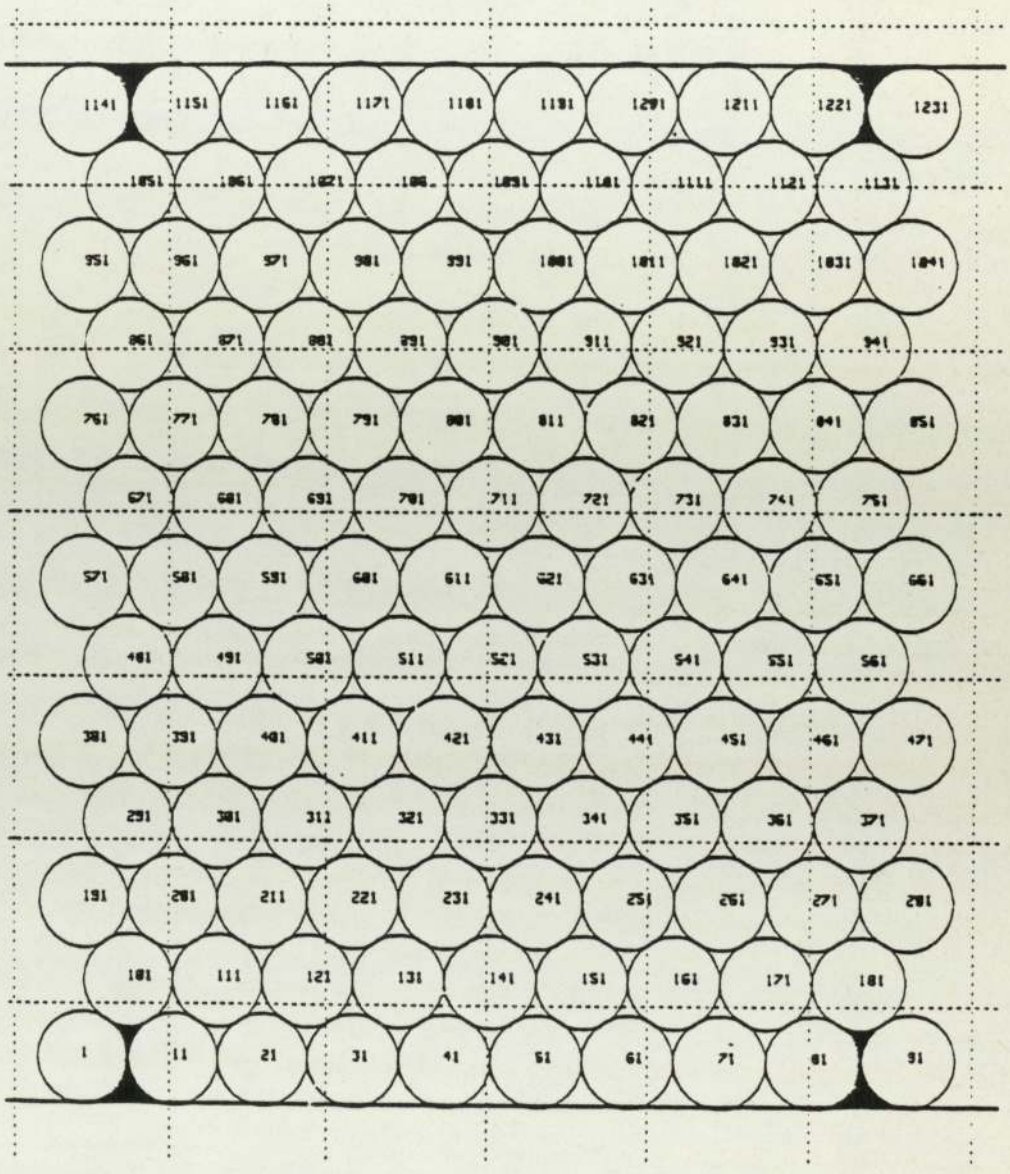

DISC FRICTION = 0.3

PLATTEN FRICTION = 0.0

ALL DISCS FREE TO ROTATE

FIGURE 8.34 DEFORMATION OF A 124 DISC PACKING AT 1.97% STRAIN WITH FRICTIONLESS PLATTENS

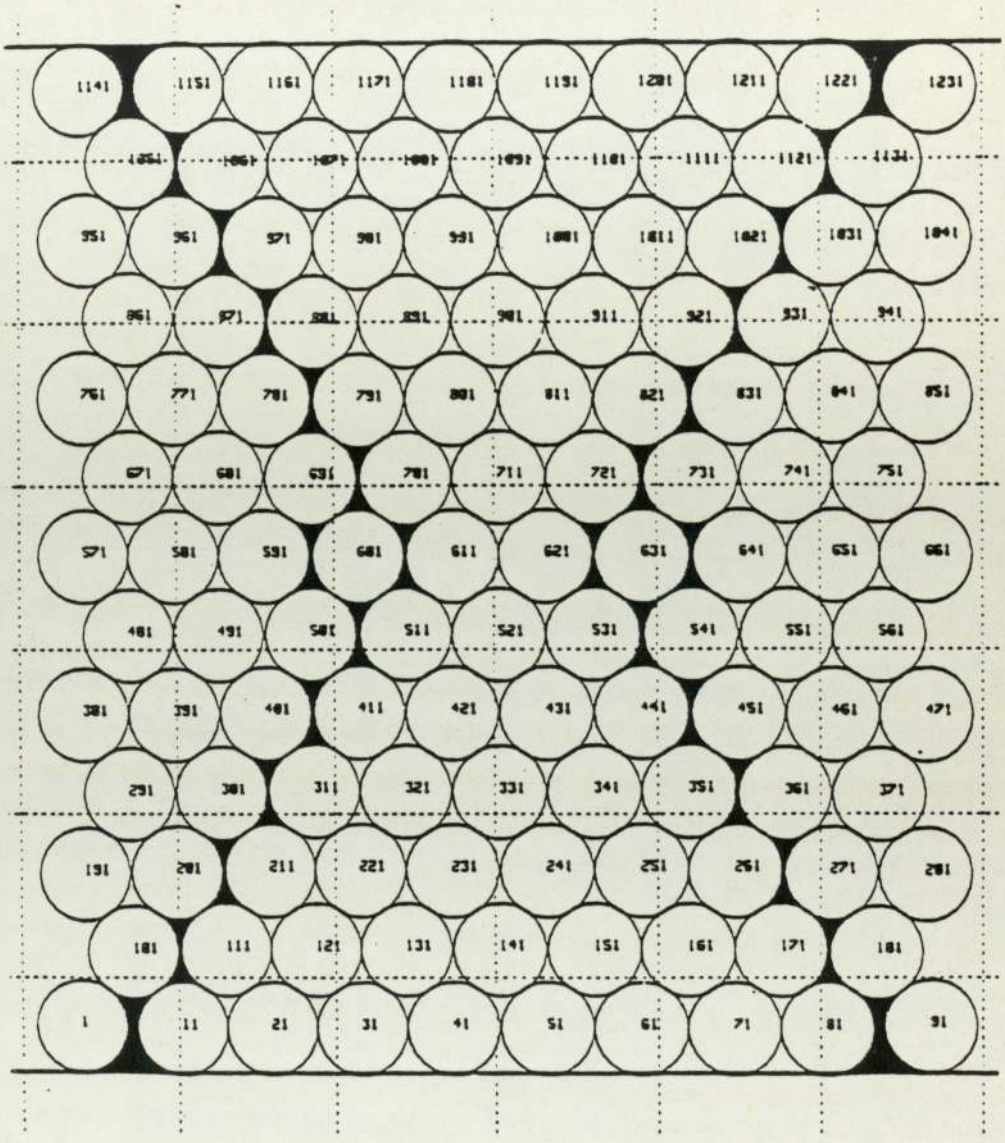

DISC FRICTION = 0.3

PLATTEN FRICTION = 0.0

ALL DISCS FREE TO ROTATE

FIGURE 8.35 DEFORMATION OF A 124 DISC PACKING AT 2.9% STRAIN WITH FRICTIONLESS PLATTENS

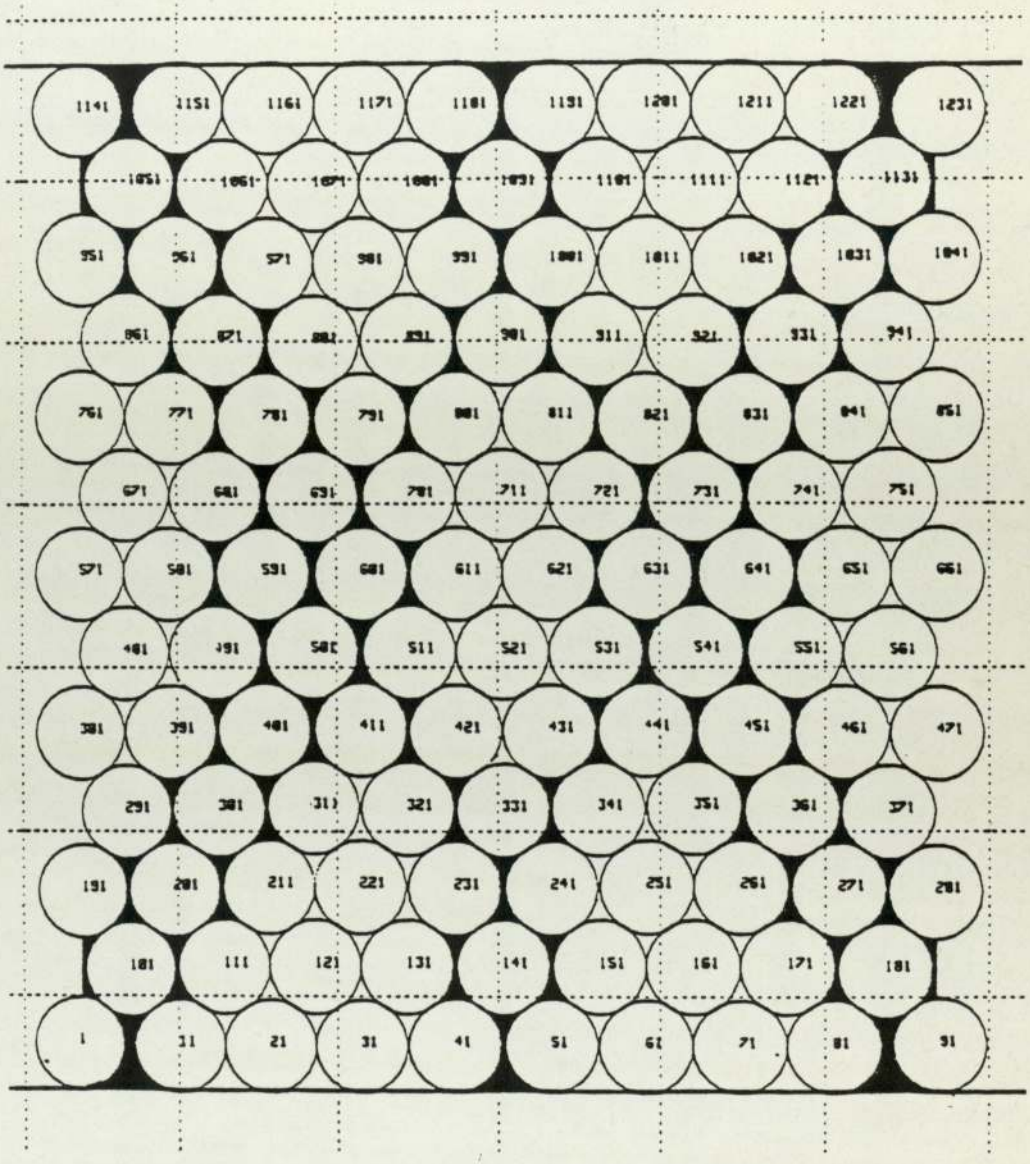

DISC FRICTION = 0.3

PLATTEN FRICTION = 0.0

ALL DISCS FREE TO ROTATE

FIGURE 8.36 DEFORMATION OF A 124 DISC PACKING AT 3.10% STRAIN WITH FRICTIONLESS PLATTENS

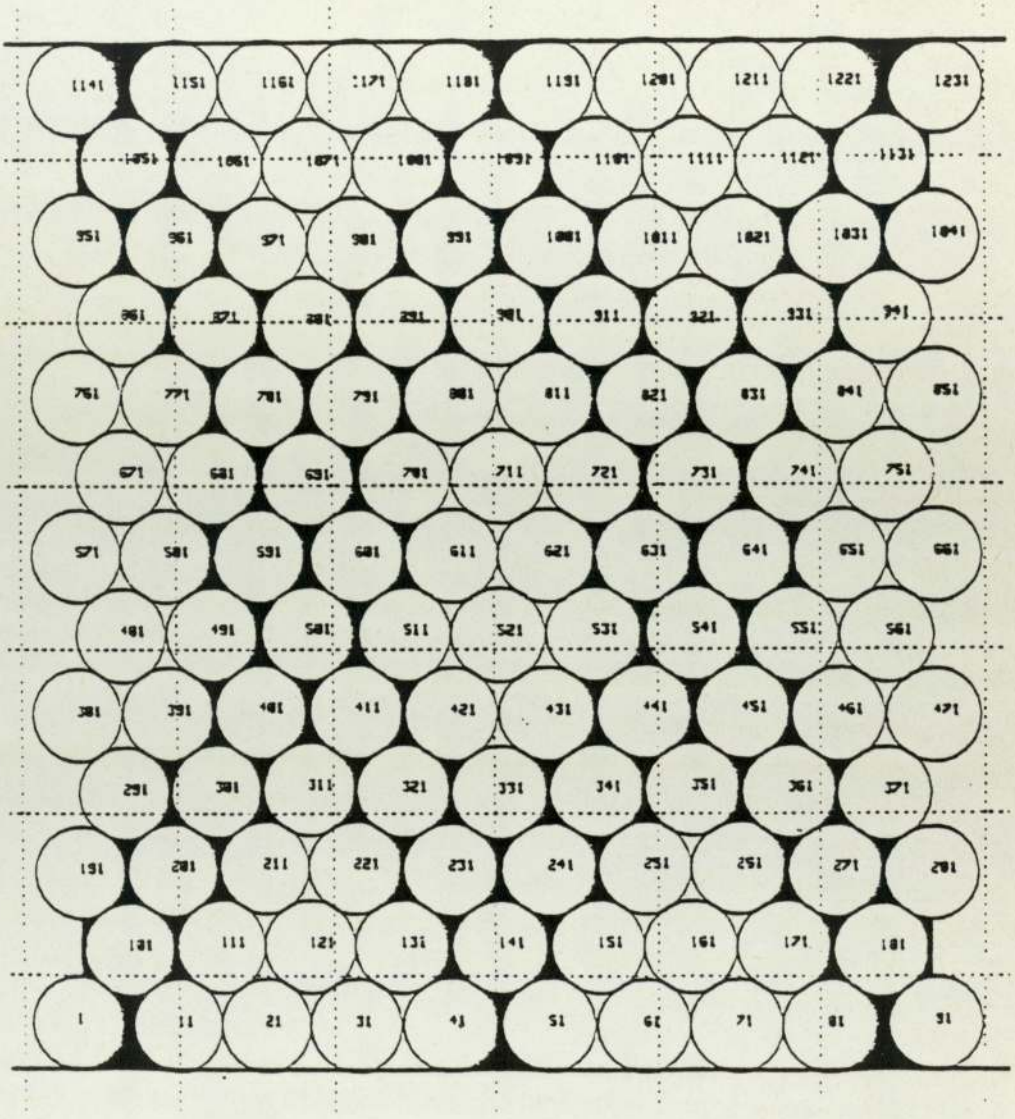

DISC FRICTION = 0.3

PLATTEN FRICTION = 0.0

ALL DISCS FREE TO ROTATE

FIGURE 8.37 DEFORMATION OF A 124 DISC PACKING AT 3.18% STRAIN WITH FRICTIONLESS PLATTENS

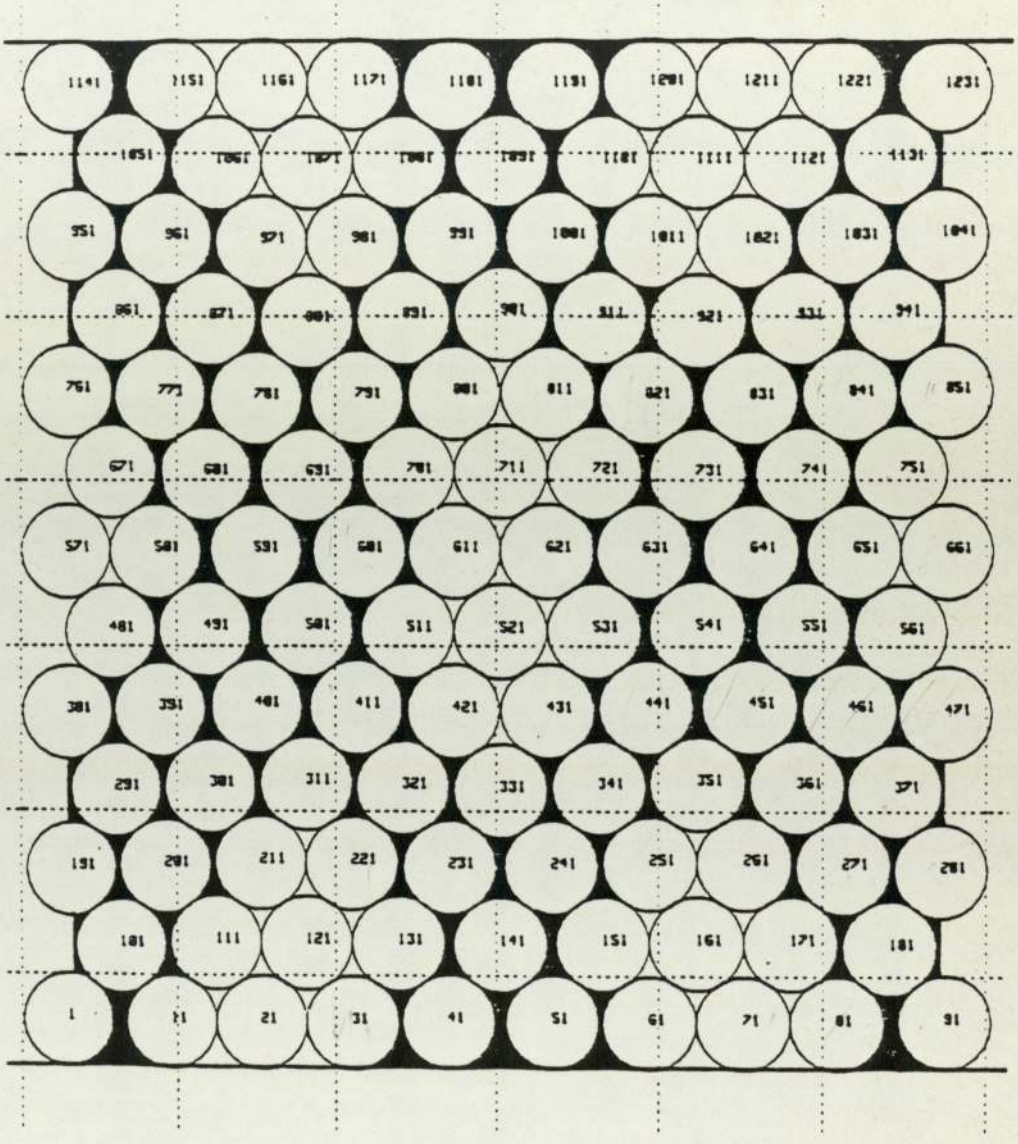

DISC FRICTION = 0.3

PLATTEN FRICTION = 0.0

ALL DISCS FREE TO ROTATE

FIGURE 8.38 DEFORMATION OF A 124 DISC PACKING AT 3.58% STRAIN WITH FRICTIONLESS PLATTENS

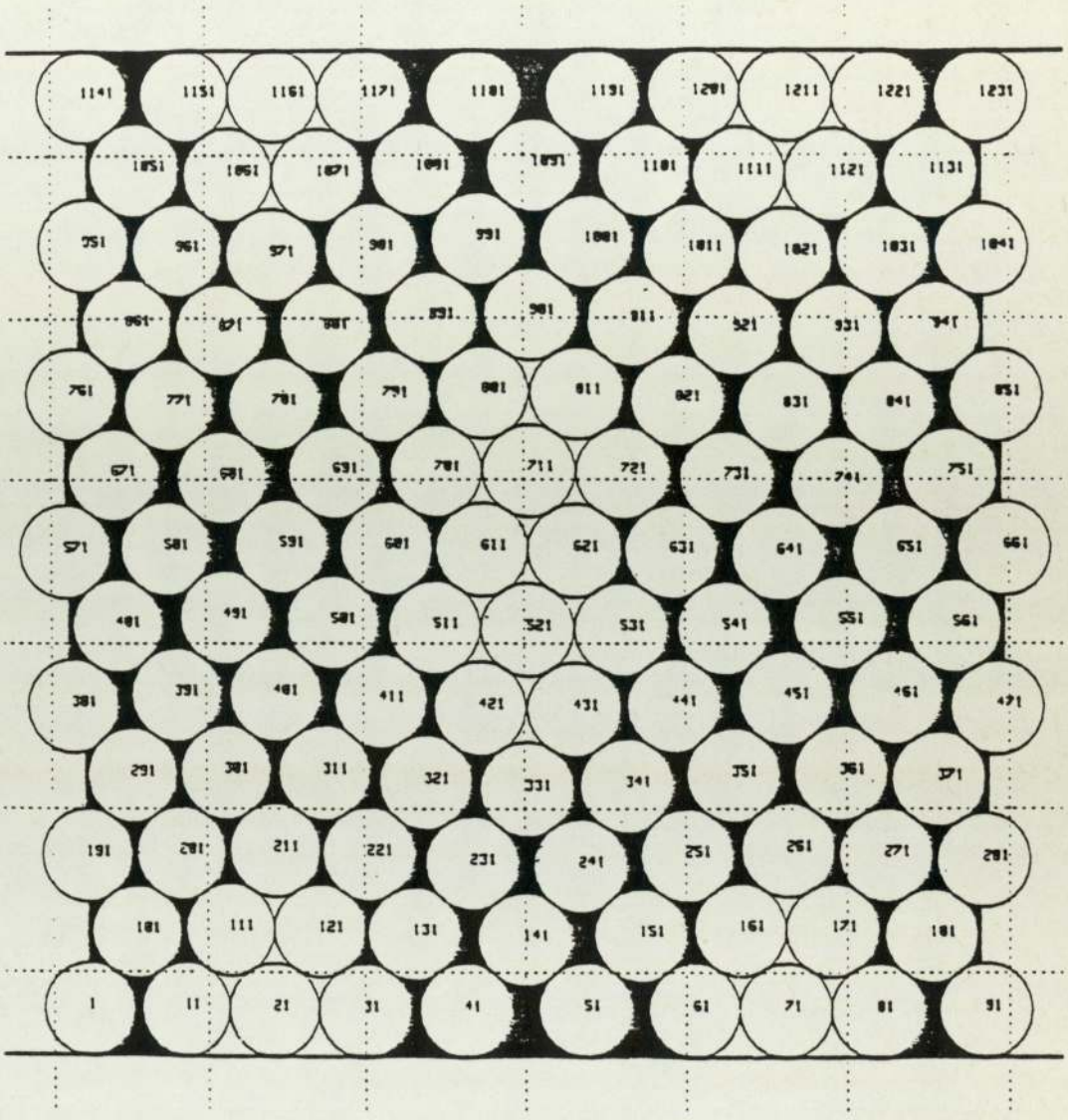

DISC FRICTION = 0.3

PLATTEN FRICTION = 0.0

ALL DISCS FREE TO ROTATE

FIGURE 8.39 DEFORMATION OF A 124 DISC PACKING AT 5.19% STRAIN WITH FRICTIONLESS PLATTENS

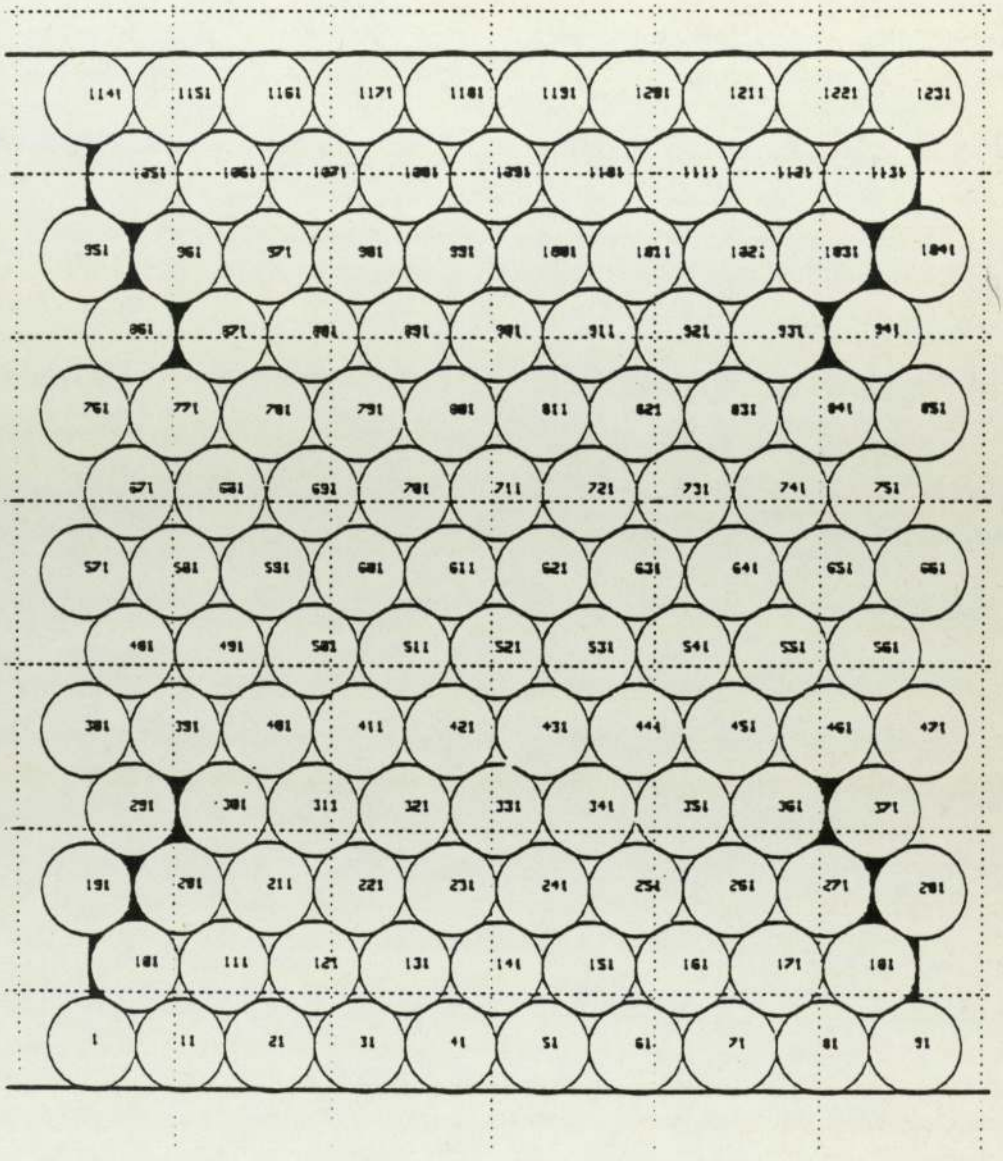

DISC FRICTION = 0.3

PLATTEN FRICTION = 0.3

ALL DISCS ARE FREE TO ROTATE

FIGURE 8.40 DEFORMATION OF A 124 DISC PACKING AT 2.49% STRAIN WITH FRICTIONAL PLATTENS

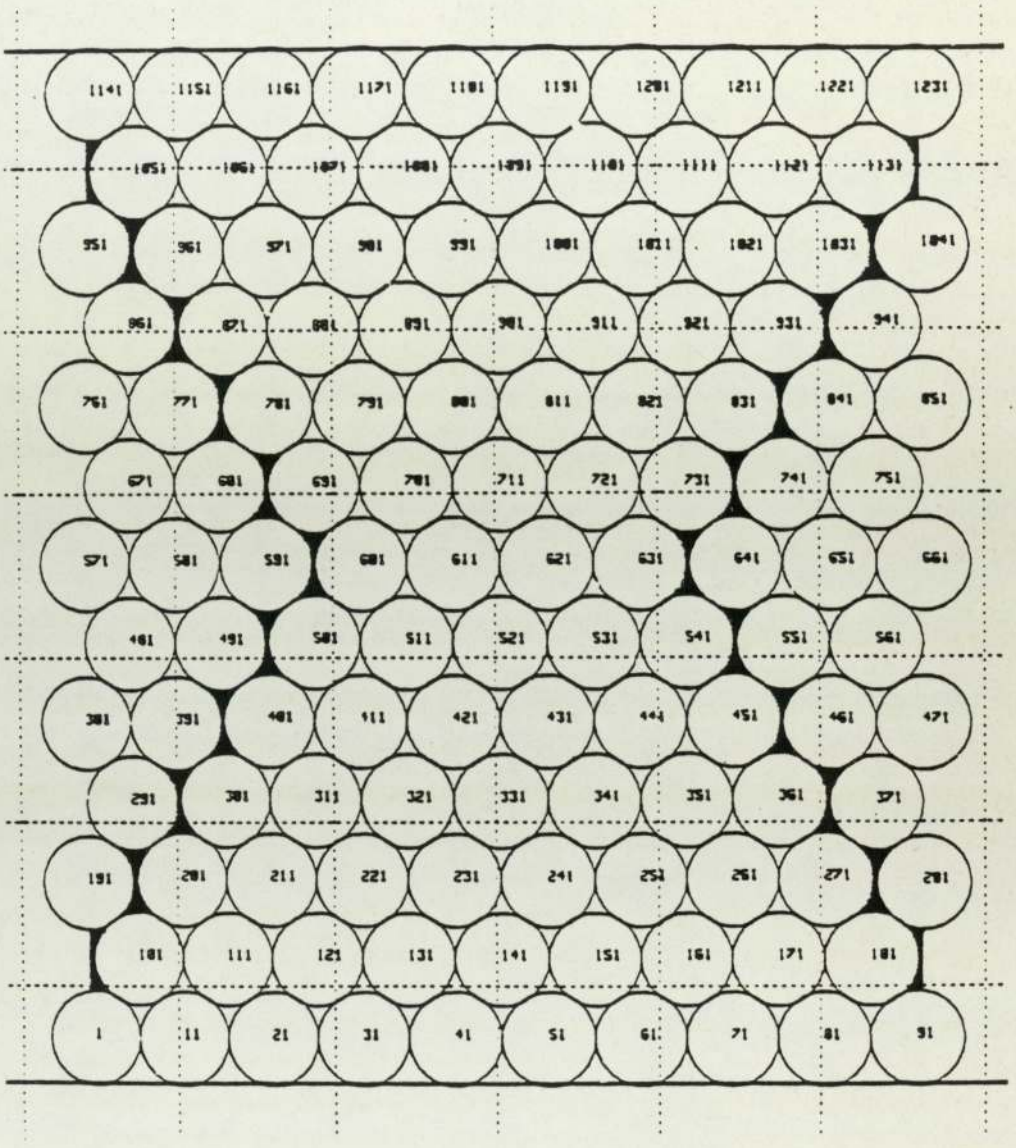

DISC FRICTION = 0.3

PLATTEN FRICTION = 0.3

ALL DISCS FREE TO ROTATE

FIGURE 8.41 DEFORMATION OF A 124 DISC PACKING AT 2.70% STRAIN WITH FRICTIONAL PLATTENS

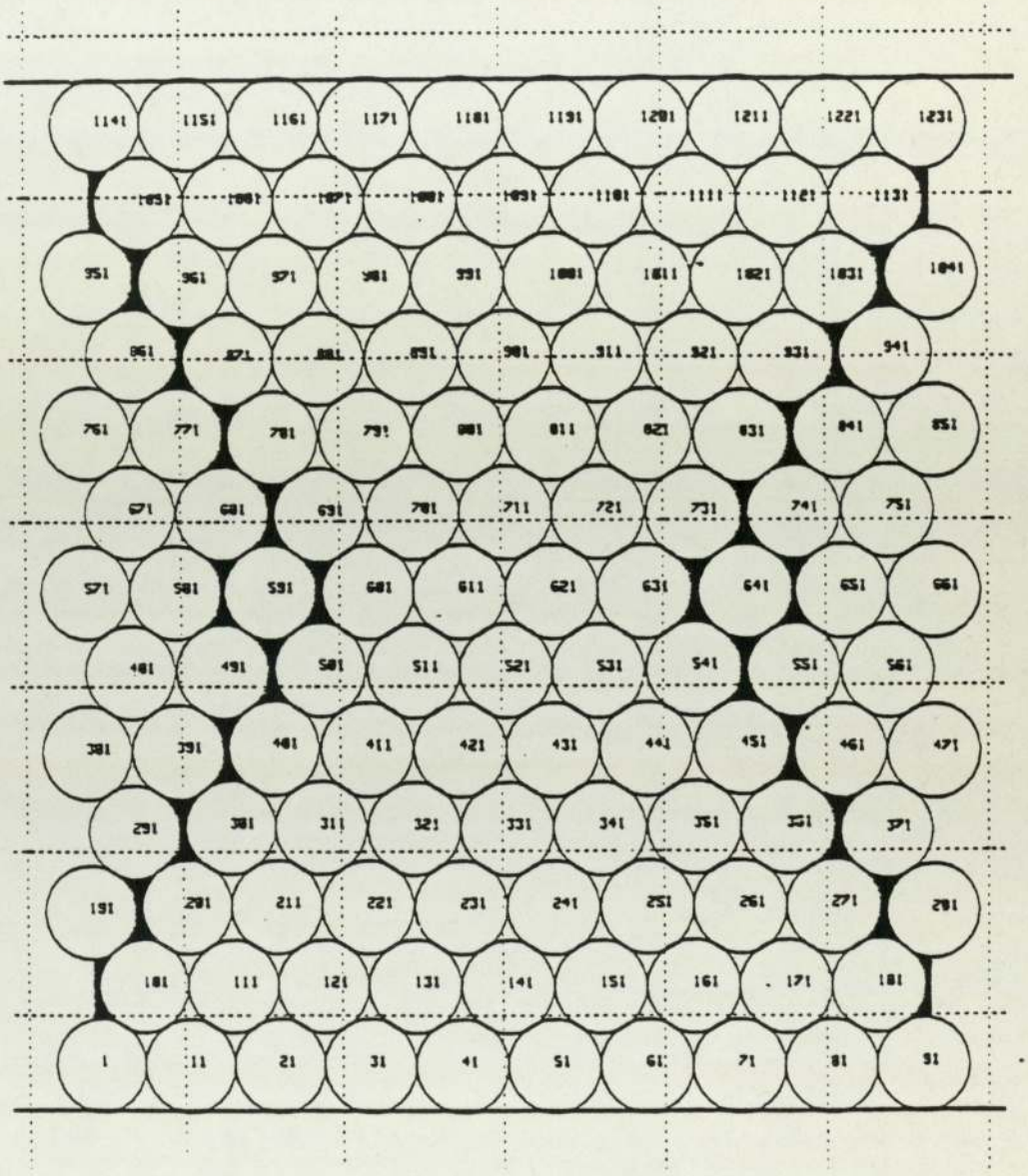

DISC FRICTION = 0.3

PLATTEN FRICTION = 0.3

ALL DISCS ARE FREE TO ROTATE

FIGURE 8.42 DEFORMATION OF A 124 DISC PACKING AT 3.10% STRAIN WITH FRICTIONAL PLATTENS

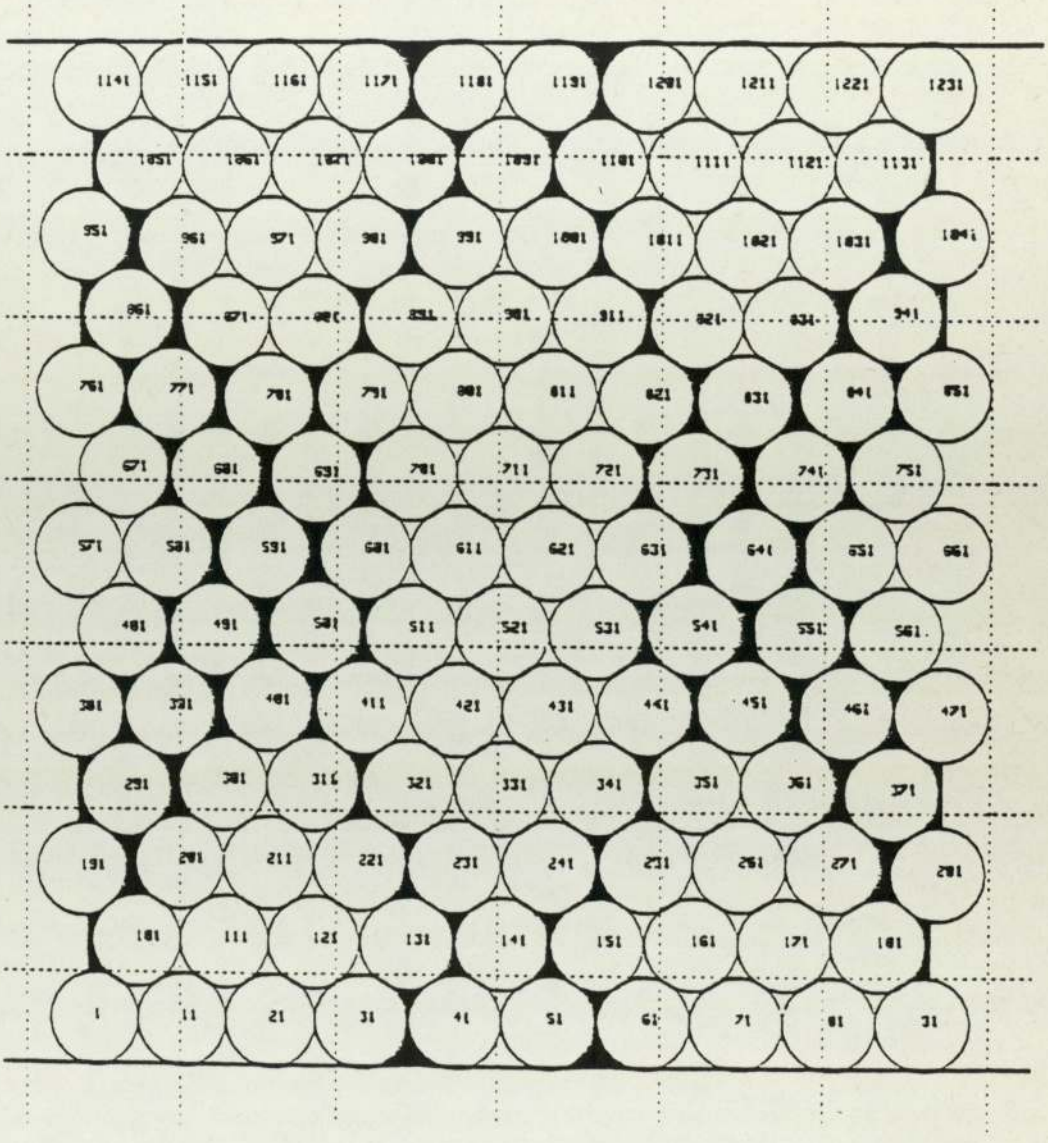

DISC FRICTION = 0.3

PLATTEN FRICTION = 0.3

ALL DISCS ARE FREE TO ROTATE

FIGURE 8.43 DEFORMATION OF A 124 DISC PACKING AT 3.58% STRAIN WITH FRICTIONAL PLATTENS

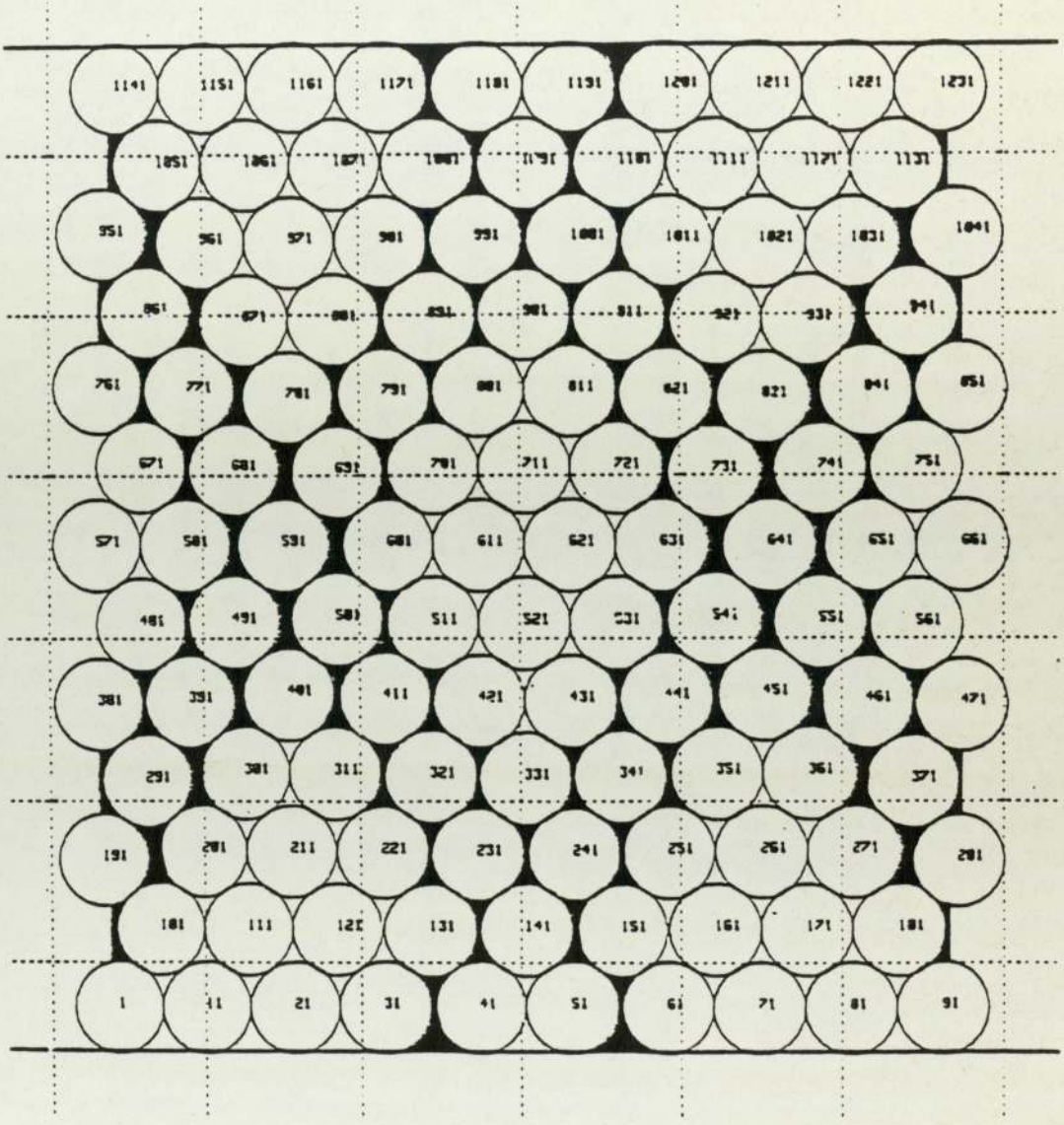

DISC FRICTION = 0.3

PLATTEN FRICTION = 0.3

ALL DISCS ARE FREE TO ROTATE

FIGURE 8.44 DEFORMATION OF A 124 DISC PACKING AT 3.90% STRAIN WITH FRICTIONAL PLATTENS

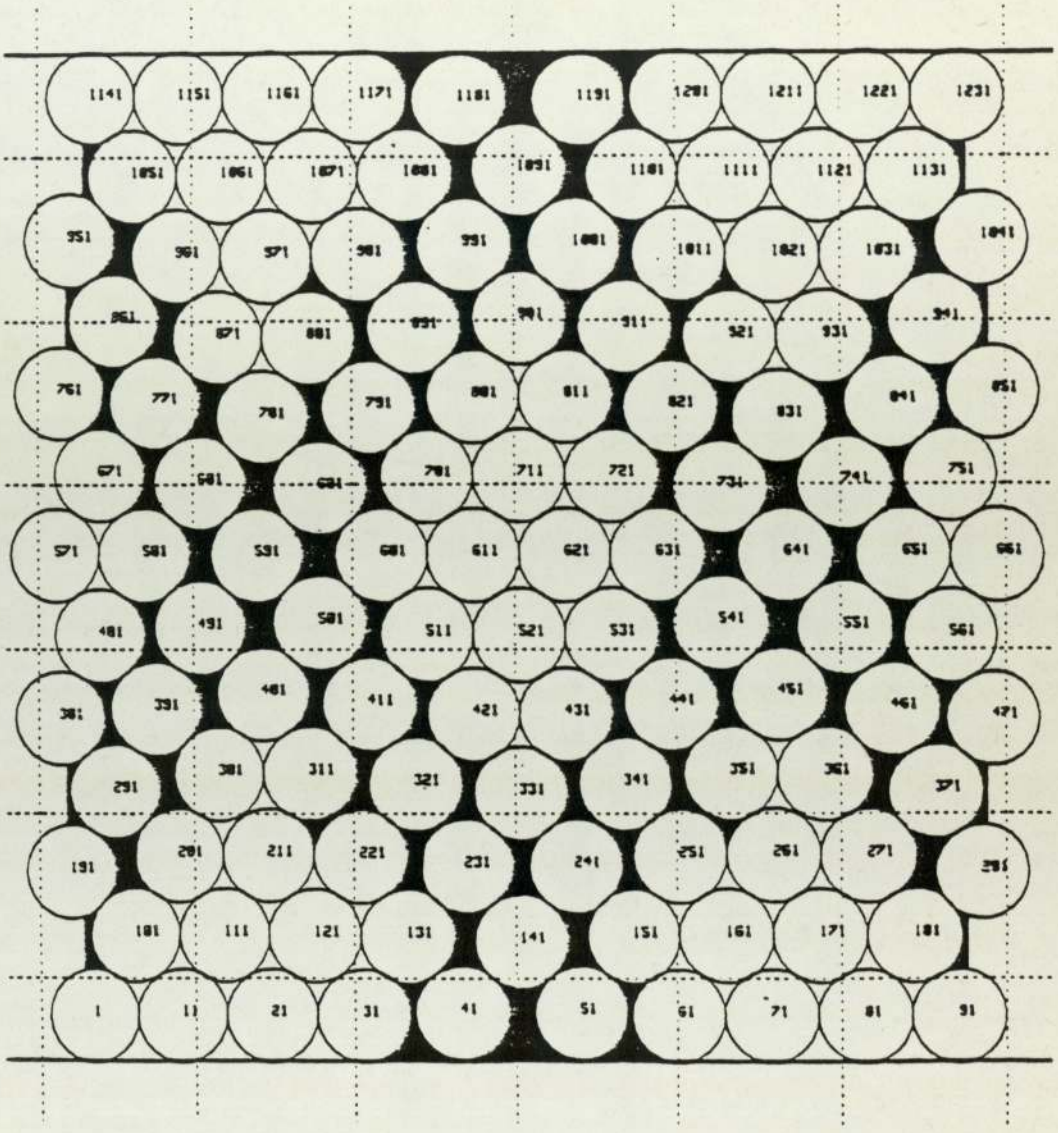

DISC FRICTION = 0.3

PLATTEN FRICTION = 0.3

ALL DISCS ARE FREE TO ROTATE

FIGURE 8.45 DEFORMATION OF A 124 DISC PACKING AT 5.31% STRAIN WITH FRICTIONAL PLATTENS

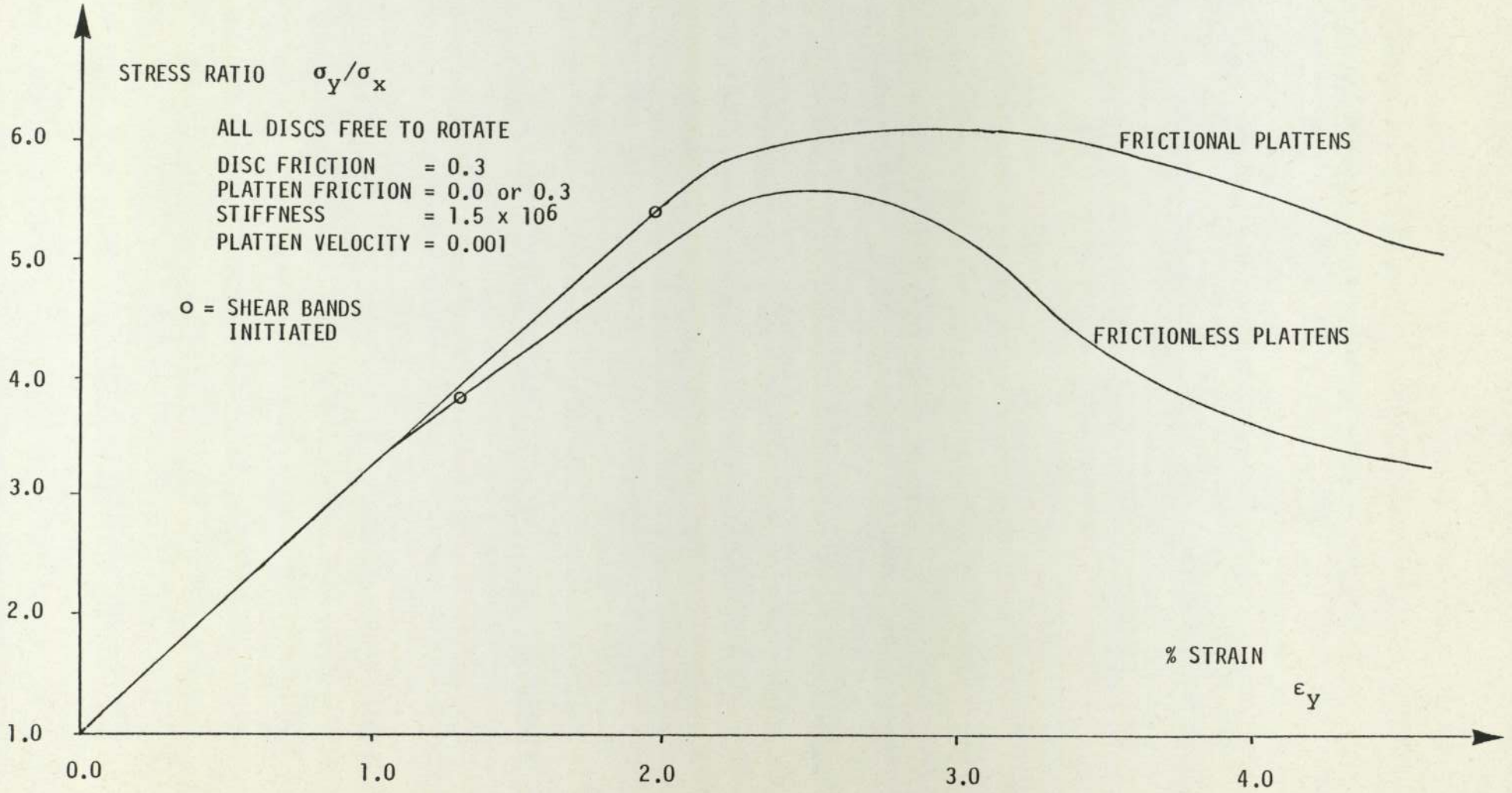

FIGURE 8.46 STRESS RATIO - STRAIN CURVES FOR 124 DISC PACKINGS COMPARING FRICTIONLESS AND FRICTIONAL PLATTENS

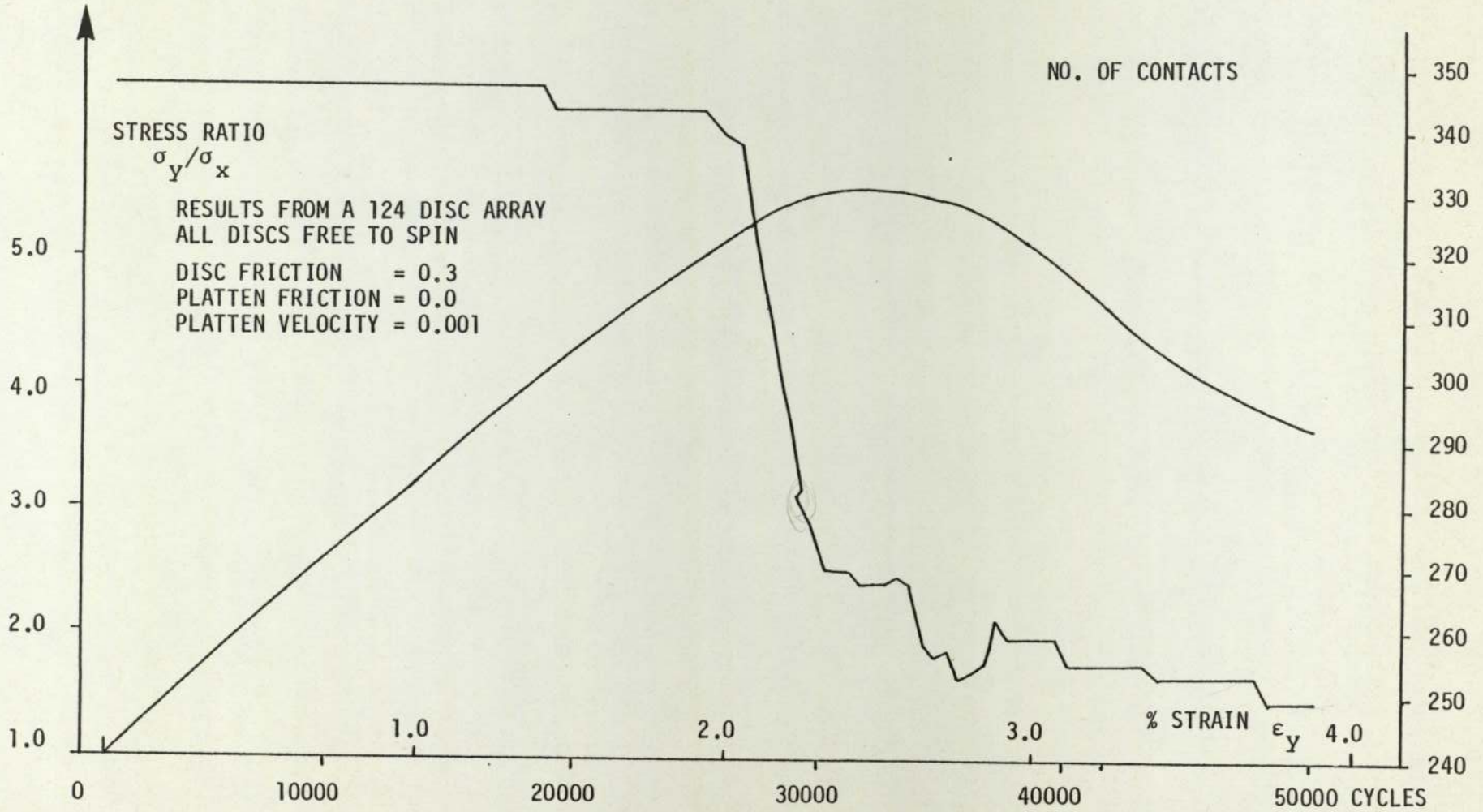

FIGURE 8.47 STRESS RATIO AND CONTACT NUMBERS PLOTTED AGAINST STRAIN (CALCULATION CYCLES)

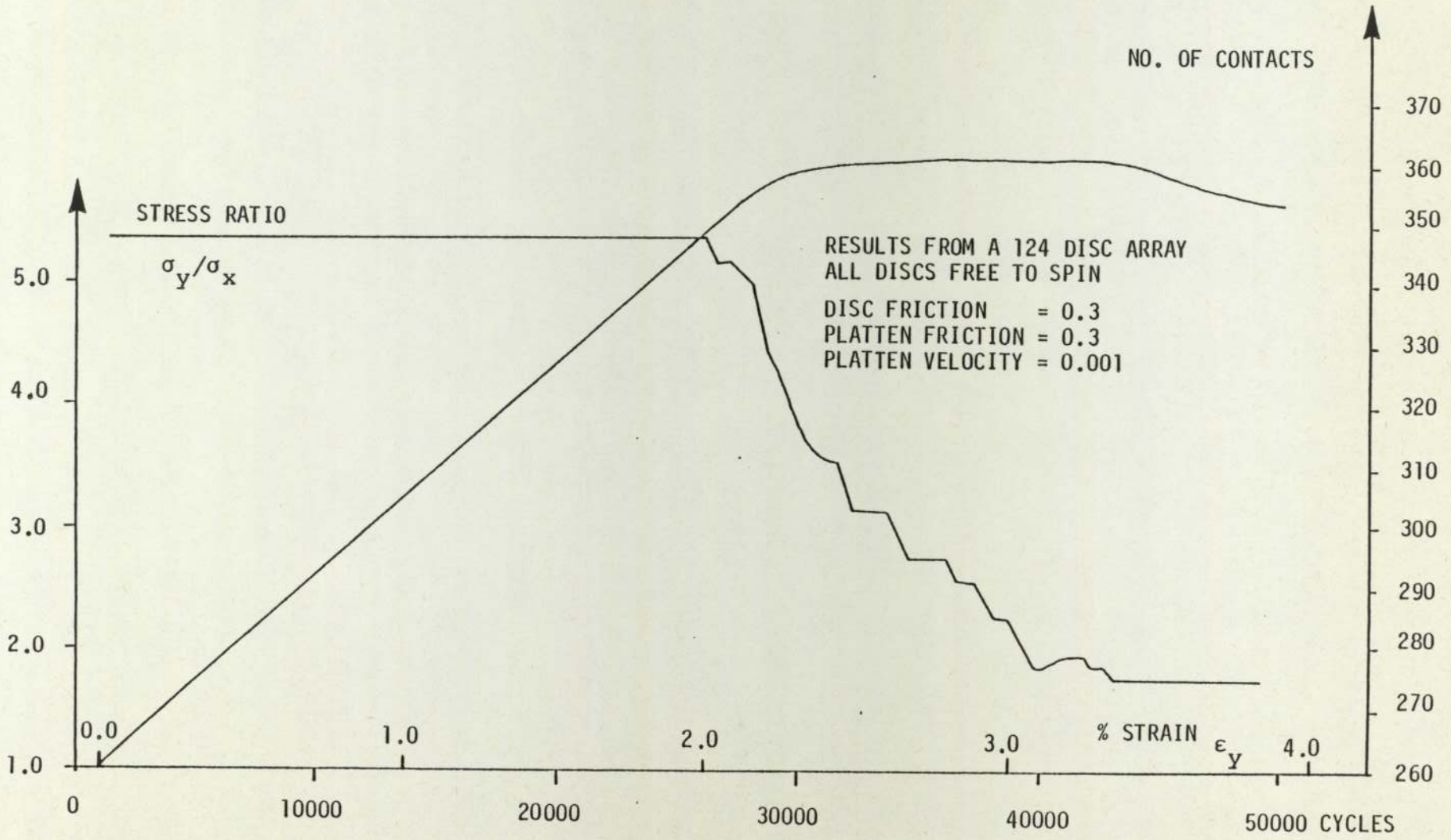

FIGURE 8.48 STRESS RATIO AND CONTACT NUMBERS AGAINST STRAIN (CALCULATION CYCLES)

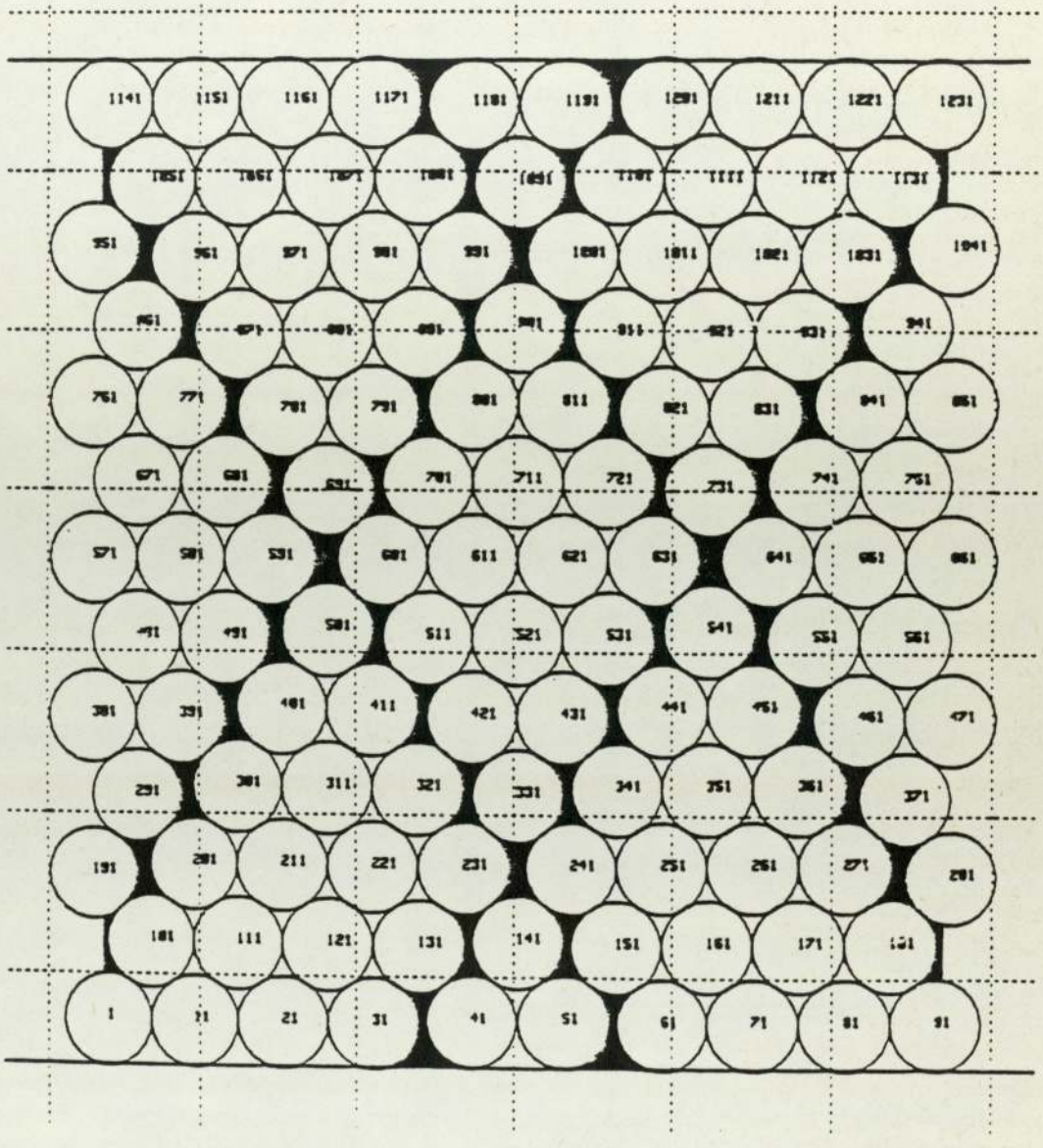

DISC FRICTION = 0.3

PLATTEN FRICTION = 0.0

ALL DISCS IRROTATIONAL

FIGURE 8.49 DEFORMATION OF A 124 DISC PACKING AT 3.58% STRAIN, WITH ALL DISCS IRROTATIONAL

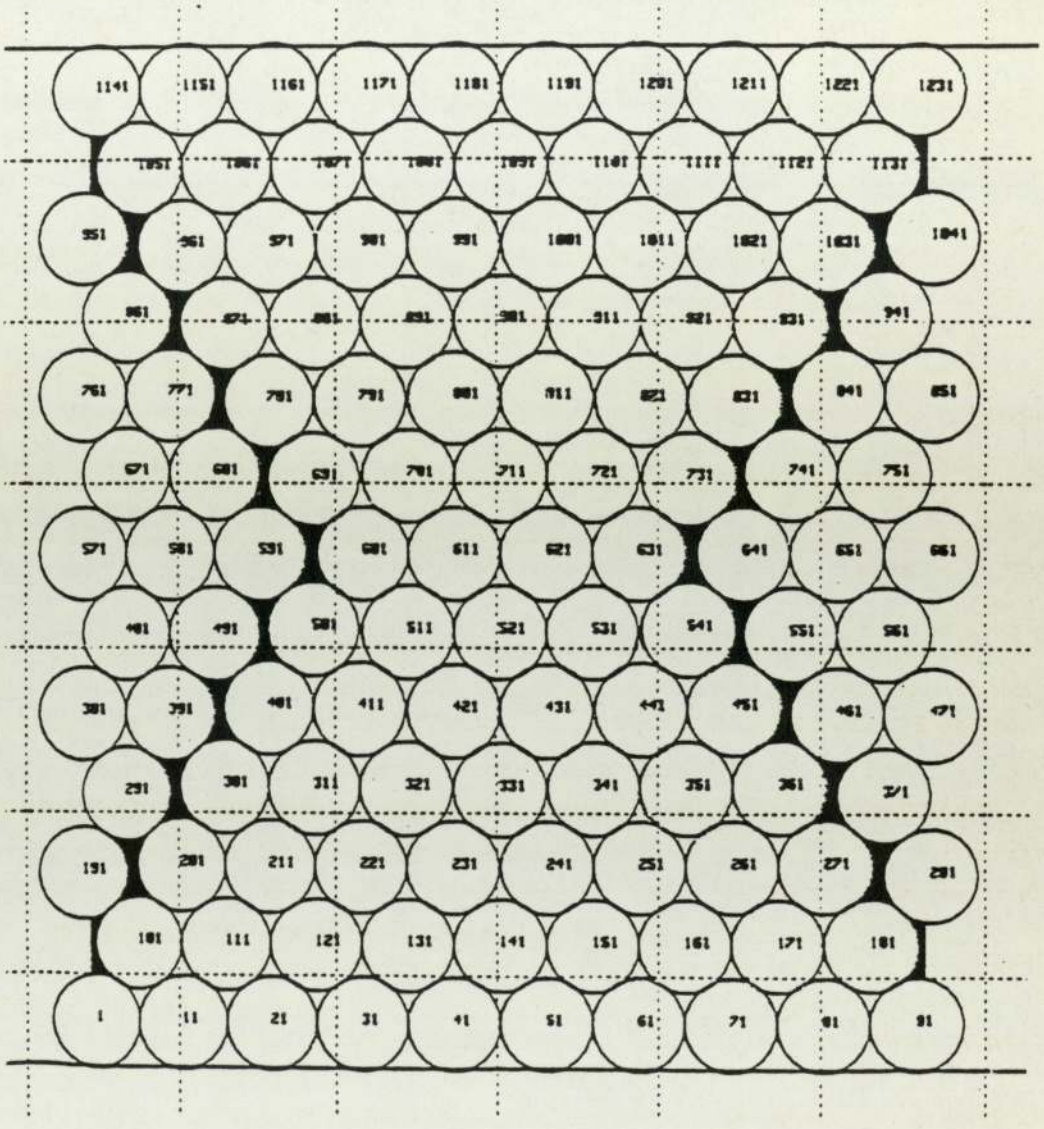

DISC FRICTION = 0.3

PLATTEN FRICTION = 0.3

ALL DISCS IRROTATIONAL

FIGURE 8.50 DEFORMATION OF A 124 DISC PACKING AT 3.58% STRAIN, WITH ALL DISCS IRROTATIONAL

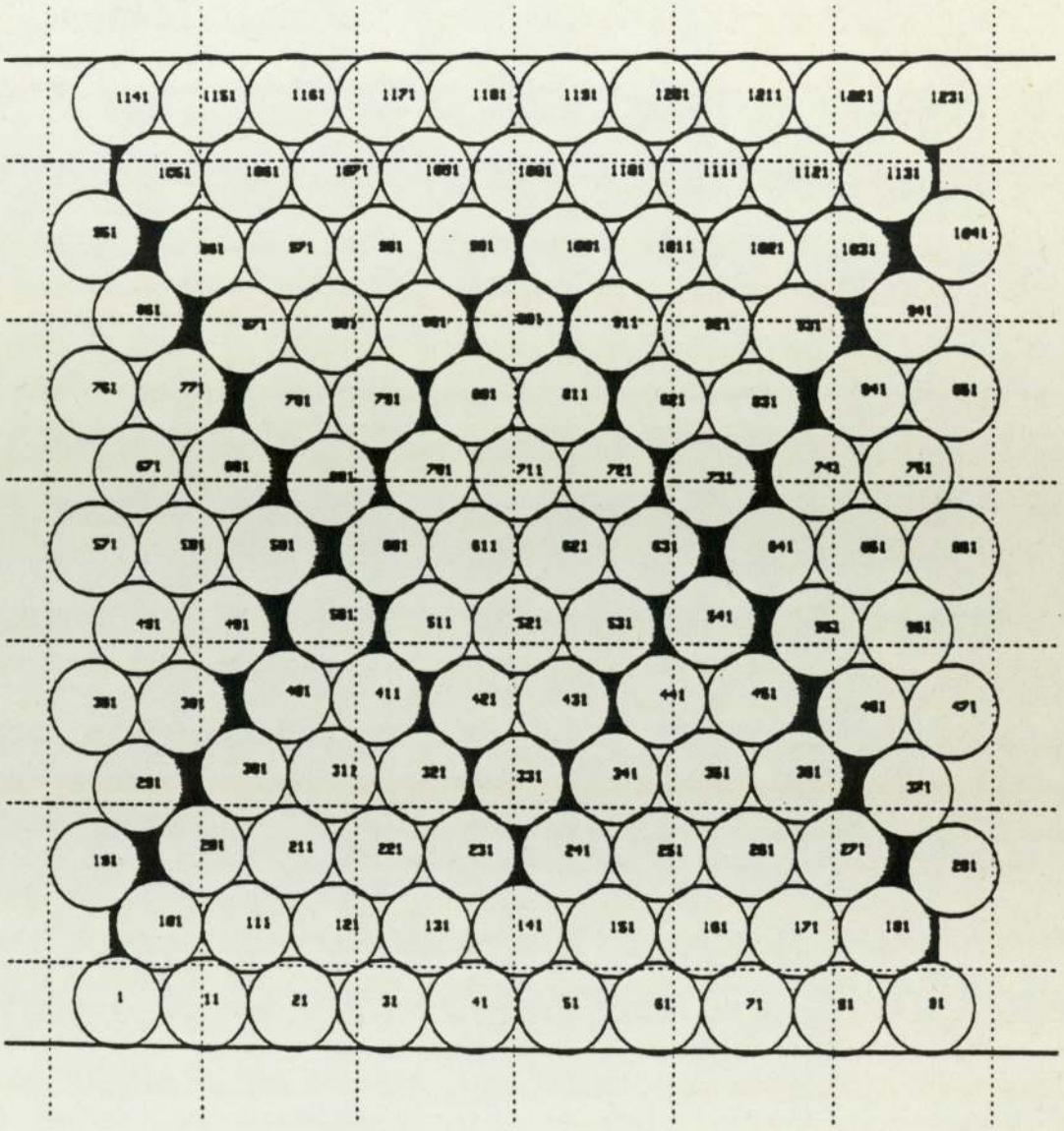

DISC FRICTION = 0.3

PLATTEN FRICTION = 0.3

ALL DISCS IRROTATIONAL

FIGURE 8.51 DEFORMATION OF A 124 DISC PACKING AT 5.19% STRAIN, WITH ALL DISCS IRROTATIONAL

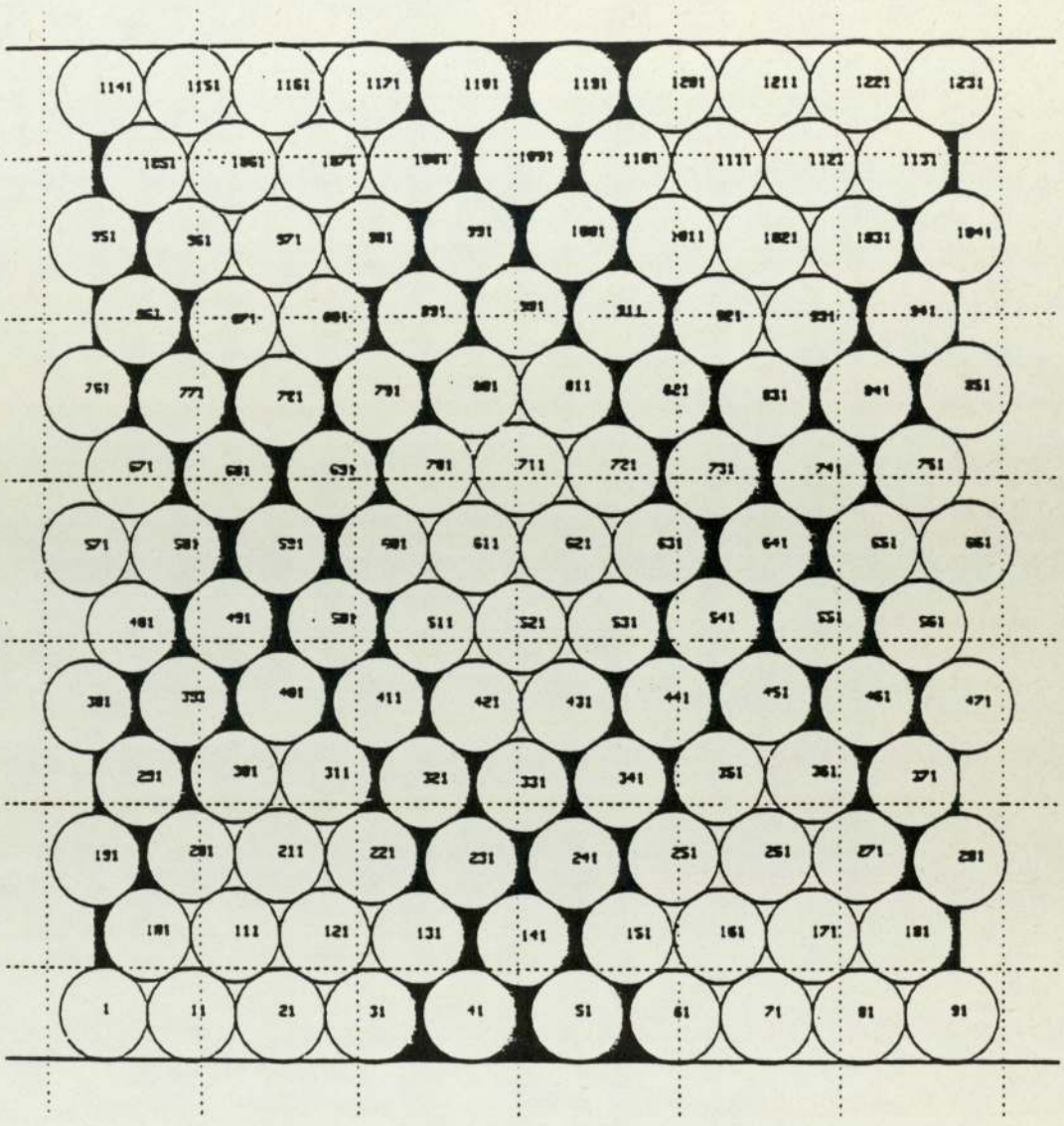

DISC FRICTION = 0.3

PLATTEN FRICTION = 0.0

BOUNDARY DISCS IRROTATIONAL

FIGURE 8.52 DEFORMATION OF A 124 DISC PACKING AT 3.58% STRAIN, WITH BOUNDARY DISCS IRROTATIONAL

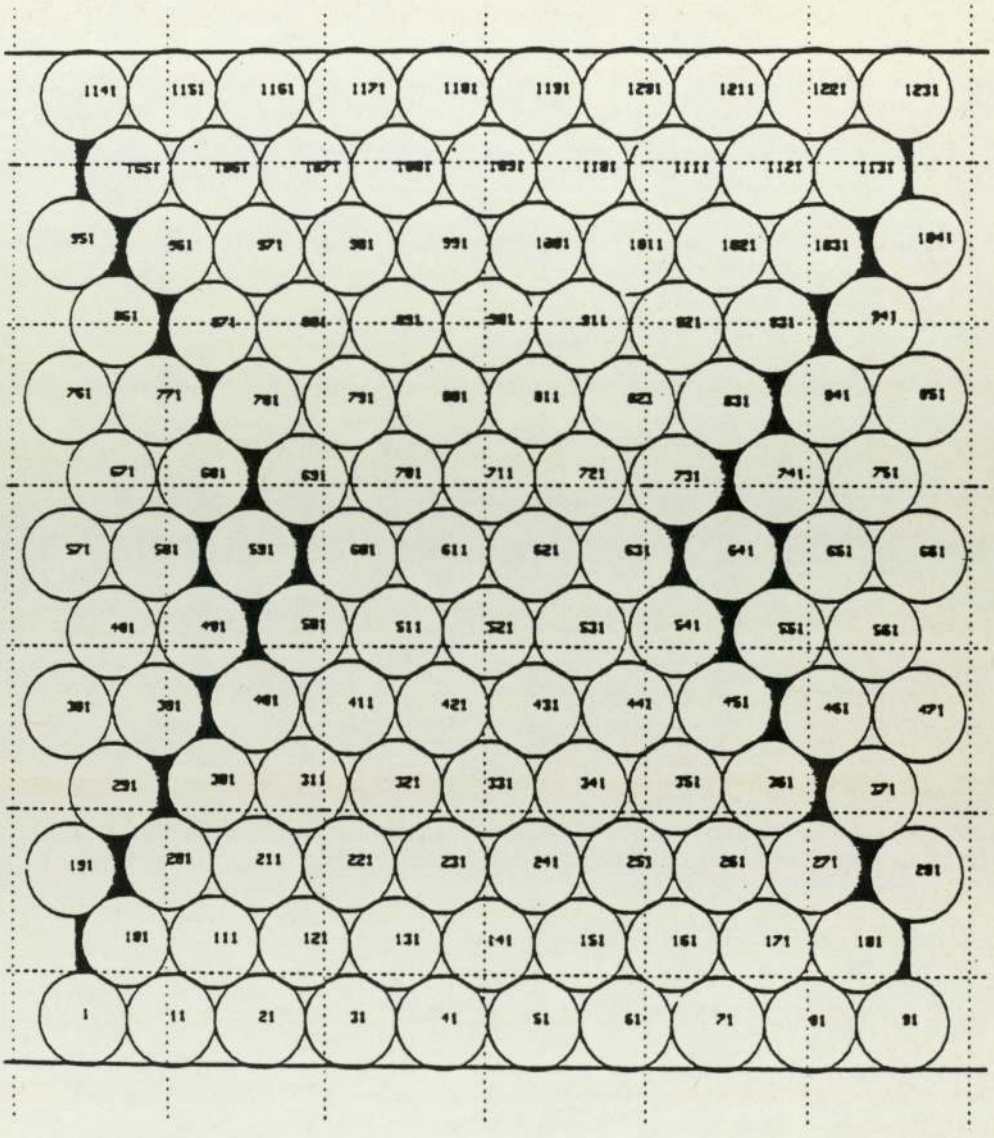

DISC FRICTION = 0.3

PLATTEN FRICTION = 0.3

BOUNDARY DISCS IRROTATIONAL

FIGURE 8.53 DEFORMATION OF A 124 DISC PACKING AT 3.58% STRAIN, WITH BOUNDARY DISCS IRROTATIONAL

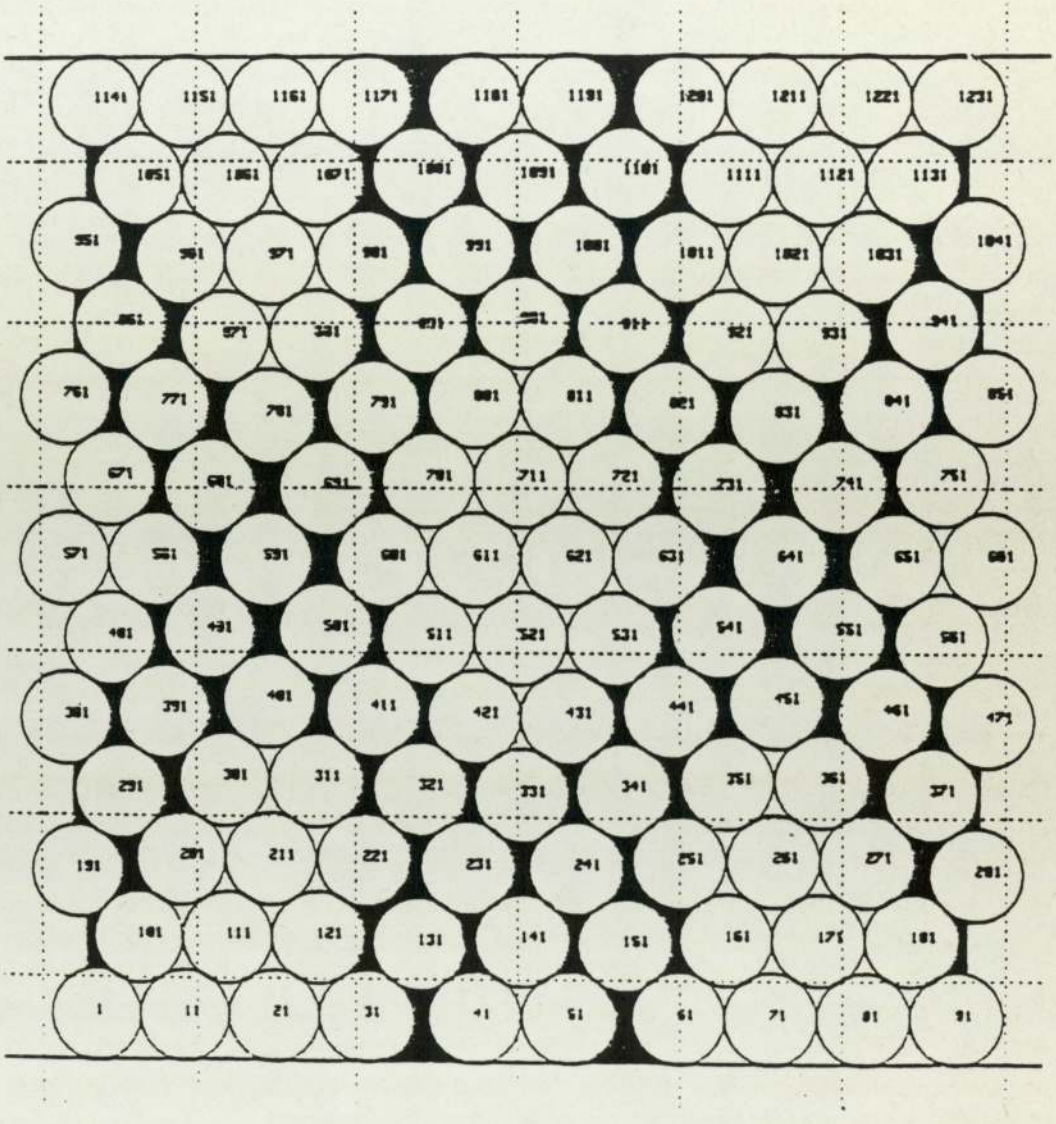

DISC FRICTION = 0.3

PLATTEN FRICTION = 0.3

BOUNDARY DISCS IRROTATIONAL

FIGURE 8.54 DEFORMATION OF A 124 DISC PACKING AT 5.19% STRAIN, WITH BOUNDARY DISCS IRROTATIONAL

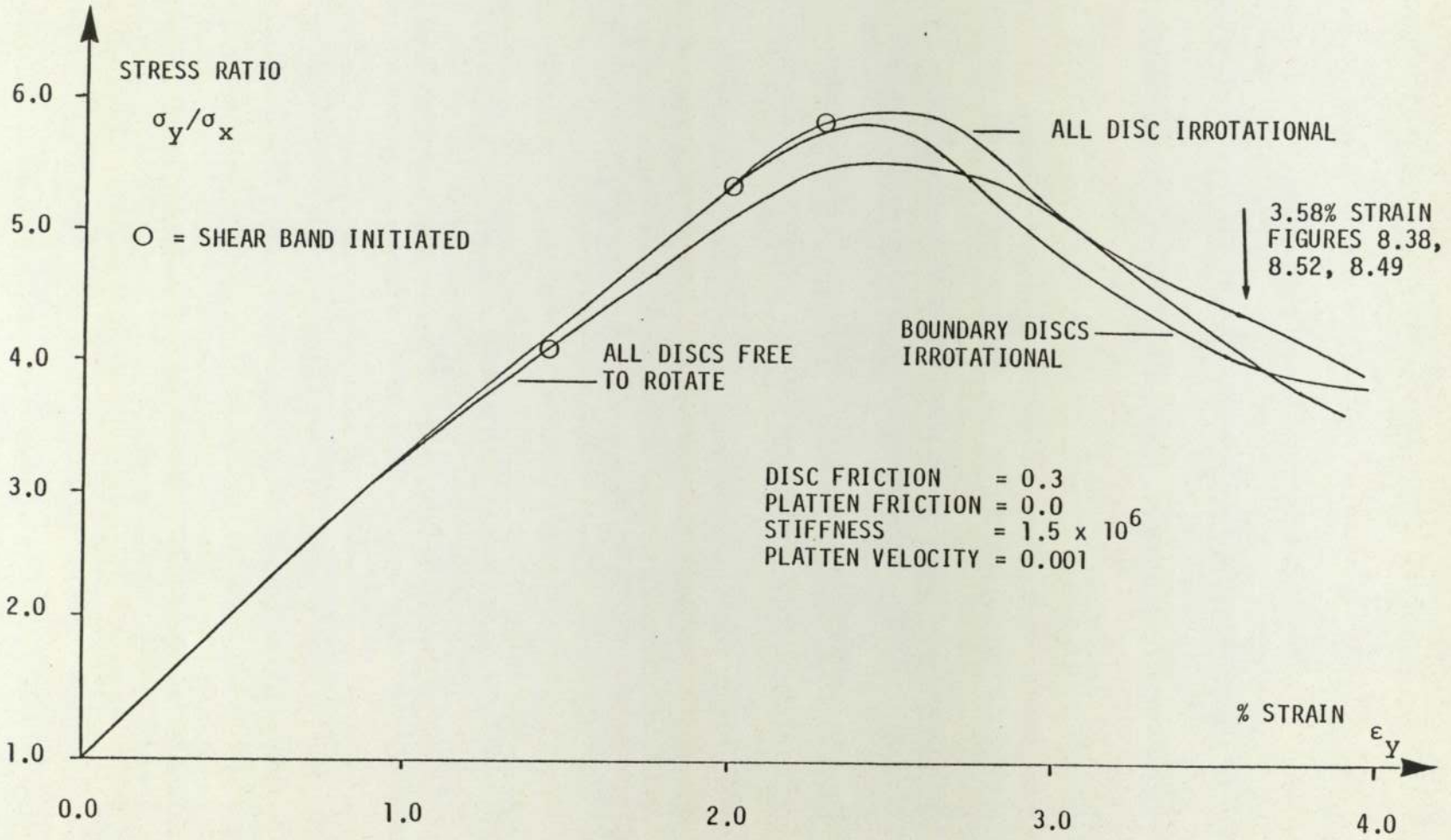

FIGURE 8.55 STRESS RATIO - STRAIN CURVES FOR 124 DISC PACKINGS (FRICTIONLESS PLATTENS) ILLUSTRATING THE EFFECT OF SPIN RESTRAINT

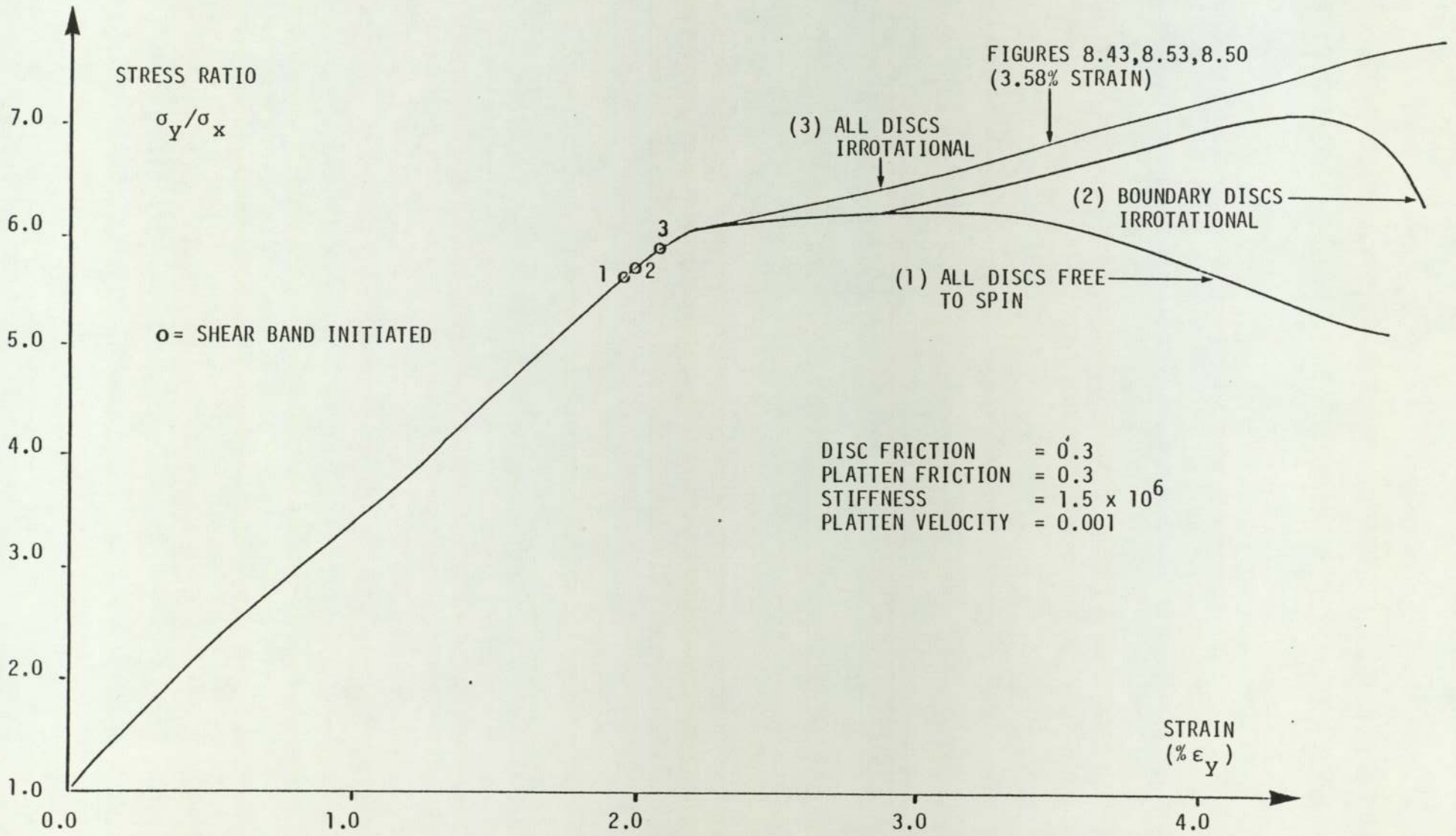

FIGURE 8.56 STRESS RATIO-STRAIN CURVES FOR 124 DISC PACKINGS (PLATTEN FRICTION) ILLUSTRATING THE EFFECTS OF SPIN RESTRAINT

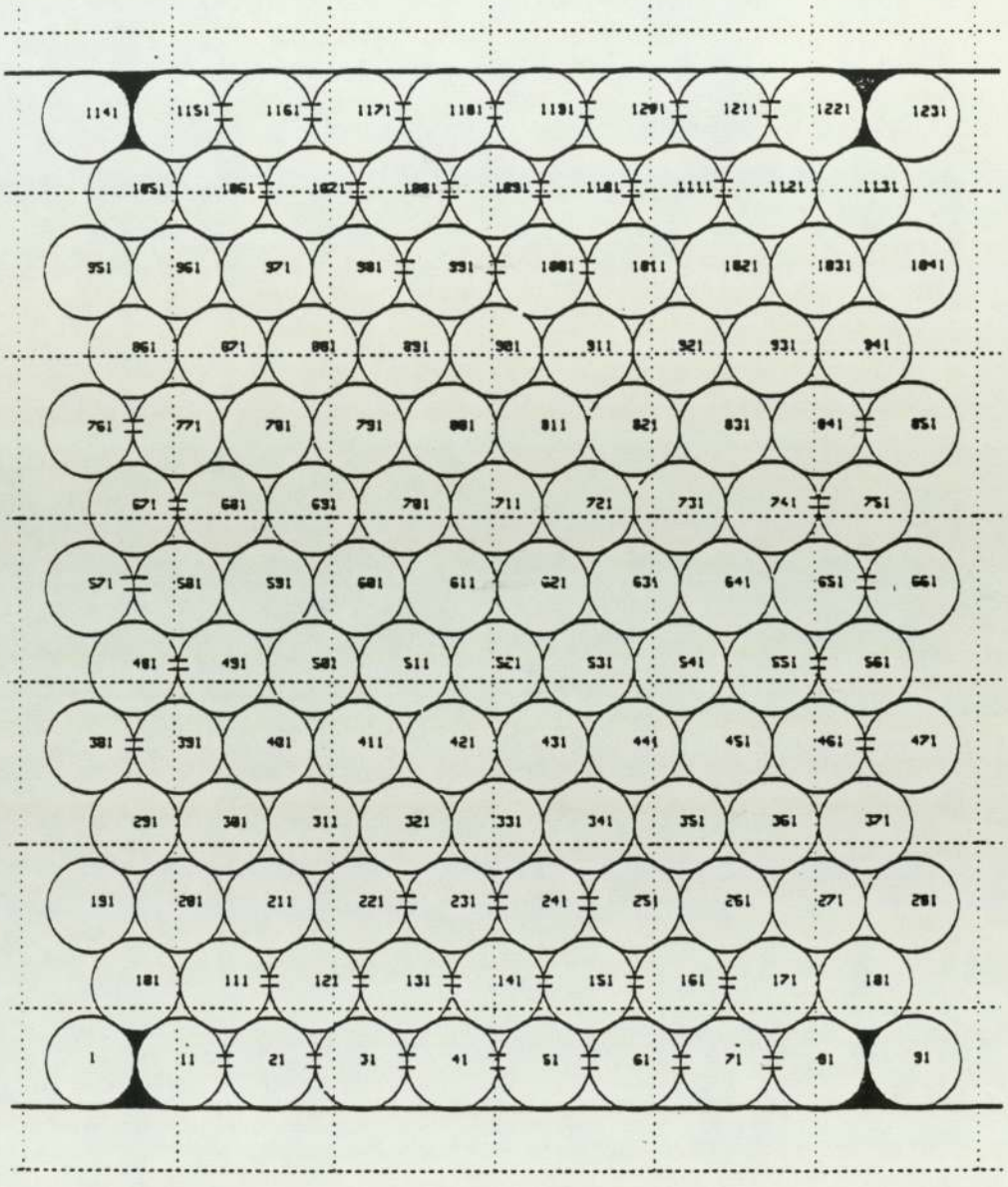

DISC FRICTION = 0.3

PLATTEN FRICTION = 0.0

ALL DISCS FREE TO ROTATE

HORIZONTAL CONTACT FORCE = =

FIGURE 8.57 DEFORMATION OF A 124 DISC PACKING AT 1.97% STRAIN WITH FRICTIONLESS PLATTENS SHOWING THE POSITION OF HORIZONTAL CONTACT FORCES

CHAPTER NINE

9. CONCLUDING REMARKS

Throughout the text of this thesis, comments and conclusions have been provided where appropriate and it is, therefore, necessary to add only a few closing remarks in this final chapter.

The research described in this thesis has been concerned with the mechanics of regular arrays of discs and spheres. It was shown in Chapter 2 that a wide range of packing geometries can be described as Body-Centred Orthorhombic. From the analysis of Body-Centred Tetragonal packings presented in Chapter 4 it was found that yield conditions were represented in principal stress space by skew cones whose apex was at the origin and whose base planes were parallel to the deviatoric planes. The strain-increment vectors were found to be normal to the axis, rather than the surface,of the cone and hence the normality rule frequently adopted in plasticity theory does not apply. For each yield cone, plastic potential surfaces could be defined by an infinite number of equally skew cylinders. During deformation the deviatoric yield loci translate and change shape. Hence the axis of the yield cone rotates about the origin of principal stress space during deformation. The shape of the yield surface was shown to be related to the structure of the packing and the size

of the yield surface was found to be dependent on the inter-particle friction and the mean stress.

The second part of this thesis was concerned with computer simulation tests on regular packings of discs using the Distinct Element Method. Results obtained from the simulation tests were presented in Chapter 8. The observed mechanism of failure was described as gap creation along inclined discrete shear bands and post-peak softening behaviour was associated with the widening of existing gaps. Platten friction, and to a lesser extent spin restraint, was found to inhibit the speed of propagation of shear bands through the samples, thus delaying the attainment of peak stress ratios.

Significant irregularities were seen to be introduced into the packings by the boundaries, so in future it would be worthwhile to use a more sophisticated boundary control facility when performing similar tests on regular arrays.

Two methods have been reported showing how the behaviour of regular packings can be studied, one using an analytical approach and the other making use of large scale computing facilities. It is anticipated that, arising from these studies, further work will be carried out on random arrays and on packings of irregular shaped particles.

This will, in turn, lead to a greater understanding of the behaviour of granular material.

Appendix A

Two Dimensional Analysis of Regular Rigid Disc Arrays

The analysis of two dimensional arrays of regular rigid discs follows closely the method described in Chapter 4.

The strain-increment tensor for two dimensional packings is similar to that presented in (4.10),

$$d\varepsilon_{ij} = \begin{bmatrix} c/l^2 & 0 \\ 0 & a/n^2 \end{bmatrix} \qquad \ldots(A.1)$$

where $a+c = 0$ and $l^2 + n^2 = 1$.
The range for l and n is between $\sqrt{3}/2$ and $\frac{1}{2}$ inclusive and for the case of a close packing $l = \sqrt{3}/2$ and $n = \frac{1}{2}$.
As in (4.7) and (4.9)

$$a = \delta u/(8D^2) \qquad \ldots(A.2a)$$

$$c = \delta v/(8D^2) \qquad \ldots(A.2b)$$

where $\delta v = 16 \Delta_1 Dl$ and $\delta u = 16 \Delta_2 Dn$

therefore $c = \frac{2\Delta_1 l}{D}$, $a = \frac{2\Delta_2 n}{D}$

where Δ_1 and Δ_2 are the vertical and horizontal displacements, respectively, of each disc.

For the same tangential displacement at each contact, say Δp

$$\Delta_1 = n\Delta p \quad \text{and} \quad \Delta_2 = -l\Delta p$$

therefore

$$d\varepsilon_{ij} = \frac{2\Delta p}{D} \begin{bmatrix} n/l & 0 \\ 0 & -l/n \end{bmatrix} \qquad \ldots(A.3)$$

The average stress tensor is obtained by summing the normal force and tangential force contributions as in (4.14).

$$\bar{\sigma}_{ij} = \bar{\sigma}_{ij\,(N)} + \bar{\sigma}_{ij(T)} \qquad \ldots(A.4)$$

But for the two dimensional analysis the contributions are

$$\bar{\sigma}_{ij(N)} = \frac{2pD}{V} \begin{bmatrix} l^2 & 0 \\ 0 & n^2 \end{bmatrix} \qquad \ldots(A.5)$$

and

$$\bar{\sigma}_{ij(T)} = \frac{2fD}{VF} \begin{bmatrix} c & 0 \\ 0 & a \end{bmatrix} \qquad \ldots(A.6)$$

where $F = (D/2) \cdot \sqrt{c^2/l^2 + a^2/n^2}$

Summing the two contributions results in the average stress tensor,

$$\bar{\sigma}_{ij} = \frac{2pD}{V} \begin{bmatrix} l^2 + \mu c/F & 0 \\ 0 & n^2 + \mu a/F \end{bmatrix} \qquad \ldots(A.7)$$

Solutions corresponding to the average stress tensor for cases where $\mu = 0.0$ and $\mu = 0.3$ are shown in Figure A.1.

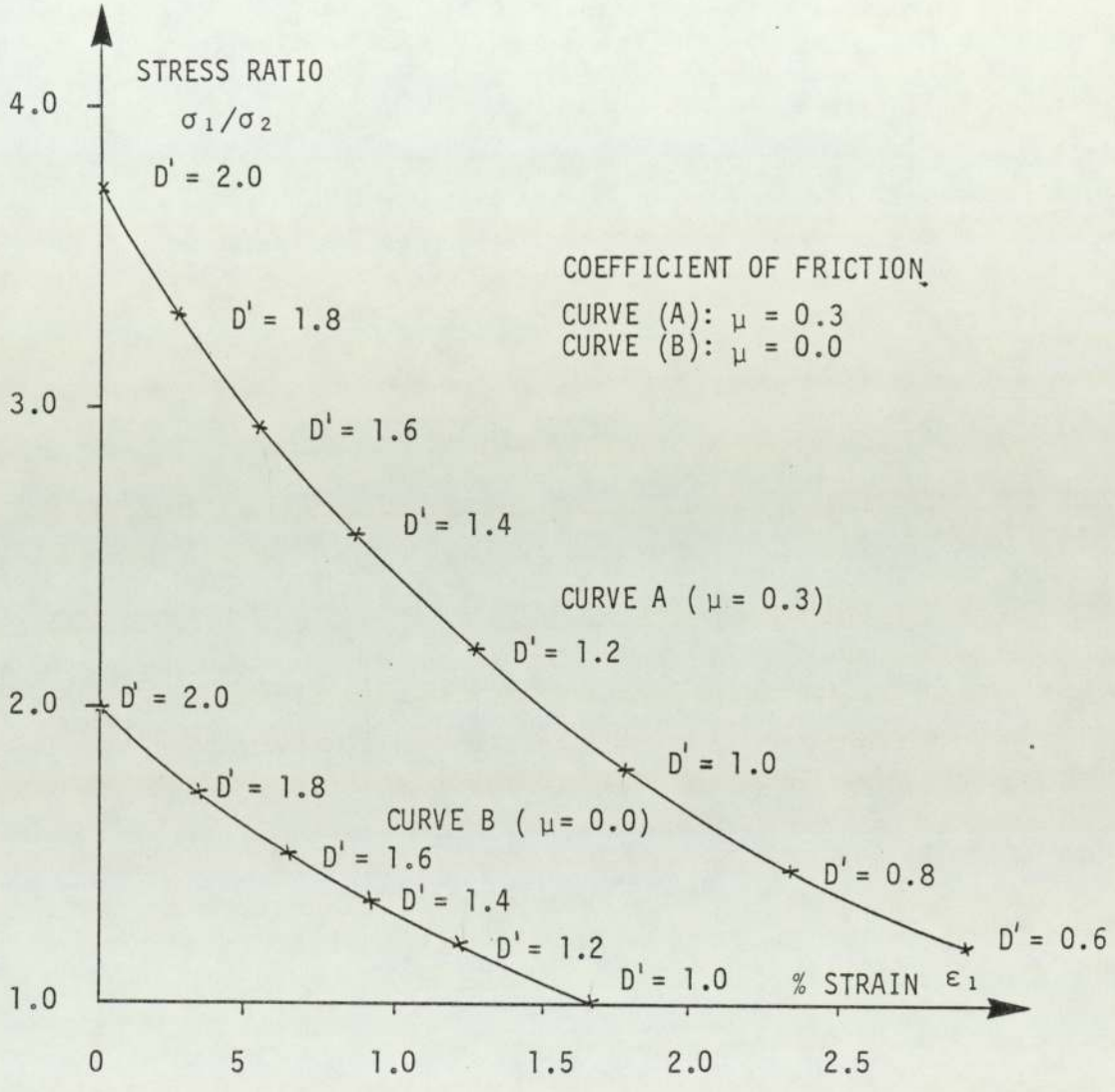

FIGURE A.1 PLOT OF YIELD STRESS AGAINST DEFORMATION SHOWING THE POINTS CORRESPONDING TO VARIOUS INTERMEDIATE PACKING TYPES

APPENDIX B

COMMANDS AVAILABLE FOR "BALL"

To set up and run the program "BALL", it is necessary to use some, or all, of the following commands - depending on the simulation desired. The format for all commands is the first four letters of the command word on one line, and then the correct number of parameters on the following lines. In this appendix, the first four letters of each command word underlined are to be typed exactly, while the variables shown merely stand for numerical values. The majority of these commands remain unaltered from their original form, as found in Cundall (1978). The usual Fortran convention is used, where variables beginning with the letters I,J,K,L,M or N represent integer values, while all others indicate real values. The first command must be either

START

W H NBOX NBALL NWALL

or

RESTART

If the first command is START, the parameters have the following meanings:

W	width of the grid area (x-dimension)
H	height of the grid area (y-dimension)
NBOX	number of grid boxes requested
NBALL	maximum number of discs that are likely to be used.

NWALL maximum number of walls to be used.

The next line must be a heading and can consist of any characters.

The Restart card is used when it is desired to continue a run that was previously terminated normally. The previous run must have written a restart file before stopping. To indicate whether this is so, or not, a message is printed out at the end of each successful run. If the Restart command is used, the next commands should be from those listed below.

The following commands may be issued in any order, unless it is stated otherwise.

STOP	This stops the simulation run and a restart file is written.
RADIUS	Defines the radius,R, of type ITYPE discs.
R ITYPE	
SHEARSTIFFNESS	Defines the shear stiffness,K, of type
K ITYPE	ITYPE elements.
NORMALSTIFFNESS	Defines the normal stiffness,K, of
K ITYPE	type ITYPE elements.
DENSITY	Defines the density,RHO, of type
RHO ITYPE	ITYPE elements.
FRICTION	Defines the coefficient of friction,
U ITYPE	u, for type ITYPE elements.
COHESION	Defines the cohesion,c, for type
C ITYPE	ITYPE particles.

DAMPING

LMIN FMIN IM IK

Sets the damping parameters for Rayleigh damping, where FMIN is the frequency at which minimum damping occurs, and LMIN is the fraction of critical damping at that frequency. Where Rayleigh damping takes the form

$$[C] = \alpha [M] + \beta [K]$$

If IM=1, α is set to zero

If IK=1, β is set to zero

If IM=IK=0, normal Rayleigh damping is used.

CYCLE

N

The simulation performs N calculation cycles, under the current boundary conditions.

FRACTION

F

This sets the fraction of the critical time-step used, to F. Recommended values are: 0.2 to 0.5 for loose packings, 0.1 for dense packings.

XGRAVITY

XG

YGRAVITY

YG

Sets the gravitational accelerations in the x and y directions.

CREATE

X Y ITYPE

Creates a type, ITYPE, disc with its centre at (X,Y). A radius must have been defined previously for this type number.

AUTO

XL XU YL YU N NTRY SEED

Automatically generates particles. The program tries to generate N particles within the area XL≤X≤XU and YL≤Y≤YU, using a random number generator whose seed value is SEED. If the simulation has not produced N particles after NTRY tries, it gives up and writes a message informing the user how many discs were actually generated. This command, because of its random packing ability was not used for the research reported in this thesis. Used instead was;

FORM

NCOLS NROWS ITYPE RAD

Forms a tight packing of discs, NCOLS by NROWS, using discs of radius RAD and of properties associated with type ITYPE particles.

DEFWALL

NAME XC YC θC H1 H2 $\dot{X}$V $\dot{Y}$V $\dot{\theta}$V ITYPE

Defines a wall as follows:

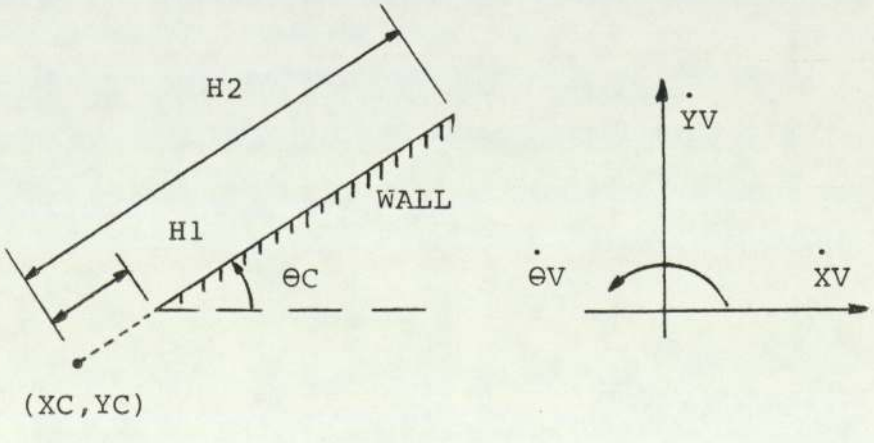

	where; ITYPE is the type number, NAME is an alphanumeric name (4 characters) θC and $\dot{\theta}V$ are in degrees and degrees/second respectively.
ALTWALL NAME $\dot{X}V$ $\dot{Y}V$ $\dot{\theta}V$ ITYPE	Causes the velocities or the type of the named wall, to be altered.
ZERO	Sets all particle velocities to zero.
RESET	Resets the radius vectors of all particles to zero.
RETURN	Zeros the cycle counter.
HISTORY RESET	Rewinds the 'history file' causing the erasure of whatever is in there.
HISTORY REPEAT N	Sets the value N such that the 'history file' will be added to after every N time cycles.
PRINT WALL XL XU YL YU or BALL XL XU YL YU or CONT XL XU YL YU	Prints out data on WALLS or DISCS or CONTACTS, within the area $XL \leq X \leq XU$, $YL \leq Y \leq XU$ If XL=XU=YL=YU=0 then data on all WALLS/DISCS/CONTACTS will be printed out.
DUMP N1 N2	Dumps out memory from locations N1 to N2 in the working array.
PLOT MEDIA NCYCLES	Selects the output media for graphics (MEDIA=35 results in Microfiche) (MEDIA=16 results in cinefilm)

A graphics plot is automatically produced every NCYCLES.

WINDOW
XL XU YL YU

Sets the area of the simulation that is to be plotted. The window size is initially set equal to the total grid area.

CHECK

Prints out the kinetic energy and momentum sums for all particles.

ISET
IL(1) IL(2) ILOC

Sets directly the first and second parts of the memory word at location ILOC in the working array.

RSET
RV ILOC

Sets directly the memory word at location ILOC to the real value RV.

GO BACK OVER A SERIES OF COMMANDS
NCYCLES HSTRESS VSTRESS N(1) N(2) N(3) N(4)

Cycle through the simulation for NCYCLES with the current boundary conditions and the horizontal and vertical restraining stresses kept at HSTRESS and VSTRESS respectively. The four discs at the corners of the packing are N(1) N(2) N(3) and N(4).

HORIZONTALLY CONSTRAINED DISCS
VERTICALLY CONSTRAINED DISCS
NUMBER
I1
I2
.
.
.
IN

Specifies the following number (NUMBER) of discs to be either Vertically or Horizontally constrained. Where I1, I2 etc are the discs that will be affected, there must be NUMBER discs specified.

SPIN CONSTRAINED DISCS

	Basically the same as for Horizontally
NUMBER	and Vertically constrained discs,
I_1	except that the discs specified are
I_2	held irotational. If the value
⋮	of NUMBER equals 9999, then no disc
⋮	numbers need be specified as all
I_N	discs will be held irotational.

PLATTEN PACKING AND AUTOMATIC DEFINITION

CONSTS I1 I2 I3 I4	Automatically define plattens along the top and bottom of the packing, using the co-ordinate of the corner discs (I1-I4) and under an isotropic stress of CONSTS.

APPENDIX C

PROGRAM LISTING OF "BALL"

A program listing of the computer simulation "BALL", will be found on a microfiche bound inside the back cover of this thesis.

REFERENCES

BUERGER, M.J. (1970)
"Contemporary Crystallography."
McGraw - Hill.

BRAVAIS, A. (1851)
Part 1 of "Crystal form and structure." SCHNEER, C.J. (Ed.) (1977)
Dowden, Hutchinson and Ross Inc.

CATTENEO, C. (1938)
"Sul contatto di due corpi elastici."
Accademia Dei Lincei, Rendiconto, Series 6, Vol.27, pp 342-348, pp 434-436, pp 474-478.

CUNDALL, P.A. (1971)
"A computer model for simulating progressive large scale movements in blocky rock systems."
Symp. Soc. Int. Mecanique des Roches, Nancy.

CUNDALL, P.A. (1978)
"BALL - A program to model granular media using the Distinct Element Method."
Dames and Moore, Advanced Technology Group, London.

CUNDALL, P.A. and STRACK, O.D.L. (1978)
"The Distinct Element Method as a tool for research in granular media - Part 1."
Report to National Science Found. NSF GRANT ENG76-20711.
Dept. Civil and Mineral Eng., Univ. Minnesota.

CUNDALL, P.A. and STRACK, O.D.L. (1979a)
"A discrete numerical model for granular assemblies."
Geotechnique Vol. 29, pt. 1, pp 47-65.

CUNDALL, P.A. and STRACK, O.D.L. (1979b)
"The Distinct Element Method as a tool for research in granular media - Part 2."
Report to National Science Found. NSF GRANT ENG76-20711.
Dept. Civil and Mineral Eng., Univ. Minnesota.

DANTU, P. (1961)
"Etude mechanique d'un milieu pulverulent forme de spheres egales de compaicte maxima."
Proc. 5th Int. Conf. Soil Mech. Found. Eng. Vol. 1, pp 61-70.

DERESIEWICZ, H (1958)
"Mechanics of granular matter"
Adv.App. Mech. VOL 5, pp 233-306.

DUFFY, J. (1959)
"A differential stress-strain relation for the hexagonal close packed array of elastic spheres."
J.APPL. Mech. TRANS ASME. pp 88-94.

DUFFY, J. and MINDLIN, R.D. (1957)
"Stress strain relations and vibrations of a granular medium."
J.APPL. Mech. TRANS ASME. pp 585-593.

GOODMAN, R.E., TAYLOR, R.L. and BREKKE, T.L. (1968)
"A model for the mechanics of jointed rock."
J.Soil Mech. and Found. Div., Proc. ASCE VOL 94, PT.SM3, pp 637-661.

GRATTON, L.C. and FRASER, H.J. (1935)
"Systematic packing of spheres - with particular relation to porosity and permeability."
J.Geology VOL.43, NO.8, PT.1.

JOHNSON, K.L. (1955)
"Surface interaction between elastically loaded bodies under tangential forces."
Proc. Roy. Soc. (London) Ser.A.230 pp 531-548.

JOSSELIN DE JONG, G.DE. and VERRUIJT, A. (1969)
"Etude photo-elastique d'un empilement de disques."
Cah. Grpe. Fr. Etud. Rheol.,2, pp 73-86.

KEPLER, J. (1611)
Part 1 of "Crystal form and structure." SCHNEER, C.J. (Ed.) (1977)
Dowden, Hutchinson and Ross Inc.

LEUSSINK, H and WITTKE, W. (1963)
"Difference in triaxial and plane strain shear strength."
Symp. Lab. Shear Testing of Soils, OTTOWA, ASTM, STP.361, pp 77-89.

MINDLIN, R.D. (1949)
"Compliance of Elastic Bodies in Contact."
J.APPL. MECH. Vol.16, pp 259-268.

MINDLIN, R.D. and DERESIEWICZ, H (1953)
"Elastic spheres in contact under varying oblique forces."
J.APPL. MECH., Vol.20, pp 327-344.

MINDLIN, R.D., MASON, W.P., OSMER, T.F. and DERESIEWICZ, H. (1951)
"Effects of an oscillating tangential force on the contact surfaces of elastic spheres."
Proc. First Nat. Cong. Appl. Mech., Chicago, pp 203-208.

MOLENKAMP, F. (1980)
"Some aspects of constitutive equations for sand."
Proc. Int. Symp. on Soils under Cyclic and Transient Loading, Swansea.

ODA, M. and KONISHI, J. (1974)
"Microscopic deformation mechanism of granular material in simple shear."
Jap. Soc. Soil Mech. and Found. Eng., Vol 14, No.4, pp 25-38.

PARKIN, A.K. (1964)
"The application of discrete unit models to studies of the strength of granular materials."
Ph.D. Thesis, Univ. Melbourne.

PARKIN, A.K. (1965)
"ON THE STRENGH OF PACKED SPHERES."
J.Aust. Math. Soc., Vol.5, pp 443-452.

PARKIN, A.K. (1981)
Correspondence on Thornton (1979)
Geotechnique 31

PRIKSTER, A.A. and PEGDEN, C.D. (1979)
"Introduction to Simulation and SLAM."
John Wiley and Sons, New York.

RENNIE, B.C. (1959)
"On the strength of sand."
J.Aust. Math. Soc., Vol.1, pp 71-79.

ROSENBLUETH, L.M. and WIENER, H. (1945)
"The role of models in science."
Philosophy of Science, Vol.12, No.4, pp 316.

ROWE, P.W. (1962)
"The stress-dilating relation for static equilibrium of an assembly of particles in contact."
Proc. Roy. Soc. 269, No. 1339 pp 500-527.

SERRANO, A.A. and RODRIGUEZ-ORTIZ, J.M. (1973)
"A contribution to the mechanics of hetrogeneus granular media."
Proc. Symp. Plasticity and Soil Mech., Cambridge.

THORNTON, C. (1974)
"Deformation of sand in plane strain and axisymmetric compression."
Ph.D. Thesis, University of Aston in Birmingham.

THORNTON, C. (1977)
"Deformation of a simple particulate model."
Proc. Speciality Session 9, ICSMFE, TOKYO.

THORNTON, C. (1979)
"The conditions for failure of a face-centred cubic array of uniform rigid spheres."
GEOTECHNIQUE, 29, No.4., pp 441-459.

THORNTON, C. (1981)
Author's reply to discussion on Thornton (1979)
Geotechnique 31.

THORNTON, C. and BLACKBURN, D.J. (1981)
"A microstructural approach to soil plasticity theory."
Paper presented at Int. Colloquium on Plastic Behaviour of Anistropic Solids, Grenoble. To be published 1983.

THURSTON, C.W. and DERESIEWICZ, H. (1959)
"Analysis of a compression test of a model of a granular medium."
J.Appl. Mech., Vol.26, pp 251-258.

TIMOSHENKO, S. and GOODIER, J.H. (1951)
"Theory of Elasticity."
McGraw - Hill, New York.

TROLLOPE, D.H. and BURMAN, B.C. (1980)
"Physical and numerical experiments with granular wedges."
Geotechnique, 30, No.2., pp 137-157.

WALTON, K. (1978)
"The oblique compression of two elastic spheres."
J.Mech. Phys. Solids, Vol.26, pp 139-150.

ZIENKIEWICZ, O.C. BEST, B., DULLAGE, C.and STAGG, K.G. (1970)
"Analysis of non-linear problems in rock mechanics - with particular reference to jointed rock."
Proc. 2ND CONG. Int. Soc. Rock Mech., Pt.(8-14), pp 501-509.

BIBLIOGRAPHY

BUERGER, M.J (1970)
"Contemporary Crystallography."
McGraw - Hill.

EMSHOFF, J.R. and SISSON, R.L. (1970)
"Design and Use of Computer Simulation Models."
MacMillan, New York.

GUY, A.G. (1951)
"Elements of Physical Metallurgy."
Addison - Wesley.

HUDSON, M. (1971)
"Crystals and Crystal Structure."
Longmans, Green and Co.

NAYLOR, T.H. BALINTFY, J.L. BURDICK, D.S. AND CHU, K. (1966)
"Computer Simulation Techniques."
John Wiley and Sons.

SCHNEER, C.J. (ED.) (1977)
"Crystal Form and Structure."
Dowden, Hutchinson and Ross Inc.